


A STUDY OF  
THE FISCHER-TROPSCH SYNTHESIS AT  
ELEVATED TEMPERATURES IN A SHOCK TUBE

by

RAYMOND JAMES KELLY M. Sc. (Chem. Eng.)

A thesis submitted in partial fulfilment  
of the requirements for the degree of  
Doctor of Philosophy in the Department of  
Chemical Engineering, University of Natal



Johannesburg

July, 1973

This work was carried out in the Chemical Engineering Department of the University of Natal. The author was assisted in various ways by members of staff of the University and of the South African Coal, Oil and Gas Corporation; formal reference to this is made in the Acknowledgements. Otherwise, unless specifically indicated to the contrary in the text, this thesis is entirely the work of the author.

R. J. KELLY

DEDICATION

To my parents and Noreen

### ABSTRACT

The shock tube was used to investigate the product spectrum of the initial stages of the Fischer-Tropsch synthesis carried out at elevated temperatures. Special attention was paid to the relationship between methane selectivity and temperature.

The range of reaction environments studied are summarised below:-

Reaction temperature	-	780°K - 1425°K
Reaction pressure	-	160 psia - 330 psia
Mean reaction time	-	628 $\mu$ sec. - 727 $\mu$ sec.
Test gas composition	-	argon 81 - 87 mol.%
	-	hydrogen 6,5 - 9 mol.%
	-	carbon monoxide 6,5 - 9,5 mol.%
Catalyst type	-	fused iron, triply promoted
Catalyst loading	-	0,12 - 0,14 $\frac{\text{mass catalyst}}{\text{mass gas}}$

The experiments were conducted in the incident shock region and quenching was achieved by the reflected rarefaction wave.

Percentage conversion of hydrogen and carbon monoxide to useful products (hydrocarbons) varied between 0,1 and 2. Products detected in measurable quantities were methane, ethylene, ethane and propylene.

The theory of shock tube wave propagations through heterogeneous media was studied in detail and unique theory developed for handling conditions of varying temperature and pressure. This enabled characterisation of the reaction environment so that multilinear regression could be used to find a correlation between  $H_2 + CO$  consumption and system variables.

Major information gleaned on the initial stages of the Fischer-Tropsch synthesis at elevated temperatures was;

- (i) contrary to observed trends under normal synthesis conditions, methane selectivity decreased and propylene selectivity increased with increasing temperature;
- (ii) the process appeared to be hydrogen adsorption rate controlled;

- (iii) molecular degradation processes played a negligible part in the formation of final reaction products,  
and
- (iv) oxygen compounds, such as methanol, did not appear to be important intermediate products.

It has been shown that the heterogeneous shock tube offers a possible means of obtaining initial reaction rate data for highly complex systems.

### ACKNOWLEDGEMENTS

The author wishes to express sincere thanks to the supervisor of this project, Professor E.T. Woodburn of the University of Natal, for his interest, advice and encouragement throughout the course of this work.

Financial and material support from the South African Coal, Oil and Gas Corporation is gratefully acknowledged.

The author wishes also to acknowledge the invaluable support given by Dr L.J. Dry, Dr J.D. Louw and Dr M.E. Dry, all of the Research Division of the South African Coal, Oil and Gas Corporation, including the analytical work of Mr. E. Malan and his team.

Special thanks are due to the following members of staff of the University of Natal;

Mr R.J.J. Egenes who carried out the mechanical design of the shock tube itself.

Messrs D. Penn, E. Magnus and J. Botha for the construction, erection and maintenance of the experimental equipment.

Mr A. Achurch for his help and advice on electronic circuitry.

Messrs A. Perumal and N. David for their assistance in photographic matters.

LIST OF FIGURES AND PLATES

FIGURE (PLATE where indicated)		Page No.
2.1.I	SHOCK TUBE	18
2.1.I (PLATE)	DIAPHRAGM STATION	19
2.2.I	REACTION MIXTURE CIRCULATING SYSTEM	21
2.4.I	AIR SEGREGATOR AND PRODUCT GAS MIXER	23
2.5.2.I	CATALYST REDUCTION EQUIPMENT	24
2.5.2.I (PLATE)	CATALYST REDUCTION EQUIPMENT	24a
2.6.4.I (PLATE)	OSCILLOGRAPH AND CAMERA	28
2.6.4.II(PLATE)	PHOTO RECORD OF OSCILLOGRAPH TRACE - SHOCK SPEED MEASUREMENT	29
2.7.3.I	METHANE CALIBRATION CURVE FOR GAS CHROMATOGRAPH	32
3.1.1.I	(a) SHOCK TUBE (b) DISTANCE-TIME DIAGRAM SHOWING WAVE PATTERNS (c) PRESSURE DISTRIBUTION AT TIME $t_1$ (d) TEMPERATURE DISTRIBUTION AT TIME $t_1$	34
3.1.2.I	GAS FLOW THROUGH STATIONARY SHOCK FRONT	35
3.1.3.I	NON-IDEAL WAVE PATTERNS; $x-t$ DIAGRAM FOR HOMOGENEOUS SYSTEM	39
3.2.1.I	WAVE PATTERNS FOR HETEROGENEOUS SYSTEM SHOWING SOLID SLIP	43
3.2.2.I	RELAXATION ZONE - STATIONARY SHOCK FRONT	44
3.2.2.II	VARIATIONS OF THE GAS TEMPERATURE, VELOCITY AND PRESSURE, AND PARTICLE TEMPERATURE AND VELOCITY BEHIND THE SHOCK FRONT (RUN 36)	49
3.2.2.III	VARIATIONS OF THE GAS TEMPERATURE, VELOCITY AND PRESSURE, AND PARTICLE TEMPERATURE AND VELOCITY BEHIND THE SHOCK FRONT (RUN 16)	50
3.2.2.IV	VARIATIONS OF THE GAS TEMPERATURE, VELOCITY AND PRESSURE, AND PARTICLE TEMPERATURE AND VELOCITY BEHIND THE SHOCK FRONT (RUN 5)	51
3.2.3.I	CORRELATIONS FOR DRAG COEFFICIENT	53
3.2.4.I	SHOCK WAVE BOUNDARY LAYER FORMATION	56
3.2.4.II	$x-t$ DIAGRAM SHOWING IDEAL FLOW DURATION	57

3.2.4.III	RATIO OF EXPERIMENTALLY MEASURED FLOW DURATION TO IDEALLY PREDICTED FLOW DURATION VERSUS INITIAL CHANNEL GAS PRESSURE, HOOKER (1961)	58
3.2.4.IV	x-t DIAGRAM SHOWING IDEAL AND CORRECTED FLOW DURATION	62
3.3.2.I	RAREFACTION HEAD INTERSECTIONS	65
3.3.3.I	QUENCH BY REFLECTED RAREFACTION WAVE (RUN 36)	69
4.1.I	CATALYST PARTICLE SIZE DISTRIBUTION BY ROLLER ANALYSIS	78
4.2.I	SHOCK TUBE ELECTRICAL CONTROL CIRCUIT	81
4.2.I (PLATE)	SHOCK TUBE CONTROL PANEL	82
5.4.1.I	PRE-SHOCK CONTACT PERIOD; VARIATION IN GAS COMPOSITION WITH TIME	111
5.5.1.I	LONG CONTACT AND NO CATALYST RUNS; METHANE YIELD VERSUS SHOCK TEMPERATURE	118
5.5.1.II	LONG CONTACT AND NO CATALYST RUNS; ETHYLENE YIELD VERSUS SHOCK TEMPERATURE	119
5.5.1.III	LONG CONTACT AND NO CATALYST RUNS; ETHANE YIELD VERSUS SHOCK TEMPERATURE	120
5.5.1.IV	LONG CONTACT AND NO CATALYST RUNS; PROPYLENE YIELD VERSUS SHOCK TEMPERATURE	121
5.5.1.1.I	OBSERVED $H_2+CO$ CONSUMPTION ( $Q_{obs.A}$ ) VERSUS SHOCK TEMPERATURE ( $T_e$ ) AND CURVE FIT ( $Q_{F9}$ )	131
5.5.1.1.II	CO ADSORPTION ISOBAR, RAAL (1955)	133
5.5.2.I	LONG AND SHORT CONTACT RUNS; METHANE YIELD VERSUS SHOCK TEMPERATURE	137
5.5.2.II	LONG AND SHORT CONTACT RUNS; ETHYLENE YIELD VERSUS SHOCK TEMPERATURE	138
5.5.2.III	LONG AND SHORT CONTACT RUNS; ETHANE YIELD VERSUS SHOCK TEMPERATURE	139
5.5.2.IV	LONG AND SHORT CONTACT RUNS; PROPYLENE YIELD VERSUS SHOCK TEMPERATURE	140
5.5.2.V	STANDARD FREE ENERGY CHANGES VERSUS TEMPERATURE; HYDROCARBONS, WATER GAS, AND IRON PENTACARBONYL	143
5.5.4.I	LONG CONTACT, UNREDUCED AND RE-OXIDISED RUNS; METHANE YIELD VERSUS TEMPERATURE	152
5.5.4.II	LONG CONTACT, UNREDUCED AND RE-OXIDISED RUNS; ETHYLENE YIELD VERSUS TEMPERATURE	153



5.5.4.III	LONG CONTACT, UNREDUCED AND RE-OXIDISED RUNS; ETHANE YIELD VERSUS TEMPERATURE	154
5.5.4.IV	LONG CONTACT, UNREDUCED AND RE-OXIDISED RUNS; PROPYLENE YIELD VERSUS TEMPERATURE	155
5.6.I	STANDARD FREE ENERGY CHANGES VERSUS TEMPERA- TURE; FORMATION OF HYDROCARBONS VIA HOMO- GENEOUS REACTION	160
5.7.I	MEAN SELECTIVITIES	169
5.8.I	RECOMMENDATIONS FOR FUTURE WORK ON KELLOGG SYNTHESIS	171
C.2.I	TEMPERATURE-TIME DIAGRAM; REACTION ZONE	C3
C.2.II	ITERATIVE APPROACH OF Q TO $Q_{FA}$	C7
C.2.III	YIELD AND RATE/TIME DIAGRAMS	C8
C.2.IV	QUENCH-TEMPERATURE/TIME CURVES FOR CATEGORIES I, II AND III	C10
D.I	PRESSURE SWITCH	D1
E.I	BOTTOM SOLENOID VALVE	E2
E.II	RUPTURE PIN	E3

## CONTENTS

	Page No.
ABSTRACT	iv
ACKNOWLEDGEMENTS	vi
LIST OF FIGURES AND PLATES	vii
INTRODUCTION	1
CHAPTER 1 LITERATURE SURVEY	
Fischer-Tropsch Reaction Mechanism - Iron Catalyst	3
1.1 Background	3
1.2 Early Theories	4
1.3 Modern Theories	8
1.4 Conclusion	15
CHAPTER 2 DESCRIPTION OF EQUIPMENT	17
2.1 The Shock Tube	17
2.2 The Reaction Mixture Circulating System	20
2.3 Vacuum Pump	22
2.4 Gas Mixers	22
2.5 Catalyst Preparation Equipment	22
2.5.1 Air Segregator	22
2.5.2 Catalyst Reduction Equipment	25
2.6 Instrumentation	25
2.6.1 Pressure Gauges	25
2.6.2 Temperature Gauges	26
2.6.3 Photoelectric Cell	26
2.6.4 Shock Speed Measurement	26
2.7 Gas Analysers	30
2.7.1 Hydrocarbon and Water Analysis	30
2.7.2 Inorganic Gas Analysis	30
2.7.3 Calibration of Chromatographs	31
CHAPTER 3 THEORY	33
3.1 Wave Patterns in the Shock Tube - Homogeneous Case	33
3.1.1 Description	33
3.1.2 Basic Equations	35
3.1.3 Deviations from Ideal Behaviour	38
3.2 Conditions Behind the Shock Front - Heterogeneous Case	42
3.2.1 Description	42
3.2.2 Analysis of the Relaxation Zone	44
3.2.3 Particle Drag Coefficient	52
3.2.4 Boundary Layer Formation and its Effect on Flow Duration	56

3.3	Reaction Zone	63
3.3.1	Description	63
3.3.2	Reflected Rarefaction Head Intersections	64
3.3.3	Quench	68
3.4	Simple Fischer-Tropsch Reaction Rate Equation	73
CHAPTER 4	EXPERIMENTAL PROCEDURE	77
4.1	Reaction Mixture Preparation	77
4.2	Shock Tube Operation	80
4.3	Product Gas Mixing and Sampling	83
4.4	Catalyst Loading Determination	84
4.5	Experimental Design	85
4.5.1	Introduction	85
4.5.2	Catalyst Loading	85
4.5.3	Temperature, Partial Pressure of Reactants and Dwell Time	86
4.5.4	Catalyst Reduction	88
4.5.5	Regression Analysis	89
4.5.6	Conclusion	93
CHAPTER 5	EXPERIMENTAL RESULTS AND DISCUSSION	95
5.1	Introduction	95
5.2	Summary	95
5.3	Check on Consistency of Gas Analysis of Hydrocarbons	106
5.4	Pre-Shock Contact between Gas and Catalyst	106
5.4.1	Effect of Contact Period Duration	109
5.4.2	Effect of Hydrocarbons Present Initially	112
5.4.3	Effect of Catalyst Activity	114
5.5	Shock Contact between Gas and Catalyst	116
5.5.1	Effect of Shock Strength	117
5.5.1.1	Effect of Temperature and Pressure on the Apparent Overall Surface Reaction	127
5.5.2	Effect of Pre-Shock Contact Period	136
5.5.3	Effect of Gaseous Hydrocarbons Present before Shocking	145
5.5.3.1	Overall Homogeneous Reaction	147
5.5.3.2	Overall Heterogeneous Reaction	147
5.5.3.3	Summary of Chapter 5.5.3	150
5.5.4	Effect of Catalyst Activity	150
5.6	Homogeneous Reaction under Shock Conditions	158
5.7	Conclusion	161
5.8	Recommendations for Future Work	170
	NOMENCLATURE	173
	BIBLIOGRAPHY	178

APPENDIX A	COIL TIMER AND THYRISTOR AC LOAD CONTROLLER CIRCUITS	A1
APPENDIX B	SPECIMEN CALCULATION OF HYDROCARBON YIELDS	B1
APPENDIX C	DATA PROCESSING FOR REACTION MODEL	C1
	C.1 Analytical Expressions for Homogeneous Yields	C1
	C.2 Allowance for Quench Period	C3
APPENDIX D	PRESSURE SWITCH	D1
APPENDIX E	DETAILS OF SOLENOID OPERATED EQUIPMENT	E1
APPENDIX F	PROGRAMME ZHETRO - HETEROGENEOUS STATE 2 (FORTRAN V)	F1
APPENDIX G	AVERAGE PARTICLE DIAMETER, PARTICLE DENSITY AND SURFACE AREA	G1

## INTRODUCTION

The purpose of this work is twofold. Firstly it is an investigation into the character of the initial reaction steps of the Fischer-Tropsch synthesis at elevated temperatures with special reference to the formation of methane. Secondly it develops techniques to define the reaction environment realised when a single pulse shock tube is used as a research tool in the study of heterogeneous catalysis.

In the Fischer-Tropsch synthesis carbon monoxide and hydrogen react in the presence of a catalyst, usually cobalt or iron, to form gaseous, liquid and solid hydrocarbons of various molecular structure. The process is normally carried out at temperatures of 220 to 340°C and pressures of 25 - 30 atmospheres. Methane, the simplest hydrocarbon, is one of the products and since it has limited importance as a fuel, is often reformed to carbon monoxide and hydrogen. Naturally the economics of the synthesis would be improved if methane formation was minimised.

Formation of methane can occur by direct combination of carbon monoxide and hydrogen followed by hydrocondensation as postulated by Sternberg and Wender (1959) or by hydrocracking of larger hydrocarbon molecules as suggested by Craxford (1939 & 1946) and Eidus (1967).

The concept underlying the use of the shock tube is that of a uniform reaction environment which should result in a narrow product spectrum. The shock tube enables the first millisecond of reaction to be studied. This short reaction time simplifies matters by limiting the extent of reaction thereby reducing the possible routes by which observed products could be formed. Initial experiments indicated that in order to encourage reaction to proceed at a reasonable rate within such a short period, elevated temperatures would be necessary; greater than 500°C. Molecular degradation processes (hydrocracking) would be magnified at elevated temperatures making them easier to observe. In this way it was thought possible to add new information to the understanding of the mechanism of Fischer-Tropsch synthesis, shedding

some light on the relative importance of methane formation via hydrocondensation and degradation processes.

In the shock tube the reaction mixture, consisting of catalyst particles suspended in synthesis gas, is heated and quenched by a shock and a rarefaction wave respectively. A shock wave passing through such a suspension upsets the velocity and temperature equilibrium between the two phases and a relaxation zone is created in which the equilibrium is gradually re-established. The general equations for the analysis of such a system were apparently first presented by Carrier (1958). The theory as outlined by Rudinger (1964) is used in this work. Quenching of the reaction is analysed on the basis of quench rate equations for homogeneous systems developed by Kelly (1965) using the method of Characteristics.

The scope of this work can be outlined as follows:-

- (a) The design and construction of a suitable shock tube and ancilliary equipment including certain instrumentation.
  - (b) Conduction of Fischer-Tropsch synthesis in the shock tube under various reaction conditions never previously investigated.
  - (c) Development of a rate equation for the synthesis as conducted in (b) above, using multilinear regression analysis.
  - (d) A critical analysis of results obtained with regard to published Fischer-Tropsch reaction data.
-

## CHAPTER 1

### LITERATURE SURVEY

#### Fischer-Tropsch Reaction Mechanism - Iron Catalysts

##### 1.1 Background

Synthesis of hydrocarbons from carbon monoxide and hydrogen using an iron catalyst was realised for the first time by Franz Fischer and Hans Tropsch in Germany (1923 & 1924). Iron catalysts did not become popular until 1936-7 when Fischer and Pichler (1937) managed to achieve high yields of hydrocarbons using a precipitated iron catalyst. This led to intensive research on iron catalysts by several German laboratories, in order to develop a satisfactory iron catalyst to replace the more expensive cobalt catalysts used in the synthesis plants at the time. A certain degree of success was attained by 1943 with alkali promoted iron catalysts.

Between 1945 and 1955 much work was done in the United States with the aim of producing synthetic liquid fuel from carbon monoxide and hydrogen obtained by the partial oxidation of natural gas. However competition of natural petroleum proved overwhelming and efforts to synthesise petrol were curtailed. This period was not entirely wasted as, in the USA and in England, many of the new tools of catalytic research developed in the thirties were applied to the study of the Fischer-Tropsch reaction mechanism.

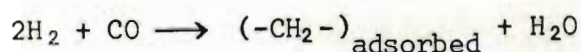
During the past eighteen years South Africa has become a world leader in a particular application of the Fischer-Tropsch synthesis employing promoted iron catalysts. In Sasolburg the South African Coal, Oil and Gas Corporation synthesises liquid fuels from coal, Hoogendoorn and Salomon (1957), using both fixed bed reactors and entrained catalyst units.

The Fischer-Tropsch process may be divided into a number of steps:-

- (a) Adsorption of reactants onto the catalyst surface,
- (b) Chain initiation,
- (c) Chain growth,
- (d) Chain termination,
- (e) Desorption of products, and
- (f) Readsorption with further reaction.

For the purposes of this study, steps (a) to (d) will be regarded as comprising the reaction mechanism.

The principal primary reaction, Anderson (1956) appears to be

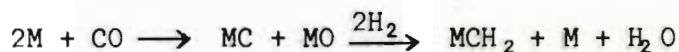


where  $(-\text{CH}_2-)_{\text{adsorbed}}$  is a chain initiator. Chain growth can be represented as the combination of two  $(-\text{CH}_2-)_{\text{adsorbed}}$  radicals to yield  $(-\text{CH}_2\text{CH}_2-)_{\text{adsorbed}}$ .

Desorption of  $(-\text{CH}_2\text{CH}_2-)_{\text{adsorbed}}$  resulting in  $\text{C}_2\text{H}_4$  or hydrogenation of  $(-\text{CH}_2\text{CH}_2-)_{\text{adsorbed}}$  giving  $\text{C}_2\text{H}_6$  is called termination.

## 1.2 Early Theories

Fischer and Tropsch (1926) postulated that carbides were important intermediates in the synthesis. Firstly synthesis gas reacted with the catalyst to form a carbide, then the carbide hydrogenated to a methylene group and thirdly methylene groups polymerised to larger molecules. Fischer (1930) modified this to include the simultaneous formation of oxide,

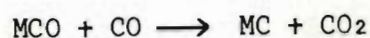
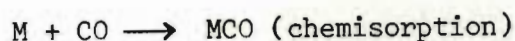


where M represents a metal atom. Hydrogenation of higher carbides containing 3 to 4 carbon atoms per atom of metal was also considered to be a possible route to methylene groups; in this case the catalyst surface would change between two carbides instead of carbide and metal. Although traces of oxygenated hydrocarbons

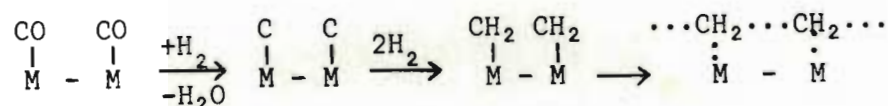


were present in the product gas Fischer regarded them as unimportant to the mechanism.

Craxford and Rideal (1939) presented a more detailed carbide hypothesis according to the following:-



or



→ higher hydrocarbons.

This reaction mechanism was studied by means of the para-to ortho-hydrogen conversion using a mixture of para-hydrogen and carbon monoxide. Craxford and Rideal conducted some experiments using (a)  $1H_2/1CO$  ratio gas at temperatures  $< 140^\circ C$ ,  $200^\circ C$  and  $> 250^\circ C$  and (b)  $24H_2/1CO$  at  $200^\circ C$ . Their observations were:-

Para to ortho conversion occurs at

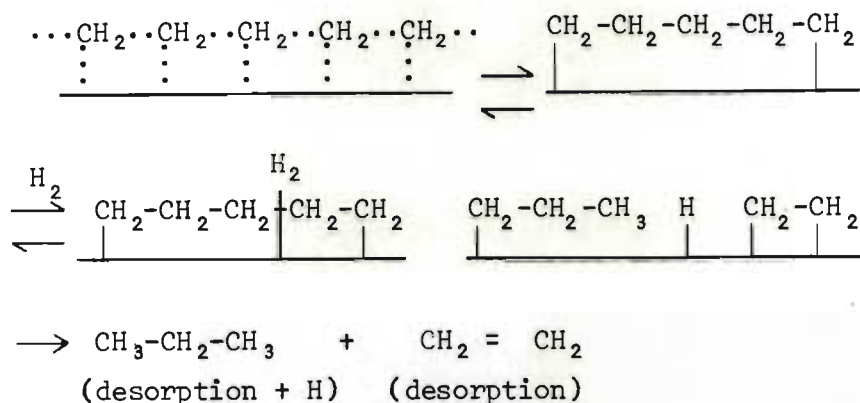
- (i) temperatures below  $140^\circ C$  with no Fischer-Tropsch reaction taking place.
- (ii) commencement of reaction at  $200^\circ C$  when methane and carbide are being formed and no oil.
- (iii) a temperature of  $200^\circ C$  with  $24H_2/1CO$  gas with methane formation and no oil.
- (iv) temperatures above  $250^\circ C$  with methane formation and no oil.

Very little para to ortho conversion occurred while oil was being formed during normal synthesis at  $200^\circ C$ . Craxford and Rideal concluded;

- (i) an insignificant amount of atomic hydrogen was present in normal synthesis,
- (ii) methane formation involved atomic hydrogen,
- (iii) high surface carbide coverage of the catalyst inhibited para-to ortho-conversion.

Their mechanism for the formation of macromolecules was therefore based on molecular hydrogen only.

Macromolecules grew until split by hydrogen;



Hydrocracking would be favoured by high amounts of chemisorbed hydrogen. In a later article Craxford (1946) postulated that methane and gaseous hydrocarbons were produced by hydrocracking. He thought that this reaction did not occur in normal synthesis where the catalyst was postulated to be covered by carbide. However it did occur on surfaces having no carbide and in the presence of atomic hydrogen.

Many aspects of Craxford's hypothesis have since been shown to be either inconsistent or incorrect. His basic assumption that surface carbide is an intermediate has been criticised. Some comments on Craxford's hypothesis by Anderson (1956) are summarised below.

- " 1 Craxford and Rideal's conclusion that insignificant amounts of atomic hydrogen were present in normal synthesis is not the only possibility in the light of low para-to ortho-hydrogen conversion. Other possibilities are (a) the adsorption of hydrogen is the rate controlling step, and (b) hydrogen desorbed from the catalyst surface would have to diffuse against a net gas flow in the pores of the catalyst caused by the gas contraction of the synthesis reaction. The detention of this hydrogen in the pores could result in its extinction by further adsorption and subsequent reaction.

- 2 Large yields of alcohols are obtained under suitable conditions of synthesis and they appear to be important primary products in the synthesis with iron catalyst. The carbide theory does not predict the formation of oxygenated compounds.
- 3 Whereas in the case of iron catalyst, samples containing carbides have activities equal to or greater than corresponding non-carburised samples, the opposite is true for cobalt catalysts."

Kummer, DeWitt and Emmett (1948) investigated the carbide intermediate hypothesis on iron and cobalt catalyst using  $^{14}\text{C}$  as a tracer. Experiments were conducted with iron catalysts in which the extent of reaction, if it proceeded entirely by the carbide mechanism, would involve only a small fraction of the catalyst surface. The results indicated that only 10 and 15 per cent of synthesis proceeded by carbide reduction at 260 and 300°C respectively. Thus, only a small fraction of the hydrocarbons was produced from surface carbide deposited on the catalyst by a pre-treatment with carbon dioxide. The authors noted that the data did not preclude the possibility that carbon atoms may exist momentarily on the catalyst surface in some step of the synthesis.

Since the carbide theory did not predict the formation of oxygenated compounds and alcohols are important synthesis products under certain experimental conditions, the postulate of an oxygenated intermediate was first made by Elvins and Nash (1926). Methanol was suggested as a possible intermediate although none was found.

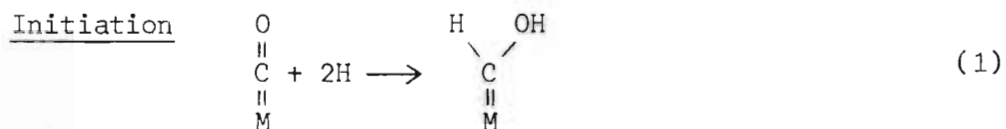
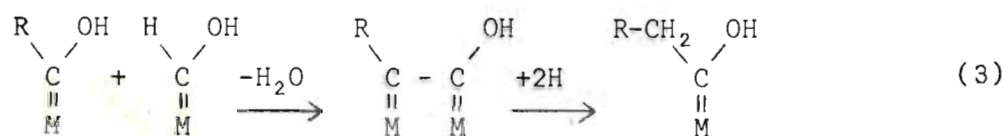
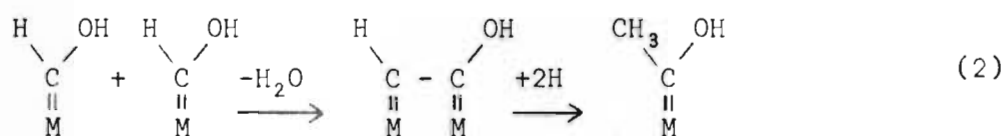
Pichler (1947) favoured the idea of carbonyl-type intermediates. He maintained that optimum synthesis conditions prevailed at temperatures and pressures where the rate of formation of volatile carbonyl remained lower than that for the supposed intermediate carbon monoxide compounds with hydrogen.

---

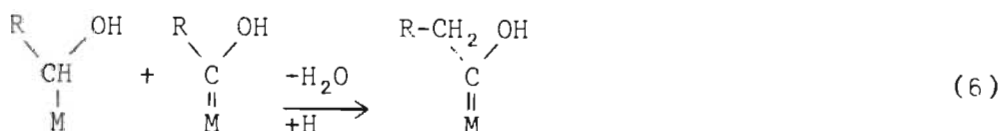
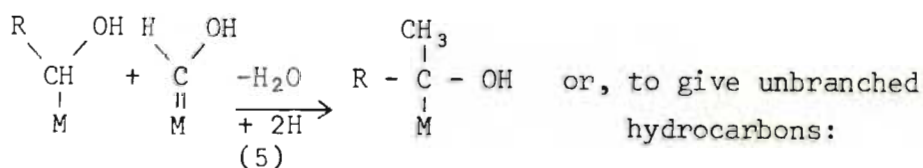
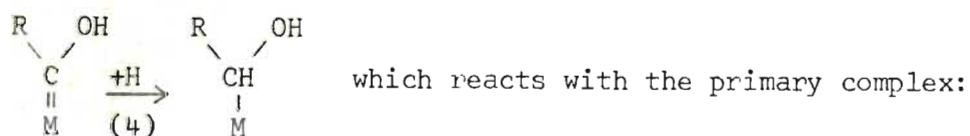


TABLE 1.3.I

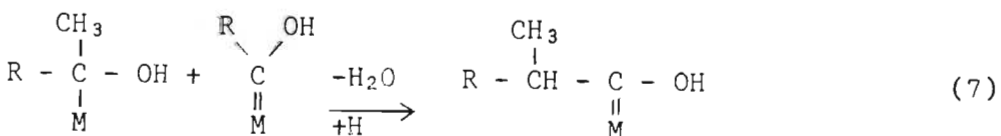
REACTION MECHANISM OF THE FISCHER-TROPSCH SYNTHESIS  
AS PROPOSED BY STORCH ET AL (1951)

Chain growth

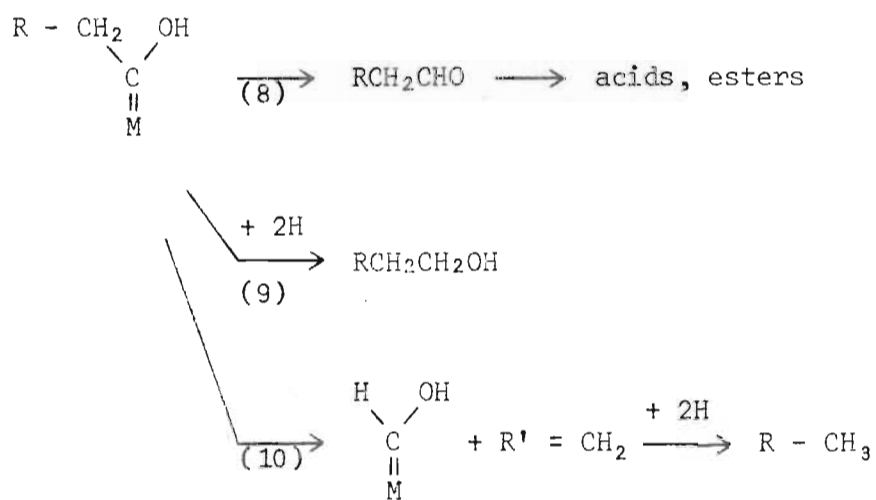
or, leading to branched hydrocarbons:



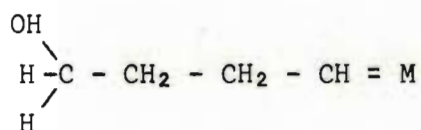
The branched isomer may further react with the primary complex:



continued

TABLE 1.3.I ContinuedTermination

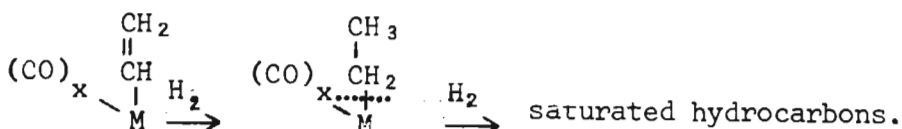
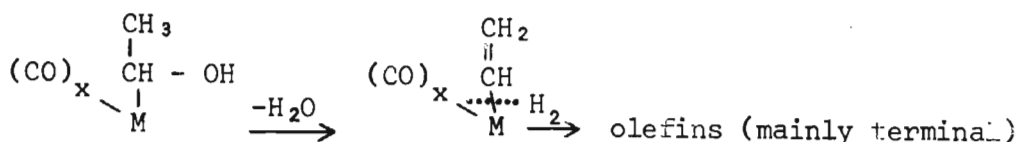
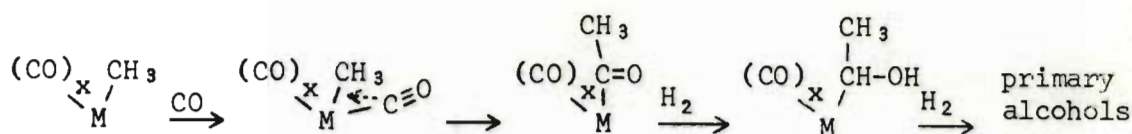
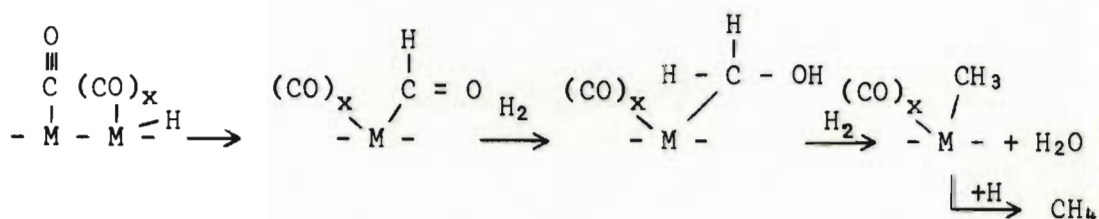
to the catalyst at the opposite end of the chain from the hydroxyl group, e.g.:-



Chain growth was postulated to proceed by addition of methylene groups at the end attached to the catalyst.

Storch, Golumbic and Anderson's reaction scheme did not include the possibility of chain extension by the reaction of olefins or alcohols produced in a primary step with hydrogen and carbon monoxide involving a carbonyl-type surface intermediate. Surface complexes of a hydrocarbonyl-type would be stabilised by the presence of alkali which may explain the promoting influence of alkali on the synthesis.

Sternberg and Wender (1959) suggested that the initial methyl group is formed through  $\text{H}\cdot\text{CO}\cdot\text{M}(\text{CO})_x$  where M is a transition metal surface, i.e. it is carbonyl-catalysed. Chain lengthening occurs through CO being inserted between the methyl group and the surface:-



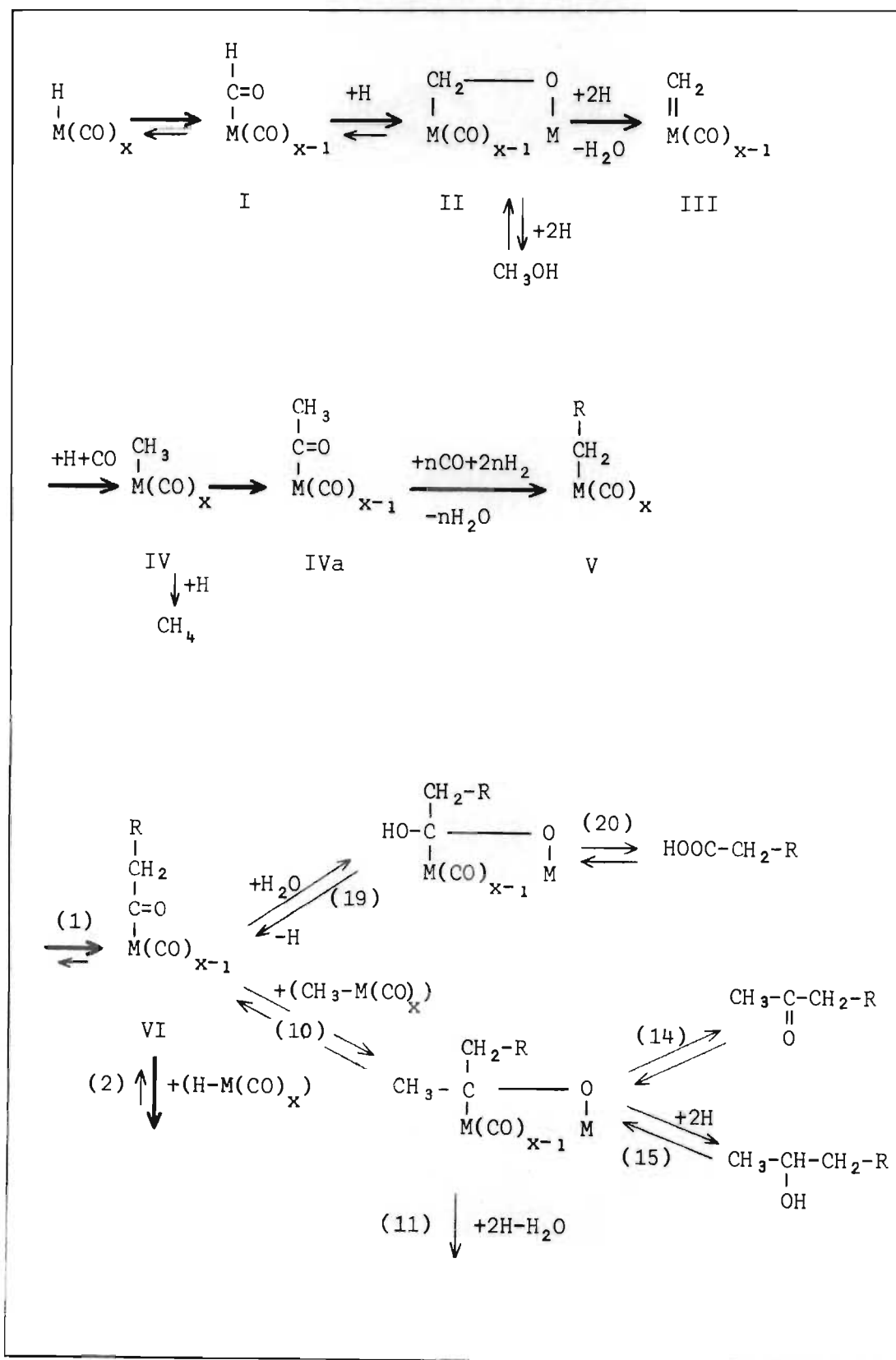
Eidus (1967) reviewed experiments in which an addition of a small quantity of compounds labelled with  $^{14}\text{C}$  to the  $\text{H}_2$ -CO mixture, had been made. These compounds could be divided into two groups - the first group included formaldehyde, methanol, methyl formate and ketene labelled in the CO group, while the second group included ethanol, propanol, acetaldehyde, ethylene, propylene and ketene labelled in the  $\text{CH}_2$  group. The first group yielded liquid products in which molar radioactivity increased regularly with increase in carbon number, whilst the second group yielded constant molar radioactivity with change in carbon number. This indicated that substances of the first group underwent preliminary decomposition forming CO which in turn reacted further, taking part in chain growth. Conversely substances of the second group did not decompose. These results supported the long standing idea of a primary complex being formed from CO and  $\text{H}_2$  on the catalyst surface and showed that this complex could have not only one but also two or more carbon atoms. The initiation of the chains by methylene radicals formed by dissociation of ketene showed convincingly that the presence of an oxygen-containing radical was not essential for chain initiation. Eidus inferred that polymerisation of  $\text{CH}_2$  radicals for C-C bond formation was a probable way in which chain lengthening occurred.

Pichler (1970) outlined his ideas on the growing of hydrocarbon chains. He believed, like Sternberg and Wender (1959) and Roginskii (1964), that the phenomenon took place by the insertion of a CO molecule between the catalyst metal atom and a hydrocarbon chain attached to the catalyst surface followed by reduction of the CO group with hydrogen to  $\text{CH}_2$ . Pichler maintained that under conditions of synthesis it was probable that several CO molecules could be chemisorbed on active catalyst sites. Chain initiation took place by reaction of chemisorbed H-atoms with CO groups to yield formyl groups I as shown in Table 1.3.II. Reaction with a second H-atom gave the intermediate II where oxygen became chemisorbed to an adjacent catalyst atom. Hydrogenolysis followed causing the oxygen to be removed by action of hydrogen. Chain growth occurred by alternating insertion of CO and hydrogenolysis.



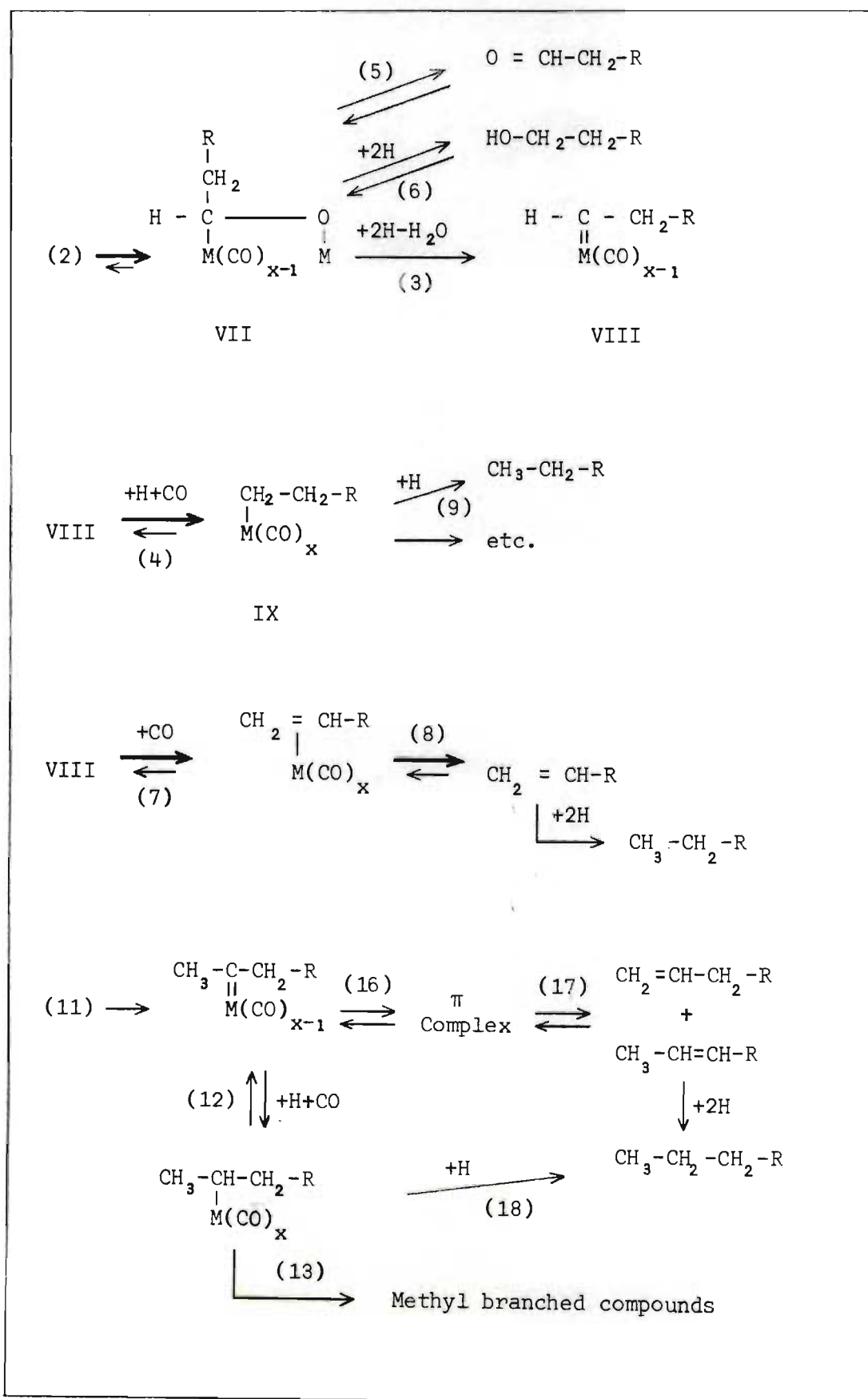
TABLE 1.3.II

## REACTION MECHANISM ACCORDING TO H. PICHLER (1970)



continued

TABLE 1.3.II Continued



By reversible desorption of the intermediate VII it was possible to form small amounts of primary aldehydes (Step 5) and by reversible hydrogenation primary alcohols could be formed (Step 6).

Non-reversible hydrocracking of the carbon-oxygen bond of VII gave the chemisorbed species VIII which may desorb reversibly via an olefin  $\pi$ -complex to an  $\alpha$ -olefin or be converted by addition of an H-atom to chemisorbed species IX, which in turn would be capable of further chain growth by insertion of CO. By action of hydrogen IX could be desorbed as a paraffin.

Pichler's proposed reversibility of the formation of olefins, alcohols and aldehydes allowed for the possibility of chain initiation by these compounds. He maintained that secondary alcohols and ketones were formed by reactions of chemisorbed acyl and alkyl radicals (Step 10). Steps 11 to 18 are analogous to Steps 3 to 9 with the exception that Step 13 leads to the formation of branched compounds. Using  $^{14}\text{C}$  tracer Pichler found that branched compounds could also be formed by the incorporation of  $\text{C}_3$  and higher olefins. His tracer experiments also showed that low molecular weight olefins took part in chain initiation and were capable of hydrosplitting to yield methane; however, paraffinic hydrocarbons were not incorporated and behaved as inerts.

Organic acids could be formed by reversible reaction with adsorbed water (Step 19) followed by desorption (Step 20).

---

#### 1.4 Conclusion

The early carbide hypothesis (Fischer and Tropsch (1926), Fischer (1930), Craxford and Rideal (1939) and Craxford (1946)) has been subjected to well-founded criticism as early as the nineteen forties (Kummer, DeWitt and Emmett (1948) Eidus and Zelinskii (1942) and Weller, Hofer and Anderson (1948)). Another hypothesis which has been refuted is the theory of a "giant" molecule, Craxford and Rideal (1939) and Craxford (1946), formed by the polymerisation of methylene radicals and which undergoes cracking by atomic hydrogen to yield the final products. The rejection (Weitkamp et al

(1953)) of this hypothesis had an undesirable effect as it led to an underestimation of the part played by molecular degradation processes in the reaction and the part played by hydrocarbon radicals in the formation of the chains.

In his review on the mechanism of the Fischer-Tropsch synthesis and related hydropolymerisation of alkenes, Eidus (1967) said that the most important theoretical problems of both reactions yet to be completely resolved were;

- " (i) the part played by oxygen compounds as intermediate products;
- (ii) the part played by heterogeneous hydrocarbon and oxygen-containing radicals at the start of chain formation and in the process of chain growth;
- (iii) the chemistry of the formation of C-C bonds between the units of the chains - the choice between polymerisation and condensation schemes, and
- (iv) the part played by degradation processes in the formation of the final reaction products. "

A primary aim of this work was to contribute to the understanding of the Fischer-Tropsch reaction especially in regard to problems (i), (ii) and (iv) above. In this way it was hoped to comment constructively on two current hypotheses namely, that of Storch, Golumbic and Anderson and that of Pichler; Sternberg and Wender; and Roginskii.

---

## CHAPTER 2

### DESCRIPTION OF EQUIPMENT

#### 2.1 The Shock Tube

The shock tube was constructed from stainless steel pipe having a constant internal diameter of 53 mm and wall thickness of 3,5 mm. Maximum operating pressure was 2000 psig or in the case of shock pressures (impulse loads) the maximum was 700 psig. Neoprene "O-rings" were used to seal flanged joints. The tube was mounted vertically as shown in Figure 2.1.I.

The tube consisted of two sections of different pressure separated by a thin diaphragm which, ideally, disappeared instantaneously on command. Diaphragm rupture was effected by means of a steel pin driven by A.C. solenoids (Figure 2.1.I and Plate 2.1.I). Details of the rupture pin and solenoid drives are given in Appendix E. The tip of the pin was star-shaped so that it made five cuts radiating from the centre of the diaphragm. Subsequent tearing of the diaphragm took place along these cuts so that good "petalling" was achieved.

Diaphragms consisted of laminations of 0,010 ins aluminium and brass sheet. Combinations of up to 0,030 ins overall thickness were used for the larger diaphragm pressure differentials.

Rapid removal of the diaphragm resulted in a pressure step which generated a shock wave in the channel section of the tube as it accelerated down the channel. In this way the reaction mixture was compressed and heated very quickly to any desired temperature. Temperatures up to 1400<sup>o</sup>K could be reached with the particular system studied in this work.

The lengths of the chamber and channel were chosen so that quenching of the reaction could be achieved by a rarefaction wave reflected from the end of the chamber; see Chapter 3 for wave patterns.

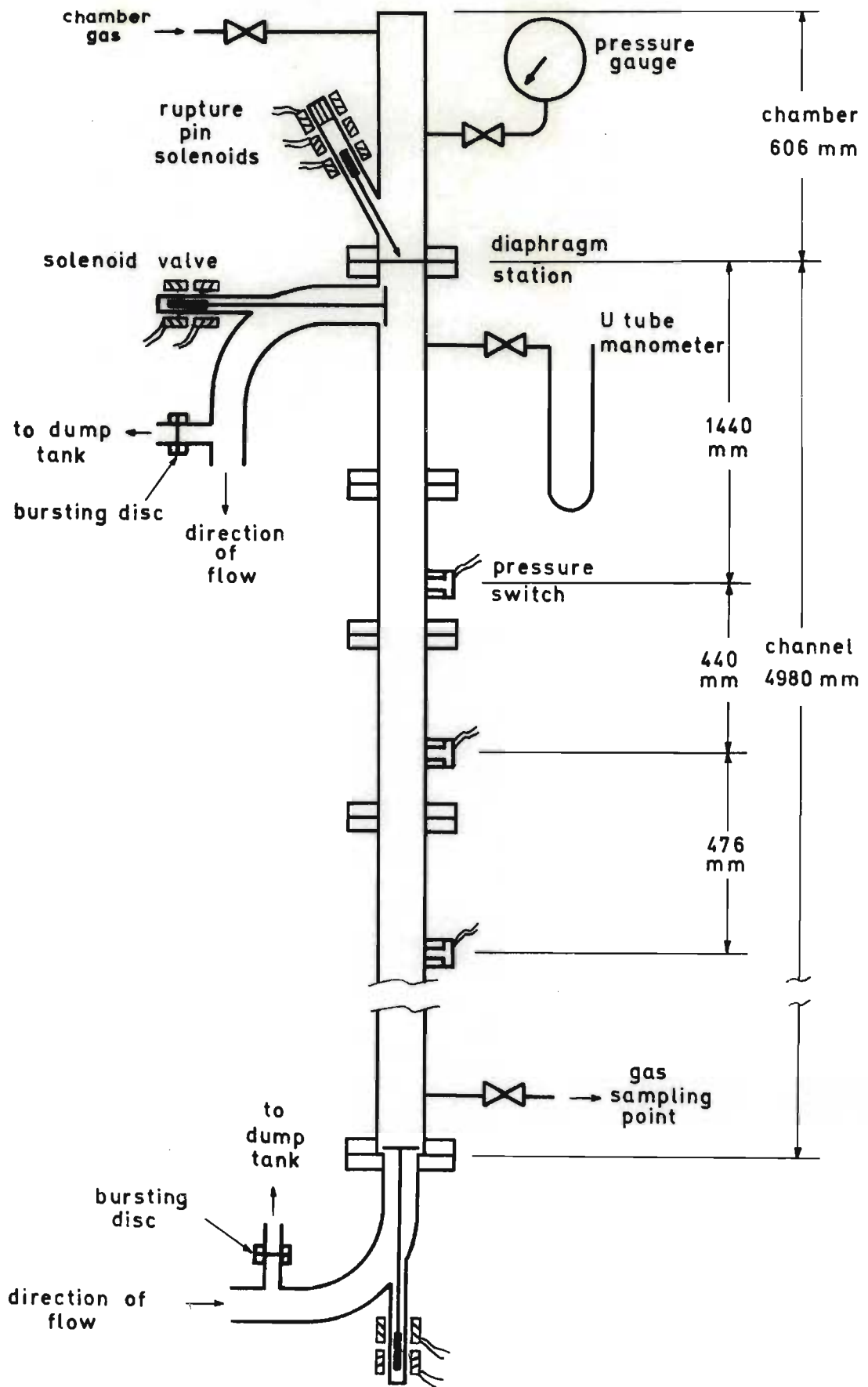


FIGURE 2.1.1 Shock Tube

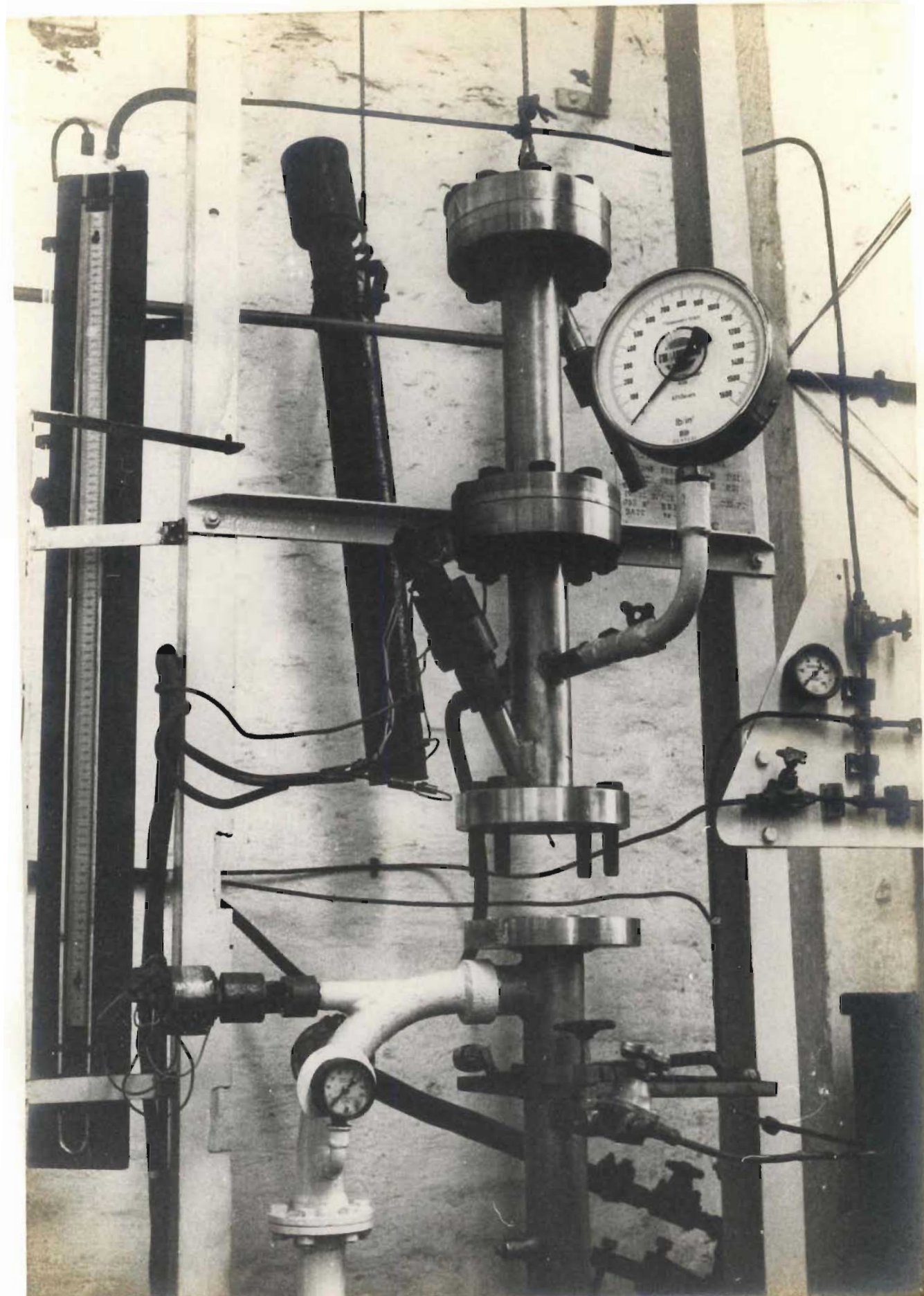


PLATE 2.1.I Diaphragm station

In order to ensure a uniform suspension of catalyst particles, sized less than  $44\mu$ , in the gas, it was necessary to circulate the mixture through the channel section. Special solenoid operated valves were used to isolate the low pressure circulating system from the channel just before diaphragm rupture. These are depicted in Figure 2.1.I (also Plate 2.1.I); further details appear in Appendix E.

---

## 2.2 The Reaction Mixture Circulating System

The reaction mixture of gas and catalyst was circulated by means of a centrifugal blower driven at 4600 rpm by a 1 HP electric motor. The blower type was SMF 7.5 manufactured by ASEA, normally used for providing an air-blast for forging hearths. It was modified for use in a gas sealed system by means of a CRANE double mechanical seal fitted to the impeller shaft.

Figure 2.2.I shows the layout of the circulating system. An upward velocity of gas in the shock tube of 64 ft/sec. was attained - measured by hot wire anemometer with no catalyst present. Various gas mixtures could be introduced into the channel through valve 1 and reduced catalyst through valve 2 by inverting the reduction vessel. A photo cell was used to check the uniformity of the catalyst suspension.

In case of premature rupturing of the diaphragm separating chamber and channel the blower casing had to be protected against shock pressures. This was achieved by means of bursting discs and large evacuated dump tanks (DT in Figure 2.2.I).

The total volume of the circulating system including the shock tube channel was 25 litres whilst that of the channel alone was 11,25 litres.  $1\frac{1}{2}$  ins I.D. mild steel pipe was used for most of the system; blower casing was cast iron and the impeller was fabricated from aluminium. Water cooled copper tubing of  $1\frac{1}{2}$  ins I.D. was used after the blower in order to cool the circulating reaction mixture.

---



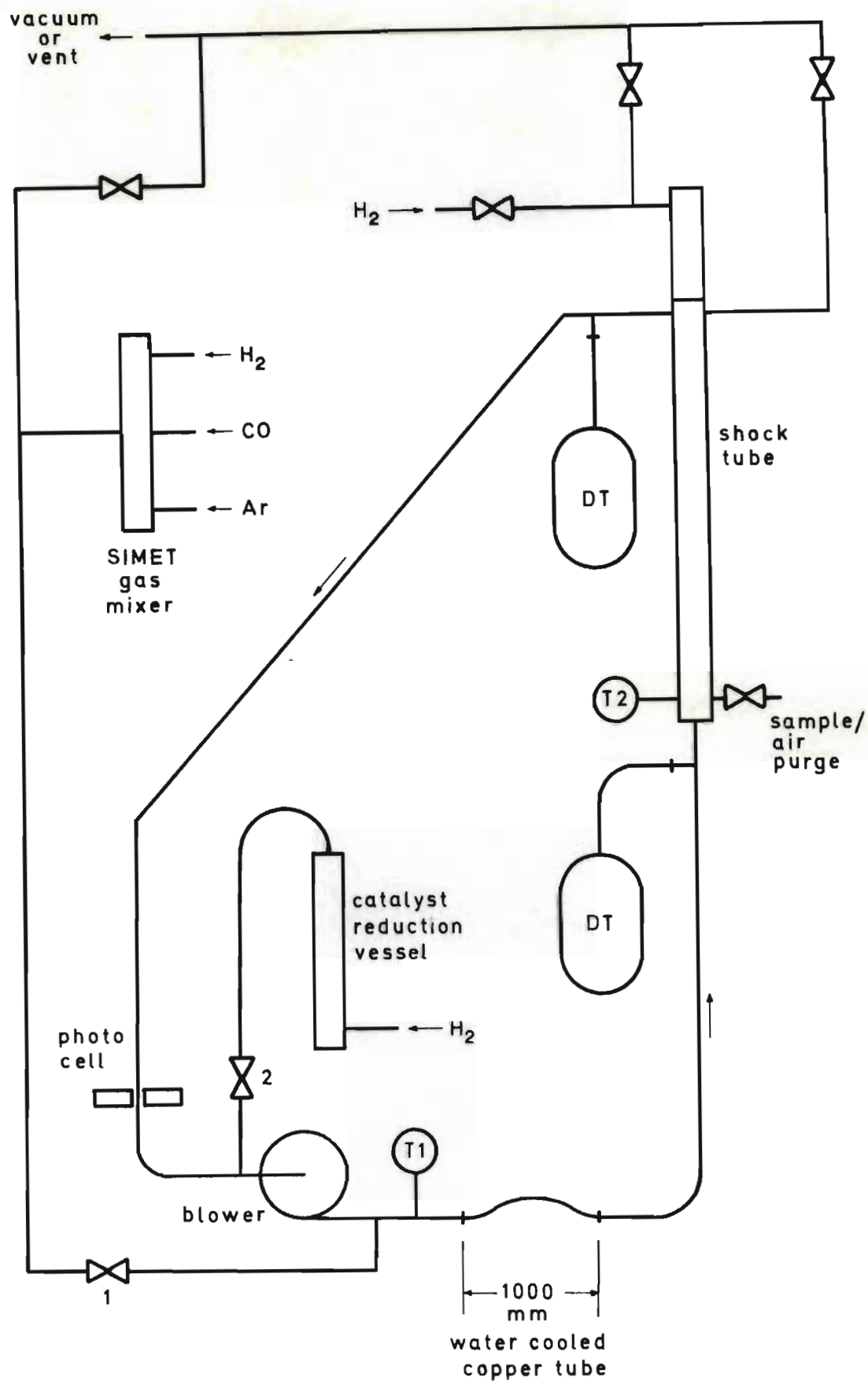


FIGURE 2.2.I Reaction mixture circulating system

### 2.3 Vacuum Pump

An oil sealed rotary pump was used to evacuate the equipment. The pump type was SPEEDIVAC ES 150 manufactured by Edwards High Vacuum Ltd., England.

Pumping of the circulation system including the shock tube channel to 2 Torr took 45 min. and the leak rate was 10 Torr per hour.

---

### 2.4 Gas Mixers

Channel gas consisted of a mixture of hydrogen, carbon monoxide and argon from cylinders, and was introduced by means of a three-turret SIMET gas mixer supplied by National Welding Equipment Co. of California. The mixer was precalibrated and was accurate to within 4 per cent.

Product gas mixing was effected by means of the stainless steel mixing vessel shown in Figure 2.4.I. The vessel was fitted internally with a movable perforated baffle and guide ring. By inverting the vessel several times the baffle could be moved to and fro through the gas. Construction was by Alfa Laval Ltd. South Africa and it had an operating pressure of 40 psig.

---

### 2.5 Catalyst Preparation Equipment

#### 2.5.1 Air Segregator

Iron catalyst received from the South African Coal, Oil and Gas Corporation was pre-screened to minus 325 mesh and contained particles below  $8\mu$  in size to the extent of 15 mass per cent. These small particles were carried over when the catalyst was fluidised during reduction. In order to know accurately the quantity of reduced catalyst

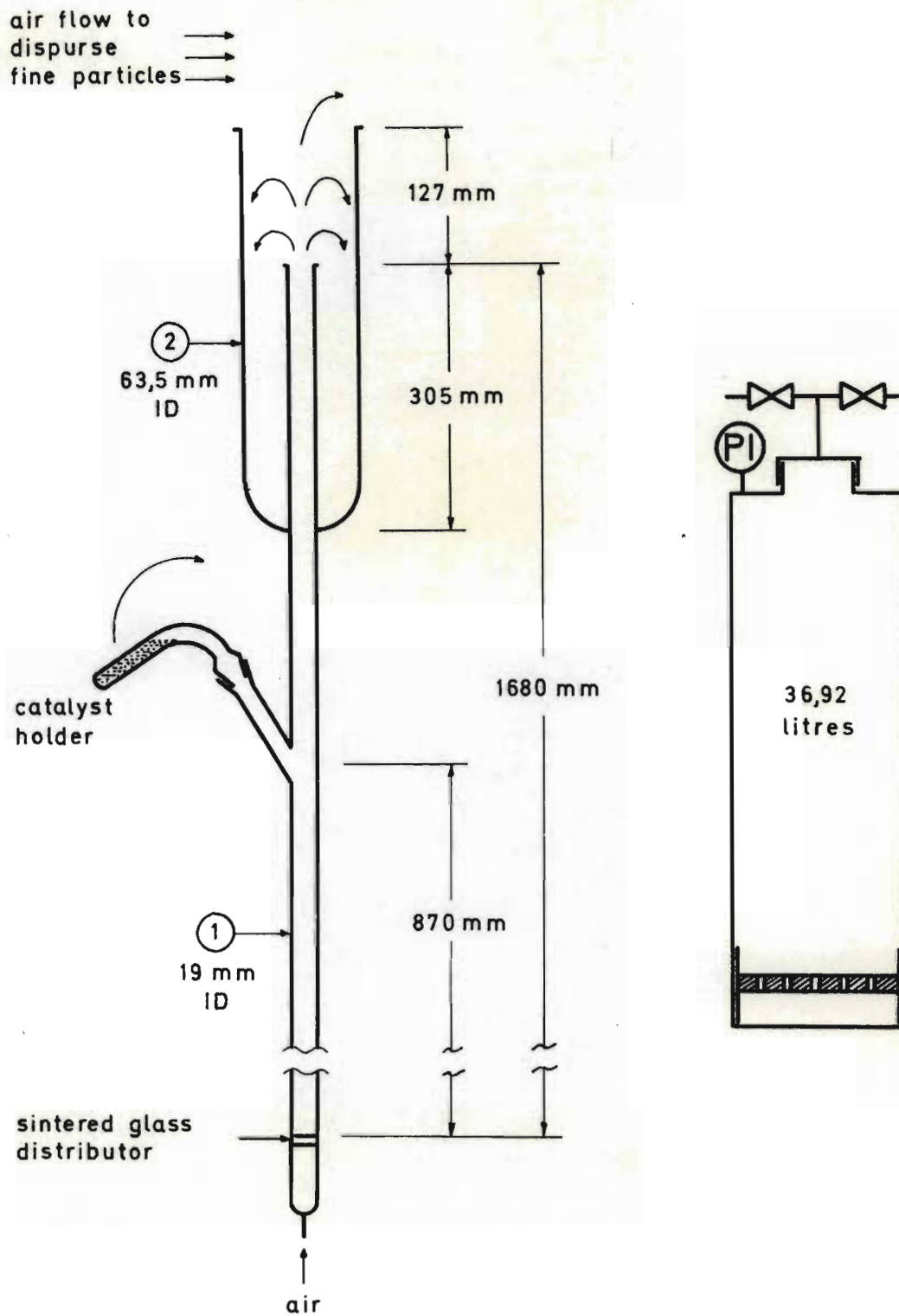


FIGURE 2.4.I Air segregator and product gas mixer

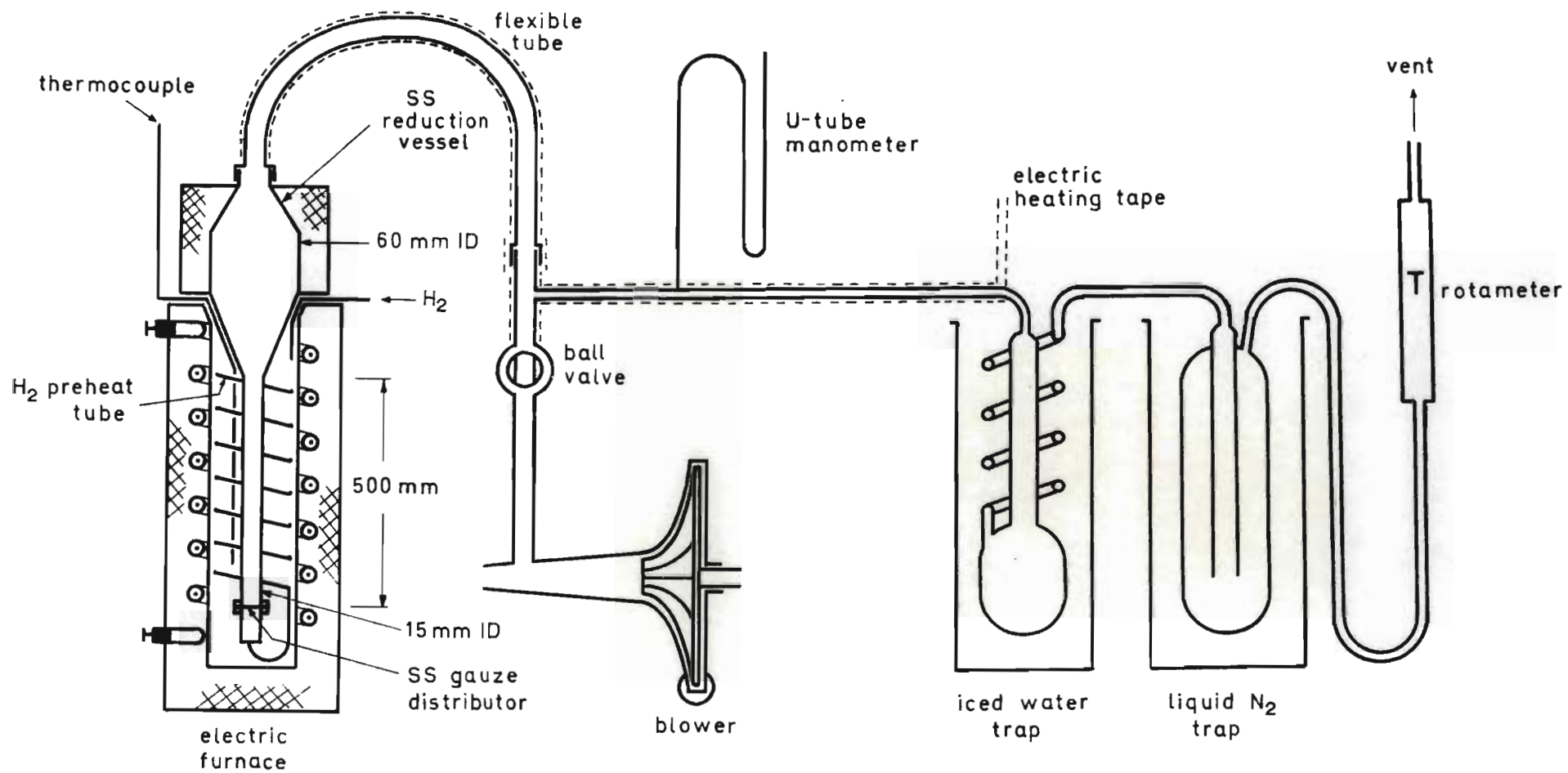


FIGURE 2.5.2.I Catalyst reduction equipment

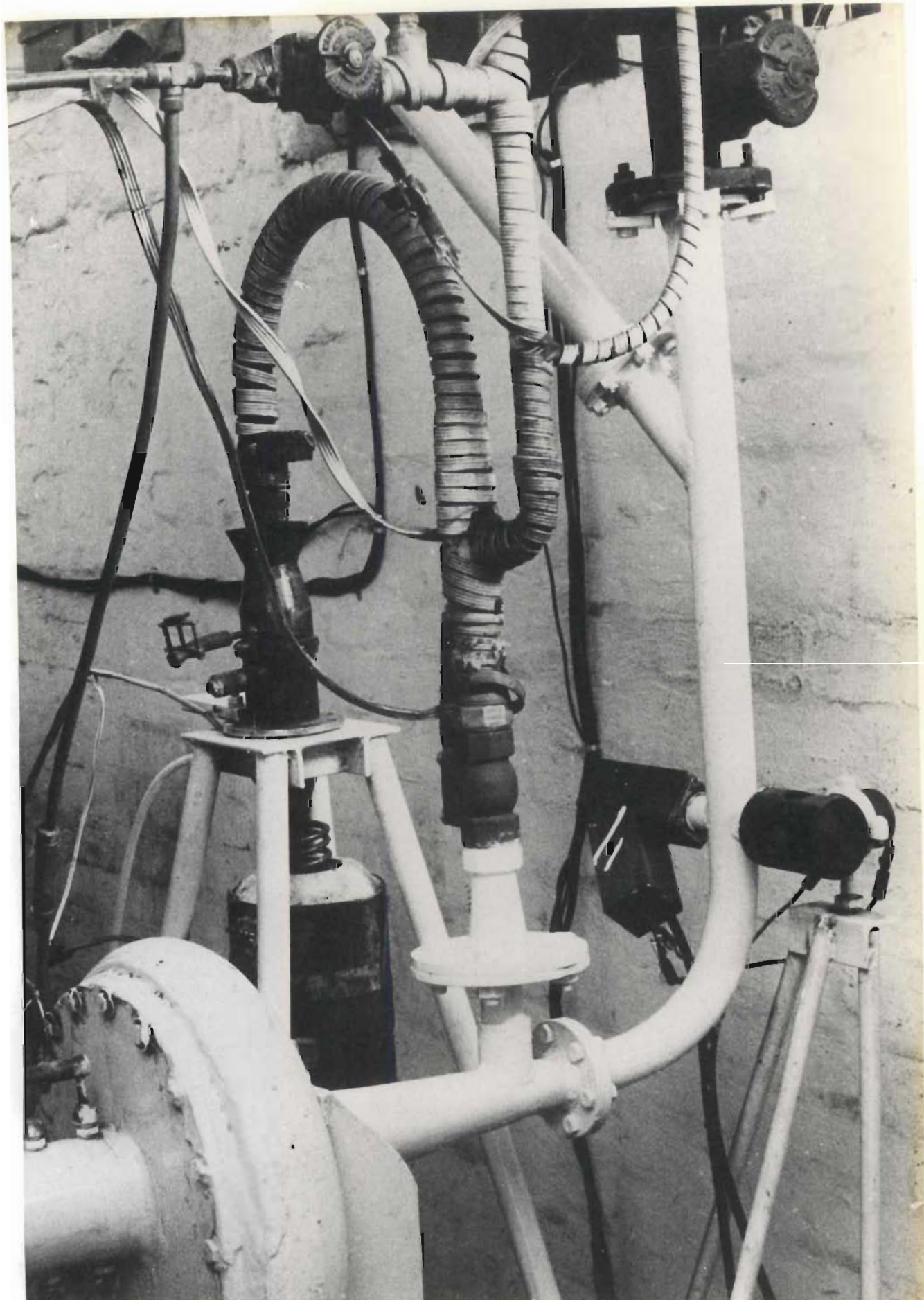


PLATE 2.5.2.I Catalyst reduction equipment; photocell and blower

introduced into the system, it was necessary to minimise carryover during reduction. Figure 2.4.I shows the air segregator constructed for this purpose. It was made of glass and fitted with a sintered glass air distributor at its lower end.

With a flow of air equal to 35 l/min. it was possible to collect catalyst in the top section (2) having only 5 mass per cent of particles below  $8\mu$ . Particles greater than  $50\mu$  remained in the narrow tube (1) and were discarded.

### 2.5.2 Catalyst Reduction Equipment

The iron catalyst used was triply promoted fused iron containing about 70 mass per cent iron and 28 mass per cent oxygen. It was necessary to reduce it with hydrogen to obtain optimum activity.

Fluidised bed reduction was employed using the stainless steel vessel shown in Figure 2.5.2.I and Plate 2.5.2.I. With a catalyst charge of 80 g, temperature of  $600^{\circ}\text{C}$  and hydrogen space velocity of  $4990\text{ h}^{-1}$ , 85 per cent reduction could be obtained in  $4\frac{1}{2}$  hours. Reduction extent was measured by trapping the water formed, see Figure 2.5.2.I. Heat source was a 3 kW electrical furnace built in the laboratory.

---

## 2.6 Instrumentation

### 2.6.1 Pressure Gauges

Chamber pressure was measured by a FEINMESS manometer calibrated in 10 psi divisions to 1600 psig. It was supplied by Dreyer, Rosenkranz und Droop, Germany. Precision of measurement was within 0,3 per cent.

Channel pressures were measured on an ordinary mercury U-tube manometer whilst atmospheric pressure was monitored by a FORTIN barometer.

### 2.6.2 Temperature Gauges

A standard mercury thermometer was used for measuring the temperature of circulating reaction mixture just after the blower (T1 in Figure 2.2.I).

An iron/constantan thermocouple was used to measure shock tube wall temperature (T2 in Figure 2.2.I).

Catalyst reduction furnace temperature was monitored by a chromel-P/alumel thermocouple (Figure 2.5.2.I).

### 2.6.3 Photoelectric Cell

Catalyst loading was observed by means of a silicon photoelectric cell and a 100 W projector lamp, the intensity of which was controlled by rheostat. Cell type was Si 07, 8 mm diameter, supplied by Dr. B. Lange & Co., Berlin.

The output of the cell was displayed on a millivoltmeter. Calibration was found to be difficult due to variable amounts of catalyst fines adhering to the windows in the pipe wall. The apparatus was used only as an indication of when steady conditions were reached after catalyst introduction. Plate 2.5.2.I shows the arrangement.

### 2.6.4 Shock Speed Measurement

Shock sensors of three different types were tried. Initially the detection of light emitted by shocked gas (Toennies & Greene (1957)) was attempted by means of Hewlett Packard ultra-fast infra red photodiodes. The voltage output of these was amplified, shaped and fed to a timing device consisting of an oscillator and counter. Unfortunately a large proportion of the light emitted was absorbed by the catalyst particles. Circuit sensitivity needed to be increased to such a degree that the system became susceptible to interference by radiation from high current mechanical switch gear used to operate the powerful solenoids

of the diaphragm rupture pin and circulating valves. This mechanical switch gear was replaced by thyristor switching but to no avail.

The photodiodes were replaced with heat transfer gauges of the baked platinum type (Gaydon and Hurlle (1963)). Again sensitivity was impaired, this time a film of catalyst deposited on the platinum forming a barrier to heat transfer.

Finally a pressure activated contact was used. Thurston (1955) describes such a contact placed behind a thin diaphragm in the wall of the shock tube. Resolution times of around  $5\mu$  sec. can be expected with this type of sensor. It has the advantage of not requiring any signal pre-amplification when coupled to the oscillograph. This arrangement was completely immune to external interference and proved reliable.

The pressure switch consisted of a brass diaphragm 5 mm in diameter, 0,05 mm thick, mounted in front of a contact pin. The gap between the diaphragm and pin was adjustable by means of a 10 BA screw thread. A drawing of the unit appears in Appendix D. A voltage of 27 volts D.C. was applied across the gap and the sensor connected to the vertical amplifier input of a 535 A Tektronix oscillograph. The oscillograph's electron beam was oscillated horizontally at a suitable frequency by means of a HEATH signal generator. Movement of the electron beam was recorded on film by a 16 mm FASTAX high speed smear camera; see Plate 2.6.4.I. The type of trace obtained is shown in Plate 2.6.4.II, three vertical displacements of the electron beam are clearly visible. These corresponded to the closing of each of the three pressure switches (Figure 2.1.I). Since the time interval between the displacements was given by the frequency setting of the signal generator, two shock speed measurements were obtained.

The camera was operated via a GOOSE control unit supplied by Wollensak, USA. This unit contained two timing circuits and a variac for camera speed adjustment; its use is described in Chapter 4.

---



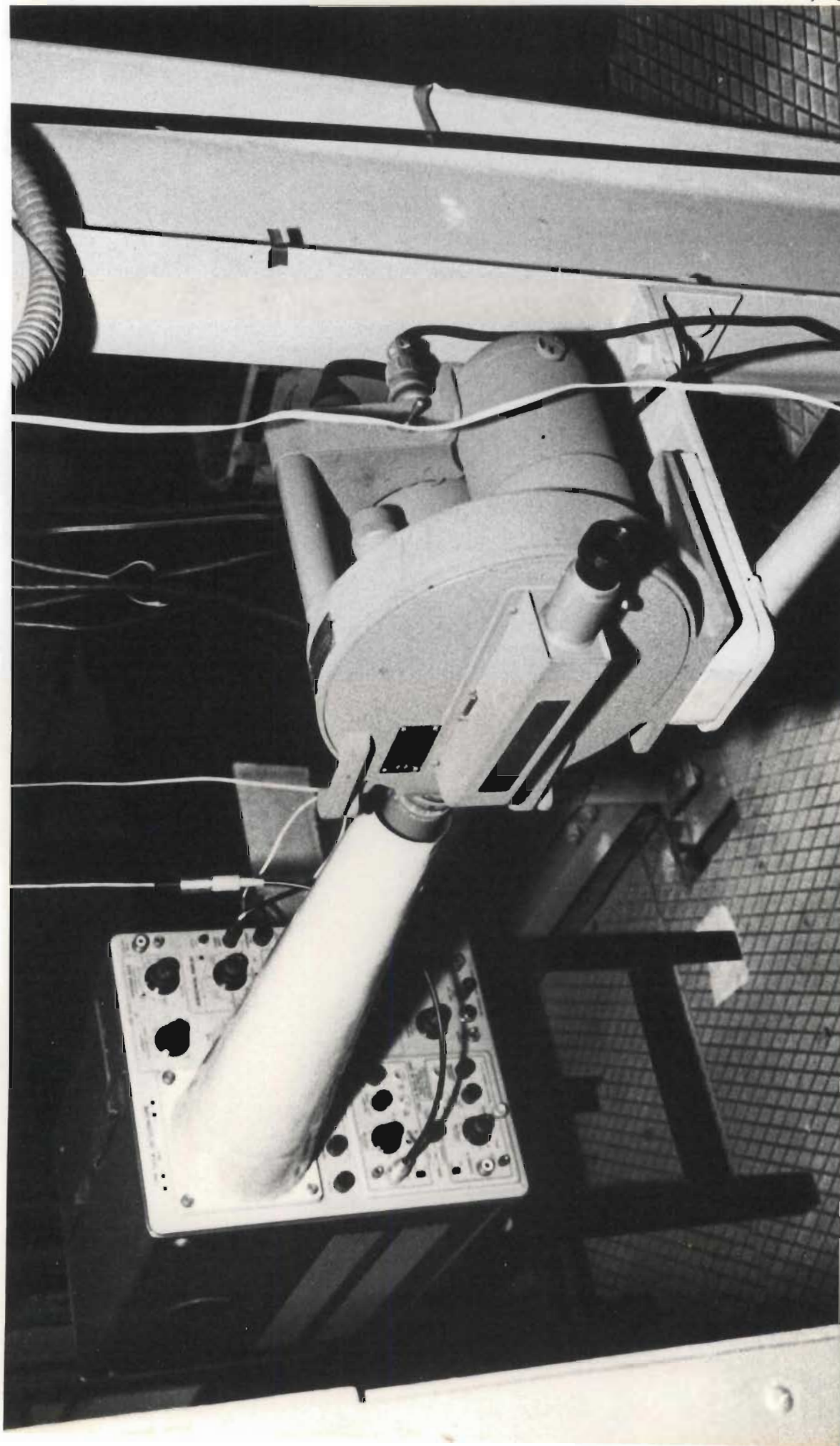
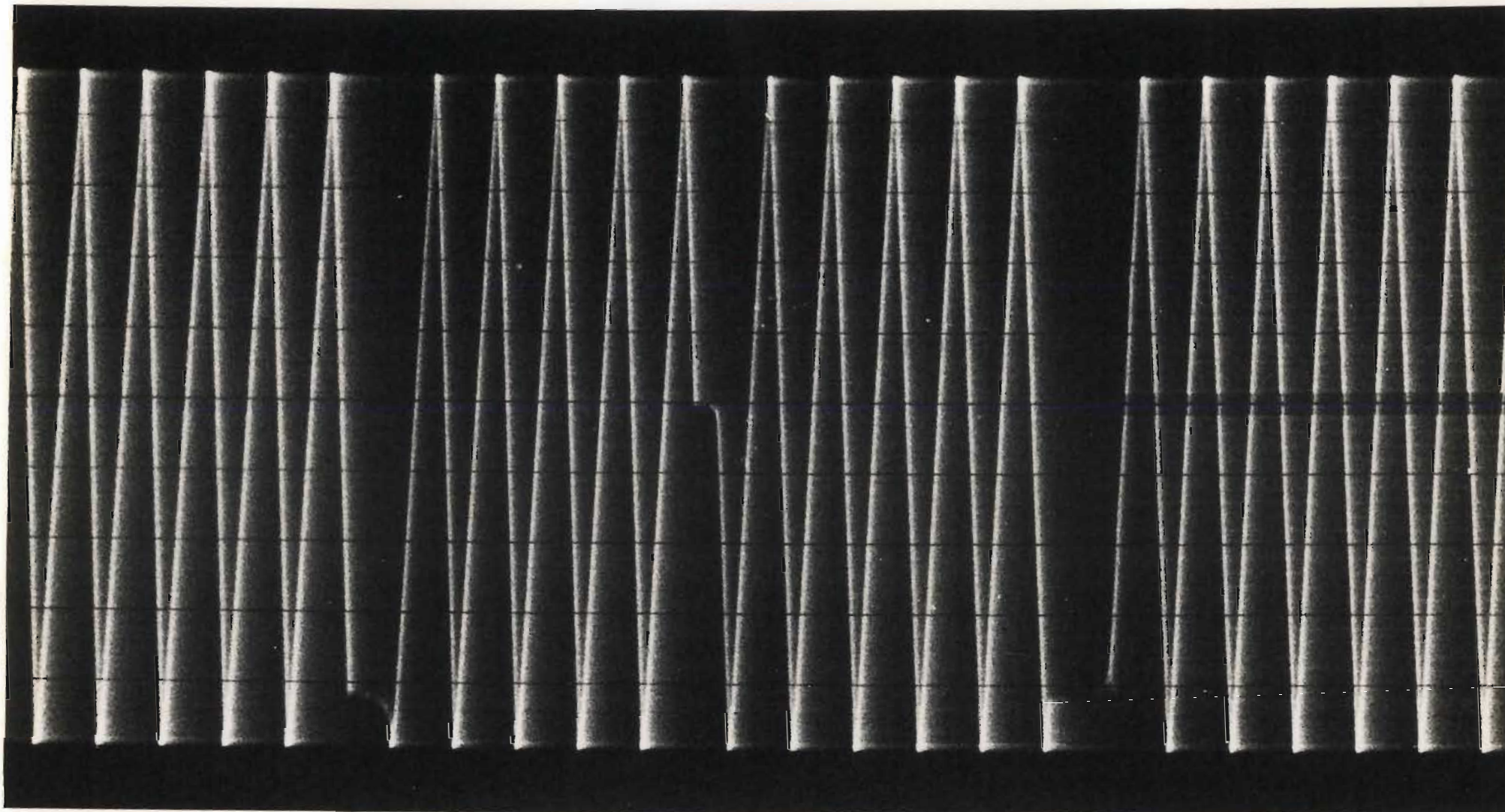


PLATE 2.6.4.I Oscilloscope and Camera



TIME →

PLATE 2.6.4.II Photo record of oscillograph trace-shock speed measurement.  
Sweep frequency - 10K cycles/second. Film - Geveart pan 36.

## 2.7 Gas Analysers

Three gas chromatographs were used to analyse gas samples.

A Philips PV 4000 series research chromatograph with flame ionisation detector was used to measure hydrocarbons and water whilst Beckman models 2A and 4 chromatographs with thermal conductivity detectors were used for determining inorganic gases. Helium was used throughout as carrier gas and was supplied through columns containing molecular sieve 5A (400 mm long by 12 mm diameter). For the Philips unit hydrogen and air were supplied through similar molecular sieve traps.

One to two ml gas samples were introduced by syringe.

### 2.7.1 Hydrocarbon and Water Analysis

Analysis for the following compounds was considered necessary:- methane, acetylene, ethylene, ethane, propylene, propane, methanol, ethanol and water.

Methanol, ethanol and water were determined by means of a Carbowax 20 M column, 3600 mm long, 6 mm diameter, operated at 120°C. The other substances were measured using a Porapak Q column, 3600 mm long, 6 mm diameter, operated at 60°C.

Both columns were supplied by Beckman Instruments.

### 2.7.2 Inorganic Gas Analysis

Inorganic gases considered were; hydrogen, argon, oxygen, nitrogen, carbon monoxide and carbon dioxide.

Carbon dioxide was determined using Porapak V, 1800 mm long, 6 mm diameter, operated at 70°C. The other gases were measured using molecular sieve 3A, 1800 mm long, 6 mm diameter, run at 70°C.

### 2.7.3 Calibration of Chromatographs

For high concentrations, in the volume per cent range, calibration gas mixtures were prepared on a partial pressure basis. Flow dilution equipment, Zocchi (1968), was used to prepare calibration samples in the volume ppm range, nitrogen being used as diluent. Concentrations as low as 0,5 ppmv with an accuracy of within 3 per cent could be obtained with this equipment. The calibration curve for low concentrations of methane is shown in Figure 2.7.3.I.

The limits of detection of the various compounds were as follows:-

methane, acetylene, ethylene, ethane, propylene & propane	0,04 ppmv
methanol and ethanol	0,1 ppmv
hydrogen	50 ppmv
argon, oxygen & nitrogen	50 ppmv
carbon monoxide	200 ppmv
carbon dioxide	100 ppmv

Reliable water determination was not achieved.

Limits of detection were defined as those concentrations which yielded a signal to noise ratio of 1,5.

Research grade compressed gases supplied by the Matheson Co., USA, were used for all calibration samples except in the case of methanol and ethanol.

---

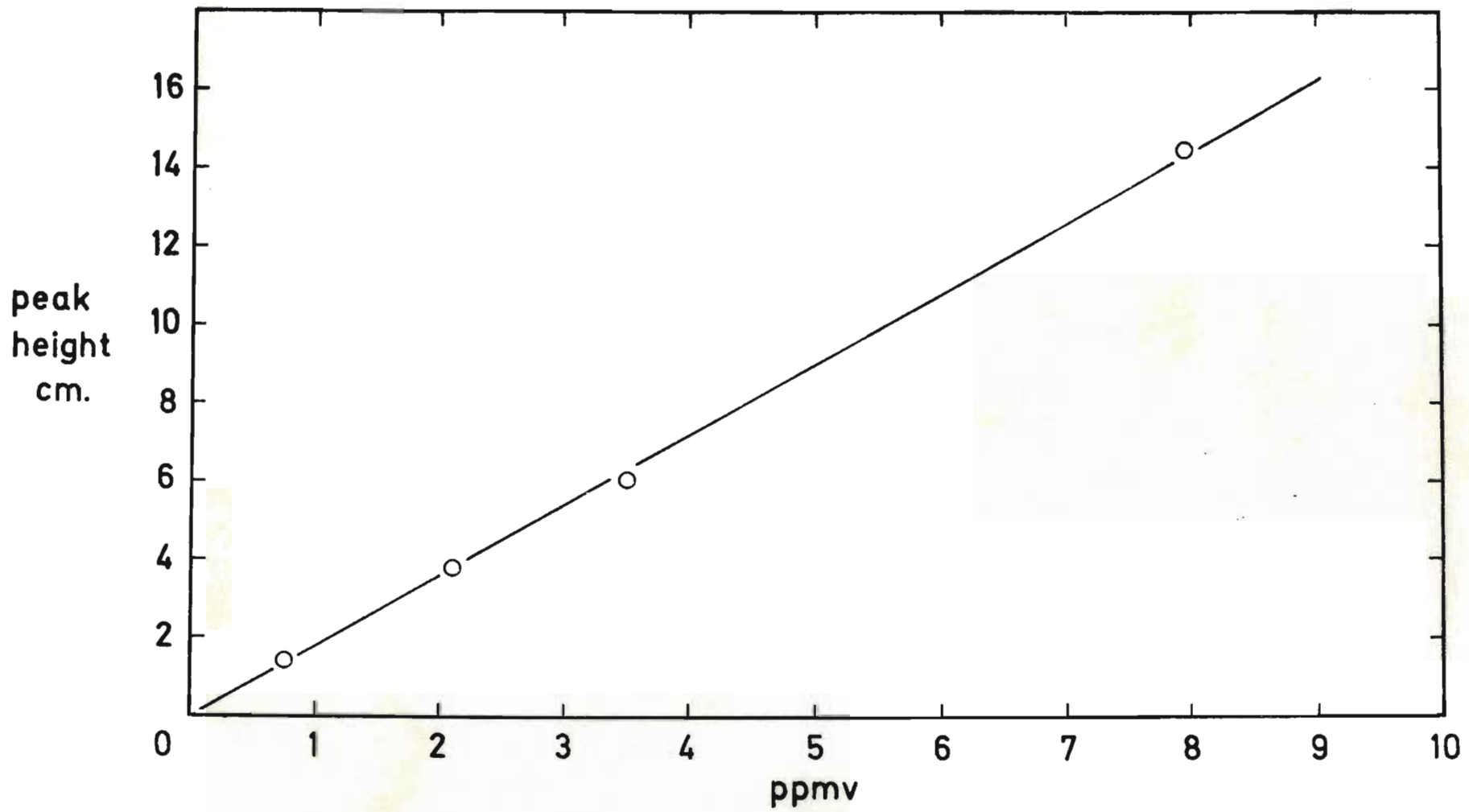


FIGURE 2.7.3.I Methane calibration curve for gas chromatograph

## CHAPTER 3

### THEORY

#### 3.1 Wave Patterns in the Shock Tube - Homogeneous Case

##### 3.1.1 Description

When the diaphragm has burst a compression wave is formed in the channel section, this rapidly steepens to form a shock front. The pressure change at the shock front is discontinuous. A very simple picture of the formation of a shock wave was given by Becker in 1922; the reader is referred to Gaydon and Hurle (1963) who relate Becker's ideas.

As the shock wave moves down the channel an expansion or rarefaction wave moves back into the chamber; the front of this rarefaction travels with the speed of sound in the chamber gas, but the drop in pressure is continuous and the rarefaction wave is often referred to as a "fan". The chamber and channel gases make contact at the "contact surface" which moves rapidly down the channel. The wave patterns of interest here are shown in the x-t diagram, Figure 3.1.1.I. The variation of pressure along the tube at a particular moment is illustrated in Figure 3.1.1.I (c), and the variation of temperature in Figure 3.1.1.I (d). Ideally the temperature rises abruptly at the shock front, remains steady up to the contact surface where it falls quickly to a value well below the initial temperature of the chamber gas. In the rarefaction fan the temperature rises smoothly to the initial value. In practice there is some mixing of gas at the contact surface, so that the temperature fall is less sudden.

Certain areas in Figure 3.1.1.I (b) are characterised by constant pressure and temperature, these are denoted;

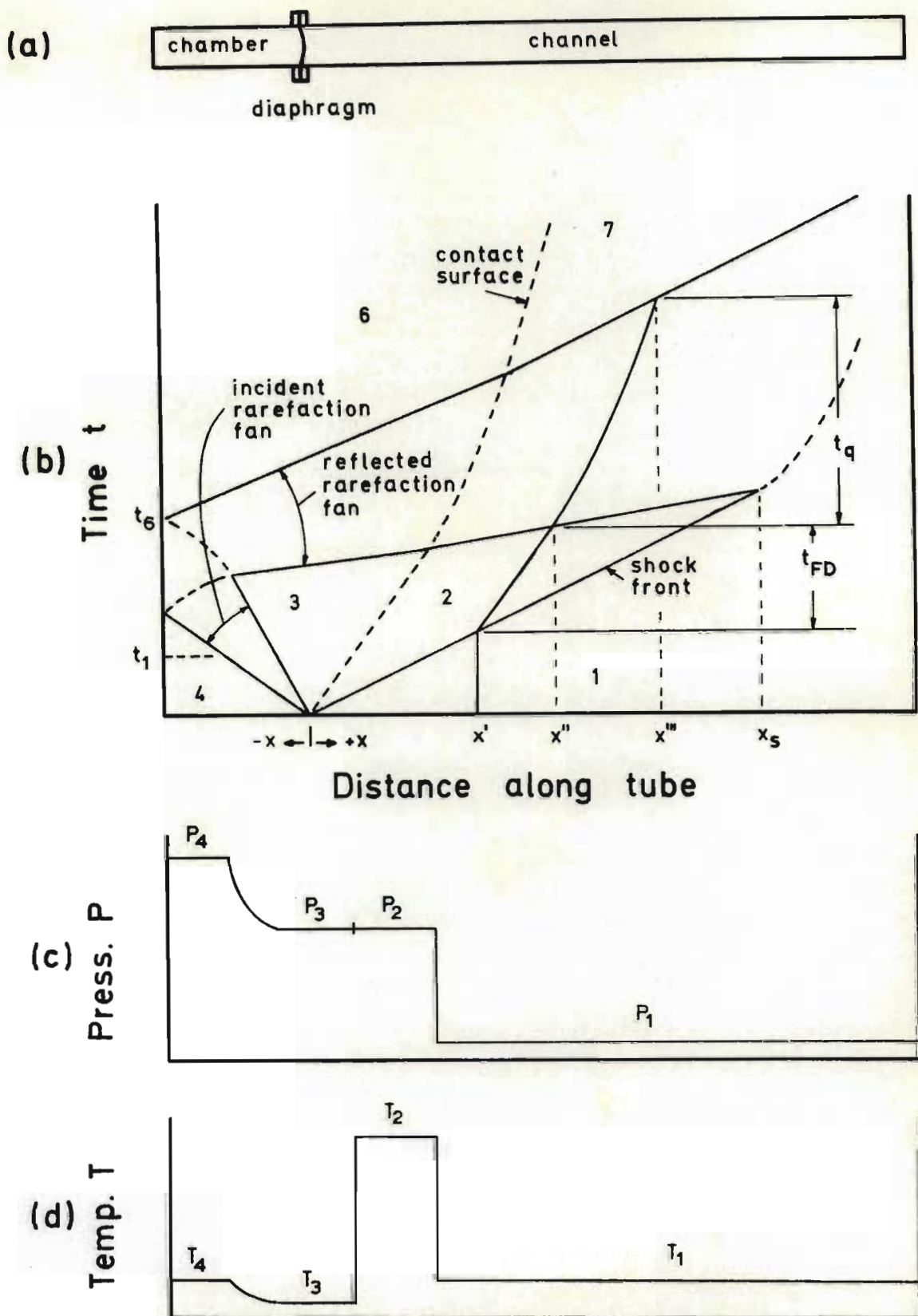


FIGURE 3.1.1.I (a) Shock tube (b) Distance-time diagram showing wave patterns (c) Pressure distribution at time  $t_1$  (d) Temperature distribution at time  $t_1$

- State 1 undisturbed channel gas,  $P_1, T_1$   
 State 2 shocked channel gas,  $P_2, T_2$   
 State 3 expanded chamber gas,  $P_3, T_3$   
 State 4 undisturbed chamber gas,  $P_4, T_4$   
 State 6 doubly expanded chamber gas,  $P_6, T_6$   
 State 7 expanded shocked channel gas,  $P_7, T_7$

Consider a gas particle initially at  $x'$ , on arrival of the shock front this particle is suddenly accelerated to the velocity of the contact surface and experiences conditions  $P_2, T_2$  for a time  $t_{FD}$  (FD denotes flow duration). At position  $x''$  this particle encounters the head of the reflected rarefaction fan and undergoes quench from conditions  $P_2, T_2$  to  $P_7, T_7$  during time interval  $t_q$ . When the particle finally attains the steady conditions of state 7 it will be at position  $x'''$ . The kineticist normally designs the system according to the chemical reaction under study so that reaction ceases at some temperature greater than  $T_7$ . Reaction time would therefore be  $t_{FD}$  plus the time to quench to zero reaction rate.

This work is concerned only with the incident shock wave and therefore the channel length was chosen so that a particle initially at  $x_s$  would attain state 7 without being reflected from the end of the channel.

### 3.1.2 Basic Equations

Full derivation of the basic equations relating to a shock wave in a tube of uniform cross-section has been given by Bradley (1962), Gaydon and Hurlle (1963) and Greene and Toennies (1957).

Consider Figure 3.1.2.I which depicts the shock front in shock-fixed coordinates, i.e. shock front at rest with gas moving through it from right to left.

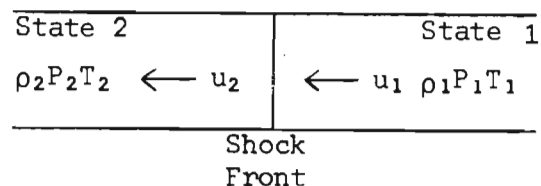


**FIGURE 3.1.2.I GAS FLOW THROUGH STATIONARY SHOCK FRONT**



From the conservation of mass, momentum and energy the following equations hold per unit area of shock front, respectively

$$\rho_1 u_1 = \rho_2 u_2 \quad 3.1.2.I$$

$$P_1 + \rho_1 u_1^2 = P_2 + \rho_2 u_2^2 \quad 3.1.2.II$$

$$H_1 + \frac{1}{2} u_1^2 = H_2 + \frac{1}{2} u_2^2 \quad 3.1.2.III$$

where  $u$  is the gas velocity,  $\rho$  is gas density,  $P$  gas pressure,  $T$  gas temperature and  $H$  the enthalpy of unit mass of gas. The subscripts refer to the two states respectively. Equation 3.1.2.III assumes no loss of heat to the shock tube walls; this is reasonable since the time of flow considered is of the order of milliseconds.

For an ideal gas,

$$H = C_p T = \frac{\gamma}{\gamma-1} \cdot RT = \frac{\gamma}{\gamma-1} \cdot \frac{P}{\rho} \quad 3.1.2.IV$$

where  $\gamma$  is the constant specific heat ratio and  $R$  the gas constant for unit mass of gas.

From equation 3.1.2.IV and the conservation equations,  $u_1$  and  $u_2$  can be eliminated yielding,

$$\frac{P_1}{P_2} = \frac{1 - \left(\frac{\gamma-1}{\gamma+1}\right) \frac{\rho_1}{\rho_2}}{\frac{\rho_1}{\rho_2} - \left(\frac{\gamma-1}{\gamma+1}\right)} \quad 3.1.2.V$$

and

$$\frac{\rho_2}{\rho_1} = \frac{\left(\frac{\gamma-1}{\gamma+1}\right) + \frac{P_2}{P_1}}{\left(\frac{\gamma-1}{\gamma+1}\right) \frac{P_2}{P_1} + 1} \quad 3.1.2.VI$$

Introducing the concept of Mach number, the ratio of the velocity of a disturbance or a flow in a gas to the local speed of sound in the gas, yields some useful equations. Shock Mach number  $M_1 = \frac{u_1}{a_1}$  where  $a_1$  is the sound speed in state 1.

By manipulation of the foregoing equations the following result,

$$\frac{P_2}{P_1} = \frac{2\gamma M_1^2 - (\gamma - 1)}{\gamma + 1} \quad 3.1.2.VII$$

$$\frac{\rho_2}{\rho_1} = \frac{(\gamma + 1) M_1^2}{(\gamma - 1) M_1^2 + 2} \quad 3.1.2.VIII$$

$$\frac{T_2}{T_1} = \frac{(\gamma M_1^2 - \frac{(\gamma - 1)}{2}) \cdot (\frac{\gamma - 1}{2} \cdot M_1^2 + 1)}{(\frac{\gamma + 1}{2})^2 M_1^2} \quad 3.1.2.IX$$

The relationships 3.1.2.V to 3.1.2.IX are known as the Rankine (1870) - Hugoniot (1887) equations.

Hence, if the initial conditions and the shock speed are known, the pressure, density and temperature in a shock wave through an ideal gas may be obtained.

By the treatment of Resler, Lin and Kantrowitz (1952) involving the analysis of flow through a rarefaction wave, it is possible to obtain an expression relating the Mach number of a shock to the initial applied pressure ratio across the diaphragm; for an ideal gas,

$$\frac{P_4}{P_1} = \frac{2\gamma_1 M_1^2 - (\gamma_1 - 1)}{\gamma_1 + 1} \cdot \left(1 - \frac{\gamma_4 - 1}{\gamma_1 + 1}\right) \cdot \frac{a_1}{a_4} \cdot \left(M_1 - \frac{1}{M_1}\right) - \left(\frac{2\gamma_4}{\gamma_4 - 1}\right)$$

3.1.2.X

### 3.1.3 Deviations from Ideal Behaviour

#### (1) Influence of diaphragm opening process

The diaphragm opening process takes several hundred microseconds to complete and the gas flow during the initial stages of this process is far from one-dimensional. The effect of the opening time is analogous to the acceleration of a piston to a constant velocity. The shock is formed by the coalescence of a series of compression waves, White (1958), and therefore accelerates to a maximum speed over the initial length of the channel. For diaphragm pressure ratios less than  $10^3$  maximum shock speeds observed are generally lower than the theoretical value given by equation 3.1.2.X. In this work shock speed was measured and equation 3.1.2.X used only in the calculation of  $t_6$ , the time at which state 6 forms. Shock speeds were measured after the shock waves had attained their maximum speeds, i.e. at a distance greater than 20 shock tube diameters from the diaphragm station, Greene and Toennies (1957). No allowance was made for shock speed variation over the first section of the channel - to do this effectively it is necessary to employ sophisticated continuous velocity measurement, Gaydon and Hurle (1963).

Figure 3.1.3.I illustrates the effect of a finite diaphragm opening time on the wave patterns (c.f. Figure 3.1.1.I). Two contact surfaces and two backward travelling rarefaction waves exist.  $P_1$  is the region in which the shock front forms through coalescence of a series of compression waves.  $P_I$  represents isentropically compressed channel gas of uniform pressure equal to  $P_2$  and of uniform temperature less than  $T_2$ . In practice the distance  $dx$  over which the shock front forms is small but its influence on the value of  $t_6$  is marked.

In Chapter 3.3.3 it will be noted that the calculation of  $t_6$  involves the pressure ratio  $P_3/P_4$ . For run 41,  $P_4/P_1$  was calculated using equation 3.1.2.X; a value of 40,2 was obtained. In practice the experimental  $P_4/P_1$  ratio was 63,3. To improve accuracy in the calculation of  $t_6$  from shock speed measurement the calculated  $P_4/P_1$  ratio was assumed to represent  $P_c/P_1$ , see



Figure 3.1.3.I. Therefore the ratio  $P_c/P_4$  instead of  $P_3/P_4$  was used for determining  $t_6$ .

Since  $dx$  is small the second rarefaction wave was assumed to have negligible width ( $x$  coordinate) and the line AB in Figure 3.1.3.I was considered to have the position A'B'.

When chamber and channel gases have different specific heats, mixing of these gases during the initial three dimensional flow affects the shock strength. White (1958) showed that volume would increase or decrease according to whether the specific heat of the chamber gas is respectively less or greater than that of the channel gas. The shock would be accelerated if volume increased and vice versa. In the case of hydrogen/argon shocks there is a volume decrease.

It is clear that equation 3.1.2.X is accurate only if it is assumed that the diaphragm is removed instantaneously.

#### (ii) Boundary layer limitations

In practice state 2 is not a uniformly flowing region of hot gas but one containing a velocity gradient normal to the flow. This is due to the viscous nature of the gas flow and gives rise to a boundary layer of gas next to the tube wall; the velocity of the gas being zero at the wall. The boundary layer thickness will be zero at the shock front and increase through the shock wave and contact surface, becoming zero again at the incident rarefaction head.

This loss of kinetic energy and gas to the boundary layer causes the shock front to be attenuated and the contact surface to be accelerated, Gaydon and Hurle (1963). Naturally this phenomenon causes a reduction in the expected flow duration,  $t_{FD}$  in Figure 3.1.1.I. Shock front attenuation has been taken into account in this work by using an average shock velocity obtained by measurement over two successive lengths of the channel. Allowance has been made for the acceleration of the contact surface; see Chapter 3.2.4 which deals with the heterogeneous case.

(iii) Real gas effects

In contrast to an ideal gas a real one processes modes of energy which are excited to degrees dependent on temperature. In the quantum partition of energy, translational and rotational modes usually have the value  $\frac{1}{2} kT$  each at about  $25^{\circ}\text{C}$ . The energy in molecular vibration approaches this value at much higher temperatures. Hence the specific heats of a polyatomic gas increase with temperature and its  $\gamma$  decreases with temperature. At  $25^{\circ}\text{C}$   $\gamma$  for a diatomic gas has the value  $7/5$ ; at high temperatures the absorption of energy by molecular vibration causes  $\gamma$  to fall to  $9/7$ , i.e. a decrease of about 8 per cent. At still higher temperatures some molecules will dissociate and even ionise.

In this work the channel gas consisted of  $\text{H}_2/\text{CO}/\text{Ar}$  in the approximate volume proportions 0,08/0,08/0,84 respectively. The highest value of  $T_2$  investigated was  $1400^{\circ}\text{K}$ . The percentage decrease in  $\gamma$  for the mixture due to the contribution of molecular vibration would be no more than 1,3 per cent. According to Rink (1962) hydrogen dissociates to the extent of 1,2 per cent at  $2832^{\circ}\text{K}$ , whilst work done by Toennies and Greene (1957) shows that negligible dissociation of carbon monoxide occurs at temperatures below  $4000^{\circ}\text{K}$ .

Use of the normal equation of state is not in error because the effect of gas imperfections due to intermolecular forces is negligible for the moderate gas densities produced in shock waves.

---

## 3.2 Conditions Behind the Shock Front - Heterogeneous Case

### 3.2.1 Description

A shock front passing through a suspension of solid particles upsets the velocity and temperature equilibrium between the two phases. Equilibrium between the phases is gradually re-established in a relaxation zone following the shock front, by means of the mechanisms of particle drag and heat transfer. General equations for analysing such systems have been presented by Carrier (1958), Soo (1961) and Rudinger (1964).

Figure 3.2.1.I is an  $x-t$  diagram for a shock wave propagating through a suspension of uniformly distributed solid particles in gas. It is assumed that the relative velocity between gas and solid particles is zero in state 1 and also that thermal equilibrium exists between the two phases. Consider gas and solid initially at  $x'$ . After passage of the shock front, gas molecules follow curve G while solid particles travel along curve S. At the shock front the gas is heated instantaneously whereas the temperature of the solid particles is subject to heat transfer processes and therefore lags well behind that of the gas. Velocity and temperature equilibrium is established by the end of the relaxation zone.

Similarly the deceleration of solid particles lags behind that of the gas in the reflected rarefaction fan. Whether or not the two curves cross as shown in Figure 3.2.1.I depends on many properties of the system under investigation.

Flow conditions in the relaxation zone do not always vary monotonically between the "frozen" state immediately behind the shock front and the ultimate equilibrium state; Rudinger (1964). Under certain conditions particle drag can cause the gas to decelerate initially.

The conditions in the relaxation zone cannot be analysed rigorously on theoretical grounds because the dependence of the particle drag coefficient on the particle Reynolds number is still uncertain.

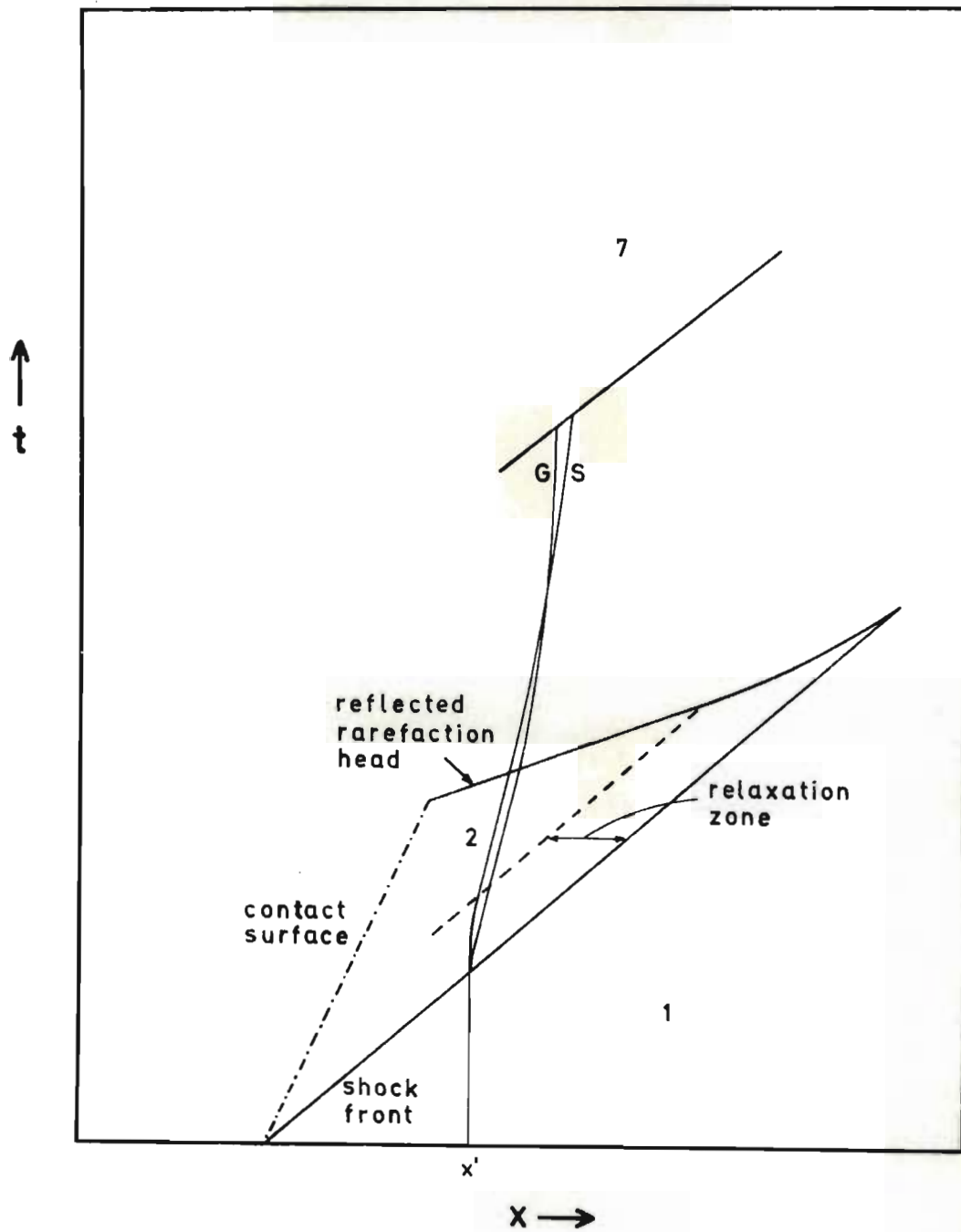


FIGURE 3.2.1.I Wave patterns for heterogeneous system showing solid slip



Normal practice is to determine experimentally the drag coefficient by shock tube techniques, Rudinger (1963).

Analysis of conditions in the rarefaction fan appears in Chapter 3.3 where it is assumed the gas/solid mixture behaves as a gas with modified properties. For rigorous analysis of the heterogeneous rarefaction fan reference should be made to Rudinger and Chang (1964).

### 3.2.2 Analysis of the Relaxation Zone

For a more complete analysis see Rudinger (1964).

Consider a shock front propagating in a tube filled with a uniform suspension of small rigid particles. The following assumptions are made:-

- (a) the gas obeys the perfect gas law,
- (b) the particle volume in the suspension is negligible,
- (c) the particles are spherical and of uniform diameter,
- (d) ahead of the shock front the particles are in temperature and velocity equilibrium with the gas,
- (e) boundary layer effects are negligible, and
- (f) the system is non turbulent.

Let the gas conditions be described by the temperature  $T$ , pressure  $P$ , density  $\rho$ , sound speed  $a$  and velocity relative to the shock wave  $u$ . The particles are characterised by their temperature  $T$ , velocity  $v$ , density  $d$ , specific heat  $c$  and diameter  $D$ .

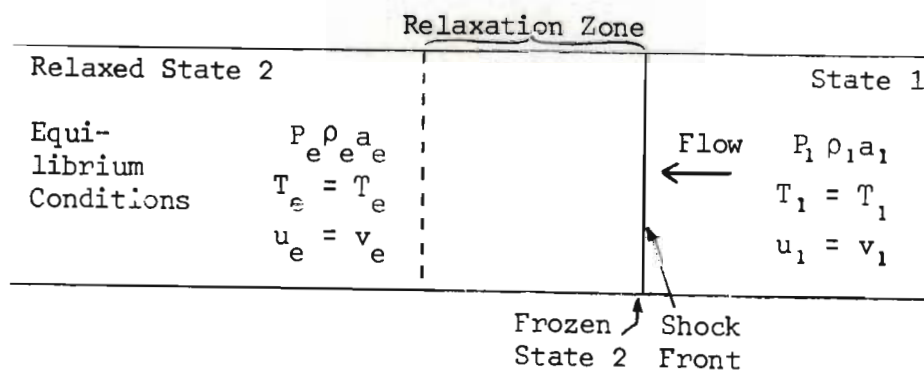


**FIGURE 3.2.2.I RELAXATION ZONE - STATIONARY SHOCK FRONT**

Figure 3.2.2.I depicts the relaxation zone in shock-fixed coordinates. The conditions immediately behind the shock front are called "frozen state 2" and denoted by subscript f. The equilibrium conditions outside the relaxation zone behind the shock front, are sometimes called "relaxed state 2" but are denoted by subscript e.

It is convenient to introduce the dimensionless variables

$$\theta = \frac{T}{T_1}, \quad \phi = \frac{T}{T_1}, \quad U = \frac{u}{a_1} \quad \text{and} \quad V = \frac{v}{a_1}.$$

Let the flow rate of particles per unit area of shock front be  $n$  and the corresponding flow rate of gas be  $m$ . Therefore the momentum equation 3.1.2.II becomes, for the heterogeneous case

$$P_1 + (m+n)u_1 = P + mu + nv \quad 3.2.2.I$$

Let  $\eta = \frac{n}{m}$  the mass flow ratio. Combining

$m = \rho u = \rho_1 u_1$  and the perfect gas law, yields

$$\frac{P}{P_1} = \theta \frac{U}{U_1} \quad 3.2.2.II$$

Writing equation 3.2.2.I in terms of the dimensionless variables and eliminating pressure by using 3.2.2.II, the following can be derived

$$U + \eta V + \frac{\theta}{\gamma U} = (1+\eta)U_1 + \frac{1}{\gamma U_1} \quad 3.2.2.III$$

where  $\gamma = C_p/C_v$  is the ratio of specific heats for the gas.

Similarly the energy equation 3.1.2.III can be written as

$$\frac{1}{2}(U^2 + \eta V^2) + (\theta + \eta \delta \phi)/(\gamma - 1) = \frac{1}{2}(1+\eta)U_1^2 + (1+\eta \delta)/(\gamma - 1) \quad 3.2.2.IV$$

where  $\delta = c/C_p$  which is temperature dependent.

Soo (1961) has shown that the equilibrium conditions  $V_e = U_e$  and  $\theta_e = \phi_e$  can be computed from the Rankine-Hugoniot equations

if the specific heat ratio of the gas/solid mixture

$$\Gamma = \gamma(1+\eta\delta)/(1+\gamma\eta\delta) \quad 3.2.2.V$$

is used and the shock Mach number is defined as  $M_s = \frac{u_1}{\alpha_1}$  where  $\alpha_1$  is the sound speed for the mixture ahead of the shock wave, which can be expressed

$$\frac{\alpha_1}{a_1} = \frac{U_1}{M_s} = \left( \frac{\Gamma}{\gamma(1+\eta)} \right)^{\frac{1}{2}} \quad 3.2.2.VI$$

As in the case of  $\gamma$ ,  $\Gamma$  is assumed to be temperature independent. It is fairly insensitive to variations in  $\delta$  for the iron catalyst used here. For example, in run 36  $\Gamma$  decreased from 1,51 to 1,47 as  $\delta$  increased from 0,786 to 1,26.

The conditions of the gas in frozen state 2 can be determined by the Rankine-Hugoniot equations (3.1.2.V to 3.1.2.IX) for a shock in the gas phase alone;  $U_1 = M_1$  the shock Mach number. The particles pass through the shock front unchanged,  $V_f = U_1$  and  $\phi_f = 1$ .

Before the flow conditions in the relaxation zone itself can be determined, equations describing momentum and heat exchange between the two phases are required. Using the derivations of Soo (1961) and introducing the dimensionless variables, the change in momentum and temperature of a particle with respect to the distance  $x$  behind the shock front, can be expressed thus

$$\frac{dV}{dx} = - \frac{3\rho_1 U_1 C_D}{4Dd} \cdot \frac{(V-U)^2}{UV} \quad 3.2.2.VII$$

$$\frac{d\phi}{dx} = \frac{6\mu Nu}{D^2 da_1 \delta Pr} \cdot \frac{(\theta-\phi)}{V} \quad 3.2.2.VIII$$

where  $C_D$  is the drag coefficient,  $Nu$  the Nusselt number,  $Pr$  the Prandtl number and  $\mu$  the dynamic viscosity of the gas.  $C_D$  and  $Nu$  are both functions of the particle Reynolds number

$$Re = \rho(v-u)D/\mu = \left( \frac{\rho_1 a_1 U_1 D}{\mu} \right) \cdot \frac{(V-U)}{U} \quad 3.2.2.IX$$

Some assumptions must be made for particle drag and heat transfer. Rudinger (1964) performed calculations on plausible variations of the customarily used formulae and showed that the results are significantly affected by choice of particle drag correlation but only to a minor extent by that for heat transfer.

In this work the following correlation was used for the drag coefficient

$$C_D = \frac{339}{Re^{0,82}} + \frac{2700}{Re^2} \quad 3.2.2.X$$

This relationship has not been reported in the literature; its origin is discussed in Chapter 3.2.3. The well-known Nusselt correlation by Knudsen and Katz (1958) for steady flow around a single sphere (forced convection)

$$Nu = 2 + 0,6 Pr^{0,33} Re^{0,50} \quad 3.2.2.XI$$

was used.

Solving equations 3.2.2.III and 3.2.2.IV for U in terms of V, one obtains

$$\begin{aligned} & \frac{(\gamma+1)U^2}{2} + (\eta\gamma V - (1+\eta)\gamma U_1 - \frac{1}{U_1}) \cdot U + 1 \\ & - \frac{(\gamma-1)}{2} (\eta V^2 - (1+\eta) U_1^2) - \eta\delta(\phi-1) = 0 \end{aligned} \quad 3.2.2.XII$$

a quadratic in U. Solutions are

$$U = \frac{-B \pm \sqrt{B^2 - 4AC}}{2A} \quad 3.2.2.XIII$$

where  $A = (\gamma+1)/2$

$$B = \eta\gamma V - (1+\eta)\gamma U_1 - \frac{1}{U_1}$$

$$\text{and } C = 1 - \frac{(\gamma-1)}{2} (\eta V^2 - (1+\eta) U_1^2) - \eta\delta(\phi-1)$$

Equations 3.2.2.II/VII/VIII/XIII may be solved numerically for the unknowns  $U$ ,  $V$ ,  $Q$ ,  $\phi$  and  $P$  for a particular shock velocity  $U_1$  and known conditions in state 1.

The computations were performed with the aid of a digital computer (UNIVAC 1108) via a Fortran V programme (ZHETRO) specially written for the purpose. The logical flow diagram, programme print-out and nomenclature are given in Appendix F.

Figure 3.2.2.II shows a typical set of results (run 36) for 24  $\mu$  iron particles suspended in 0,09 H<sub>2</sub>/0,09 CO/0,82 Ar gas mixture at initial conditions of 25°C and 20 psig. The mass flow ratio  $\eta$  was 0,135 and the shock Mach number ( $U_1$ ) 3,35 which corresponds to  $M_s = 3,67$ . For the gas alone  $\gamma = 1,61$  and since  $\delta_1 = 0,79$  for this mixture,  $\Gamma = 1,52$ . Velocity equilibrium occurs 205 mm behind the shock front. However temperature equilibrium has not been reached even though the temperature rate of change for each phase has become small. A possible reason for this might be the assumption of non-turbulent flow; the rate of heat transfer would be enhanced by turbulence especially at low particle Reynolds numbers (see Chapter 3.2.3). Soo (1961) predicted that thermal equilibrium would lag behind that of momentum if the steady flow heat transfer correlations were used. For a particular system, Nettleton (1966) has estimated the heat transfer coefficient for particles in shock-heated gases.

Relaxation zone computation results for runs 5 and 16 are depicted in Figures 3.2.2.IV and 3.2.2.III respectively.

The important result is that the gas has approached its calculated equilibrium conditions thus enabling the reaction zone to be determined according to the considerations of Chapter 3.3.  $\phi$  is a measure of the bulk temperature of the particles which is not considered to be highly significant in the study of heterogeneous catalysis involving particles of low specific surface area. It is assumed that a mono-molecular layer of exposed catalyst surface will rapidly reach a temperature close to that of the gas bulk.

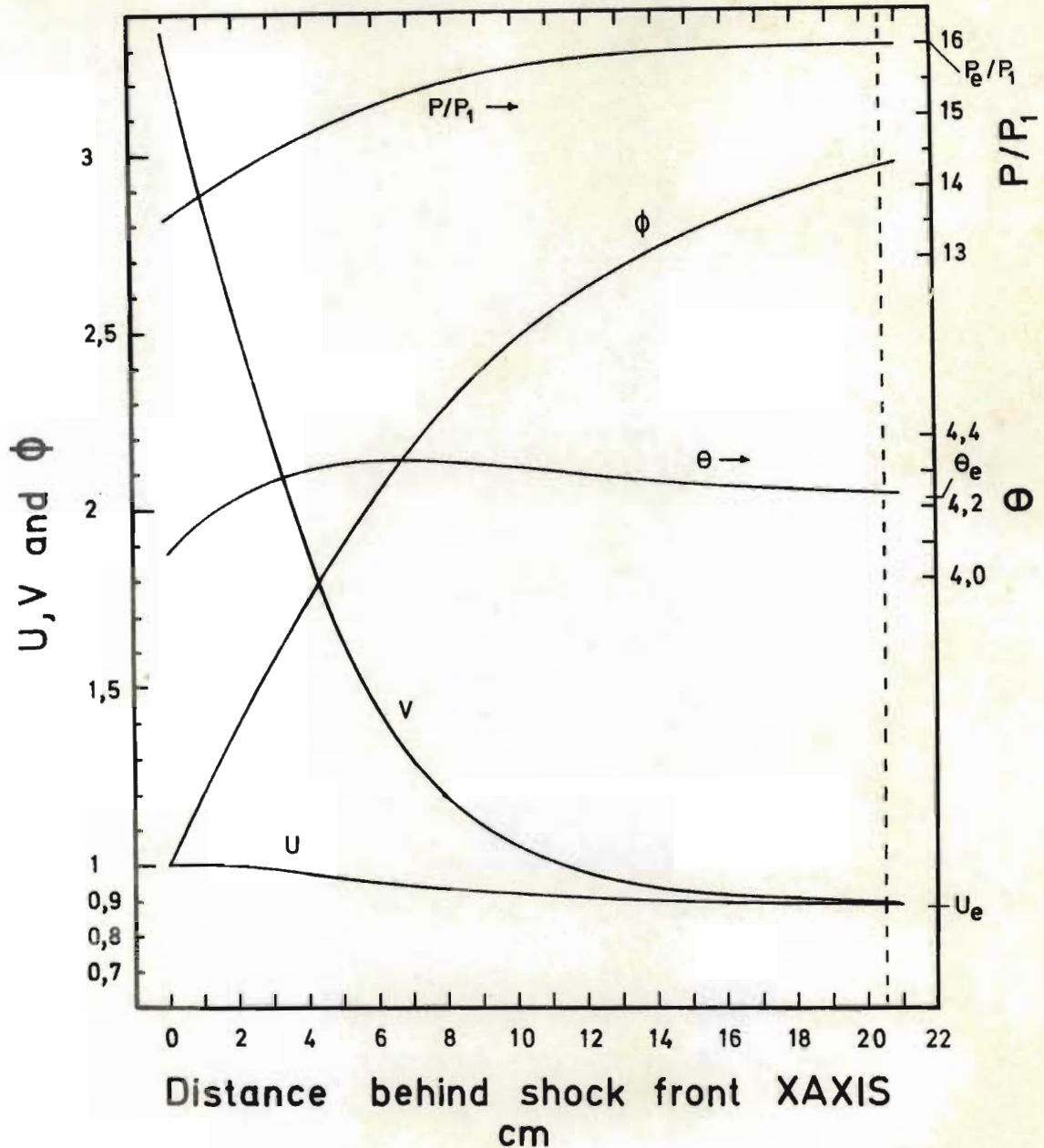


FIGURE 3.2.2.II Variations of the gas temperature, velocity and pressure, and particle temp. and velocity behind the shock front (run 36)

Computed for  $24 \mu$  iron particles in channel gas at a mass flow ratio  $\eta = 0.135$  (corresponding to  $\Gamma = 1.52$ ) and a shock velocity  $U_1 = 3.35$  ( $M_S = 3.67$ ); based on equations 3.2.2.X and 3.2.2.XI

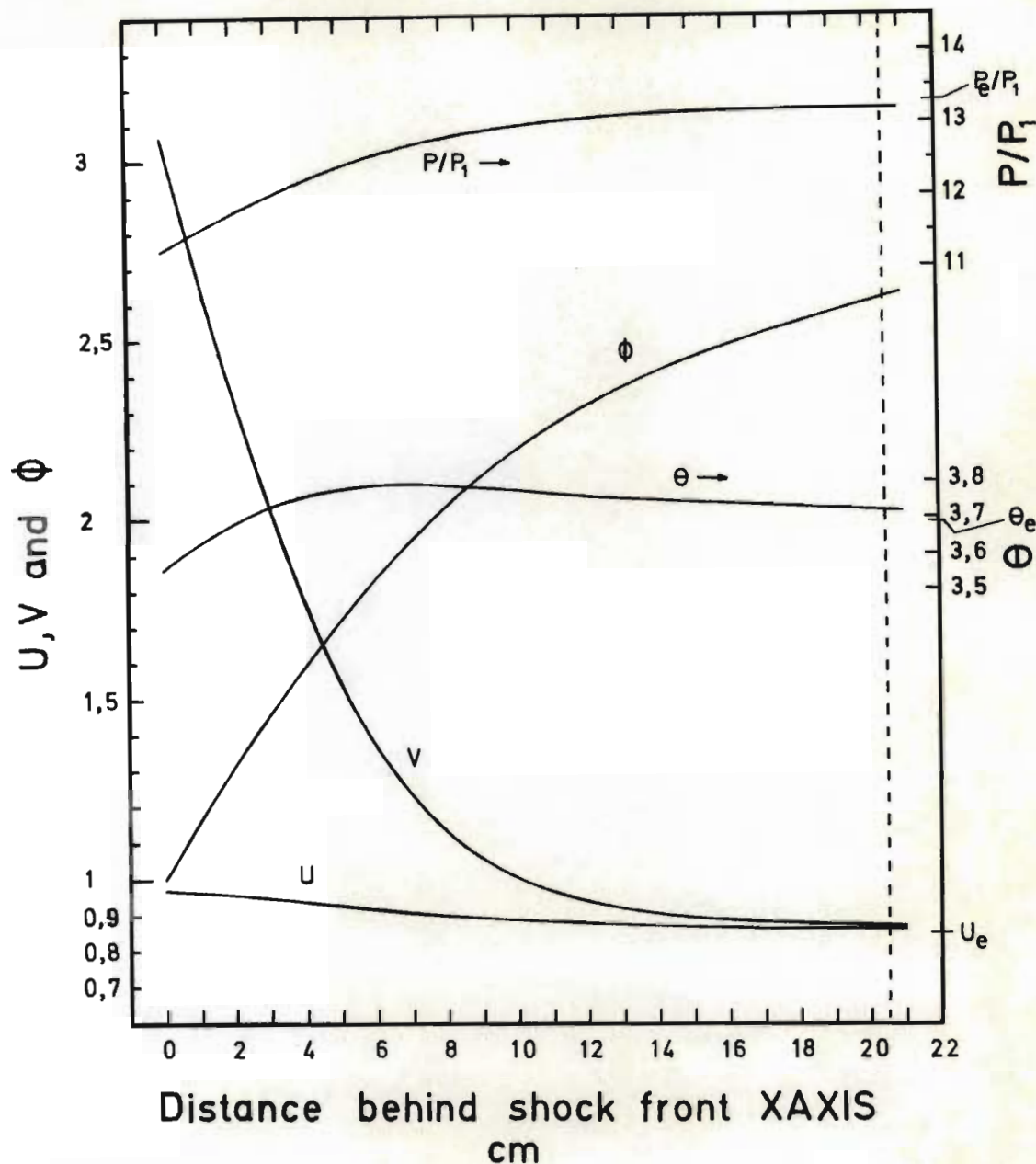


FIGURE 3.2.2.III Variations of the gas temperature, velocity and pressure, and particle temp. and velocity behind the shock front (run 16)

Computed for  $24\ \mu$  iron particles in channel gas at a mass flow ratio  $\eta=0,135$  (corresponding to  $\Gamma=1,52$ ) and a shock velocity  $U_1=3,05$  ( $M_S=3,34$ ); based on equations 3.2.2.X and 3.2.2.XI

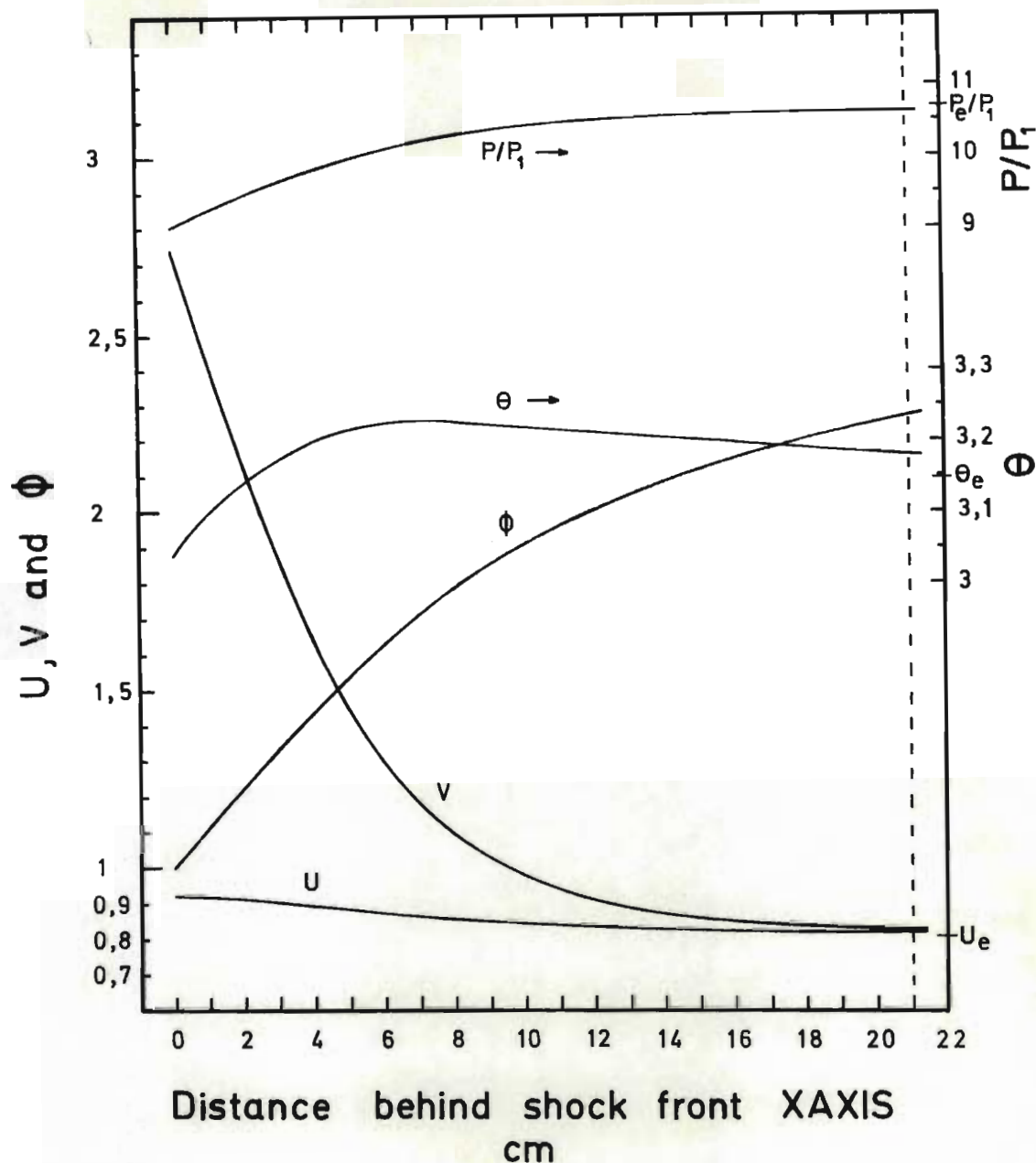


FIGURE 3.2.2.IV Variations of the gas temperature, velocity and pressure, and particle temp. and velocity behind the shock front (run 5)

Computed for 24  $\mu$  iron particles in channel gas at a mass flow ratio  $\eta=0,134$  (corresponding to  $\Gamma=1,52$ ) and a shock velocity  $U_1=2,74$  ( $M_S=3,00$ ); based on equations 3.2.2.X and 3.2.2.XI



### 3.2.3 Particle Drag Coefficient

The iron catalyst particles used here were of highly irregular shape which made it very difficult to define properly a particle diameter. Torobin and Gauvin (1960) reviewed the work of many investigators and showed that the effect of particle shape on the drag coefficient was more complex than had been suggested by previously published analyses. They discussed the available correlations and noted many contradictions between the findings of different investigators.

A theoretical analysis of particle drag is further complicated when a cloud of particles is considered. The dependence of  $C_D$  on the particle Reynolds number becomes uncertain due to the influence of particle-particle collisions (Hoglund (1962)), turbulence (Torobin and Gauvin (1960, 1961), Clamen and Gauvin (1969)) and electric charges on the particles (Rudinger (1963) and Soo (1964)).

It was decided to try some of the published correlations for regular shaped particles and one for particles such as coal and pyrites. For the system studied here, particle Reynolds number decreased from about 1500 in frozen state 2 to zero in relaxed state 2. A necessary condition is that  $U$  and  $V$  converge asymptotically to the equilibrium value ( $U_e = V_e$ ). The following are some of the correlations that were tried; see Figure 3.2.3.I.

<u>Correlation</u>	<u>Origin</u>	<u>Range of Validity</u> <u>Re</u>
$C_D = 0,48 + 28 Re^{-0,85}$	Gilbert, Davis & Altman (1955)	$0,1 - 10^6$
$C_D = 27 Re^{-0,84}$	Ingebo (1956)	10 - 1000
$C_D = 6000 Re^{-1,7}$	Rudinger (1963)	50 - 300
$C_D = \frac{24}{Re} + 0,5$	Rumpf (1960)	$< 10^5$
$C_D = \frac{24}{Re} + \frac{2,8}{\sqrt[4]{Re}}$	Leschonski (1970)	0,1 - 4000
$C_D = \frac{24}{Re} + \frac{6}{\sqrt{Re}} + 0,28$	Leschonski (1970)	0,1 - 4000
Numerical values	Miller & McNally (1936)	$0,1 - 10^4$

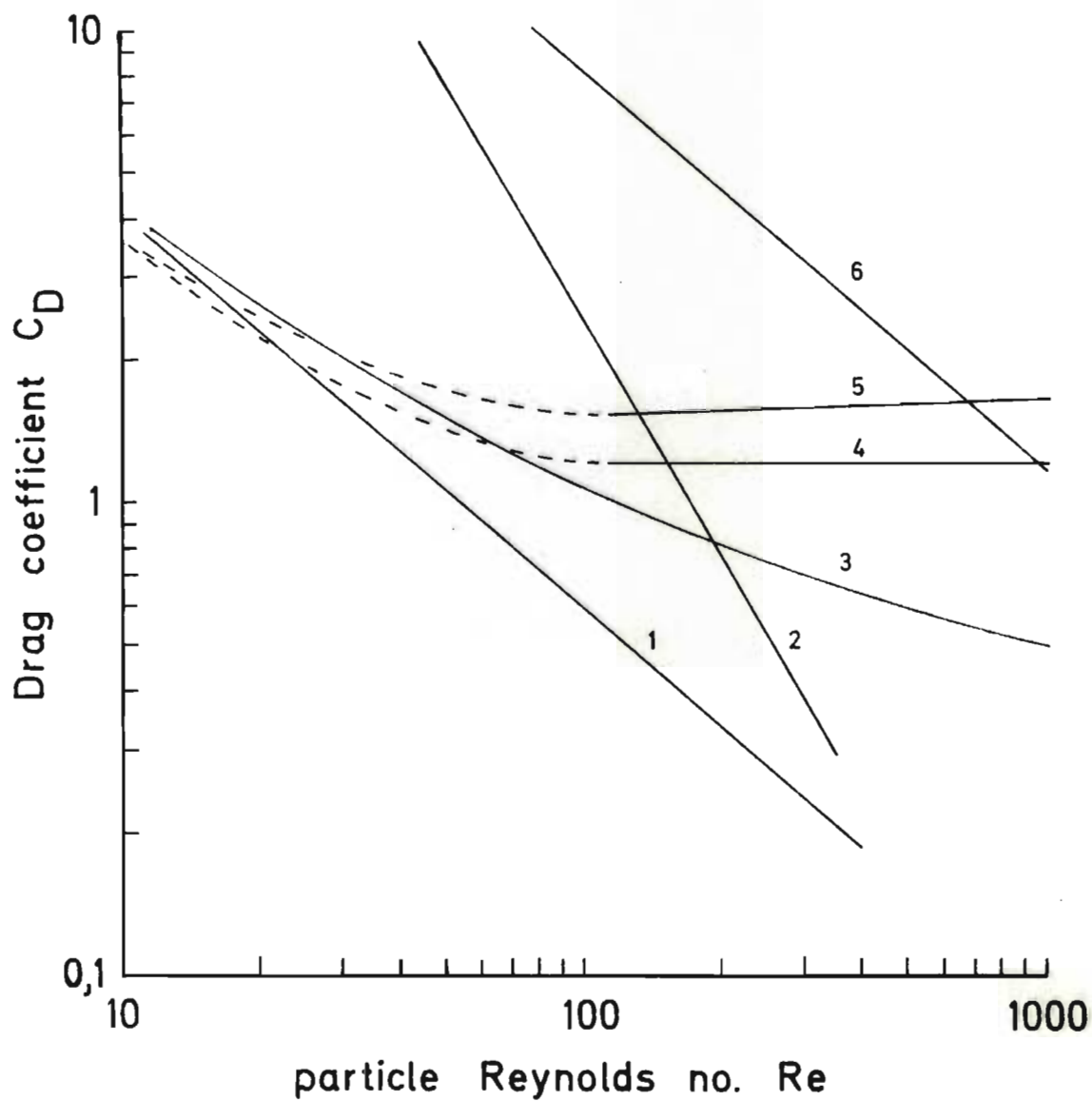


FIGURE 3.2.3.I Correlations for drag coefficient

LEGEND

- 1 Ingebo (1956) spheres
- 2 Rudinger (1963) spheres
- 3 Gilbert et al (1955) spheres
- 4 Miller and McNally (1936) coal, pyrites etc.
- 5 " " " shale
- 6 equation 3.2.2.X

The above correlations either resulted in non-asymptotic convergence of  $U$  and  $V$  or convergence only initially.

Torobin and Gauvin (1961) noted significant alterations to the steady flow drag correlation due to turbulence in the range  $500 < Re < 1500$ . They found the drag coefficient to be a function of  $Re$  and of the relative intensity of turbulence.

$$\text{Relative intensity of turbulence } I_R = \sqrt{u^{*2}}/U_R$$

where  $u^*$  is the fluctuating component of the gas velocity in the direction of travel and  $U_R$  is the relative velocity between gas and particle. Using the Von Kármán equations (1939)  $u^{*2}$  was calculated at a number of radial positions in the shock tube for argon gas and a shock velocity of 112100 cm/sec. (Mach No. = 3.5).  $I_R$  was then determined for decreasing  $U_R$  through the relaxation zone. Table 3.2.3.I shows the results compared with  $I_R$  values which have a significant influence on the steady flow drag correlation for corresponding  $Re$  values, obtained from Torobin and Gauvin (1961). The level of significance chosen is a change in  $C_D$  greater than 10 per cent. The degree of turbulence in the system studied here could become important at low Reynolds numbers, however the matter was not taken any further.

Miller and McNally (1936) found that data for coal, anthracite, sandstone and pyrite particles fell near the same curve; Figure 3.2.3.I. The values of  $C_D$  for flat shale particles were higher and showed a tendency to increase slightly with  $Re$  above  $Re = 100$ .

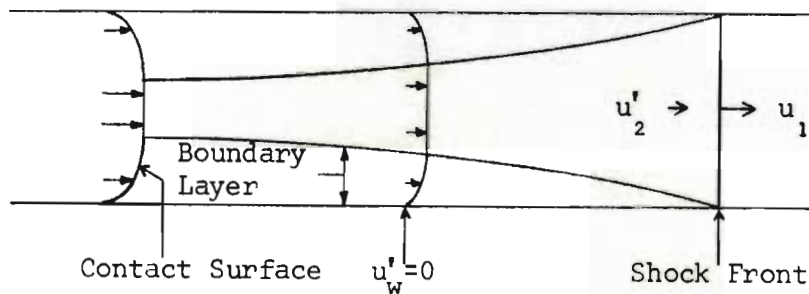
Equation 3.2.2.X was obtained by incorporating high  $C_D$  values for  $Re$  lower than 100 (Rudinger (1963)) and for  $100 < Re < 1000$  (Miller and McNally (1936)). The data shown in Figure 3.2.2.II was obtained using the relationship between  $C_D$  and  $Re$  as given by equation 3.2.2.X. This equation was a reasonable correlation for the type and concentration of particles handled in this work. It is true that a family of similar correlations would also apply. This indicates the importance of studying each system individually and developing unique correlations. Such a study (Rudinger (1963), Clamen and Gauvin (1969) and Torobin and Gauvin (1961)) was considered outside the scope of this work.

TABLE 3.2.3.1

System:- Argon Gas Mach No. 3,5 24 $\mu$ Iron Particles		System:- Air 1 mm Spheres (Torobin & Gauvin (1961))	
Re	$I_R\%$		$I_R\%$
1370	2,76		> 12
953	4,17		> 20
518	9,15		> 25
407	13,80		-
299	27,6		-

### 3.2.4 Boundary Layer Formation and its Effect on Flow Duration

Boundary layer growth in the shocked gas causes deviation from one-dimension flow assumed in ideal shock theory. The boundary layer is the region of flow where viscous forces and heat losses cause the gas velocity and temperature to decrease from their values behind the shock to much lower values at the shock tube walls; see Figure 3.2.4.I. The low speed gas in the boundary layer "leaks" past the contact surface which in turn is accelerated. Duff (1959) found that the contact surface accelerates to a terminal speed equal to that of the shock front.



**FIGURE 3.2.4.I SHOCK WAVE BOUNDARY LAYER FORMATION**

Flow duration  $FD$  is defined as the elapsed time between the arrival of the shock front and contact surface at a particular observation point on the shock tube wall; Figure 3.2.4.II.

Ideally the length  $l_1$  of the cylinder of shocked gas contained between the shock front and contact surface satisfies the relationship  $\rho_2 l_1 = \rho_1 x$  3.2.4.I

where  $x$  is the distance along the channel measured from the diaphragm,  $\rho_1$  and  $\rho_2$  are the initial and shocked densities of the gas.

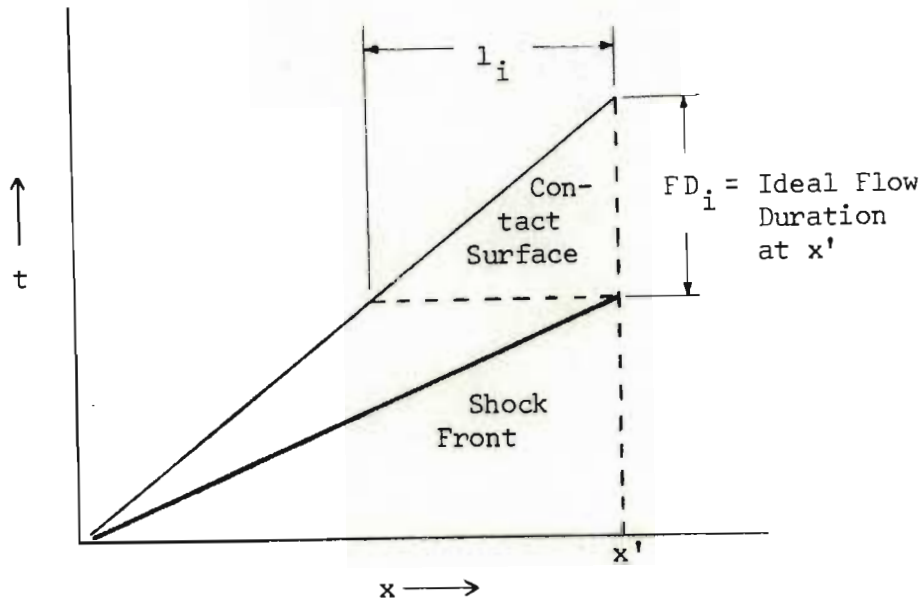


FIGURE 3.2.4.II x-t DIAGRAM SHOWING IDEAL FLOW DURATION

The velocity  $u_2'$  of the shocked gas is related to the shock speed  $u_1$  by the continuity equation  $\rho_2 u_2' = \rho_1 (u_1 - u_2')$  which gives

$$u_2' = u_1 \left( \frac{\rho_2}{\rho_1} - 1 \right) / \left( \frac{\rho_2}{\rho_1} \right) \quad 3.2.4.II$$

The flow duration can be expressed as

$$FD_i = l_i / u_2' \quad 3.2.4.III$$

combining equations 3.2.4.I, 3.2.4.II and 3.2.4.III

$$FD_i = x / (a_1 M_1 \left( \frac{\rho_2}{\rho_1} - 1 \right)) \quad 3.2.4.IV$$

where  $a_1$  is the sound speed in the undisturbed gas and  $M_1 = u_1/a_1$  is the shock Mach number.

It is well known that experimental flow durations are shorter than the calculated ideal values. The discrepancy increases with increasing Mach number and decreasing initial pressure  $P_1$ . Roshko (1960), Hooker (1961) and Mirels (1963) reported experimentally measured flow durations for initial pressures less than 110 mm Hg. Some of Hooker's results are shown in Figure 3.2.4.III.

Initial pressures used in this work were of the order of 1000 mm Hg.,  $2,4 < M_1 < 3,7$  and shock tube diameter was 5,3 cm. Since  $FD/FD_i$  is a very slowly varying ratio for pressures above 5 mm Hg. it was necessary to estimate it for the conditions used in this work. A correction factor was then applied to the ideal contact surface velocity so that more

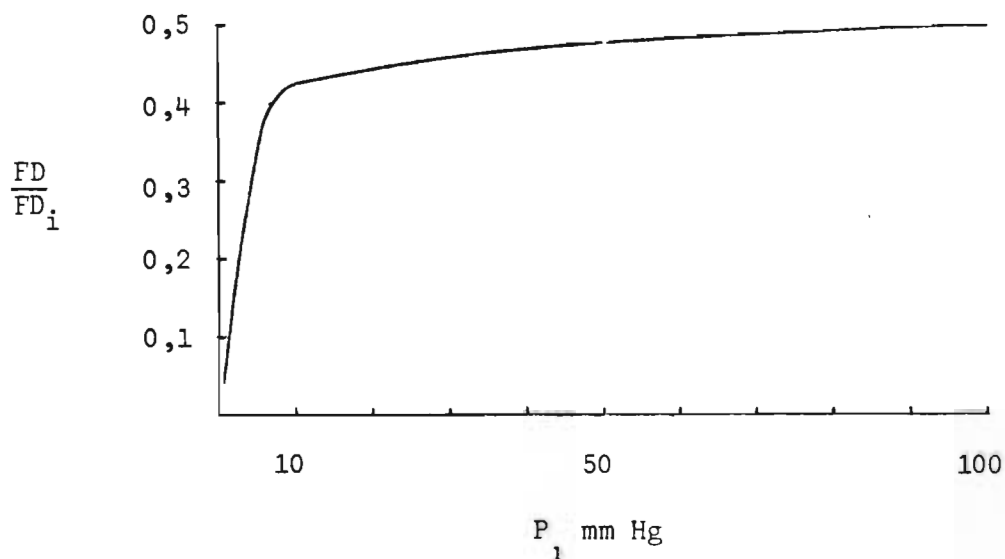


FIGURE 3.2.4.III Ratio of Experimentally Measured Flow Duration to Ideally Predicted Flow Duration Versus Initial Channel Gas Pressure.  $CO_2/Ar$ ;  $2,4 \leq M_1 \leq 4,8$ ; 3,94 cm Diameter Shock Tube - Hooker (1961)

accurate estimates of reaction times could be generated.

Roshko (1960) analysed the effects of the laminar boundary layer behind the shock front. He developed a shock tube similarity length parameter  $X$ , which depends on  $P_1$ , diameter of the tube and  $M_1$ , and a flow duration parameter FDP;

$$X = 16 \left( \frac{\mu P}{\rho a} \right)_S \beta^2 F(M_1) \frac{x}{P_1 d_{ST}^2} \quad 3.2.4.V$$

$$FDP = 16 \left( \frac{\mu P}{\rho a} \right)_S \beta^2 G(M_1) \frac{a_1 FD}{P_1 d_{ST}^2} \quad 3.2.4.VI$$

where  $\mu_s$ ,  $P_s$ ,  $\rho_s$  and  $a_s$  are standard (room temperature and atmospheric pressure) values of viscosity, pressure, density and sound velocity respectively.  $d_{ST}$  is the shock tube internal diameter.  $\beta$  is a boundary layer parameter which Roshko determined empirically to be  $\sqrt{3}$ . The functions  $F(M_1)$  and  $G(M_1)$  are defined as

$$F(M_1) = \frac{1}{Z_2} \cdot \frac{T_2}{T_1} \cdot \frac{\rho_2/\rho_1 - 1}{\rho_2/\rho_1} \cdot \frac{1}{M_1} \quad 3.2.4.VII$$

$$G(M_1) = \frac{1}{Z_2} \cdot \frac{T_2}{T_1} \cdot \frac{(\rho_2/\rho_1 - 1)^2}{\rho_2/\rho_1} \quad 3.2.4.VIII$$

where  $Z_2$  is the compressibility factor (1 for a perfect gas) and  $T_2/T_1$  is the temperature ratio across the shock front.

Roshko plotted  $F(M_1)$  and  $G(M_1)$  versus  $M_1$  for gases of different specific heat ratios  $\gamma$ . In this work  $F(M_1)$  and  $G(M_1)$  were calculated from equations 3.2.4.VII and 3.2.4.VIII using the corresponding properties for the heterogeneous mixture of gas and catalyst.

X and FDP are related by the following equation

$$\frac{X}{2} = -\ln (1 - FDP^{\frac{1}{2}}) - FDP^{\frac{1}{2}} \quad 3.2.4.IX$$

Roshko's equations were used for the heterogeneous system by assuming the mixture of gas and catalyst to be a gas with modified properties; see Chapter 3.2.2. Viscosity remains that of the gas alone since the volume occupied by the catalyst particles is assumed negligible. Density, specific heat ratio, sound speed and Mach number become new values for the mixture.

A shock Mach number  $M_s = 3.67$  was chosen for the specimen calculation; run 36.

$M_s$  is the shock Mach number with respect to the sound speed of the gas/catalyst mixture ahead of the shock front. The necessary properties for the gas/catalyst mixture in state 1 and state 2-relaxed were obtained via computer programme ZHETRO (Appendix F). The following is an example of the calculation procedure used. Values of properties and certain parameters used are listed in Table 3.2.4.i.



TABLE 3.2.4.1 VALUES USED TO ESTIMATE LAMINAR BOUNDARY LAYER EFFECT ON FLOW DURATION -  
SPECIMEN CALCULATION (RUN 36)

Item	Value	Units	Symbol Used In Text	Fortran Symbol (ZHETRO)
Shock tube diameter	2,09	in.	$d_{ST}$	-
Initial pressure in state 1	1034	mm Hg	$P_1$	-
Heterogeneous shock Mach no.	3,67	none	$M_S$	FM2
Shock velocity	112100	$\text{cm}\cdot\text{sec}^{-1}$	VEL	VEL
Sound speed in state 1	30554	$\text{cm}\cdot\text{sec}^{-1}$	$a_s, a_1$	A1
Viscosity of gas mixture in state 1	0,00022	$\text{g}\cdot\text{sec}^{-1}\cdot\text{cm}^{-1}$	$\mu_s$	FMU
Pressure of standard state	760	mm Hg	$P_s$	-
Density of heterogeneous mixture in state 1	0,001647	$\text{g}\cdot\text{cm}^3$	$\rho_s, \rho_1$	RHOH1
Density of heterogeneous mixture in relaxed state 2	0,006208	$\text{g}\cdot\text{cm}^3$	$\rho_2$	RHOH2
Distance along channel	250	cm	x	-
Ideal contact surface velocity	82522	$\text{cm}\cdot\text{sec}^{-1}$	$UE_i$	UE
Compressibility factor for gas mixture in relaxed state 2	1	none	$Z_2$	-
Temperature ratio of <u>relaxed state 2</u> state 1	4,225	none	$T_2 / T_1$	THEE

$$\begin{aligned}
 \text{Let } A &= 16 \left( \frac{\mu P}{\rho a} \right)_S \beta^2 \\
 &= 16 \left( \frac{0,000220 \cdot 760}{0,001647 \cdot 30554} \right) \cdot 3 \cdot \frac{1}{2,54} \\
 &= 0,06270 \text{ in.} \cdot \text{mm Hg.}
 \end{aligned}$$

$$X = 0,06270 \cdot 0,847 \cdot \frac{98,5}{1034 \cdot (2,09)^2} = 0,001158$$

where 0,847 is the value of  $F(M_S)$  from equation 3.2.4.VII.

This is the value of  $X$  at  $x = 98,5$  in. (250 cm) which is a point just before that where the reflected rarefaction wave catches the shock front;  $x_S = 106,7$  in. (271 cm). This value of  $x$  was chosen so that reasonably large numbers could be handled in the calculation in order to minimise inaccuracies. Since  $X$  is  $\ll 0,1$  the relationship between  $X$  and  $FDP$  will be linear for  $0 < x \leq 102,3$  (Roshko (1960)).

Solution of equation 3.2.4.IX yields  $FDP = 0,00105$ . From equation 3.2.4.VI

$$FD = \frac{0,00105 \cdot 1034 \cdot (2,09)^2 \cdot 2,54}{0,06270 \cdot 8,67 \cdot 30554} = 0,725 \text{ m.sec.}$$

where 8,67 is the value of  $G(M_S)$  from equation 3.2.4.VIII.

$$\begin{aligned}
 \text{Now } FD_i &= FD \cdot \frac{X}{FDP} = 0,725 \cdot \frac{1158}{1050} \\
 &= 0,800 \text{ m.sec.}
 \end{aligned}$$

Also, using equation 3.2.4.IV

$$FD_i = 0,800 \text{ m.sec.}$$

which is identical.

$$\frac{FD}{FD_i} = 0,905 \text{ which means that the ideal contact surface}$$

velocity needs to be corrected. The Fortran symbol for contact surface velocity is used here and is subscripted to signify assumed ideal one dimensional theory,  $UE_i$ . It can be shown using Figure 3.2.4.IV that the following relation is true

$$UE = \frac{VEL}{\frac{FD}{FD_i} \cdot \left(\frac{VEL}{UE_i} - 1\right) + 1} \quad 3.2.4.X$$

$$UE_i = \frac{x_1}{FD_i + t_1} \quad 3.2.4.XI$$

$$UE = \frac{x_1}{FD + t_1} \quad 3.2.4.XII$$

$$VEL = \frac{x_1}{t_1} \quad 3.2.4.XIII$$

dividing the R.H.S. of equation 3.2.4.XII top and bottom by  $t_1$  yields

$$UE = \frac{\frac{x_1}{t_1}}{\frac{FD}{t_1} + 1} = \frac{VEL}{\frac{FD}{t_1} + 1}$$

now  $\frac{FD}{t_1} = \frac{FD}{FD_i} \left(\frac{FD_i}{t_1}\right)$

from equation 3.2.4.XI  $FD_i = \frac{x_1}{UE_i} - t_1$

$\therefore \frac{FD_i}{t_1} = \frac{VEL}{UE_i} - 1$  hence equation 3.2.4.X.

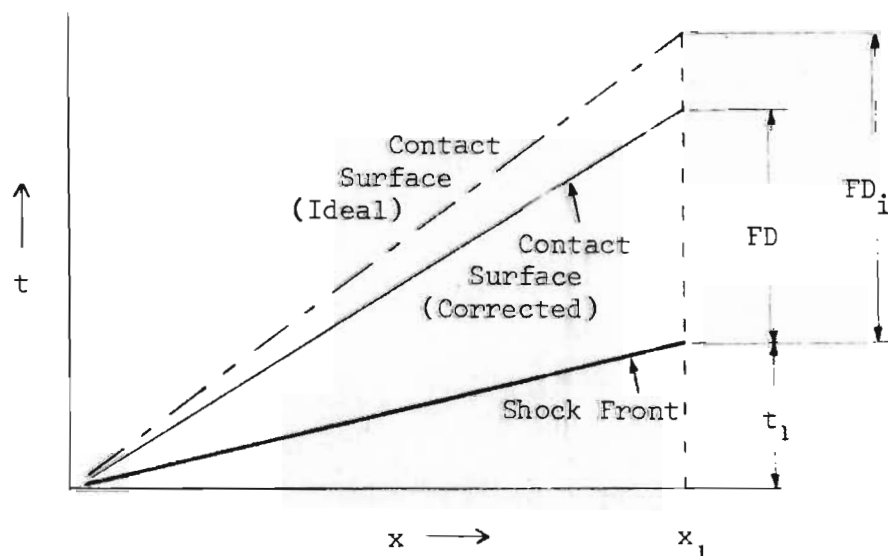


**FIGURE 3.2.4.IV** x-t DIAGRAM SHOWING IDEAL AND CORRECTED FLOW DURATION

$$\text{For this case } UE = \frac{112100}{0,907 \left( \frac{112100}{82522} - 1 \right) + 1} = 84700 \text{ cm/sec.}$$

$$\text{hence } \frac{UE - UE_i}{UE_i} \cdot 100 = 2,64 \%, \text{ say } 2,7 \%.$$

The above considerations have assumed that the boundary layer is laminar at all times. This is true immediately behind the shock, but under many conditions transition to turbulent flow occurs a certain distance behind the shock. The significance of this transition is that the turbulent boundary layer grows at a more rapid rate and hence causes a further increase in the effective contact surface velocity. The process of transition is extremely complicated and has still not been predicted for any given shock tube to an accuracy better than a factor of two or three (Hartunian (1968)).

---

### 3.3 Reaction Zone

#### 3.3.1 Description

Consider a heterogeneous reaction which possesses a finite rate above a certain temperature  $T_z$ . In the shock tube the reaction zone would be that slug of suspension which experiences temperatures greater than  $T_z$ . In Figure 3.3.3.I this slug has length  $x_{RZL}$  (RZL denotes reaction zone length) if the line O"HG represents the temperature  $T_z$  in the  $x$ "- $t$ " diagram. The area OFHGS therefore represents the reaction zone in the  $x$ - $t$  diagram. This has been explained in more detail in Chapter 3.3.3.

Clearly the temperature-time history of each element of shocked reaction mixture is different. The variation in flow duration  $t_{FD}$  and quench time  $t_q$  through the reaction zone is linear;  $t_{FD}$  varying from a maximum for an element initially at 0 to zero at point S and vice versa for  $t_q$ .

In the following Chapters equations for the construction of the x-t diagram have been presented. In the case of quench it has been assumed that the suspension is merely a gas of modified properties - slip between gas and solid has been neglected.

Further, the temperature-time history of an element initially at  $x_{RZL}/2$  has been assumed to hold for all elements. This assumption was necessary as the reaction mixture was analysed before and after reaction only and lack of published kinetic data for the various steps of the Fischer-Tropsch reaction made it impossible to estimate the contribution made by each element.

### 3.3.2 Reflected Rarefaction Head Intersections

Figure 3.3.2.I shows the head of the reflected rarefaction wave overtaking the contact surface at point  $x_c, t_c$  and the shock front at point  $x_s, t_s$ . The relaxation zone is denoted XAXIS and  $x_E, t_E$  is the point where the reflected rarefaction head enters this zone.

The equation of the tail of the rarefaction in the x, t plane is

$$x = (u_3' - a_3) t$$

$$\text{or } x = (u_e'' - a_3) t \quad 3.3.2.I$$

where  $u_e''$  is the equilibrium gas velocity in relaxed state 2 corrected for boundary layer formation (see Chapter 3.2.2 and 3.2.4).

The equation of the head between its reflection at the end wall and intersection with the tail may be shown (by the method of characteristics, Bradley (1962)) to be

$$\frac{x}{x_4} = \frac{\gamma_4 + 1}{\gamma_4 - 1} \left(\frac{t}{t_4}\right)^{\frac{3-\gamma_4}{\gamma_4+1}} - \frac{2}{\gamma_4-1} \left(\frac{t}{t_4}\right) \quad 3.3.2.II$$

where  $x_4 = a_4 t_4$  is the length of the chamber and  $\gamma_4$  is assumed to be constant during expansion. The point  $x_3, t_3$  at which this curve intersects the tail is obtained by equating 3.3.2.I and II

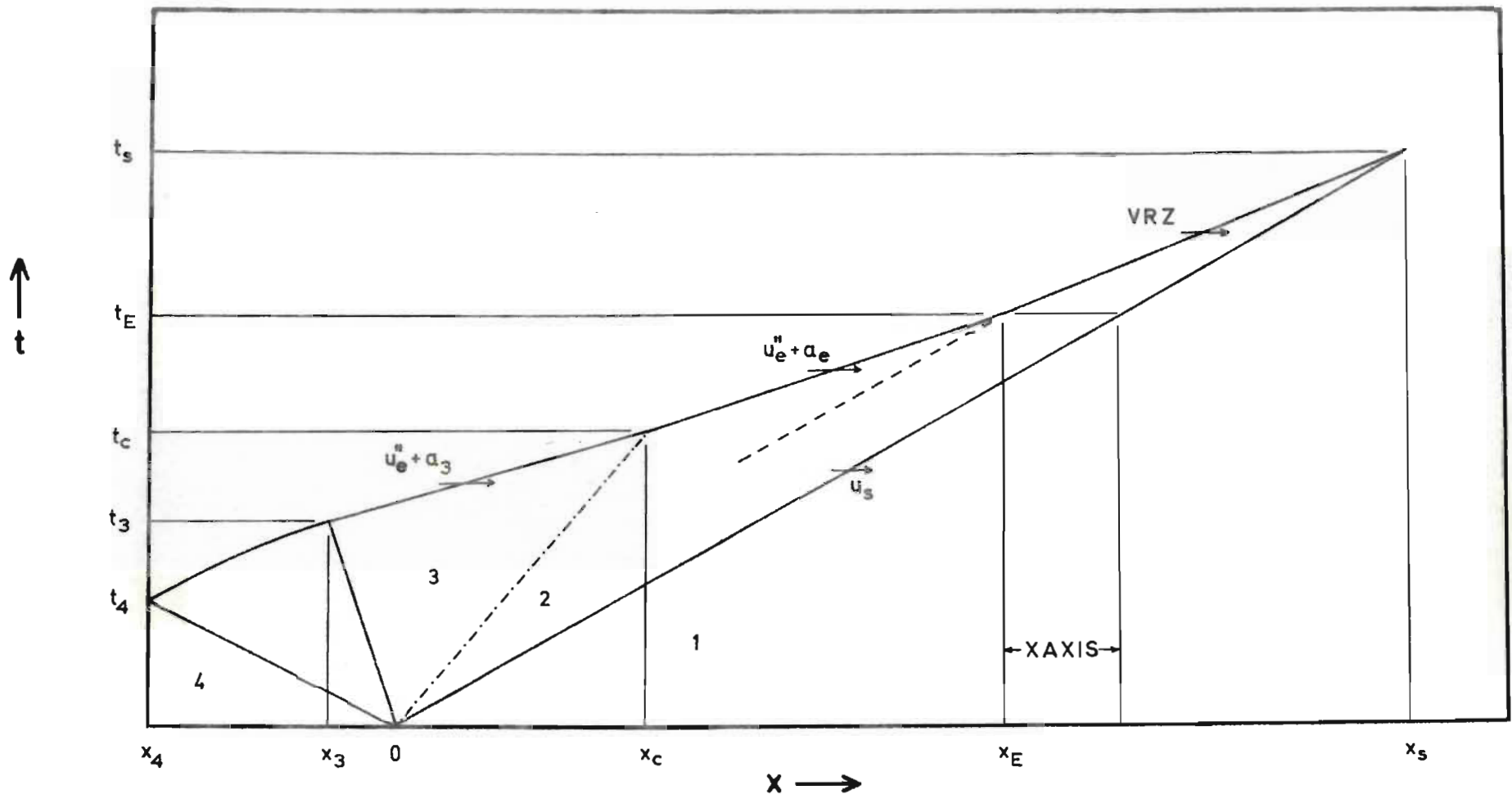


FIGURE 3.3.2.I Rarefaction head intersections

and eliminating  $a_3$  by use of the Q-characteristic equation (Bradley (1962)),

$$\frac{2}{\gamma_4 - 1} \cdot a_4 = \frac{2}{\gamma_4 - 1} \cdot a_3 + u''_e \quad 3.3.2.III$$

for isentropic expansion ( $u'_4 = 0$ ). This gives

$$x_3 = x_4 (M'_3 - 1) \cdot \left(1 + \frac{(\gamma_4 - 1)}{2} \cdot M'^2_3\right)^{\frac{3 - \gamma_4}{2(\gamma_4 - 1)}} \quad 3.3.2.IV$$

$$t_3 = \frac{x_4}{a_4} \left(1 + \frac{(\gamma_4 - 1)}{2} \cdot M'^2_3\right)^{\frac{\gamma_4 + 1}{2(\gamma_4 - 1)}} \quad 3.3.2.V$$

where  $M'_3 = \frac{u''_e}{a_3} = M_3$  correction factor for boundary layer formation (Chapter 3.2.4).

It can be shown that

$$M_3 = \frac{2}{\gamma_4 - 1} \left( \left( \frac{P_e}{P_4} \right)^{\frac{\gamma_4 - 1}{2\gamma_4}} - 1 \right) \quad 3.3.2.VI$$

In the region between  $x_3$  and  $x_c$  the head travels at the constant speed  $a_3 + u''_e$ ; hence

$$t_c = t_3 + \frac{(x_c - x_3)}{a_3 + u''_e} \quad 3.3.2.VII$$

Putting  $x_c = u''_e t_c$ , equation 3.3.2.VII, after rearrangement, becomes

$$t_c = t_3 (1 + M'_3) - x_3 \frac{M_3}{u''_e} \quad 3.3.2.VIII$$

For distances greater than  $x_c$  the rarefaction head moves through a suspension of gas and solid. Its speed relative to the gas will be the local sound speed of the gas and is not influenced by the presence of solid particles (Rudinger and Chang (1964)).

$$\text{Now } x_E = u_s t_E - \text{XAXIS} \quad 3.3.2.IX$$

$$\text{and } t_E = \frac{x_c}{u_e''} + \left( \frac{x_E - x_c}{u_e'' - a_e} \right) \quad 3.3.2.X$$

putting 3.3.2.IX into 3.3.2.X and rearranging, the following can be obtained

$$t_E = (\text{XAXIS} + x_c - (u_e'' + a_e) t_c) / (u_s - (u_e'' + a_e)) \quad 3.3.2.XI$$

where  $u_s$  is the shock velocity.

In the relaxation zone the speed of the head of the reflected rarefaction wave varies continuously. Since the variation is small the arithmetic mean speed is used

$$\text{VRZ} = \frac{u_e'' + u_2}{2} + \text{ARZ}$$

where VRZ = velocity of head in relaxation zone and ARZ = sound speed in relaxation zone.

$$\text{ARZ} = \left( \frac{\gamma_1 R}{M} \frac{(T_e + T_2)}{2} \right)^{\frac{1}{2}}$$

where M = molecular weight of the gas alone.

$$\text{Now } x_s - x_E = \text{VRZ} (t_s - t_E) \quad 3.3.2.XII$$

$$\text{also } x_s - x_E - \text{XAXIS} = u_s (t_s - t_E) \quad 3.3.2.XIII$$

subtracting 3.3.2.XIII from 3.3.2.XII yields

$$\text{XAXIS} = (\text{VRZ} - u_s) \cdot (t_s - t_E)$$

substituting for XAXIS from equation 3.3.2.IX gives

$$u_s t_E - x_E = (\text{VRZ} - u_s) t_s - t_E$$

$$\text{rearranging } t_s = \frac{\text{VRZ } t_E - x_E}{u_s - \text{VRZ}} \quad 3.3.2.XIV$$

$$\text{hence } x_s = u_s t_s \quad 3.3.2.XV$$



### 3.3.3 Quench

Consider the quenching of chamber gas by the reflected rarefaction wave. The process is state 3 to state 6 in Figure 3.3.3.I. The line OFHC represents the path of a molecule of chamber gas at the contact surface.

P-characteristic slope (for a centred wave)

$$\frac{x'}{t'} = u' + a \quad 3.3.3.I$$

For the entire region of the reflected fan, characteristic Q = characteristic Q<sub>3</sub>

$$\therefore u' - \frac{2a}{\gamma_4 - 1} = u'_3 - \frac{2a_3}{\gamma_4 - 1} \quad 3.3.3.II$$

combining 3.3.3.I and 3.3.3.II, and solving for u

$$u' = \frac{2}{\gamma_4 + 1} \cdot \frac{x'}{t'} - \frac{2a_3}{\gamma_4 + 1} + \left(\frac{\gamma_4 - 1}{\gamma_4 + 1}\right) \cdot u'_3 \quad 3.3.3.III$$

Now u' can be expressed as  $\frac{dx'}{dt'}$  and within the fan

$$\frac{dx'}{dt'} = u' + t' \frac{du'}{dt'} \quad 3.3.3.IV$$

Integrating 3.3.3.IV yields  $\frac{x'}{t'} = u'$

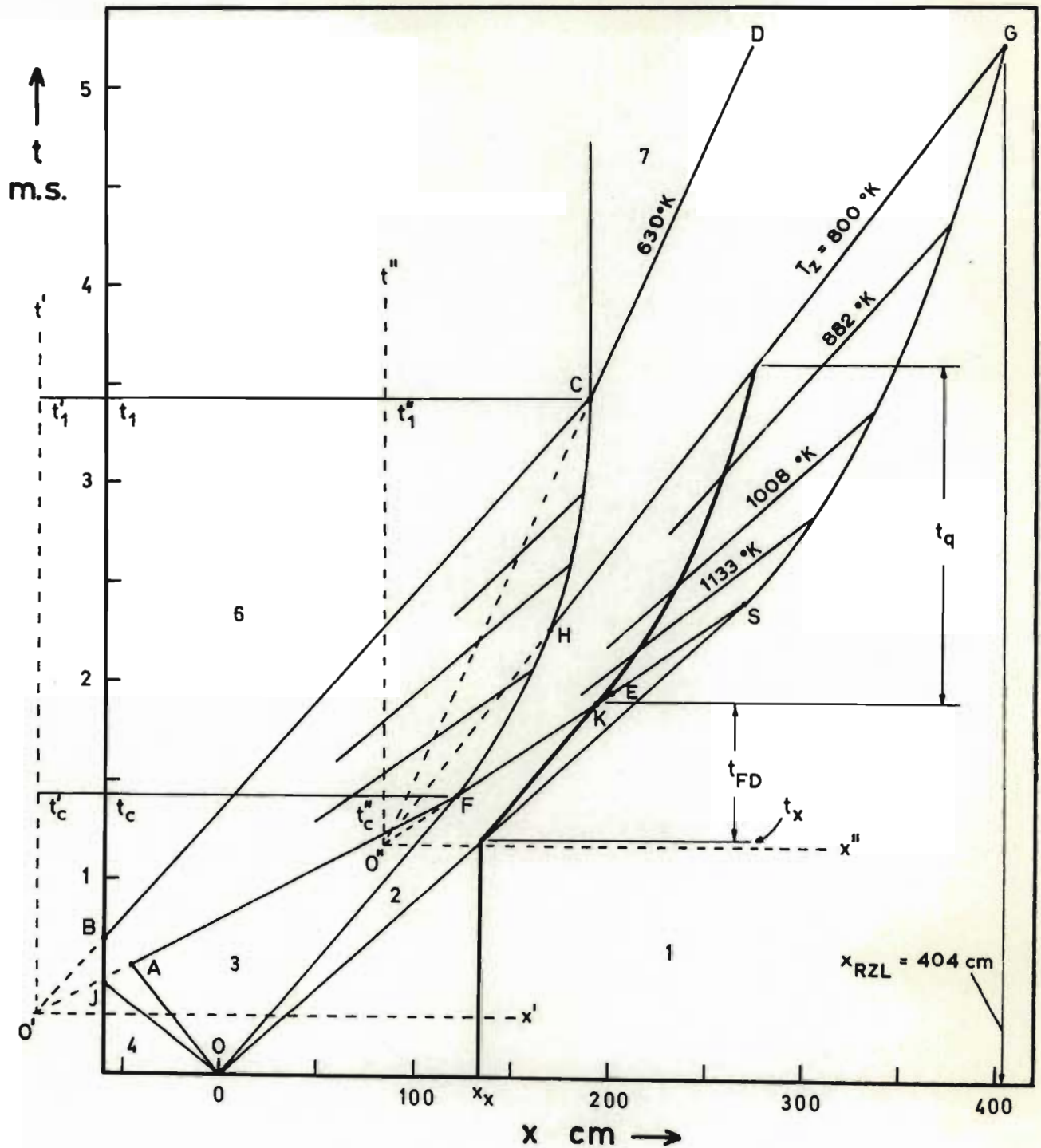
Hence 3.3.3.III becomes

$$u' + t' \frac{du'}{dt'} = \frac{2}{\gamma_4 + 1} \cdot u' - \frac{2}{\gamma_4 + 1} \cdot a_3 + \left(\frac{\gamma_4 - 1}{\gamma_4 + 1}\right) \cdot u'_3$$

Integrate

$$\left(\frac{\gamma_4 + 1}{\gamma_4 - 1}\right) \int_{u'_3}^{u'} \frac{du'}{u'_3 - \frac{2}{\gamma_4 - 1} \cdot a_3 - u'} = \int_{t'_c}^{t'} \frac{1}{t'} dt'$$

where  $t'_c$  is the time at which the molecule enters the rarefaction fan.



$$\frac{x'}{t'} = \left( \frac{\gamma_4 + 1}{\gamma_4 - 1} \right) \cdot a_3 \left( \frac{T}{T_3} \right)^{0,5} + u_e'' - \left( \frac{2a_3}{\gamma_4 - 1} \right)$$

$$\frac{x''}{t''} = \left( \frac{\Gamma + 1}{\Gamma - 1} \right) \cdot a_e \left( \frac{T}{T_e} \right)^{0,5} + u_e'' - \left( \frac{2a_e}{\Gamma - 1} \right)$$

Characteristic slopes obtained from equations 3.3.3.II and 3.3.3.III

FIGURE 3.3.3.I QUENCH by reflected rarefaction wave (run 36)

The result is

$$\left( \frac{\frac{2}{\gamma_4 - 1} \cdot a_3}{u' - u_3' + \frac{2}{\gamma_4 - 1} \cdot a_3} \right)^{\left( \frac{\gamma_4 + 1}{\gamma_4 - 1} \right)} = \frac{t'}{t'_c} \quad 3.3.3.V$$

Substituting for  $u'$  from 3.3.3.II

$$\left( \frac{a_3}{a} \right)^{\left( \frac{\gamma_4 + 1}{\gamma_4 - 1} \right)} = \frac{t'}{t'_c} \quad 3.3.3.VI$$

For isentropic expansion  $\frac{T_3}{T} = \left( \frac{a_3}{a} \right)^2$  and equation 3.3.3.VI

becomes

$$\frac{t'}{t'_c} = \left( \frac{T_3}{T} \right)^{\frac{\gamma_4 + 1}{2(\gamma_4 - 1)}} \quad 3.3.3.VII$$

Similarly for the channel gas

$$\frac{t''}{t''_c} = \left( \frac{T_e}{T} \right)^{\frac{\Gamma + 1}{2(\Gamma - 1)}} \quad 3.3.3.VIII$$

It has been assumed here that the conditions of the gas within the rarefaction fan can be calculated to a reasonable degree of accuracy by considering the gas/solid mixture to behave as a gas having a specific heat ratio  $\Gamma$ ; see Chapter 3.2.2. For a pure gas, the characteristics of the rarefaction wave form a fan of straight lines. In the heterogeneous system, only the head of the expansion wave is straight since the solid particles require a finite time to respond to changes in the gas ("frozen flow"). Subsequently, as a result of the developing interaction between the gas and particles, the characteristics become curved.

Rudinger and Chang (1964) discuss the P waves of such a modified system for  $10\mu$  diameter glass spheres; curvature of the characteristics was slight becoming more pronounced towards the tail of the expansion wave. The tendency was for  $t''/t''_c$  to have larger values than in the homogeneous system. For the purpose of this

work the use of  $\Gamma$  instead of  $\gamma_1$  ( $\Gamma < \gamma_1$ ) was regarded as sufficient correction in the right direction.

In Figure 3.3.3.I it has been assumed for simplicity, that the interaction of the reflected rarefaction wave and the contact surface results in a stationary contact surface. This is true only if

$$\frac{(C_v T)_e}{(C_v T)_3} = 1$$

Since in the system studied here  $\frac{(C_v T)_e}{(C_v T)_3} \neq 1$

the contact surface will possess a velocity after interaction with the reflected rarefaction. The above assumption is not in serious error when compared with another assumption made earlier, namely that the contact surface is a well defined plane.

The times at which the stationary states 6 and 7 are attained can be calculated from

$$\frac{t'_c}{t'_c} = \left( \frac{T_3}{T_6} \right)^{\frac{\gamma_4 + 1}{2(\gamma_4 - 1)}} \quad 3.3.3.IX$$

and

$$\frac{t''_c}{t''_c} = \left( \frac{T_e}{T_7} \right)^{\frac{\Gamma + 1}{2(\Gamma - 1)}} \quad 3.3.3.X$$

Equations for the characteristic slopes  $x'/t'$  and  $x''/t''$  are given in Figure 3.3.3.I.

#### Graphical procedure for calculating quench rates

Reference should be made to Figures 3.3.2.I and 3.3.3.I.

Known data: Points,  $A = x_3, t_3$   
 $F = x_c, t_c$   
 $E = x_s, t_s$   
 $K$  as chosen  $\frac{T}{T_1}^{\frac{1}{2}}$   
 Slopes,  $BC = a_6 = a_4 \left( \frac{6}{T_1} \right)$

$$\text{where } T_6 = T_3 \left( 1 - \frac{(\gamma_4 - 1)}{2} \cdot \frac{u''_e}{a_3} \right)^2$$

$$CD = a_7 = a_e \left( \frac{T_7}{T_e} \right)^{\frac{1}{2}}$$

$$\text{where } T_7 = T_e \left( 1 - \frac{(\Gamma - 1)}{2} \cdot \frac{u''_e}{a_e} \right)^2$$

$$AF = u''_e + a_3$$

$$FS = u''_e + a_e$$

Note that relaxation has not been accounted for here. In practice the alteration to the slope of FS by relaxation was found to be very small; refer Figure 3.3.3.I, FE is almost parallel to ES.

### Procedure

- 1 Determine point B =  $x_4, t_6$ .

For hydrogen as chamber gas, i.e. diatomic

$$t_6 = \frac{x_4}{a_4} \left( \frac{1}{(2P_{34}^{1/7} - 1)^3} + \frac{6P_{34}^{2/7} (1 - P_{34}^{1/7})^2}{(2P_{34}^{1/7} - 1)^5} \right) \quad \text{Bradley (1962)}$$

$$\text{where } P_{34} = P_3 / P_4$$

To allow for a finite diaphragm opening time  $P_3$  was replaced by  $P_c$ ; see Chapter 3.1.3.

$$P_{34} = \frac{P_c}{(P_4)_{\text{experimental}}} = \left( \frac{P_4}{P_1} \right)_{\text{calculated eqn. 3.1.2.X}} \times \left( \frac{P_1}{P_4} \right)_{\text{experimental}}$$

- 2 With points A, B and F, and slopes AF and BC known, it is possible to calculate  $t'_c$  graphically.
- 3 Using  $t'_c$  and  $T_6$  calculate  $t'_1$  from equation 3.3.3.IX.

$$4 \quad t_1 \text{ is obtained by } t_1 = t'_1 - (t'_c - t_c).$$

Hence point C is determined.

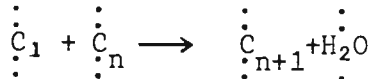
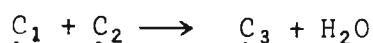
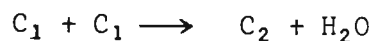
5 With points F, S and C, and slopes FS and CD known,  $t''_c$  can be calculated graphically.

6 Using  $t''_c$  and  $T_7$ ,  $t''_1$  can be calculated from equation 3.3.3.X.

By using the above procedure it is possible to determine the time for which a molecule of gas exists at a temperature above a certain value. A typical path for a gas molecule initially at  $x_x$  is shown by the bold line in Figure 3.3.3.I. It enters the reaction zone at time  $t_x$ , remains at a temperature  $T_e$  (or  $T_2$  for homogeneous system) for a time  $t_{FD}$  then cools to say  $T_Z$  in time  $t_q$ . If the reaction is terminated at temperature  $T_Z$  then the total reaction time for a particular gas molecule is  $t_{FD} + t_q$ . In this case HG in Figure 3.3.3.I is a P-characteristic for the  $x''$ ,  $t''$  diagram along which the temperature is  $T_Z$ ; therefore the distance-time region for chemical reaction is the figure OFHGSO and the reaction zone length is  $x_{RZL}$ .

### 3.4 Simple Fischer-Tropsch Reaction Rate Equation

A simple rate equation applicable to shock conditions has been developed here, based on a simplified version of the scheme of chain growth postulated by Storch et al (1951),



An intermediate  $C_1$  is formed on the catalyst surface and it reacts with other intermediates  $C_1, C_2 \dots C_n$  to form a higher intermediate or is removed by reaction with water vapour. Intermediates  $C_i$  desorb from the surface at a rate proportional to their surface concentration to form product of carbon number  $i$ . The rate of this can be expressed as

$$k_t \theta_1 \sum_{i=1}^{\infty} \theta_i$$

where  $k_t$  is the termination rate constant

$\theta_1$  is the fraction of surface covered by  $C_1$

$\theta_i$  is the fraction of surface covered by intermediate  $C_i$

At steady state conditions the following holds for the overall process;

$$k_a \theta_H^2 \theta_{CO} = k_t \theta_1 \sum_{i=1}^{\infty} \theta_i + k'_t \theta_1 \theta_{H_2O}$$

$$\text{or } r_{(H_2+CO)} = k_a \theta_H^2 \theta_{CO} - k'_t \theta_1 \theta_{H_2O}$$

where  $k_a$  is the rate constant for reaction 3.4.I

$k'_t$  is the termination rate constant for reaction 3.4.II

$\theta_H, \theta_{CO}$  and  $\theta_{H_2O}$  are respectively the fractional coverage of the surface by hydrogen atoms, CO and  $H_2O$

$r_{(H_2+CO)} = k_t \theta_1 \sum_{i=1}^{\infty} \theta_i =$  rate of consumption of  $H_2 + CO$  or the rate of production of hydrocarbons.

It should be noted here that reactions such as  $C_n + C_{n+1} \rightarrow C_{2n+1} + H_2O$  have been neglected in this simplified scheme.

Non steady state conditions exist at the start of reaction and with reaction times of the order of 1 m.sec., it is reasonable to assume that this situation might exist for a large part if not the whole of the reaction period. For unsteady state the rate controlling reaction will be 3.4.I above; i.e. the overall rate of consumption of  $H_2 + CO$  may then be expressed as

$$r_{(H_2+CO)} = k_a \theta_H^2 \theta_{CO}$$

Now, it is assumed that surface coverages may be approximated by Freundlich isotherms, i.e. the coverage by a substance is proportional to its partial pressure to a positive exponent less than one. This approximation has been shown to be valid in a number of systems (Boudart (1956), Stelling and Krustenstierna (1958) and Weller (1956)). Then

$$r = k P_{H_2}^{2m} P_{CO}^q \quad (0 < m, q < 1) \quad 3.4.III$$

In general (Anderson et al (1964)) the rate under commercial reaction conditions may be approximated by

$$r = (1-x)^{0.5 \text{ to } 1.0} \cdot P^n e^{-\frac{20000}{RT}}$$

where  $x$  is the fraction of  $H_2 + CO$  reacted and  $P$  is the total operating pressure (absolute).  $n$  is approximately unity. For shock conditions  $x$  is small so that

$$r = k' P^n e^{-\frac{E}{RT}} \quad 3.4.IV$$

would be expected to hold.  $E$  is the activation energy. From equation 3.4.III

$$r = k (PN_{H_2})^{2m} \cdot (PN_{CO})^q$$

where  $N$  is the mole fraction of the component. Since  $H_2/CO = 1$  and  $N$  are constant in the system under investigation here,

$$r = k' P^n$$

where  $n$  is  $\geq 1$

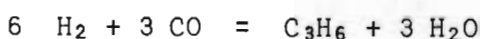
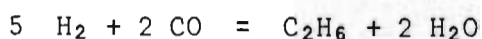
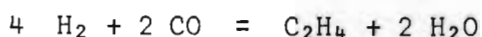
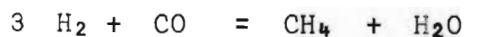
Inserting the exponential term,

$$r = k'' P^n e^{-\frac{E}{RT}} \quad 3.4.V$$

Equation 3.4.V has the same form as equation 3.4.IV.



Normally reaction rates for the Fischer-Tropsch synthesis are expressed in terms of  $H_2 + CO$  moles consumed. Owing to the extremely high space velocities and very short reaction times employed in this work, the extent of reaction was very small, making it impossible to measure directly the quantities of  $H_2 + CO$  consumed. Hence to compare results with published literature the following stoichiometry was assumed,



methane, ethylene, ethane and propylene were the only products detected in this work.

It should be noted that  $H_2 + CO$  consumed in this case implies the formation of useful products only, i.e. hydrocarbons. Carbon formation has not been accounted for in this scheme. The water gas shift reaction would not affect the total moles of  $H_2 + CO$  consumed since for each mole of  $CO$  consumed one mole of  $H_2$  is formed.

---

## CHAPTER 4

### EXPERIMENTAL PROCEDURE

#### 4.1 Reaction Mixture Preparation

Crushed fused iron catalyst supplied by the S. A. Coal, Oil and Gas Corporation (SASOL) had the following composition;

	$\text{Fe}^{2+}$	27,1	mass per cent
	$\text{Fe}^{3+}$	43,0	mass per cent
	$\text{O}_2$	28,0	mass per cent
promoters	$\text{MgO}$	} 1,9	mass per cent
	$\text{SiO}_2$		
	$\text{K}_2\text{O}$		

The material was first dried and then subjected to air segregation as previously described in Chapter 2.5.1. Figure 4.1.I shows the typical particle size distribution that resulted.

Fluidised bed reduction of the catalyst by hydrogen at  $600^\circ\text{C}$  followed. Each experimental run required 80 g of catalyst to be treated until 85 per cent of the oxygen had been removed. The apparatus used for this operation has been discussed in Chapter 2.5.2. Once the catalyst had been reduced it was cooled and kept under hydrogen atmosphere until introduction into the shock tube circulation system.

The shock tube and circulation system were evacuated down to 2 Torr and dump tanks to 20 Torr. Hydrogen was then introduced into the chamber to just above one atmosphere absolute. The channel and circulation system were filled to approximately 1450 Torr with the reaction gas mixture and evacuated again to about 380 Torr. This was repeated three times; the final filling pressure was 1300 Torr; the blower was then started. In this way the oxygen content of the reaction gas was reduced to below 30 ppmv.

The reaction gas mixture consisted of hydrogen, carbon monoxide and argon approximately in the proportion 0,08/0,08/0,84 by volume re-

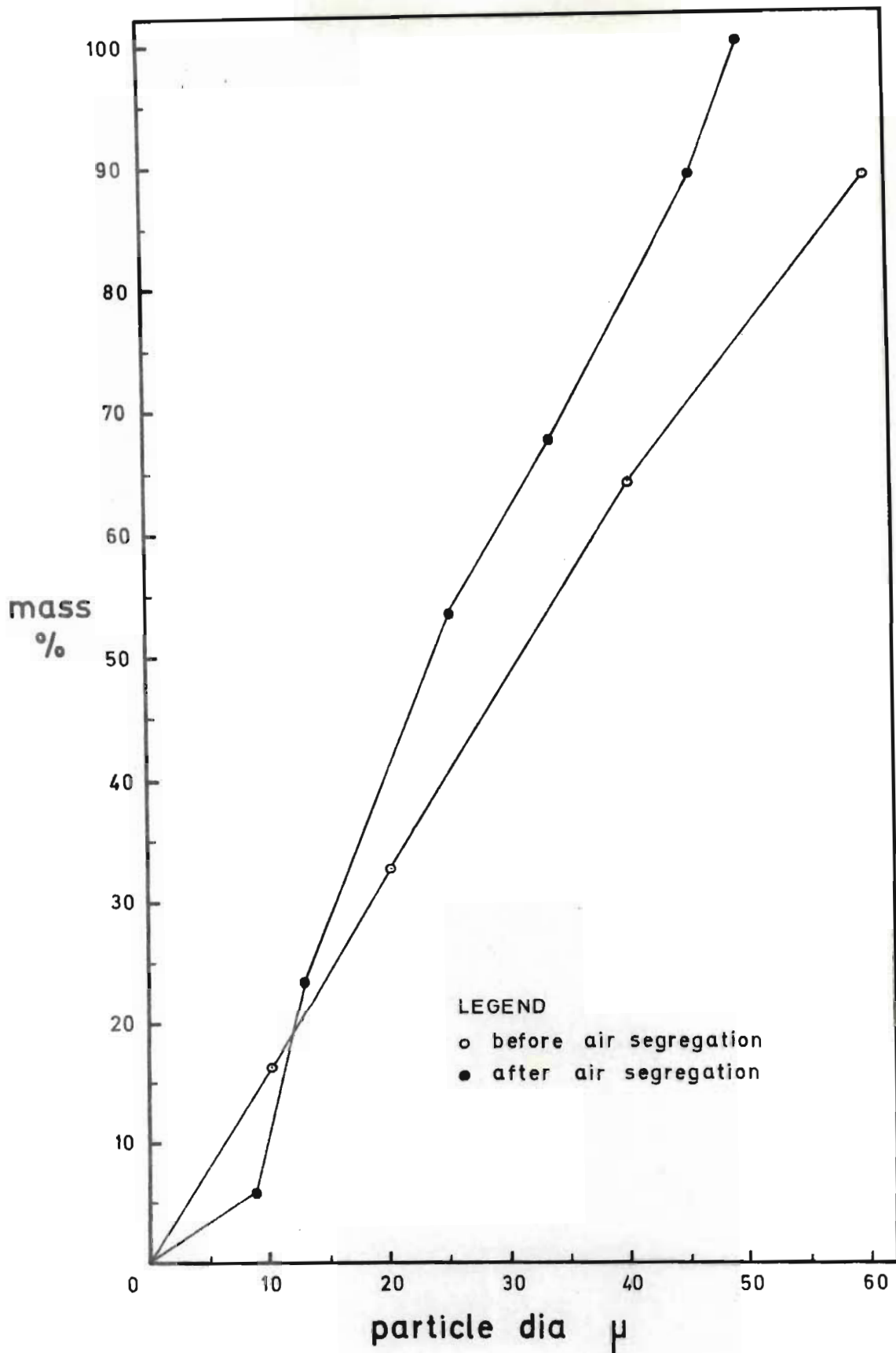


FIGURE 4.1.I Catalyst particle size distribution by Roller analysis

spectively. These gases were supplied in compressed gas cylinders, hydrogen and argon from African Oxygen Ltd. and carbon monoxide from SASOL. Average compositions were;

Hydrogen:	oxygen	90	ppmv
	methane	2	ppmv
	ethylene	< 0,5	ppmv
	ethane	< 0,5	ppmv
Argon:	oxygen	<< 50	ppmv
	nitrogen	50	ppmv
	hydrogen	<< 50	ppmv
	carbon monoxide	<< 100	ppmv
	carbon dioxide	<< 200	ppmv
	methane	5	ppmv
Carbon monoxide:	oxygen	<< 50	ppmv
	nitrogen	100	ppmv
	methane	2	ppmv
	ethylene	2	ppmv
	ethane	< 0,5	ppmv

The hydrogen pressure in the catalyst reduction vessel was then increased to 10 Torr below that of the blower suction and the ball valve, Figure 2.5.2.I, opened. By inversion of the reduction vessel the catalyst charge was introduced gradually into the circulation system. Catalyst loading of the reaction gas was observed by means of a photoelectric cell. When all the catalyst had been introduced the ball valve was closed and the system allowed at least five minutes to attain uniform catalyst loading, i.e. steady output from the photoelectric cell. The period of circulation varied from 10 to 95 minutes depending on the type of experiment being carried out, see Chapter 5. At the end of the circulation period two gas samples of 1 litre each were taken and the system pressure (measured at the top of the channel) was reduced to 1030 Torr ready for shock wave introduction.

## 4.2 Shock Tube Operation

Having completed reaction mixture circulation the chamber pressure was gradually increased to the desired value depending on the required shock strength. Before the shock wave could be introduced three operations had to be completed successfully in quick succession. These were,

- (i) closure of the circulation solenoid valves
- (ii) operation of the diaphragm rupture pin, and
- (iii) start of the high speed camera.

This was effectively accomplished by the circuitry shown in Figure 4.2.I, mounted on the rear of a control panel depicted in Plate 4.2.I.

The sequence of events is discussed here with reference to items shown in Figure 4.2.I. With switches A, C, D, G and H closed, K in the "close" position and E in its uppermost position, button F was depressed to trigger part of the thyristor AC load controller which in turn closed the solenoid valves. Not shown in Figure 4.2.I is the electrical safety circuit and indicator bulb used to ensure that both valves did in fact close; the indicator bulb is visible in Plate 4.2.I, below switches G and H (see also Appendix E). If both valves did not close the experiment was aborted at this stage.

Having shut the valves successfully switch E was thrown immediately into its lowest position and button J depressed simultaneously. The Goose control unit immediately brought into operation the coil timer and thyristor controller and switched out the electro-magnet holding the rupture pin. Thus coils A and B of the diaphragm rupturing mechanism were powered alternatively, each at a frequency of twice per second via the coil timer. After a delay of 0,2 sec. the Goose unit started the high speed camera which recorded the oscillograph sweep for shock speed measurement.

The coil timer and thyristor AC load controller were constructed in the laboratory and their circuit details are given in Appendix A. The purpose of the coil timer was to return the rupture pin after

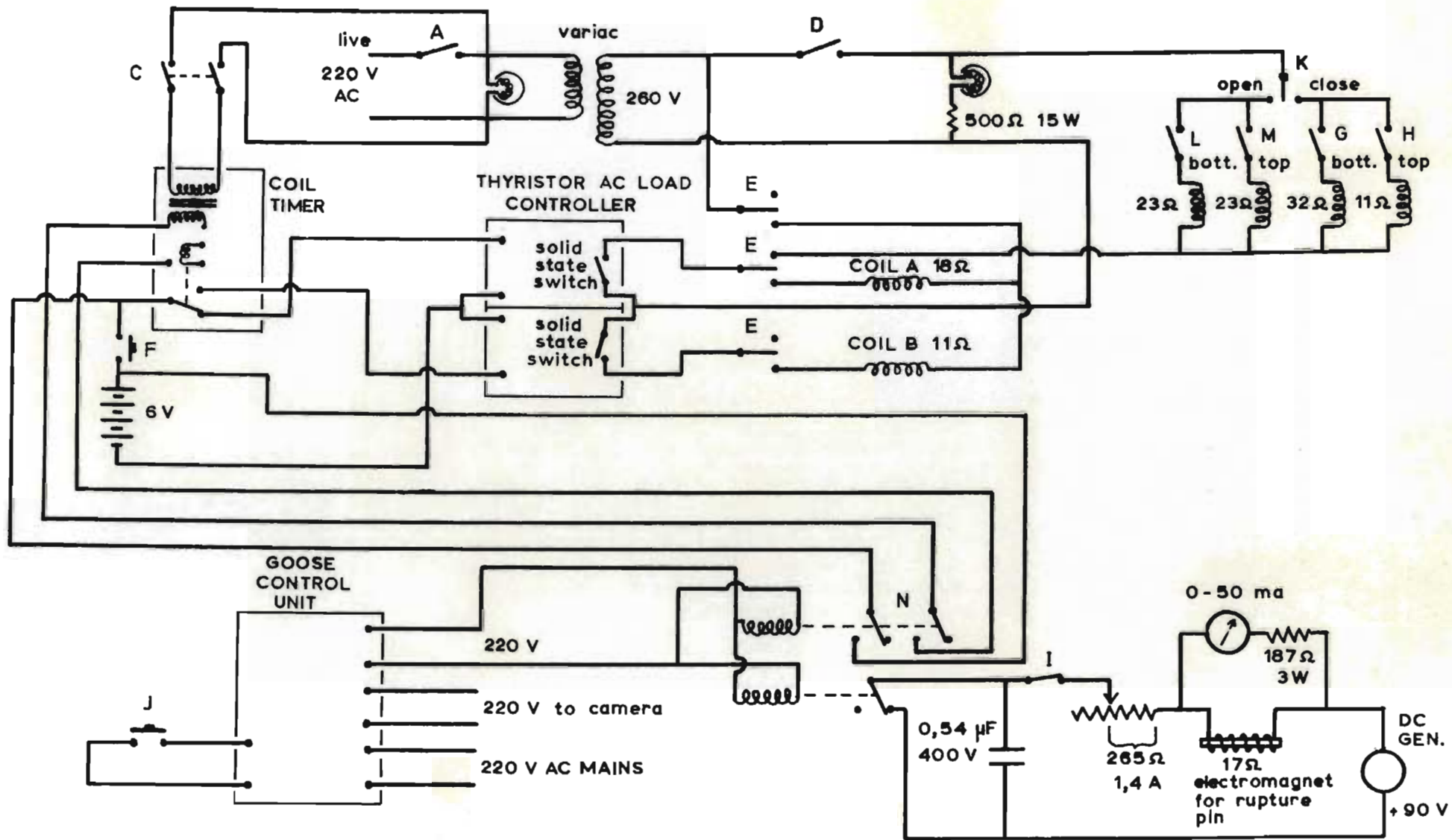


FIGURE 4.2.I Shock tube electrical control circuit

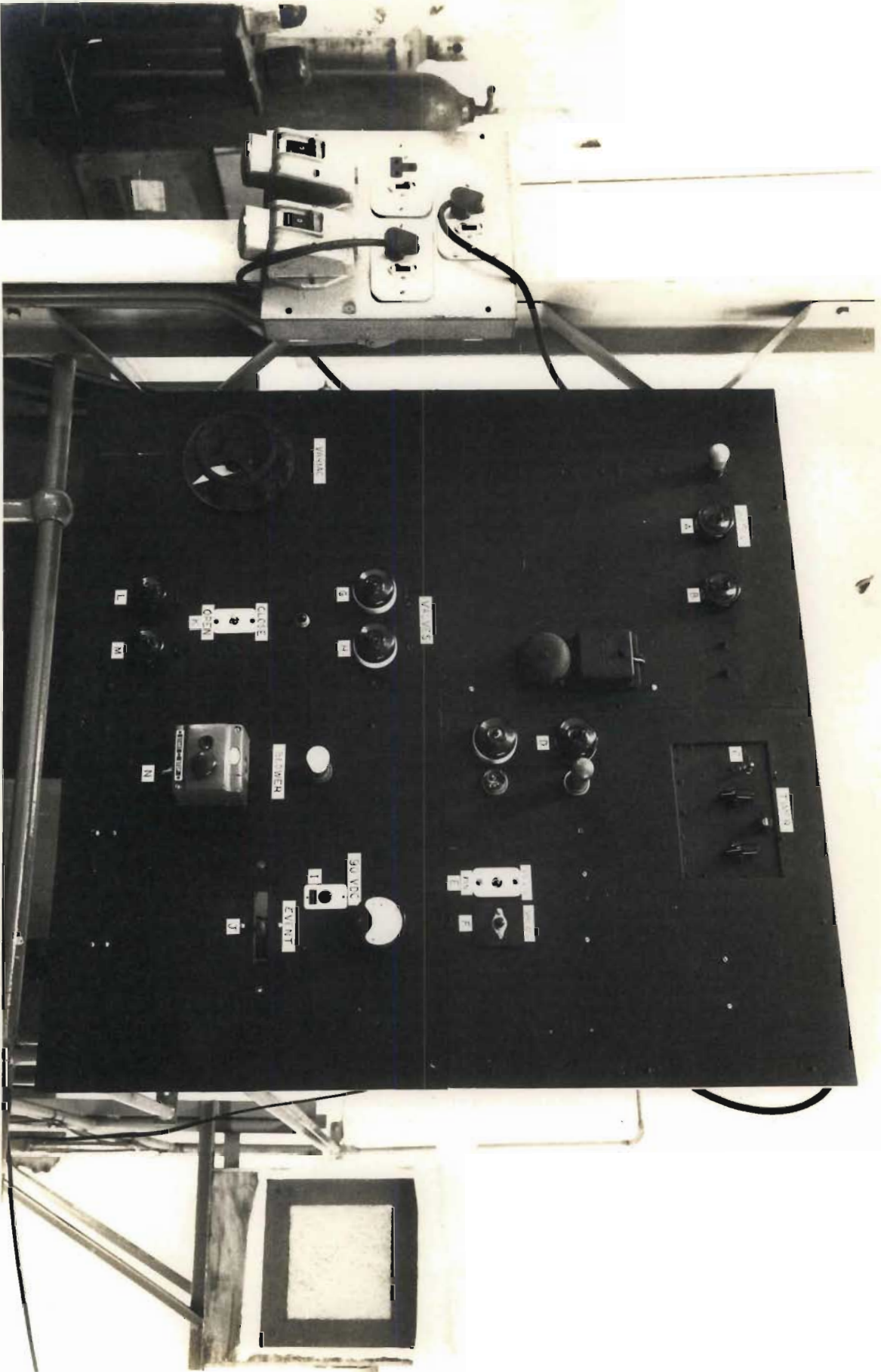


PLATE 4.2.1 Shock tube control panel

the initial forward thrust so that the tip of the pin would not obstruct the initial flow of hydrogen through the punctured diaphragm and hence slow down the diaphragm opening process.

---

#### 4.3 Product Gas Mixing and Sampling

After shocking, the product gas was contained in the shock tube at a pressure in the region of 100 psig depending on the shock strength employed. It was imperfectly mixed with chamber hydrogen and therefore a tedious procedure had to be adopted in order to ensure accurate sampling.

Time was allowed for the catalyst to settle to the bottom of the channel and then gas was tapped off into the evacuated product gas mixing vessel described in Chapter 2.4. The final positive pressure in the mixing vessel was noted and after mixing of its contents, two gas samples were taken. This was repeated a number of times until the pressure in the shock tube approached that in the circulation system at which point the solenoid valves were opened and the circulation blower started. Gas and catalyst were circulated for about 10 minutes in order to attain good mixing and then circulation was stopped, catalyst allowed to settle and system pressure noted. Final gas samples were then taken direct from the shock tube.

From a knowledge of pressures and volumes, gas analysis was converted to absolute quantities of the various compounds present in the system. A worked example of how product yields were calculated is given in Appendix B.

---



#### 4.4 Catalyst Loading Determination

After the final sampling of the gas in the system the pressure was reduced to 10 Torr above atmospheric pressure and the vent cock at the top of the system opened. A small purge of reaction gas mixture was introduced at the bottom of the system through valve 1 (Figure 2.2.I). With the bottom solenoid valve closed the circulation system was allowed 10 volume changes in order to expel the excess hydrogen. Similarly with the top solenoid valve closed the shock tube itself was purged. Now the whole system once again, contained the reaction gas mixture.

With both solenoid valves open and the purge gas still flowing, the diaphragm station was opened a minimum amount to allow withdrawal of the burst diaphragm and its replacement with a temporary one. Purging was necessary during this operation due to the pyrophoric nature of the reduced catalyst. System pressure was increased to its value before introduction of the shock wave and circulation begun. The piping was tapped in a number of places in order to enable the flowing gas to pick up catalyst which had settled in "dead spots". When the photocell indicated the same catalyst loading as registered just before shocking, the solenoid valves were closed and the catalyst allowed to settle. The channel was then purged with nitrogen and then very slowly with air from bottom to top in order to re-oxidise the catalyst before it could be removed. The bottom flange of the channel was opened, the catalyst removed, dried and weighed.

Owing to shrinkage during reduction the catalyst does not return to its former state. It was found to take up only about 80 per cent of the oxygen it had lost during reduction. Allowance was made for this in determining the catalyst to gas mass ratio  $\eta$ .

---

## 4.5 Experimental Design

### 4.5.1 Introduction

Initially it was necessary to choose realistic value ranges for certain variables of the system. Variables considered were;

reaction temperature	$T^{\circ}\text{K}(T_2 \text{ or } T_e)$
reactants' partial pressure	P atmos.
average dwell time ( $t_{\text{FD}}$ at $x_{\text{RZL}}/2$ )	$t_{\text{FD}}$ m.sec.
catalyst loading	$\eta$ mass of catalyst/mass of gas
catalyst reduction extent	$R_D$ mass % of $\text{O}_2$ removed
apparent product yield	Y cc at N.T.P.

Apparent product yields were used because the actual reacting mixture volume and real average reaction times for each run were unknown - a method for their estimation had still to be developed (see Chapter 3.3). The dwell time or flow duration used does not include the quench period.

### 4.5.2 Catalyst Loading

Catalyst loading of the test gas was expected to be critical.

Since reaction times in the shock tube were to be extremely short it was deemed imperative to secure as large a catalyst loading factor  $\eta$  as possible. To achieve this the reactants ( $\text{H}_2 + \text{CO}$ ) were diluted with argon resulting in a channel gas mixture of higher density and viscosity which could transport larger amounts of catalyst. It was found by experiment that a channel gas of greater than 70 volume per cent argon and a total pressure of 1,3 atmospheres would consistently yield  $\eta$  of between 0,120 and 0,140. Below 70 volume per cent greater pressures were necessary to obtain reproducible catalyst loadings. Naturally it would have been theoretically possible to reduce the catalyst particle size and employ higher channel pressures. However from practical considerations these variables were near their limiting values already because of the following reasons;

- (a) too small a particle size resulted in difficult control of the fluidised catalyst reduction process often resulting in carry-over and sintering.
- (b) too high a channel pressure necessitated high diaphragm pressure differentials to attain temperatures in the region of  $1300^{\circ}\text{K}$ . With differentials greater than 85 atmospheres good petalling of the diaphragm was difficult to achieve and instead the diaphragm shattered, propelling fragments down the channel.

It was decided therefore, to allow  $\eta$  to take on values between 0,120 and 0,140.

#### 4.5.3 Temperature, Partial Pressure of Reactants and Dwell Time

Temperatures between 600 and  $1400^{\circ}\text{K}$  were desired. By manipulating the following variables it is possible to obtain different shocked gas temperatures, pressures and dwell times.

- 1 Chamber gas composition and temperature
- 2 Diaphragm pressure ratio  $P_4/P_1$
- 3 Channel fluid composition (gas plus catalyst)

Temperature and partial pressure of reactants in the shocked state are very closely linked to  $P_4/P_1$  and fluid properties, whereas the dwell time is a function mainly of shock tube geometry. Temperature and pressure could be varied independently of each other by manipulating  $P_4/P_1$  ratio and channel fluid composition simultaneously. However since variations in the channel fluid composition were greatly restricted by catalyst transportation requirements no attempts were made to effect such independent variations.

In the heterogeneous shock tube dwell times are most effectively altered by changing the length of the chamber. The tube was therefore provided with a chamber consisting of two parts of equal length. It was decided to begin tests using the longer chamber and if hydrocarbon yields were high enough and shock deceleration low enough then the shorter chamber would be employed.

From inspection of equation 3.1.2.X the strongest possible shock is obtained when

$$P_4/P_1 \rightarrow \infty \text{ and then } M_1 \rightarrow \frac{\gamma_1+1}{\gamma_4-1} \cdot \frac{a_4}{a_1}$$

The strongest shocks are thus obtained by using a chamber gas having a high speed of sound and low specific heat ratio. For these reasons a low density gas such as hydrogen or helium is often used. As channel pressures would be high (by shock tube standards) in order to facilitate catalyst transport, it was decided to use hydrogen as chamber gas so that diaphragm pressure differentials could be minimised; see Chapter 4.5.2, paragraph (b). According to preliminary calculations facilities for heating the chamber gas would not be required for shock temperatures up to 1400°K provided, (a) hydrogen was used, (b) channel fluid pressure  $P_1$  did not exceed 1,5 atmospheres, and (c) channel fluid consisted of at least 80 volume per cent argon.

Two aspects disfavoured the use of hydrogen as chamber gas; (i) hydrogen was a reactable and would increase the  $H_2/CO$  ratio in the vicinity of the contact surface, and (ii) hydrogen would upset hydrogen balance calculations performed in the gas mixture after shocking. These objections were over-ruled by the following reasoning. Firstly the rapidly expanded low temperature hydrogen in the vicinity of the contact surface would merely quench reaction and secondly a hydrogen balance would be very difficult anyway as it was expected that conversion would be extremely low.

Since only one ratio of  $H_2/CO$  was to be investigated, the most suitable had to be chosen.

Anderson et al (1964) studied the effect of  $H_2/CO$  ratio on selectivity. Table 4.5.3.I summarises some of their findings. One objective of this work was to determine the extent of degradation, if any, of hydrocarbons to methane within the first milli-second of reaction. Using the results of Anderson et al, an  $H_2/CO$  ratio of 1 was chosen since the selectivity of methane was average and the differential reaction rate was in the upper regions.

TABLE 4.5.3.I

INFLUENCE OF H<sub>2</sub>/CO RATIO ON METHANE SELECTIVITY  
(ANDERSON ET AL (1964))

System:- Nitrided iron catalyst, 21,4 atmospheres and 240°C		
H <sub>2</sub> /CO	Methane production at 10% conversion. moles CH <sub>4</sub> /mole of H <sub>2</sub> + CO consumed	Maximum differential reaction rate at zero conversion.
2	0,07	300
1	0,045	290
0,7	0,045	275
0,25	0,025	210

#### 4.5.4 Catalyst Reduction

The extent of catalyst reduction was not expected to be important provided it was greater than 50 per cent (Dorling et al (1958)). In the short reaction periods only surface in the outer crust of the catalyst particle would be effective; see Chapter 3.2.2. Reduction extents between 77 and 85 per cent were employed.

Reduction temperature was expected to be very important as it has a great influence on catalyst surface area (Anderson et al (1964)). For reasons stated in Chapter 5.1 it was necessary to ensure that total surface areas of unreduced and reduced catalysts did not vary substantially hence a reduction temperature of 600°C was chosen; (see also Appendix G).

Surface area of unreduced catalyst                      1,0 m<sup>2</sup>/g

surface area of reduced catalyst (600°C)            1,4 m<sup>2</sup>/g.

#### 4.5.5 Regression Analysis

Twelve experiments were conducted and regression analysis used to determine major variables. Variables took on the following values,

reaction temperature T	782 - 1121 <sup>o</sup> K
reactables partial pressure P	1,61 - 3,03 atmos.
channel pressure P <sub>1</sub>	1,36 atmos. (constant)
channel gas composition	argon 80-87 vol.per cent, H <sub>2</sub> /CO=1
average dwell time t <sub>FD</sub>	0,628 - 0,681 m.sec.
catalyst loading η	0,120 - 0,140
catalyst reduction R <sub>D</sub>	0,77 - 0,85

Linear and exponential models were found suitable for the two major products, methane and ethylene. A Computer Sciences Sigma Ltd. library programme entitled \*\*\*STEPW1 which performed a stepwise multilinear regression analysis was used.

Independent variables were taken to be reaction temperature T, reactants' partial pressure P, average dwell time t<sub>FD</sub>, catalyst loading η, and catalyst reduction R<sub>D</sub>. The dependent variable was apparent hydrocarbon yield Y.

Models took the forms,

$$Y = \alpha_0 + \alpha_1 T + \alpha_2 P + \alpha_3 t_{FD} + \alpha_4 \eta + \alpha_{12} P T + \alpha_{13} T t_{FD} + \alpha_{14} T \eta + \alpha_{23} P t_{FD} + \alpha_{34} t_{FD} \eta \quad (i)$$

or (i) with  $\alpha_{24} P \eta$  instead of  $\alpha_{34} t_{FD} \eta$  (ii)

or (i) with  $\alpha_{4D} R_D$ ,  $\alpha_{14D} T R_D$  and  $\alpha_{34D} t_{FD} R_D$  instead of  $\alpha_4 \eta$ ,  $\alpha_{14} T \eta$  and  $\alpha_{34} t_{FD} \eta$  respectively (iii)

or (iii) with  $\alpha_{24D} P R_D$  instead of  $\alpha_{34D} t_{FD} R_D$  (iv)

or (i), (ii), (iii) and (iv) excluding one or more terms

$$Y = \alpha_0 P^{\alpha_2} t_{FD}^{\alpha_3} \eta^{\alpha_4} R_D^{\alpha_5} e^{(-\frac{E}{RT})} \quad (v)$$

or (v) excluding one or more terms.

Table 4.5.5.I depicts the regression results for methane with model types (i), (ii), (iii), (iv) and (v), while ethylene model types (i), (ii), (iii), (iv) and (v) are contained in Table 4.5.5.II.

Variables immediately beneath the horizontal dashed line in Tables 4.5.5.I & II having partial F values below the 5 per cent level are regarded insignificant for experimental design purposes: Note

$F_{1,9} (5\%) = 5,12$ . Coefficients for variables were:-

Methane models	Coefficient	Standard Deviation
(i) to (iv)	$\alpha_{12} (PT) = 0,00131$	0,000316
	$\alpha_2 (P) = -1,11$	0,473
(i) to (iv) excl. PT,	$\alpha_{13} (Tt_{FD}) = 0,00436$	0,000265
(i) to (iv) excl. PT & $Tt_{FD}$ ,	$\alpha_1 (T) = 0,00357$	0,000231
Methane model (v)	$\alpha_3 (\ln t_{FD}) = 13,35$	0,814
excl. $t_{FD}$ ,	E/R = 3070	213
excl. $t_{FD}$ & T,	$\alpha_2 (\ln P) = 1,83$	0,145
Ethylene models		
(i) to (iv)	$\alpha_{12} (PT) = 0,000329$	0,0000436
(i) & (ii) excl. PT,	$\alpha_{23} (Pt_{FD}) = 11,44$	4,38
	$\alpha_2 (P) = -8,08$	3,29
(iii) & (iv) excl. PT,	$\alpha_{23} (Pt_{FD}) = 19,19$	3,82
	$\alpha_2 (P) = -13,38$	2,77
	$\alpha_{14} (TR_D) = -0,00262$	0,00079
(i) to (iv) excl. PT & $Pt_{FD}$ ,	$\alpha_3 (t_{FD}) = 11,94$	1,68
(v)	$\alpha_3 (\ln t_{RD}) = 35,15$	1,70
	$\alpha_5 (\ln R_D) = -4,95$	1,92
	$\alpha_4 (\ln \eta) = -2,67$	1,12
(v) excl. $t_{RD}$ ,	$\alpha_2 (\ln P) = 4,40$	0,340
(v) excl. $t_{RD}$ & P,	E/R = 7279	618

TABLE 4.5.5.I

## REGRESSION RESULTS - METHANE

Model type	Re-gres-sion step	Variable	Proportion of vari-able of Y reduced	Partial F	F for analysis of variance	Multiple correlation coefficient
CH <sub>4</sub> (i)	1	PT	0,968	1-10=302	1-10=302	0,9838
	2	P	0,0122	1-9=5,54	2-9=222	0,9900
	3	Pt <sub>FD</sub>	0,00155	1-8=0,679		
excl.PT	1	Tt <sub>FD</sub>	0,964	1-10=271	1-10=271	0,9820
	2	T	0,00509	1-9=1,50		
excl.PT & Tt <sub>FD</sub>	1	T	0,960	1-10=238	1-10=238	0,9796
	2	Pt <sub>FD</sub>	0,00758	1-9=2,08		
CH <sub>4</sub> (ii)	1	PT	0,968	1-10=302	1-10=302	0,9839
	2	P	0,122	1-9=5,54	2-9=222	0,9900
	3	Pt <sub>FD</sub>	0,00155	1-8=0,679		
excl.PT	1	Tt <sub>FD</sub>	0,964	1-10=271	1-10=271	0,9820
	2	P $\eta$	0,00588	1-9=1,78		
excl.PT & Tt <sub>FD</sub>	1	T	0,960	1-10=238	1-10=238	0,9796
	2	P $\eta$	0,00918	1-9=2,65		
CH <sub>4</sub> (iii)	1	PT	0,968	1-10=302	1-10=302	0,9839
	2	P	0,0122	1-9=5,54	2-9=222	0,9900
	3	Pt <sub>FD</sub>	0,00155	1-8=0,679		
excl.PT	1	Tt <sub>FD</sub>	0,964	1-10=271	1-10=271	0,9820
	2	T	0,00509	1-9=1,50		
excl.PT & Tt <sub>FD</sub>	1	T	0,960	1-10=238	1-10=238	0,9796
	2	Pt <sub>FD</sub>	0,00758	1-9=2,08		
CH <sub>4</sub> (iv)	1	PT	0,968	1-10=302	1-10=302	0,9838
	2	P	0,0122	1-9=5,54	2-9=222	0,9900
	3	Pt <sub>FD</sub>	0,00155	1-8=0,679		
excl.PT	1	Tt <sub>FD</sub>	0,964	1-10=271	1-10=271	0,9820
	2	T	0,00509	1-9=1,50		
CH <sub>4</sub> (iv) excl.PT & Tt <sub>FD</sub>	1	T	0,960	1-10=238	1-10=238	0,9796
	2	Pt <sub>FD</sub>	0,00758	1-9=2,08		
CH <sub>4</sub> (v)	1	ln t <sub>FD</sub>	0,964	1-10=269	1-10=269	0,9819
	2	ln $\eta$	0,001711	1-9=0,451		
excl.t <sub>FD</sub>	1	-1/T	0,954	1-10=208	1-10=208	0,9768
	2	ln P	0,00576	1-9=1,29		
excl.t <sub>FD</sub> & T	1	ln P	0,941	1-10=160	1-10=160	0,9701
	2	ln $\eta$	0,00219	1-9=0,349		



TABLE 4.5.5.II

## REGRESSION RESULTS - ETHYLENE

Model type	Re-gres-sion step	Variable	Proportion of vari-able of Y reduced	Partial F	F for analysis of variance	Multiple correlation coefficient
C <sub>2</sub> H <sub>4</sub> (i)	1	PT	0,850	1-10=56,7	1-10=56,7	0,9220
	2	T η	0,0171	1- 9 =1,16		
excl.PT	1	Pt <sub>FD</sub>	0,839	1-10=52,3	1-10=52,3	0,9162
	2	P <sub>FD</sub>	0,0646	1- 9 =6,05	2- 9 =42,4	0,9508
excl.PT & Pt <sub>FD</sub>	3	T η	0,0346	1- 8 =4,52		
	1	t <sub>FD</sub>	0,835	1-10=50,6	1-10=50,6	0,9138
C <sub>2</sub> H <sub>4</sub> (ii)	2	P	0,00538	1- 9 =0,303		
	1	PT	0,850	1-10=56,7	1-10=56,7	0,9220
C <sub>2</sub> H <sub>4</sub> (ii)	2	P η	0,0356	1- 9 =2,80		
	1	Pt <sub>FD</sub>	0,839	1-10=52,3	1-10=52,3	0,9162
excl.PT	2	P	0,0646	1- 9 =6,05	2- 9 =42,4	0,9508
	3	T η	0,0346	1- 8 =4,52		
excl.PT & Pt <sub>FD</sub>	1	t <sub>FD</sub>	0,835	1-10=50,6	1-10=50,6	0,9139
	2	P	0,00538	1- 9 =0,303		
C <sub>2</sub> H <sub>4</sub> (iii)	1	PT	0,850	1-10=56,7	1-10=56,7	0,9220
	2	R <sub>D</sub>	0,0179	1- 9 =1,22		
excl.PT	1	Pt <sub>FD</sub>	0,839	1-10=52,3	1-10=52,3	0,9162
	2	P <sub>FD</sub>	0,0646	1- 9 =6,05	2- 9 =42,4	0,9508
excl.PT & Pt <sub>FD</sub>	3	TR <sub>D</sub>	0,0555	1- 8 =10,97	3- 8 =63,2	0,9795
	4	t <sub>FD</sub>	0,00171	1- 7 =0,308		
excl.PT & Pt <sub>FD</sub>	1	t <sub>FD</sub>	0,835	1-10=50,6	1-10=50,6	0,9138
	2	R <sub>D</sub>	0,0162	1- 9 =0,981		
C <sub>2</sub> H <sub>4</sub> (iv)	1	PT	0,850	1-10=56,7	1-10=56,7	0,9220
	2	PR <sub>D</sub>	0,0288	1- 9 =2,14		
excl.PT	1	Pt <sub>FD</sub>	0,839	1-10=52,3	1-10=52,3	0,9162
	2	P <sub>FD</sub>	0,0646	1- 9 =6,05	2- 9 =42,4	0,9508
excl.PT & Pt <sub>FD</sub>	3	TR <sub>D</sub>	0,0555	1- 8 =10,97	3- 8 =63,2	0,9795
	4	t <sub>FD</sub>	0,00171	1- 7 =0,308		
excl.PT & Pt <sub>FD</sub>	1	t <sub>FD</sub>	0,835	1-10=50,6	1-10=50,6	0,9138
	2	R <sub>D</sub>	0,0162	1- 9 =0,981		
C <sub>2</sub> H <sub>4</sub> (v)	1	ln t <sub>FD</sub>	0,960	1-10=240	1-10=240	0,9798
	2	ln R <sub>D</sub>	0,0142	1- 9 =4,94	2- 9 =170	0,9870
	3	ln η	0,0108	1- 8 =5,73	3- 8 =174	0,9924
	4	-1/T	0,00222	1- 7 =1,21		
excl.t <sub>FD</sub>	1	ln P	0,944	1-10=168	1-10=168	0,9714
	2	ln η	0,0117	1- 9 =2,36		
excl.t <sub>FD</sub> & P	1	-1/T	0,933	1-10=139	1-10=139	0,9658
	2	ln η	0,0167	1- 9 =2,97		

Clearly the important variables are  $T$ ,  $P$ ,  $t_{FD}$ ,  $PT$  and  $Pt_{FD}$ . Variations in catalyst reduction and loading over the ranges used are insignificant since negative coefficients for these two variables, as obtained in the ethylene model (v), are meaningless. This is supported by the results of ethylene model (v) with  $t_{FD}$  and  $t_{FD}$  plus  $P$  excluded.

Since  $\alpha_2$  is negative and  $\alpha_1$  positive in the linear models for methane,  $T$  itself must make a large positive contribution. The negative  $\alpha_2$  is in agreement with Anderson et al (1964) who found that methane production over iron catalyst decreased with increasing pressure. Negative values for  $\alpha_2$  in the case of ethylene is contradictory to the findings of Anderson et al who reported olefin production to be independent of pressure.

#### 4.5.6 Conclusion

Since hydrocarbon yields were very small, the question of increasing the dwell times was re-considered at this stage. A preliminary estimate of real reaction time was obtained; see Chapter 3.3. It was found that for run 16 the average time to quench from  $1100^\circ\text{K}$  to  $800^\circ\text{K}$  was approximately 1 millisecond which meant an average real reaction time of about 1,7 milliseconds; there being no significant reaction at  $800^\circ\text{K}$ . If run 16 were to be repeated using a longer chamber, quenching would be even slower. As the accuracy of the method used to determine quench rate was unknown it was decided not to embark on experiments having slower quench rates for fear of incorporating greater errors.

Further experiments were carried out at higher temperatures, pressures and dwell times by varying only the diaphragm pressure ratio  $P_4/P_1$ . No attempt was made to vary any particular variable independently. Since it is impossible to reproduce exactly a particular reaction environment in a heterogeneous shock tube, scatter in variables would always be present.

It was clear at this stage that special attention would have to be paid to assessing the extent of reaction during quenching of

the incident shock wave by the reflected rarefaction wave.

Experiments without catalyst would be undertaken to check for possible homogeneous reaction and hence determine yield due to surface reaction only.

---

## CHAPTER 5

### EXPERIMENTAL RESULTS AND DISCUSSION

#### 5.1 Introduction

The purpose of this work was twofold. Firstly it was an investigation into the character of the initial reaction steps of the Fischer-Tropsch synthesis at elevated temperatures with special reference to the formation of methane. Secondly it developed techniques for defining the reaction environment realised when a shock tube is used as a research tool in the study of heterogeneous catalysis.

The experiment was designed to establish the extent of the dependence of reaction on the degree of activity of the catalyst and whether there was a parallel gas phase reaction. Hence a set of runs was carried out utilising catalysts of varying degree of activity and another set with no catalyst at all but with low concentrations of gaseous hydrocarbons to act as possible chain initiators.

Information gleaned on the Fischer-Tropsch synthesis has been discussed in Chapters 5.1 through 5.8, while the development of a rate equation for the synthesis as carried out in a shock tube, using multilinear regression analysis, has been presented in Chapter 5.5.1.1. The usefulness of such initial rate data for the development of new concepts in commercial reactor design has been discussed in Chapter 5.8.

#### 5.2 Summary

For ease of reference this summary has been depicted in the form of a logic diagram, see overleaf. In the blocks constituting the diagram, reference has been made to the Chapters in which the particular topic is discussed. Paragraph designation below corresponds to that of the blocks in the logic diagram.

A Consistency of hydrocarbon analysis  
Chapter 5.3

Reasonable consistency was observed.

Homogeneous

Heterogeneous

B Pre-shock circulation of test gas  
Chapter 5.3

Composition remained essentially constant during circulation period.

D Pre-shock contact between test gas & catalyst  
Chapter 5.4

Increase in hydrocarbon content was observed.

E Shock results (heterogeneous case)  
Chapter 5.5

Synthesis of hydrocarbons was observed

C Shock results (homogeneous case)  
Chapters 5.5.1 & 5.6

Synthesis of hydrocarbons was observed.

D1 Rate dependence on contact period duration  
Chapter 5.4.1

Rate remained constant but reaction extent varied directly with contact period duration.

D2 Rate dependence on initial hydrocarbon content of test gas  
Chapter 5.4.2

Methane synthesis rate varied inversely with initial hydrocarbon content.

D3 Rate dependence on catalyst activity  
Chapter 5.4.3

No significant dependence was observed.

Rate dependence on Temperature & Pressure  
Chapters 5.5.1 & 5.6

Rate was only slightly dependent on these parameters.

C2 Rate dependence on hydrocarbons initially present  
Chapters 5.5.3

No dependence observed.

E1 Rate dependence on temperature and pressure  
Chapter 5.5.1

Hydrocarbon synthesis rate varied directly with shock strength. No pressure dependence was observed.

E2 Rate dependence on contact period duration  
Chapter 5.5.2

Hydrocarbon synthesis rate varied directly with contact period duration.

E3 Rate dependence on initial hydrocarbon content of test gas  
Chapter 5.5.3

Hydrocarbon synthesis was not influenced by these impurities.

E4 Rate dependence on catalyst activity  
Chapter 5.5.4

Synthesis rate varied directly with catalyst activity for paraffin production: No dependence in case of olefins.

F Conclusion and Recommendations for future work  
Chapters 5.7 & 5.8

See text.

Table 5.2.I summarises the scope of the experimental runs performed in this work, while Table 5.2.II contains particulars of all successful shock wave experiments carried out.

A, B Consistency of hydrocarbon analysis and pre-shock circulation of test gas

Chapters 5.3 and 5.4.1

Before being introduced into the shock tube system gases were mixed in a Simet gas mixer. By analysing these gases before mixing and, after mixing and circulating in the shock tube system for different periods of time, it was possible to check whether the system had any influence on the hydrocarbon impurities present in these gases as supplied.

Overall the hydrocarbon concentrations appeared to be stable in the equipment. Variations observed were significantly smaller than changes due to low temperature Fischer-Tropsch reaction. It was concluded that adsorption onto or desorption from equipment surfaces was negligible.

C Shock results (homogeneous case)

Chapters 5.5.1 and 5.6

Test gas was subjected to shock waves of various strengths; Mach numbers 2,4 - 3,4; and it was observed that hydrocarbon synthesis took place. The inference was that Fischer-Tropsch synthesis had proceeded without the aid of a catalyst at elevated temperatures (900 - 1300<sup>o</sup>K). The products detected, in order of descending amounts, were methane, ethylene, propylene and ethane.

C1 Rate dependence on temperature and pressure

Chapters 5.5.1 and 5.6

Slight rate dependence on these parameters was observed. Reaction rate varied directly with shock strength up to 1100<sup>o</sup>K, thereafter it appeared to stabilise.

TABLE 5.2.I

Item	Specification
Chamber Gas	Hydrogen
Channel Gas	Argon 81 - 87 mol.% Hydrogen 6,5 - 9 mol.% Carbon Monoxide 6,5 - 9,5 mol.%
Catalyst Loading	0 - 0,140 mass ratio (catalyst/gas)
Type of Catalyst	Fused iron triply promoted with K <sub>2</sub> O, MgO and SiO <sub>2</sub>
Catalyst Pre-Treatment	Reduced - 77 - 92 % reduction Reoxidised - reduced & exposed to air Unreduced - as received from supplier
Catalyst Surface Area	Unreduced - 1,0 m <sup>2</sup> /g Reduced (600°C) - 1,4 m <sup>2</sup> /g
Reaction Temperature	780 - 1425 °K
Reaction Pressure	160 - 330 psia
Mean Reaction Times	0,628 - 0,727 milliseconds

TABLE 5.2.II SHOCK WAVE EXPERIMENTS

Run No.	Relaxed State 2		Mean Shock Velocity cm/sec.	Channel Gas Composition vol. %			Channel Gas		Catalyst Loading Mass Cat. Mass Gas $\eta$	Catalyst Reduction Fraction of Oxygen Removed $R_D$	Chamber Gas (Hydrogen)		Diaphragm Pressure Ratio $P_4/P_1$	Partial Press. of Reactants (H <sub>2</sub> +CO) in Relaxed State 2 atm.(abs.)	Mean Dwell Time $t_{FD}$ m.sec.
	Temp. $T_e$ $^{\circ}K$	Press. $P_e$ psia		Ar	H <sub>2</sub>	CO	Temp. $T_1$ $^{\circ}K$	Press. $P_1$ psia			Temp. $T_4$ $^{\circ}K$	Press. $P_4$ psia			
4	932	210	91200	84	8	8	298	20,0	,120	,82	298	765	38,25	2,14	,655
5	938	214	91040	85	7,5	7,5	"	"	,134	,80	"	765	38,25	2,18	,655
6	782	162	80070	85	7,5	7,5	"	"	,120	,79	"	615	30,75	1,65	,628
8	953	218	91740	86	7	7	"	"	,130	,77	"	765	38,25	2,07	,655
9	916	205	89700	85	7,5	7,5	"	"	,125	,82	"	765	38,25	2,09	,653
0	825	177	82750	86	7	7	"	"	,133	,80	"	615	30,75	1,68	,633
2	804	169	81250	86	7	7	"	"	,130	,82	"	615	30,75	1,61	,631
4	1079	262	100900	83	8,5	8,5	"	"	,140	,82	"	965	48,25	3,03	,681
5	1048	249	98700	84	8	8	"	"	,130	,80	"	965	48,25	2,71	,679
5	1100	266	101300	85	7,5	7,5	"	"	,135	,85	"	965	48,25	2,71	,680
7	1121	273	102600	85	7,5	7,5	"	"	,136	,81	"	965	48,25	2,78	,681
8	914	213	90500	85	7,5	7,5	"	"	,134	0	"	765	38,25	2,18	,656
1	1024	248	97500	86	7	7	"	"	,130	0	"	965	48,25	2,36	,678

continued

Page 33



TABLE 5.2.II SHOCK WAVE EXPERIMENTS Continued

Run No.	Relaxed State 2		Mean Shock Velocity cm/sec.	Channel Gas Composition vol. %			Channel Gas		Catalyst Loading Mass Cat. Mass Gas $\eta$	Catalyst Reduction Fraction of Oxygen Removed $R_D$	Chamber Gas (Hydrogen)		Diaphragm Pressure Ratio $P_4/P_1$	Partial Press. of Reactants ( $H_2+CO$ ) in Relaxed State 2 atm(abs.)	Mean Dwell Time $t_{FD}$ m.sec.
	Temp. $T_e$ $^{\circ}K$	Press. $P_e$ psia		Ar	$H_2$	CO	Temp. $T_1$ $^{\circ}K$	Press. $P_1$ psia			Temp. $T_4$ $^{\circ}K$	Press. $P_4$ psia			
20	1103	267	102100	84	8	8	298	20,0	,130	,80	298	965	48,25	2,90	,681
21	830	177	83100	86	7	7	"	"	,128	,86	"	615	30,75	1,69	,634
22	932	211	90140	86	7	7	"	"	,138	,86	"	765	38,25	2,01	,654
23	1125	273	101850	87	6,5	6,5	"	"	,140	,86	"	965	48,25	2,42	,679
24	1216	268	110100	86	7	7	"	"	0	0	"	965	48,25	2,55	,693
25	1085	259	99940	86	7	7	"	"	,133	,86	"	965	48,25	2,47	,679
26	948	216	91300	86	7	7	"	"	,133	,82	"	765	38,25	2,05	,655
27	797	167	80800	86	7	7	"	"	,128	,78	"	615	30,75	1,59	,630
28	1221	270	110900	85	7,5	7,5	"	"	0	0	"	965	48,25	2,76	,694
29	1015	247	96850	86	7	7	"	"	,135	0	"	965	48,25	2,35	,678
30	1034	252	98150	86	7	7	"	"	,130	0	"	965	48,25	2,40	,679
31	843	162	86200	86	7	7	"	"	0	0	"	615	30,75	1,55	,634
32	863	168	87650	86	7	7	"	"	0	0	"	615	30,75	1,60	,637

continued

TABLE 5.2.II SHOCK WAVE EXPERIMENTS Continued

Run No.	Relaxed State 2		Mean Shock Velocity cm/sec.	Channel Gas Composition vol. %			Channel Gas		Catalyst Loading Mass Cat. Mass Gas $\eta$	Catalyst Reduction Fraction of Oxygen Removed $R_D$	Chamber Gas (Hydrogen)		Diaphragm Pressure Ratio $P_4/P_1$	Partial Press. of Reactants ( $H_2 + CO$ ) in Relaxed State 2 atm(abs.)	Mean Dwell Time $t_{FD}$ m.sec.
	Temp. $T_e$ $^{\circ}K$	Press. $P_e$ psia		Ar	$H_2$	CO	Temp. $T_1$ $^{\circ}K$	Press. $P_1$ psia			Temp. $T_4$ $^{\circ}K$	Press. $P_4$ psia			
34	1194	297	109000	81	9,5	9,5	298	20,0	,125	,80	298	1265	63,25	3,86	,712
36	1259	320	112100	82	9	9	"	"	,135	,80	"	1265	63,25	3,90	,713
37	1240	313	111000	82	9	9	"	"	,134	,82	"	1265	63,25	3,82	,712
38	1269	314	110200	87	6,5	6,5	"	"	,123	,92	"	1265	63,25	2,80	,709
39	1305	329	111950	87	6,5	6,5	"	"	,135	,90	"	1265	63,35	2,89	,709
40	1287	321	111150	87	6,5	6,5	"	"	,125	,92	"	1265	63,25	2,85	,709
41	1342	307	118800	83	8,5	8,5	"	"	0	0	"	1265	63,25	3,55	,726
42	1392	322	121500	83	8,5	8,5	"	"	0	0	"	1265	63,25	3,72	,727
43	1130	284	105450	83	8,5	8,5	"	"	,125	0	"	1265	63,25	3,29	,710
44	1107	277	104050	83	8,5	8,5	"	"	,125	0	"	1265	63,25	3,20	,708
45	1366	312	118950	85	7,5	7,5	"	"	0	0	"	1265	63,25	3,18	,725

continued

TABLE 5.2.II SHOCK WAVE EXPERIMENTS Continued

Run No.	Relaxed State 2		Mean Shock Velocity cm/sec.	Channel Gas Composition vol. %			Channel Gas		Catalyst Loading Mass Cat. Mass Gas $\eta$	Catalyst Reduction Fraction of Oxygen Removed $R_D$	Chamber Gas (Hydrogen)		Diaphragm Pressure Ratio $P_4/P_1$	Partial Press. of Reactants ( $H_2+CO$ ) in Relaxed State 2 atm. (abs.)	Mean Dwell Time $t_{FD}$ m. sec.
	Temp. $T_e$ $^{\circ}K$	Press. $P_e$ psia		Ar	$H_2$	$CO$	Temp. $T_1$ $^{\circ}K$	Press. $P_1$ psia			Temp. $T_4$ $^{\circ}K$	Press. $P_4$ psia			
46	1423	328	121950	85	7,5	7,5	298	20,0	0	0	298	1265	63,25	3,34	,725
48	1409	323	120650	86	7	7	"	"	0	0	"	1265	63,25	3,07	,724
52	1239	307	109170	86	7	7	"	"	,123	,80	"	1265	63,25	2,92	,710
53	1363	310	118250	86	7	7	"	"	0	0	"	1265	63,25	2,95	,724
55	1243	309	109250	86	7	7	"	"	,128	,86	"	1265	63,25	2,95	,709
56	1292	326	112030	86	7	7	"	"	,130	,80	"	1265	63,25	3,10	,710
58	1260	315	110200	86	7	7	"	"	,130	,82	"	1265	63,25	3,00	,710
0	1017	212	98500	85	7,5	7,5	"	"	0	0	"	765	38,25	2,16	,667
1	1023	214	98900	85	7,5	7,5	"	"	0	0	"	765	38,25	2,18	,667

From thermodynamic considerations it was reasoned that the homogeneous reaction was probably not one involving polymerisation of  $\text{CH}_2$  free radicals but simply a molecular process.

C2 Rate dependence on hydrocarbons initially present

Chapter 5.5.3

No correlation was observed between shock yields and quantities of hydrocarbons present initially. The range of initial hydrocarbon concentrations investigated was 0,3 - 70 volume ppm.

D Pre-shock contact between test gas and catalyst

Chapter 5.4

Test gas and catalyst were circulated in the shock tube system for varying times before introduction of the shock wave. This was done primarily to obtain even distribution of the catalyst within the gas, but also to observe to what extent adsorption of hydrocarbon impurities onto the catalyst would take place. During this period of circulation, or contact period, hydrocarbon synthesis was observed.

Owing to the low temperature,  $40^\circ\text{C}$ , the extent of synthesis was small but nevertheless detectable. Products were methane, ethylene, ethane and propylene in order of descending quantities. A very interesting feature of this reaction was that methane was by a large margin the major product even at such low temperatures.

D1 Rate dependence on contact period duration

Chapter 5.4.1

As the contact period was extended the observed rate of hydrocarbon synthesis was essentially unaffected. The extent of reaction (amounts of hydrocarbons produced) was directly dependent on contact period duration.

Owing to the very small extent of reaction and also on account of the experimental conditions not having been carefully controlled during this pre-shock period, it was difficult to comment on reaction characteristics under these conditions.

D2 Rate dependence on initial hydrocarbon content of test gas

## Chapter 5.4.2

As the gas bulk concentration of methane increased suppression of methane production was observed. It was concluded that the rate of desorption of methane was controlled by its gas bulk concentration.

It was impossible to comment on the other reaction products due to their very much lower concentrations being more severely influenced by experimental error.

D3 Rate dependence on catalyst activity

## Chapter 5.4.3

During the contact period no significant relationship between reaction rate and catalyst pre-treatment could be detected and it was inferred that the surface reaction was not a limiting step at these low temperatures.

E Shock results (heterogeneous case)

## Chapter 5.5

Shock strengths between Mach numbers 2,4 and 3,4 were passed through test mixtures of gas and catalyst. Detectable yields of methane, ethylene, ethane and propylene were observed. In all cases the lighter molecular weight hydrocarbons were formed in preference except that propylene was formed in preference to ethane.

E1 Rate dependence on temperature and pressure

## Chapter 5.5.1

Generally, the rate of hydrocarbon synthesis was observed to vary directly with shock strength. In the case of very active catalysts (reduced type) synthesis rate increased exponentially with increasing shock strength. With inactive catalyst this dependence was much lower.

A rate equation was developed and fitted to the observed overall surface reaction. From the form of this equation and other consi-

derations it was concluded that the process as conducted in the shock tube was hydrogen adsorption controlled, but independent of pressure.

#### E2 Rate dependence on contact period duration

##### Chapter 5.5.2

It was observed that a long contact period was advantageous for Fischer-Tropsch synthesis to proceed under shock conditions. The main reason for this appeared to be the relatively slow rate of adsorption of carbon monoxide during the contact period; long contact period runs had larger CO/H<sub>2</sub> ratios on the catalyst surface when the shock reaction began.

#### E3 Rate dependence on initial hydrocarbon content of test gas

##### Chapter 5.5.3

The results and discussion showed that hydrocarbons present in the gas before shocking had no observable effect on reaction rate or product spectrum.

#### E4 Rate dependence on catalyst activity

##### Chapter 5.5.4

Paraffin yields increased with increasing catalyst activity. Conversely, olefin production appeared to be independent of catalyst activity between 900°K and 1150°K.

#### F Conclusion and recommendations for future work

##### Chapters 5.7 and 5.8

Inspection of product selectivities led to the conclusion that even at elevated temperatures degradation processes were negligible and for the most part, methane was formed at the beginning of reaction. Results favoured Pichler's reaction mechanism.

Conclusions drawn from the results pointed to aspects worth investigation in regard to decreasing methane yield and narrowing the product spectrum of the Kellogg synthesis; namely (i) higher initial reaction temperature, (ii) lower H<sub>2</sub>/CO ratio and (iii) steam, carbon dioxide and carbon monoxide injection at various stages of reaction.

---

### 5.3 Check on Consistency of Gas Analysis of Hydrocarbons

A comparison has been made between the gas analysis expected after passage through the Simet gas mixer and that actually obtained from samples taken after a given period of circulation in the shock tube system. The expected hydrocarbon analysis was calculated from the analysis of the individual gases which appears in Table 5.3.II.

The test gas for runs 41 and 42 comprised hydrogen, carbon monoxide and argon (cylinder 3) in a volume ratio of 1:1:8 respectively.

Hence the expected hydrocarbon composition of the mixture would be as shown in Table 5.3.I. In the other cases the test gas was SASOL gas: argon as 1:4; SASOL gas being hydrogen: carbon monoxide as 1:1.

Generally, for each run there was good agreement between gas samples taken from the apparatus at different times after the start of circulation; see Table 5.3.I. Runs 60, 32, 28 and 30 showed some scatter in the analyses.

Expected hydrocarbon compositions have been tabulated in order to check whether the apparatus had any influence on the hydrocarbon content of the gas. Differences are present but it has been taken that the the hydrocarbon concentrations were stable in the equipment.

### 5.4 Pre-Shock Contact between Gas and Catalyst

On addition of catalyst to the premixed test gas it was observed that the hydrocarbon content of the gas increased with time. Since desorption of hydrocarbons previously adsorbed to the walls of the shock tube system could not explain the large increases in hydrocarbons observed here it was concluded that reaction at room temperature had occurred.

The effects of the following have been discussed in this section.

- 5.4.1 Contact period duration,
- 5.4.2 Hydrocarbons present initially,
- 5.4.3 Catalyst activity.

TABLE 5.3.I

Run No.	Expected Hydrocarbon Composition Vol.ppm					Measured Hydrocarbon Composition Vol.ppm					Sample Time After Starting Circulatory Blower Min.
	CH <sub>4</sub>	C <sub>2</sub> H <sub>4</sub>	C <sub>2</sub> H <sub>6</sub>	C <sub>3</sub> H <sub>6</sub>	C <sub>3</sub> H <sub>8</sub>	CH <sub>4</sub>	C <sub>2</sub> H <sub>4</sub>	C <sub>2</sub> H <sub>6</sub>	C <sub>3</sub> H <sub>6</sub>	C <sub>3</sub> H <sub>8</sub>	
21	1,0	<0,1	<0,1	<0,1	<0,1	2,39	0,06	0,06	<0,04	<0,04	5
						1,82	0,07	0,09	"	"	10
22	"	"	"	"	"	1,65	0,09	0,13	"	"	5
						1,48	0,11	0,07	"	"	10
23	"	"	"	"	"	1,66	0,10	0,15	"	"	5
						2,04	0,09	0,10	"	"	10
25	"	"	"	"	"	1,36	-	-	0,47	0,99	5
						-	0,07	0,12	<0,04	<0,04	10
26	"	"	"	"	"	0,27	0,11	0,13	"	"	5
						0,19	0,08	0,04	"	"	10
27	"	"	"	"	"	0,51	0,05	0,05	"	"	5
29	1,0	<0,1	<0,1	<0,1	<0,1	0,38	<0,04	<0,04	<0,04	<0,04	15
						0,46	"	"	"	"	20
30	"	"	"	"	"	2,76	"	"	"	"	15
						3,41	0,08	0,25	"	"	20
24	1,0	<0,1	<0,1	<0,1	<0,1	1,17	0,05	0,07	<0,04	<0,04	25
						2,38	0,13	0,19	"	"	30
28	"	"	"	"	"	1,23	<0,04	<0,04	"	"	25
						0,19	"	"	"	"	30
60	19	<0,1	<0,1	<0,1	<0,1	11,0	0,16	0,27	<0,04	<0,04	50
						8,5	0,06	0,06	"	"	60
32	"	"	"	"	"	16,09	0,06	0,08	"	"	50
						13,42	0,16	0,30	0,19	0,17	60
41	0,8	<0,1	<0,1	<0,1	<0,1	0,70	<0,04	<0,04	<0,04	<0,04	60
42	"	"	"	"	"	0,30	"	"	"	"	60



TABLE 5.3.II

Gas Cylinder	Measured Hydrocarbon Composition					Run No.
	Vol. ppm					
	CH <sub>4</sub>	C <sub>2</sub> H <sub>4</sub>	C <sub>2</sub> H <sub>6</sub>	C <sub>3</sub> H <sub>6</sub>	C <sub>3</sub> H <sub>8</sub>	
Argon Cyl. 1	24,02	<0,04	<0,04	<0,04	<0,04	60 & 32
Argon Cyl. 2	1,21	"	"	"	"	21 to 30
Argon Cyl. 3	0,79	"	"	"	"	41 & 42
SASOL Cyl. 1	<0,10	<0,10	<0,10	<0,10	<0,10	60 & 32
SASOL Cyl. 2	<0,10	"	"	"	"	all except 41 & 42
Hydrogen Cyl.1	1,5	0,3	0,3	<0,04	<0,04	41 & 42
Carbon Mon- oxide Cyl.1	1,2	1,8	0,2	"	"	41 & 42

#### 5.4.1 Effect of Contact Period Duration

It was found necessary to allow the gas and catalyst to circulate for at least five minutes in order to obtain even distribution of the catalyst particles. Catalyst distribution in the gas was observed by means of a photocell. It was during this period that changes in gas composition were noticed.

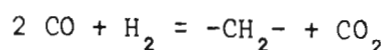
In Table 5.4.1.I, runs with similar initial concentrations of hydrocarbons and catalyst activity were compared in order to determine whether the increase in hydrocarbons observed was a function of contact period duration.

Run 12 exhibited a large increase in all hydrocarbons during the contact period. Comparing this with run 37 it was observed that methane had not increased over the extended contact time but that other hydrocarbons had done so by rather large factors. Essentially there was no difference between catalyst batches A and C once reduction had taken place; further discussed in section 5.4.3.

Analysis of gas samples taken at various stages during the contact period in runs 49, 50, 51 and 55 revealed very interesting trends shown in Figure 5.4.1.I. In these cases the rate of 'production' of hydrocarbons was fairly constant during the contact period. This 'production' seemed to persist after 90 minutes of contact whereas in the case of run 37 the 'production' (of methane) appeared to level off at that stage. This phenomenon is discussed in section 5.4.2. For convenience contact periods in excess of 90 minutes were not employed.

It was postulated that Fischer-Tropsch synthesis had occurred at very low temperature in the pre-shock contact period. The extent of synthesis obviously depended on the contact period duration. Furthermore it was noticed that even at such low temperatures methane production was favoured.

During the contact period the temperature of the mixture rose to a maximum of about 40°C after 35 minutes. Kölbel et al (1966) discuss Fischer-Tropsch at a temperature of only 50°C according to the overall reaction,



$$\Delta H = -43,6 \text{ kcal/mol}$$

TABLE 5.4.1.I

Run No.	Measured Hydrocarbon Composition before Contact Period (estimated where stated)					Measured Hydrocarbon Composition after Contact Period (estimated where stated)					Contact Period or Sample Time Min.	Catalyst Batch and Pre-Treatment
	Vol.ppm					Vol.ppm						
	CH <sub>4</sub>	C <sub>2</sub> H <sub>4</sub>	C <sub>2</sub> H <sub>6</sub>	C <sub>3</sub> H <sub>6</sub>	C <sub>3</sub> H <sub>8</sub>	CH <sub>4</sub>	C <sub>2</sub> H <sub>4</sub>	C <sub>2</sub> H <sub>6</sub>	C <sub>3</sub> H <sub>6</sub>	C <sub>3</sub> H <sub>8</sub>		
12	0,6	<0,04	<0,04	<0,04	<0,04	12,0	0,20	0,20	0,10	0,10	20	A
	1,9	"	0,04	"	"	20,8	0,30	"	"	"	30	82%red.
37	0,8*	<0,1*	<0,1*	<0,1*	<0,1*	17,97	1,59	0,54	0,75	0,32	80	C
						18,21	2,70	0,73	1,29	0,29	90	82%red.
49	0,55	0,16	<0,04	<0,04	<0,04	4,50	0,95	0,25	<0,04	<0,04	30	C
						8,90	2,00	0,53	"	"	70	89%red.
51	0,50	<0,04	"	0,15	"	3,20	0,80	0,20	0,20	"	30	C
						6,90	1,50	0,40	0,55	"	70	85%red.
50	0,45	"	"	0,20	"	7,20	1,65	0,35	0,35	"	60	C
						9,70	2,13	0,55	0,35	"	90	85%red.
41	0,80*	<0,1*	<0,1*	<0,1*	<0,1*	0,70	<0,04	<0,04	<0,04	<0,04	60	None
42	0,80	"	"	"	"	0,30	"	"	"	"	60	None

Remarks: \* estimated via Simet setting

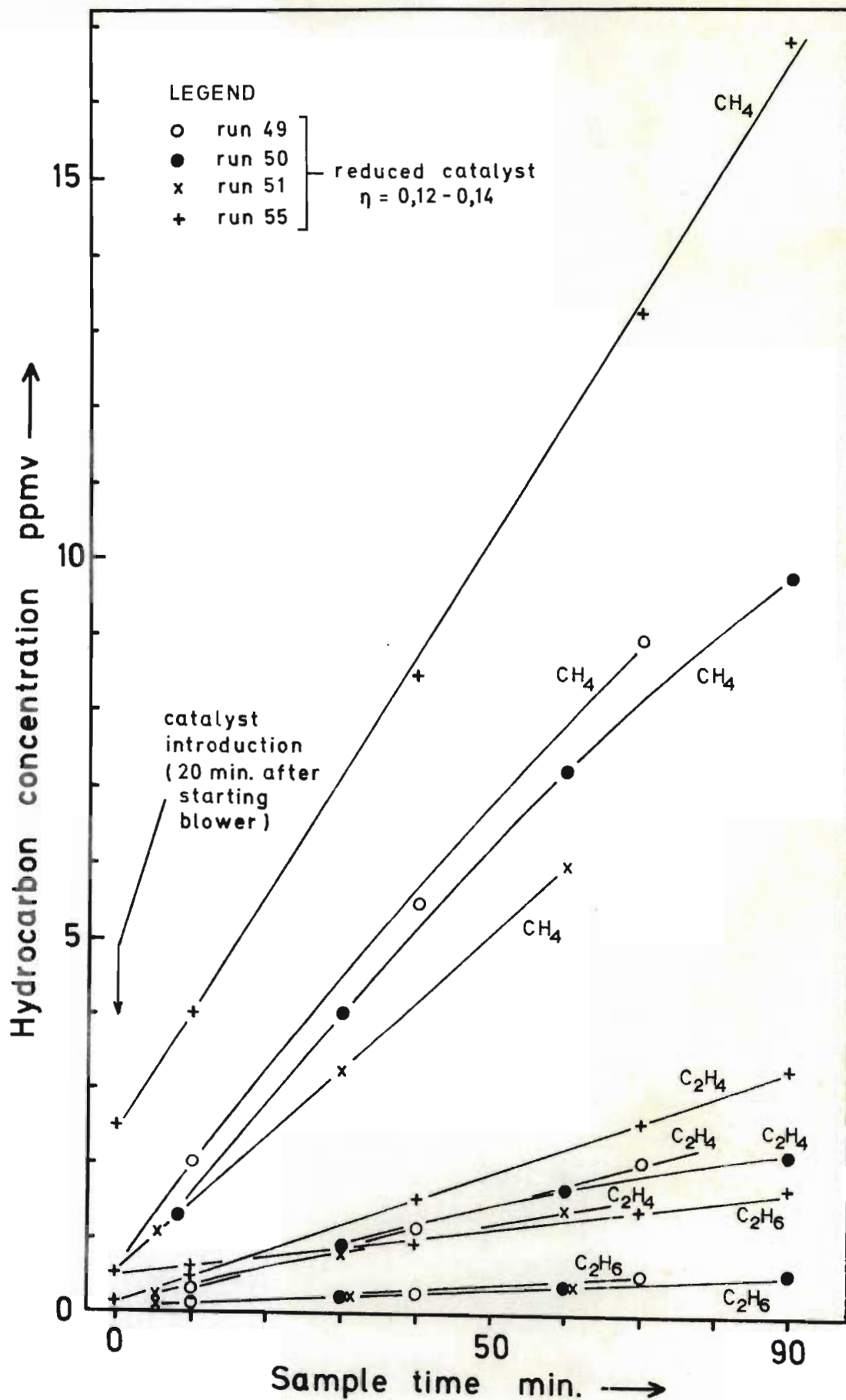


FIGURE 5.4.1.1 Pre-shock contact period ; variation in gas composition with time

They detected  $C_2H_6$  and  $C_3H_8$ , 1 and 0,2 per cent by volume respectively, after a contact period of 135 minutes with hydrogen: carbon monoxide as 1:1. These are very high values compared with ppm observed in this work and were probably due to the much higher concentrations of reactants and much lower space velocities used by Kölbel.

The increase in temperature observed during the contact period was attributed to compression and frictional heat and not to reaction for the following reason. Consider run 37, the increase in methane concentration was approximately 17 ppm - equivalent to 0,43 cc at N.T.P. or 0,43/22400 mol. The heat released by this reaction would have been about 1 calorie which would have raised the temperature by only 0,2°C.

Probst et al (1952) have shown that iron pentacarbonyl is formed at low temperatures, 0 - 100°C, with potassium carbonate promoted catalysts. At 25°C they detected 0,6 volume per cent of carbonyl after 144 hours. Although this compound was not observed in this work it was thought possible that it could have initiated reaction (see Chapter 5.5.2).

On the basis of results obtained here speculation as to the mechanism of possible heterogeneous reactions at these low temperatures would be meaningless. There was no comparable homogeneous reaction as was observed from the analyses of runs 41 and 42 where samples were taken after 60 minutes of circulation, see Table 5.4.1.I.

#### 5.4.2 Effect of Hydrocarbons Present Initially

Table 5.4.2.I compares runs with constant contact period duration and catalyst activity but with varying initial hydrocarbon content.

In most cases there was an observable dependence of rate of formation of hydrocarbons on the quantities of hydrocarbons present initially. As initial hydrocarbon concentration was increased there appeared to be a depression of reaction rate, viz. runs 8 - 12 and 34 - 40. Runs 14 and 15 had high initial hydrocarbon concentrations and exhibited low reaction rates. However runs 49 - 51 did not

TABLE 5.4.2.I

Run No.	Measured Hydrocarbon Composition before Contact Period (estimated where stated)					Measured Hydrocarbon Composition after Contact Period (estimated where stated)					Contact Period or Sample Time Min.	Catalyst Batch and Pre-Treatment	Shock Temp. T <sub>e</sub> °K	Remarks
	Vol.ppm					Vol.ppm								
	CH <sub>4</sub>	C <sub>2</sub> H <sub>4</sub>	C <sub>2</sub> H <sub>6</sub>	C <sub>3</sub> H <sub>6</sub>	C <sub>3</sub> H <sub>8</sub>	CH <sub>4</sub>	C <sub>2</sub> H <sub>4</sub>	C <sub>2</sub> H <sub>6</sub>	C <sub>3</sub> H <sub>6</sub>	C <sub>3</sub> H <sub>8</sub>				
12	0,6	<0,04	<0,04	<0,04	<0,04	12,0	0,20	0,20	0,10	0,10	20	A	804	
	1,9	<0,04	<0,04	<0,04	<0,04	20,8	0,30	0,20	0,10	0,10	30	82% red.		
8	5,7	<0,04	<0,04	<0,04	<0,04	17,2	0,40	0,10	0,10	0,10	25	A	953	
	12,8	0,10	<0,04	<0,04	<0,04	17,2	0,30	0,20	0,10	0,10	35	77% red.		
10	9,0	0,04	0,04	<0,04	<0,04	18,3	0,10	0,10	<0,04	<0,04	20	A	825	
	10,4	0,10	0,10	0,10	0,10	18,0	0,20	0,20	0,10	0,10	30	80% red.		
9	21,4	0,04	0,04	<0,04	<0,04	21,3	0,20	0,20	0,10	0,10	25	A	916	
	19,6	0,10	0,10	<0,04	<0,04	25,7	0,10	0,10	0,10	0,10	30	82% red.		
34	0,8	<0,10	<0,10	<0,10	<0,10	18,67	0,50	<0,04	0,52	0,56	80	C	1194	Composition before Contact Period was estimated via Simet Setting
						21,59	0,55	<0,04	0,21	0,17	90	80% red.		
36	"	"	"	"	"	13,39	2,62	0,89	0,95	0,57	80	C	1259	
						19,64	2,35	0,87	1,63	1,57	90	80% red.		
37	"	"	"	"	"	17,97	1,59	0,54	0,75	0,32	80	C	1240	
						18,21	2,70	0,73	1,29	0,29	90	82% red.		
38	5,5	1,0	3,0	0,4	0,06	11,05	2,22	1,31	0,17	<0,04	80	C	1269	
						14,68	2,80	2,29	0,56	0,20	90	92% red.		
39	"	"	"	"	"	16,12	4,15	3,88	1,48	1,65	80	C	1305	
						14,99	2,71	2,06	0,41	<0,04	90	90% red.		
40	"	"	"	"	"	13,05	2,42	0,99	0,64	0,20	80	C	1287	
						11,36	3,08	2,28	1,15	<0,04	90	92% red.		
50	0,45	<0,04	<0,04	0,20	<0,04	9,70	2,13	0,55	0,35	<0,04	90	C, 85% red.	-	
55	2,25	0,10	0,50	<0,04	<0,04	16,70	3,30	1,65	0,85	0,40	90	C, 86% red.	1243	
49	0,55	0,16	<0,04	<0,04	<0,04	8,90	2,00	0,53	<0,04	<0,04	70	C, 89% red.	-	Comp. after Cont. Period estd from Fig.5.4.1.I
51	0,50	<0,04	<0,04	0,15	<0,04	6,90	1,50	0,40	0,55	<0,04	70	C, 85% red.	-	
14	19*	<0,1*	<0,1*	<0,1*	<0,1*	26,13	0,61	0,66	0,22	0,32	50	A	1079	*Estimated via Simet Setting
						25,81	0,75	0,40	0,22	0,40	60	82% red.		
15	"	"	"	"	"	23,15	0,69	0,47	0,34	0,27	50	A	1048	
						28,78	0,87	0,59	0,55	0,31	60	80% red.		

follow the tendency as their initial hydrocarbon content and reaction rate was low. Experimental conditions were not carefully controlled during this pre-shock period which could have led to large errors. Under these unfavourable reaction conditions the nature of the catalyst surface would be crucial, for example, insufficient outgassing of hydrogen from the surface after reduction would decrease the extent of CO adsorption (Brunauer and Emmett (1940)).

It was concluded that evidence for a rate dependence on initial hydrocarbon content was established and that this phenomenon indicated an equilibrium gas bulk concentration for methane of about 30 ppmv. It appeared that reaction in the case of methane could not proceed much beyond that shown by runs 9, 14 and 15; cf. section 5.4.1. Note that this did not hold for the other hydrocarbons. From this it was inferred that the rate of desorption of methane from the catalyst surface was, under these conditions, highly dependent on the gas bulk concentration of same product.

It was impossible to comment on the other reaction products due to their very much lower concentrations being more severely influenced by experimental error.

#### 5.4.3 Effect of Catalyst Activity

Comparing runs 43 and 44 with 34, 36 and 37 (Table 5.4.3.I) it was noticed that reduction of the catalyst caused a slightly greater quantity of hydrocarbons to form during the contact period.

In runs 29 and 30 the catalyst was reduced and reoxidised with air. This catalyst yielded slightly more hydrocarbons during the contact period than did reduced catalyst when run 30 was compared with 38, 39 and 40. However there was no difference when comparing reoxidised 29 and unreduced 44 with 38, 39 and 40. On the basis of these results no conclusion can be drawn concerning any difference in activity between these two cases.

Summarising, it may be said that during the contact period no significant relationship between reaction and catalyst pre-treatment

TABLE 5.4.3.I

Run No.	Measured Hydrocarbon Composition before Contact Period (estimated where stated)					Measured Hydrocarbon Composition after Contact Period (estimated where stated)					Contact Period or Sample Time Min.	Catalyst Batch and Pre-Treatment	Shock Temp. T <sub>e</sub> °K
	Vol.ppm					Vol.ppm							
	CH <sub>4</sub>	C <sub>2</sub> H <sub>4</sub>	C <sub>2</sub> H <sub>6</sub>	C <sub>3</sub> H <sub>6</sub>	C <sub>3</sub> H <sub>8</sub>	CH <sub>4</sub>	C <sub>2</sub> H <sub>4</sub>	C <sub>2</sub> H <sub>6</sub>	C <sub>3</sub> H <sub>6</sub>	C <sub>3</sub> H <sub>8</sub>			
43*	0,8	<0,1	<0,1	<0,1	<0,1	11,07	2,93	0,50	<0,04	<0,04	90	C, unred.	1130
44*	"	"	"	"	"	12,04	0,83	0,44	<0,04	<0,04	90	C, unred.	1107
34*	"	"	"	"	"	18,67	0,50	<0,04	0,52	0,56	80	C, 80% red.	1194
						21,59	0,55	<0,04	0,21	0,17	90		
36*	"	"	"	"	"	13,39	2,62	0,89	0,95	0,57	80	C, 80% red.	1259
						19,64	2,35	0,87	1,63	1,57	90		
37*	"	"	"	"	"	17,97	1,59	0,54	0,75	0,32	80	C, 82% red.	1240
						18,21	2,70	0,73	1,29	0,29	90		
44*	0,8	<0,1	<0,1	<0,1	<0,1	12,04	0,83	0,44	<0,04	<0,04	90	C, unred.	1107
29	0,38	<0,04	<0,04	<0,04	<0,04	12,35	0,14	0,23	<0,04	<0,04	80	B, 89% red. re-oxidised	1015
	0,46	"	"	"	"	13,96	0,12	0,17	<0,04	<0,04	90		
30	2,76	<0,04	<0,04	<0,04	<0,04	20,41	0,13	0,08	0,04	<0,04	80	B, 100% red. re-oxidised	1034
	3,41	0,08	0,25	"	"	23,01	0,37	0,32	<0,04	"	90		
38*	5,5	1,0	3,0	0,4	0,06	11,05	2,22	1,31	0,17	"	80	C, 92% red.	1269
						14,68	2,80	2,29	0,56	0,20	90		
39*	"	"	"	"	"	16,12	4,15	3,88	1,48	1,65	80	C, 90% red.	1305
						14,99	2,71	2,06	0,41	<0,04	90		
40*	"	"	"	"	"	13,05	2,42	0,99	0,64	0,20	80	C, 92% red.	1287
						11,36	3,08	2,28	1,15	<0,04	90		
18*	19	<0,1	<0,1	<0,1	<0,1	71,0	3,63	7,74	2,11	3,18	50	B, unred.	914
						67,3	1,46	1,03	0,51	0,18	60		
19*	"	"	"	"	"	69,1	0,86	1,41	0,14	0,07	50	B, unred.	1024
						79,7	1,49	1,04	0,39	0,26	60		
43*	0,8	"	"	"	"	11,07	2,93	0,50	<0,04	<0,04	90	C, unred.	1130
44*	"	"	"	"	"	12,04	0,83	0,94	"	"	90	C, unred.	1107
29	0,38	<0,04	<0,04	<0,04	<0,04	12,35	0,14	0,23	<0,04	<0,04	80	B, 89% red. re-oxidised	1015
	0,46	"	"	"	"	13,96	0,12	0,17	"	"	90		
30	2,76	"	"	"	"	20,41	0,13	0,08	0,04	"	80	B, 100% red. re-oxidised	1034
	3,41	0,08	0,25	"	"	23,01	0,37	0,32	<0,04	"	90		

Remarks: \*Composition before Contact Period estimated via Simet Setting



could be detected and it might be inferred that the surface reaction was not a limiting step at these low temperatures.

Although catalyst was supplied freshly manufactured from SASOL, there existed always the possibility that the catalyst received was in fact catalyst which had been used in synthesis. This could be an explanation for the exceptionally high hydrocarbon concentrations detected in the contact periods of runs 18 and 19, Table 5.4.3.I. To establish that other catalysts contained no hydrocarbons permanently adsorbed which could be desorbed in the shock tube, the re-oxidised type of catalyst was prepared by reducing catalyst as received and then deactivating it by re-oxidising with air. The effectiveness of this technique in removing gross pre-contamination of catalysts was demonstrated by runs 29 and 30 which employed batch B type catalyst as in the case of runs 18 and 19; see Table 5.4.3.I. Batch B catalyst was later found to have a much lower bulk density than batches A and C - an indication that the catalyst might have undergone carbonisation during synthesis at SASOL.

---

## 5.5 Shock Contact between Gas and Catalyst

Experiments were designed to establish the extent of the dependence of conversion at elevated temperatures on the following:-

- 5.5.1 temperature and pressure,
  - 5.5.1.1 effect of temperature and pressure on the apparent overall surface reaction,
- 5.5.2 pre-shock contact period,
- 5.5.3 gaseous hydrocarbons present before shocking.

Experiments with reduced catalyst have been classified as follows:-

- a) those where the gas and catalyst were contacted for 40 - 90 minutes, and
- b) contacted for 5 - 15 minutes,

in the pre-shock period. These have been referred to, subsequently, as long and short contact respectively.

In the reduction of the catalyst, see Chapter 2.5.2, the water formed was measured and the percentage oxygen removed calculated. The extent of reduction was normally between 77 and 92 per cent. Low catalyst activities were obtained by using unreduced catalyst and reduced catalyst which had been re-oxidised. The purpose of the low activity catalyst was to provide blanks to demonstrate the importance of the nature of the catalyst surface.

### 5.5.1 Effect of Shock Strength

Fischer-Tropsch synthesis in the shock tube has been investigated by varying the shock temperature and pressure simultaneously. Figures 5.5.1.I - IV depict the yields of methane, ethylene, ethane and propylene respectively, from shock waves of various strengths.

Table 5.5.1.I groups the runs shown in Figures 5.5.1.I - IV according to shock temperature. Columns 12 - 13 show the difference between quantities of hydrocarbons which were present in the apparatus after shocking and the quantities present before shocking, i.e. the yield of products due to the shock wave (see Appendix B for calculation). These values have been plotted against the reaction temperature in Figures 5.5.1.I - IV.

For the long contact runs production increased exponentially with increasing shock strength for all hydrocarbons detected. The exposure of catalyst which had previously participated in reaction during the contact period, to shock conditions would encourage desorption of products formed during that contact period. Evidence to confirm that yields expected via surface reaction under shock conditions would be much greater than those expected from induced desorption (shock conditions) of reaction products formed during the contact period, was provided by the following considerations:-

Yields of products plotted in Figures 5.5.1.I to IV for long contact runs can be approximated by an Arrhenius relationship between yield and temperature. The influence of pressure variation was found to be negligible, see Chapter 5.5.1.1. Choosing a shock

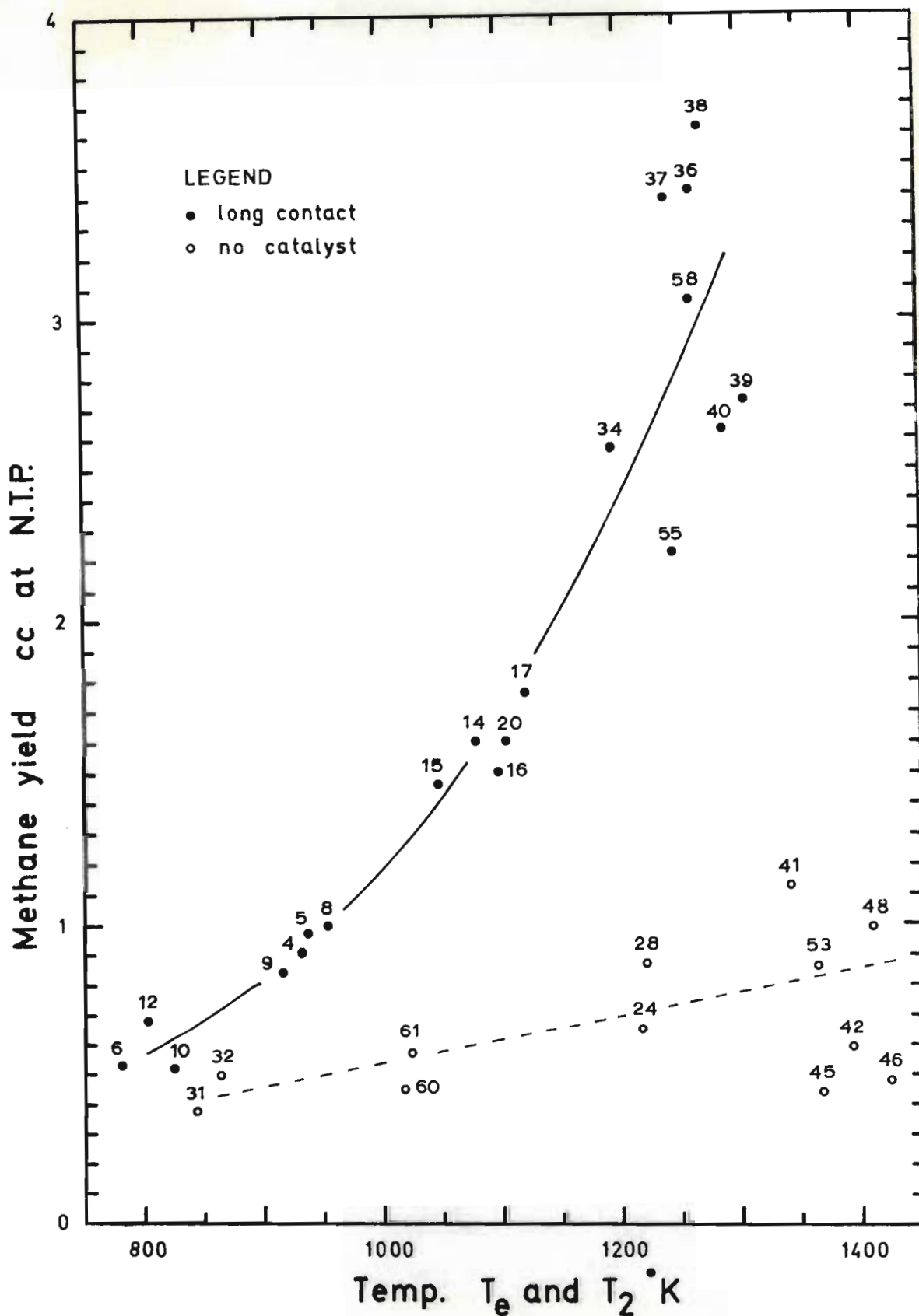


FIGURE 5.5.1.I Long contact and no catalyst runs ; methane yield v. shock temperature

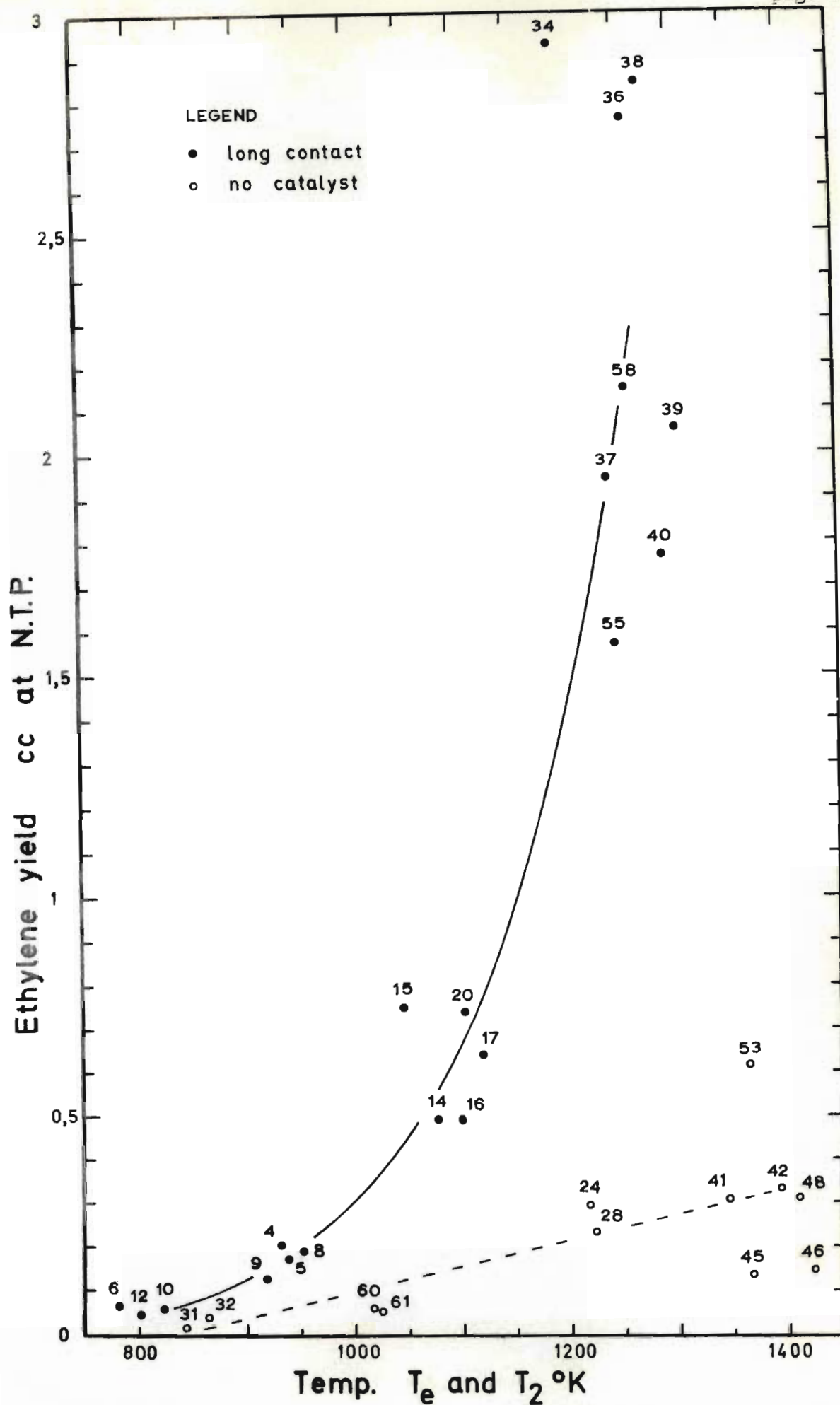


FIGURE 5.5.1.II Long contact and no catalyst runs ; ethylene yield v. shock temperature

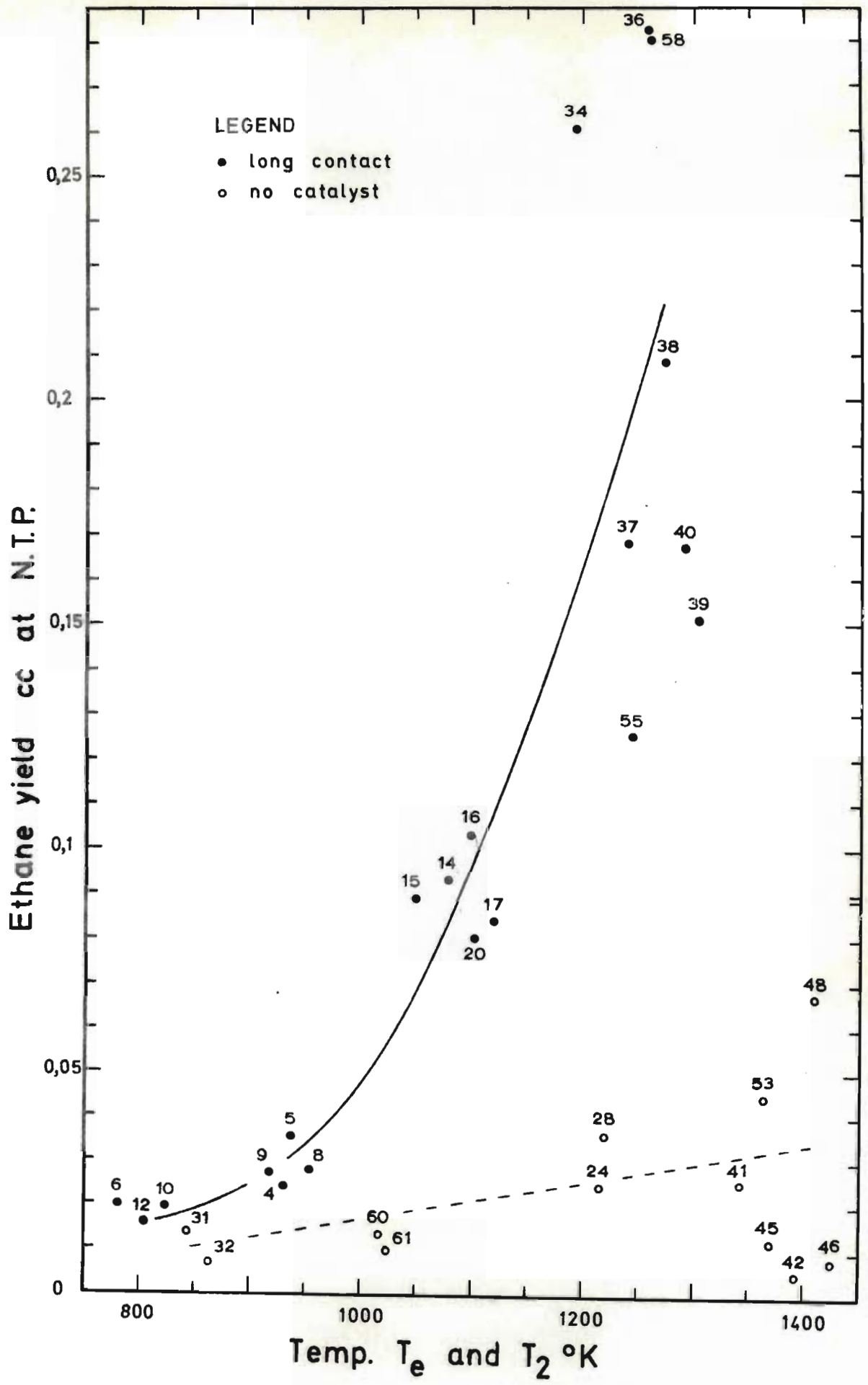


FIGURE 5.5.1.III Long contact and no catalyst runs; ethane yield v. shock temperature

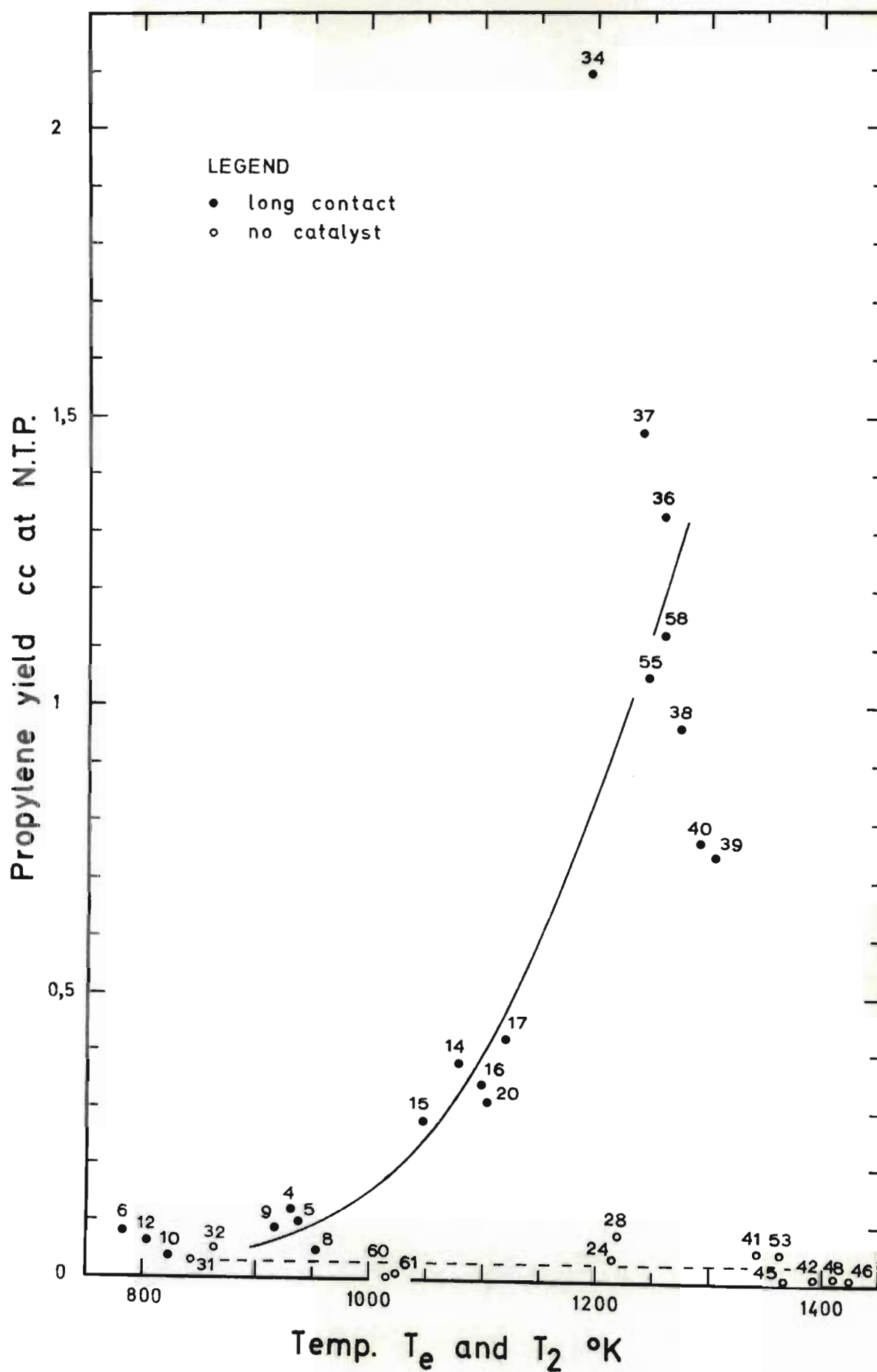


FIGURE 5.5.1.IV Long contact and no catalyst runs ;  
propylene yield v. shock temperature

TABLE 5.5.1.I

Run No.	Measured Hydrocarbon Composition before Contact Period (estimated where stated)					Measured Hydrocarbon Composition after Contact Period (estimated where stated)					Hydrocarbon Yield due to Shock Wave					Contact Period or Sample Time Min.	Catalyst Batch and Pre-Treatment	Shock Temp. T <sub>e</sub> °K
	Vol. ppm					Vol. ppm					cc at N.T.P.							
	CH <sub>4</sub>	C <sub>2</sub> H <sub>4</sub>	C <sub>2</sub> H <sub>6</sub>	C <sub>3</sub> H <sub>6</sub>	C <sub>3</sub> H <sub>8</sub>	CH <sub>4</sub>	C <sub>2</sub> H <sub>4</sub>	C <sub>2</sub> H <sub>6</sub>	C <sub>3</sub> H <sub>6</sub>	C <sub>3</sub> H <sub>8</sub>	CH <sub>4</sub>	C <sub>2</sub> H <sub>4</sub>	C <sub>2</sub> H <sub>6</sub>	C <sub>3</sub> H <sub>6</sub>	C <sub>3</sub> H <sub>8</sub>			
6	-	-	-	-	-	15,7	0,40	0,20	0,10	0,10	0,54	0,065	0,020	0,080	Nil	20	A	782
						17,8	0,40	0,10	"	"						30		
10	9,0	0,04	0,04	<0,04	<0,04	18,3	0,10	0,10	<0,04	<0,04	0,52	0,0550	0,019	0,038	0,013	20	A	825
						18,0	0,20	0,20	0,10	0,10						30		
12	0,6	<0,04	<0,04	<0,04	<0,04	12,0	0,20	0,20	0,10	"	0,68	0,044	0,016	0,064	0,01	20	A	804
						20,8	0,30	"	"	"						30		
31	12,6	0,06	0,06	0,04	<0,04	-	-	-	-	-	0,38	0,015	0,013	0,032	Nil	50	None	843
																60		
32	16,09	0,06	0,08	"	"	-	-	-	-	-	0,50	0,040	0,007	0,056	0,010	50	None	863
																60		
4	-	-	-	-	-	18,8	0,65	0,50	0,20	0,10	0,90	0,20	0,024	0,12	Nil	25	A	932
						15,3	0,60	0,40	0,20	"						35		
5	-	-	-	-	-	20,8	0,30	0,30	0,10	0,15	0,97	0,165	0,034	0,10	Nil	25	A	938
						17,8	0,40	0,20	"	0,10						35		
8	5,7	<0,04	<0,04	<0,04	<0,04	17,2	0,40	0,10	0,10	0,10	0,99	0,19	0,028	0,051	0,01	25	A	953
						17,2	0,30	0,20	"	"						35		
9	21,4	0,04	0,04	"	"	21,3	0,20	"	"	"	0,84	0,12	0,027	0,089	0,016	25	A	916
						25,7	0,10	0,10	"	"						35		
60	11,0	0,16	0,27	<0,04	<0,04	-	-	-	-	-	0,45	0,06	0,013	0,005	0,003	50	None	1017
																60		
61	6,9	0,12	0,04	0,04	"	-	-	-	-	-	0,57	0,05	0,010	0,010	Nil	50	None	1023
																60		

continued

TABLE 5.5.1.I Continued

Run No.	Measured Hydrocarbon Composition before Contact Period (estimated where stated)					Measured Hydrocarbon Composition after Contact Period (estimated where stated)					Hydrocarbon Yield due to Shock Wave					Contact Period or Sample Time Min.	Catalyst Batch and Pre-Treatment	Shock Temp. T <sub>e</sub> °K
	Vol. ppm					Vol. ppm					cc at N.T.P.							
	CH <sub>4</sub>	C <sub>2</sub> H <sub>4</sub>	C <sub>2</sub> H <sub>6</sub>	C <sub>3</sub> H <sub>6</sub>	C <sub>3</sub> H <sub>8</sub>	CH <sub>4</sub>	C <sub>2</sub> H <sub>4</sub>	C <sub>2</sub> H <sub>6</sub>	C <sub>3</sub> H <sub>6</sub>	C <sub>3</sub> H <sub>8</sub>	CH <sub>4</sub>	C <sub>2</sub> H <sub>4</sub>	C <sub>2</sub> H <sub>6</sub>	C <sub>3</sub> H <sub>6</sub>	C <sub>3</sub> H <sub>8</sub>			
14	19,0*	<0,1*	<0,1*	<0,1*	<0,1*	26,13	0,61	0,66	0,22	0,32	1,60	0,49	0,093	0,380	0,044	50	A 82%red.	1079
						25,81	0,75	0,40	0,22	0,40						60		
15	"	"	"	"	"	23,15	0,69	0,47	0,34	0,27	1,46	0,75	0,089	0,280	0,029	50	A 80%red.	1048
						28,78	0,87	0,59	0,55	0,31						60		
16	2,50*	0,10*	0,50*	<0,04*	<0,04*	21,36	0,84	0,52	0,55	0,20	1,50	0,49	0,103	0,343	Nil	90	C 85%red.	1100
17	"	"	"	"	"	19,72	1,30	0,63	0,18	0,12	1,76	0,64	0,084	0,422	Nil	90	C 81%red.	1121
20	"	"	"	"	"	22,33	1,00	0,47	0,38	0,25	1,60	0,73	0,080	0,312	Nil	90	C 80%red.	1103
24	1,17	0,05	0,07	<0,04	<0,04	-	-	-	-	-	0,65	0,29	0,024	0,040	Nil	25	None	1216
	2,38	0,13	0,19	"	"											30		
28	1,23	<0,04	<0,04	"	"	-	-	-	-	-	0,87	0,23	0,036	0,080	0,003	25	None	1221
	0,19	"	"	"	"											30		

continued



TABLE 5.5.1.I Continued

Run No.	Measured Hydrocarbon Composition before Contact Period (estimated where stated)					Measured Hydrocarbon Composition after Contact Period (estimated where stated)					Hydrocarbon Yield due to Shock Wave					Contact Period or Sample Time Min.	Catalyst Batch and Pre-Treatment	Shock Temp. T <sub>e</sub> °K
	Vol. ppm					Vol. ppm					cc at N.T.P.							
	CH <sub>4</sub>	C <sub>2</sub> H <sub>4</sub>	C <sub>2</sub> H <sub>6</sub>	C <sub>3</sub> H <sub>6</sub>	C <sub>3</sub> H <sub>8</sub>	CH <sub>4</sub>	C <sub>2</sub> H <sub>4</sub>	C <sub>2</sub> H <sub>6</sub>	C <sub>3</sub> H <sub>6</sub>	C <sub>3</sub> H <sub>8</sub>	CH <sub>4</sub>	C <sub>2</sub> H <sub>4</sub>	C <sub>2</sub> H <sub>6</sub>	C <sub>3</sub> H <sub>6</sub>	C <sub>3</sub> H <sub>8</sub>			
34	0,8*	<0,1*	<0,1*	<0,1*	<0,1*	18,67	0,50	<0,04	0,52	0,56	2,56	2,93	0,260	2,09	0,05	80	C	1194
						21,59	0,55	"	0,21	0,17					90	80%red.		
36	"	"	"	"	"	13,39	2,62	0,89	0,95	0,57	3,41	2,76	0,282	1,33	0,114	80	C	1259
						19,64	2,35	0,87	1,63	1,57					90	80%red.		
37	"	"	"	"	"	17,97	1,59	0,54	0,75	0,32	3,38	1,90	0,168	1,47	0,064	80	C	1240
						18,21	2,70	0,73	1,29	0,29					90	82%red.		
38	5,5*	1,0*	3,0*	0,4*	0,06*	11,05	2,22	1,31	0,17	<0,04	3,62	2,84	0,208	0,960	0,004	80	C	1269
						14,68	2,80	2,29	0,56	0,20					90	92%red.		
39	"	"	"	"	"	16,12	4,15	3,88	1,48	1,65	2,72	2,06	0,151	0,741	Nil	80	C	1305
						14,99	2,71	2,06	0,41	<0,04					90	90%red.		
40	"	"	"	"	"	13,05	2,42	0,99	0,64	0,20	2,62	1,77	0,167	0,762	0,035	80	C	1287
						11,36	3,08	2,28	1,15	<0,04					90	92%red.		
55	2,25	0,10	0,50	<0,04	<0,04	17,4*	3,40*	1,65*	0,85*	0,40*	2,22	1,57	0,125	1,05	Nil	95	C,86%red.	1243
58	-	-	-	-	-	56,4	5,32	3,64	1,05	0,18	3,05	2,15	0,280	1,12	0,005	90	C,82%red.	1260
41	0,70	<0,04	<0,04	<0,04	<0,04	-	-	-	-	-	1,13	0,31	0,025	0,053	Nil	60	None	1342
42	0,30	"	"	"	"	-	-	-	-	-	0,590	0,33	0,005	0,010	"	60	"	1392
45	17,5	0,17	0,07	0,85	"	-	-	-	-	-	0,44	0,134	0,012	0,005	"	15	"	1366
46	0,55	0,14	<0,04	<0,04	"	-	-	-	-	-	0,480	0,145	0,008	0,010	"	15	"	1423
48	69,7	64,0	"	"	"	-	-	-	-	-	0,994	0,312	0,067	0,013	"	15	"	1409
53	7,6	<0,04	0,55	0,15	"	-	-	-	-	-	0,861	0,614	0,044	0,050	"	15	"	1363

Remarks: \* estimated via Simet setting

\* estimated from Figure 5.4.1.I

reaction temperature of 1100°K, let  $k_1$  and  $k_2$  be the specific reaction rates of the overall reaction during the contact period and under shock conditions respectively.

$$\text{Hence } \frac{k_2}{k_1} = \frac{A_2 e^{-E_2/RT_2}}{A_1 e^{-E_1/RT_1}}$$

where  $T_2 = 1100^\circ\text{K}$ ,  $T_1 = 313^\circ\text{K}$ .

Assuming  $A_1 = A_2$  and  $E_1 = E_2 = E$  then,

$$\frac{k_2}{k_1} = e^{-E/(1100 \cdot R)} / e^{-E/(313 \cdot R)}$$

Assigning a value of 20 kcal./mole to  $E$  the activation energy (which has been reported for the overall Fischer-Tropsch reaction, Anderson et al (1964) and Dry et al (1972)) then

$$\frac{k_2}{k_1} = 8,13 \cdot 10^9$$

The reaction during the contact period lasted a maximum of 90 minutes whereas the shock reaction had a mean duration of about 0,6 millisecond. Hence,

$$\frac{\text{maximum pre-shock reaction time}}{\text{shock reaction time}} = \frac{90 \cdot 60}{0,0006} = 10^7$$

Therefore the extent of reaction under shock conditions has been estimated to be  $8,13 \cdot 10^9 / 10^7 = 8,13 \cdot 10^2$  times greater than that attained during the contact period. Consequently the contribution to the yields detected after shocking by desorbed products of the pre-shock reaction was considered negligible.

Clearly, yields obtained in the shock reaction were not as great as predicted by the above considerations. For instance, the low temperature reaction in the contact period of run 55 yielded 14 ppmv of methane equal to a production of 0,35 cc at N.T.P.; run 20 produced 1,60 cc of methane at N.T.P. from a much smaller volume

of reactants. The ratio of reacting volumes of runs 55/20 was 25/5,65; hence the overall ratio between yields was

$$\frac{1,60}{0,35} \cdot \frac{25}{5,65} = 20.$$

Reasons for this very low ratio are discussed in Chapter 5.5.1.1.

From another view point:- The adsorbed monolayer volume of one gram of reduced catalyst was 0,35 cc at S.T.P. or 0,38 cc at N.T.P. On average 1,50 g of catalyst took part in the shock reaction and if it was assumed that the monolayer volume consisted only of products then complete desorption of this monolayer would yield 0,57 cc of products at N.T.P.; run 20 yielded a total of 1,99 cc of products, see Table 5.5.1.1.I. In practice the monolayer would not consist of products only and complete desorption was very unlikely.

On the basis of the above considerations it could still be assumed that the fraction of the total shock yield resulting from the desorption of products formed during the pre-shock contact period, was negligible.

Also shown in Figures 5.5.1.I to IV are runs without catalyst which have yielded lower quantities of hydrocarbons. These runs are discussed in Chapter 5.6 but have been included here to provide a comparison of the two extremes investigated. The difference between the yield of hydrocarbons from long contact runs and runs with no catalyst, was due only to the surface reaction occurring on the catalyst.

The F-test was applied to confirm that yield means of the long contact runs, set A, and no-catalyst runs, set B, were significantly different. Results appear overleaf.

Temp. °K	Set A (Run Nos)	Set B (Run Nos)	Calculated F	F at 1% level	F at 5% level
840- 1030	4, 5, 8, 9	31, 32, 60, 61	CH <sub>4</sub> -F <sub>1,6</sub> = 72,75 C <sub>2</sub> H <sub>4</sub> -F <sub>1,6</sub> = 39,51 C <sub>2</sub> H <sub>6</sub> -F <sub>1,6</sub> = 42,13 C <sub>3</sub> H <sub>6</sub> -F <sub>1,6</sub> = 11,92	F <sub>1,6</sub> = 13,74	F <sub>1,6</sub> = 5,99
1010- 1220	14, 15, 16, 17, 20	24, 28, 60, 61	CH <sub>4</sub> -F <sub>1,7</sub> = 95,94 C <sub>2</sub> H <sub>4</sub> -F <sub>1,7</sub> = 31,46 C <sub>2</sub> H <sub>6</sub> -F <sub>1,7</sub> = 102,4 C <sub>3</sub> H <sub>6</sub> -F <sub>1,7</sub> = 95,64	F <sub>1,7</sub> = 12,25	F <sub>1,7</sub> = 5,59
1190- 1430	34, 36, 37, 38, 39, 40, 55, 58	24, 28, 41, 42, 45, 46, 48, 53	CH <sub>4</sub> -F <sub>1,14</sub> = 126,3 C <sub>2</sub> H <sub>4</sub> -F <sub>1,14</sub> = 102,2 C <sub>2</sub> H <sub>6</sub> -F <sub>1,14</sub> = 59,27 C <sub>3</sub> H <sub>6</sub> -F <sub>1,14</sub>	F <sub>1,14</sub> = 8,86	F <sub>1,14</sub> = 4,60

Except for propylene in the low temperature range the following is true; in less than 1 per cent of the cases could the observed difference in sample means be explained on the basis of the scatter of the observed data.

In Table 5.5.1.I the initial gas composition and the sample time or in the case of runs with catalyst the contact period, vary considerably. The effects of variations in the quantities of hydrocarbons present initially are discussed in Chapter 5.5.3 and the contact period is dealt with in Chapter 5.4.1. Dependence of shock reaction rate on these variables is minimal compared to that of temperature.

#### 5.5.1.1 Effect of Temperature and Pressure on the Apparent Overall Surface Reaction

Yields via the homogeneous reaction (lower curve, Figures 5.5.1.I to IV) were subtracted from the total yields (upper curve) to provide a measure of the apparent overall surface reaction. This was done in the following manner: Homogeneous reaction yields were subjected to regression analysis and the resulting analytical expressions were used to predict the extent of homogeneous reaction under the conditions of each of the heterogeneous runs. The analytical expressions for each product specie are given in Appendix C. Resultant figures appear in Table 5.5.1.1.I together with the corresponding quantities of H<sub>2</sub> + CO consumed (Q<sub>obs.I</sub>) in the formation

TABLE 5.5.1.1.I SURFACE REACTION YIELDS AND CONSUMPTION OF REACTANTS

Run No.	Reaction Temp. $T_e$ °K	Heterogeneous Yield cc at N.T.P.				Consumption of Reactants ( $H_2+CO$ ) by Heterogeneous (Surface) Reaction		Percentage Conversion of ( $H_2+CO$ ) Based on $Q_{obs.A}$
						$Q_{obs.I} \cdot 10^4$ g mole/dwell time/reacting volume	$Q_{obs.A} \cdot 10^4$ g mole/dwell time/reacting volume	
		$CH_4$	$C_2H_4$	$C_2H_6$	$C_3H_6$			
6	782	0,1511	0,05183	0,02000	0,050	0,6120	0,6120	0,163
10	825	0,1012	0,03592	0,01900	0,008	0,3356	0,3356	0,095
12	804	0,2757	0,02800	0,01600	0,034	0,6865	0,6865	0,195
4	932	0,4112	0,1586	0,02006	0,090	1,442	1,059	0,233
5	938	0,4775	0,1220	0,03029	0,070	1,416	1,051	0,250
8	953	0,4882	0,1428	0,01846	0,021	1,271	0,968	0,244
9	916	0,3613	0,08271	0,02421	0,059	1,074	0,762	0,182
14	1079	1,025	0,3966	0,0930	0,350	4,179	2,627	0,501
15	1048	0,9023	0,6699	0,08531	0,250	4,258	2,468	0,509
16	1100	0,9136	0,3870	0,09174	0,313	3,836	2,510	0,541
17	1121	1,162	0,5267	0,07221	0,392	4,814	3,264	0,700
20	1103	1,012	0,6256	0,07507	0,282	4,417	2,831	0,564
34	1194	1,925	2,777	0,2600	2,06	18,18	8,44	1,33
36	1259	2,744	2,565	0,2820	1,30	16,28	9,90	1,62
37	1240	2,723	1,718	0,1680	1,44	14,36	8,10	1,34
38	1269	2,949	2,638	0,1758	0,930	15,13	9,33	2,13
39	1305	2,033	1,832	0,1175	0,711	10,71	6,94	1,58
40	1287	1,941	1,555	0,1343	0,732	10,01	6,34	1,44
55	1243	1,561	1,386	0,1025	1,02	9,942	5,85	1,26
58	1260	2,383	1,954	0,2572	1,09	13,36	8,13	1,73

of products via the stoichiometry of Chapter 3.4.

The following exercise is an attempt to apply a simple rate equation to the apparent surface reaction. The reaction considered is not purely a surface process as some degradation of product molecules in the gas phase can be expected to occur at temperatures above 1100<sup>o</sup>K (Palmer and Hirt (1963) and Chappell and Shaw (1968)). Therefore the procedure of yield subtraction described above does not strictly result in the quantities of hydrocarbons produced by the surface reaction alone. However, degradation and interference by homogeneous reactions have been assumed negligible. Hence the product spectrum obtained by subtraction shall be used as a measure of the surface reaction.

By the regression analyses of Appendix C (Table C.3) it was shown that corrections to  $Q_{\text{obs.I}}$  for variations in mean dwell time and reacting volume were negligible. Hence  $Q_{\text{obs.I}}$  was based on a mean dwell time of 0,670 m.sec. and a reacting volume of 5,31 litres (equivalent to reacting length  $x_{\text{RZL}}$  of 235 cm).

According to the considerations of Chapter 3.4 reaction rate could be expressed in the form

$$r = k'' p^n e^{-E/RT_e}$$

Initial regression yielded,

$Q_{\text{FI}} = 3,8 \cdot 10^3 \cdot e^{\left(-\frac{7267}{T_e}\right)}$  with a multiple correlation coefficient of 0,963; refer to Table C.2 of Appendix C.  $Q_{\text{FI}} = Q_{\text{FIT,init.}}$  =  $\text{H}_2 + \text{CO}$  consumed according to initial curve fit. This relationship and the iteration procedure described in Appendix C were used to estimate the consumption of  $\text{H}_2 + \text{CO}$  assuming instantaneous quench; see Table C.4 of Appendix C. **Nine** iteration steps were required resulting in,

$$Q_{\text{Fg}} = 9,573 \cdot 10^2 \cdot e^{\left(-\frac{6221}{T_e}\right)}$$

5.5.1.1.I

with multiple correlation coefficient of 0,958. The corresponding observed values ( $Q_{\text{obs.9}} \cdot 10^4 = Q_{\text{obs.A}} \cdot 10^4$ ) have been listed in Table 5.5.1.1.I.

$E/R = 6221$ , standard deviation of  $E/R = 442$  and computed  $t = 14,1$ . Therefore  $E = 12,4$  kcal/mole. Equation 5.5.1.1.I has been drawn in Figure 5.5.1.1.I; the fit is fairly good. Note that percentage conversion of  $H_2 + CO$  has been calculated using  $Q_{\text{obs.A}}$  values; see Table 5.5.1.1.I.

Under normal synthesis conditions, Anderson et al (1964) obtained an activation energy of 17,9 kcal/mole with reduced iron catalyst and  $H_2/CO = 1$  whilst British researchers (Fuel Research Board G.B. (1953 & 1954)) reported a corresponding value of 22,3 for  $H_2/CO = 1,12$  and 27,5 kcal/mole for  $H_2/CO = 0,67$ . Dry et al (1972) using  $H_2/CO = 1,9$  and a triply promoted fused iron catalyst, reported an activation energy of 16,8 kcal/mole based on  $H_2O + CO_2$  moles produced.

Incorporation of  $P$ ,  $\eta$  and  $R_D$  into the regression (Table 5.5.1.1.II) yielded no improvement as the partial  $F$  for each variable was below the 95% level which is in the region of 4,5.

**TABLE 5.5.1.1.II** REGRESSION ANALYSIS OF  $Q_{\text{obs.A}}$

Exponential model $Q_{\text{est.A}} = A P^L \eta^M R_D^N e^{-E/RT_e}$					
Step	Variable	Proportion of Variable of $Q$ reduced	Partial $F$	$F$ for Analysis of Variance	Multiple Correlation Coefficient
1	$-1/T_e$	0,917	1-18=198	1-18 =198 1-18(99%)=8,23	0,9575
2	$\ln P$	0,0124	1-17=2,98	2-17 =112 2-17(99%)=6,11	0,9640
3	$\ln \eta$	0,0131	1-16=3,65	3-16 =87,2 3-16(99%)=5,29	0,9708
4	$\ln R_D$	0,00302	1-15=0,83	4-15 =64,9 4-15(99%)=4,89	0,9723

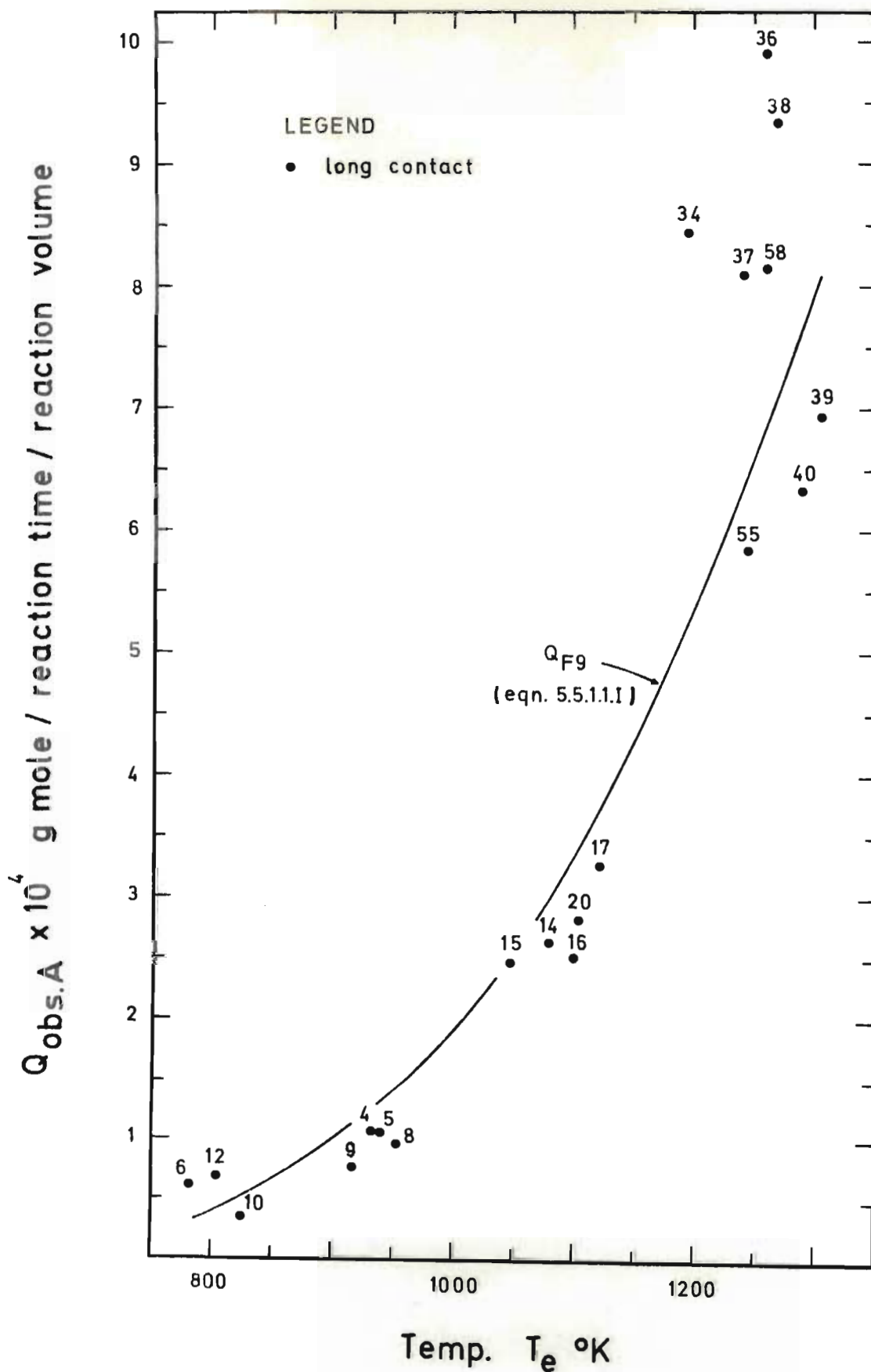


FIGURE 5.5.1.1.I Observed  $H_2 + CO$  consumption ( $Q_{obs.A}$ ) v. shock temp. ( $T_e$ ) and curve fit ( $Q_{F9}$ )



With  $T_e$  and  $P$  included the following equation was obtained

$$Q_{FA} = 78,6 \cdot P^{1,07} \cdot e^{(-\frac{4656}{T_e})}$$

Variable	Regression Coefficient	Standard Deviation of Coefficient	Computed t
$-1/T_e$	4656	999	4,66
$P$	1,07	0,617	1,73

The level of confidence in the coefficient of  $P$  was very low since the computed  $t \ll 4,5$  and was assumed to be zero; equation 5.5.1.1.I providing the best fit.

Fragmentary evidence for reduced iron catalysts (Anderson et al (1964)) suggests that reaction rate varies as the 0,5 power of the system pressure at normal operating temperatures and over the pressure range used in this work. If the reaction was reactant diffusion controlled (gas bulk to adsorbed layer) then a fairly strong dependence on pressure would emerge. The independence of rate on total reactant partial pressure found here indicated high surface coverage by reactants. This may be true before or at the beginning of shock reaction but certainly is not the case later since product yield was much lower than expected. The catalyst monolayer volume per reacting volume was 0,525 cc at S.T.P. equivalent to  $0,234 \cdot 10^4$  g mole  $H_2 + CO$ . From Table 5.5.1.1.I it can be seen that all runs except the low temperature ones (Nos 6, 10 and 12) consumed considerably more than  $0,234 \cdot 10^4$  g mole  $H_2 + CO$ .

The surface reaction appeared to be controlled by phenomena not influenced by pressure. Such phenomena could be (i) a low reactant/s adsorption rate and (ii) a slow surface intermediate step.

(i) Adsorption

If the adsorbed reactants are removed rapidly by reaction and conditions for further adsorption are unfavourable then the system is said to be adsorption controlled.

Carbon monoxide isobars for promoted fused iron Fischer-Tropsch catalysts often behave in the way shown by the solid line in Figure 5.5.1.1.II (Raal (1955)). At low temperatures physical adsorption takes place and because this process is exothermic, the amount of adsorption decreases with increase in temperature.

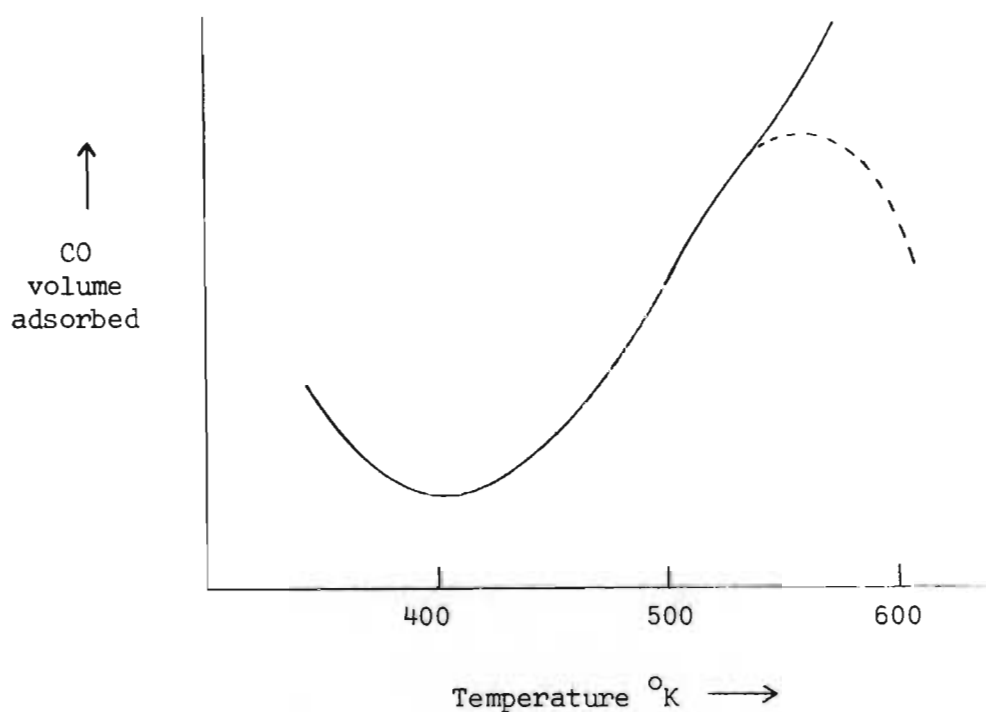


FIGURE 5.5.1.1.II CO ADSORPTION ISOBAR, RAAL (1955)

As temperature rises the rate of chemisorption increases. At sufficiently high temperatures chemisorption equilibrium is established and since this process is also exothermic, the extent of adsorption decreases again when the temperature is increased still further; see dashed line in Figure 5.5.1.1.II. However Raal observed that promoted fused iron catalysts exhibited no maximum adsorption for carbon monoxide up to 600°K and in fact the isobars still climbed steeply at this temperature. He attributed this increase to the onset of some chemical reaction whereby carbon monoxide was being

consumed. Probst et al (1952) studied carbon monoxide adsorption on potassium promoted iron catalysts between 0 and 108°C and found that chemical reactions occur which produce iron pentacarbonyl and carbon dioxide. Formation of carbides on the catalyst surface at elevated temperatures has been demonstrated by various investigators (U.S. Bureau of Mines Bulletin 544).

Raal reported a similar isobar for hydrogen but a maximum was observed at 500°K because hydrogen did not react with the catalyst surface. From Raal's work, volume ratios of CO/H<sub>2</sub> in the adsorbed layer were 1, 2 and > 6 at temperatures of 300, 500 and 600°K respectively. Dry et al (1969) using a catalyst of similar composition to that used in this work, found a ratio of 2 at 300°K. Subramanyam and Rao (1969) reported a ratio of 2,5 at 320°K for another similar catalyst; see Chapter 5.5.2. In the absence of published work on adsorption at temperatures in the region of 1000°K it was assumed that the above trends could be extrapolated. Hence the CO/H<sub>2</sub> ratio in the adsorbed phase could be expected to be extremely large under shock conditions.

On oxide promoted catalysts such as that used in this work, the heat of adsorption of hydrogen is much lower than that of carbon monoxide indicating that hydrogen is less strongly bonded to the catalyst surface; see Dry et al (1969). Chornet and Coughlin (1972) performed detailed studies of the adsorption of hydrogen on smooth clean iron surfaces in the temperature range 100 to 500°K. They obtained a rate equation for hydrogen adsorption at low surface coverage having the form

$$r_{H_2} = C p_{H_2} e^{-E_a/RT} \quad 5.5.1.1.II$$

where  $p_{H_2}$  = partial pressure of hydrogen, C is a constant and  $E_a$  = activation energy for adsorption = 500 cal/mole. This was an extremely low value for  $E_a$  and led Chornet and Coughlin to postulate that the activated complex was molecular in nature. Clearly temperature dependence of rate was low.

Raal (1955) used the following rate equation for carbon monoxide adsorption on iron surfaces at low coverage and up to 600°K

$$r_{CO} = C' p_{CO} e^{-E_a/RT} \quad 5.5.1.1.III$$

here  $E_a = 13,5$  kcal/mole.

Assuming equations 5.5.1.1.II and III hold for T up to 1300°K say, without serious error, the change in the rate of adsorption of H<sub>2</sub> and CO through the temperature range 800°K to 1300°K would involve factors of  $e^{0,12}$  and  $e^{3,23}$  respectively. The large difference effectively outweighs the effect of the change in total pressure of reactants over this temperature range.

#### (ii) Surface Reaction

Published work reports activation energies for the overall Fischer-Tropsch reaction on iron catalysts in the region of 20 kcal/mole. The lower activation energy obtained here would indicate that surface reaction intermediate steps were unlikely to be rate controlling.

For the surface reaction Ghosh et al (1952) observed activation energies of 6 - 20 kcal/mole depending on the experimental conditions. They noticed a strong dependence of activation energy on pressure suggesting that the process of adsorption was highly significant and complex, involving also diffusion within the pore system of the catalyst. Bokhoven and associates (1955) considered diffusion and reaction in iron catalysts.

From the above considerations it was postulated that at elevated temperatures the Fischer-Tropsch reaction was controlled by the rate of hydrogen adsorption. This could also explain why Craxford and Rideal (1939) did not observe para to ortho hydrogen conversion during synthesis at normal temperatures; see Chapter 1.1. Considerations of Chapters 5.5.2 and 5.7 also support this postulate.

### 5.5.2 Effect of Pre-Shock Contact Period

An interesting comparison has been made in Figures 5.5.2.I - IV where long and short contact runs have been plotted. Short contact experiments gave lower yields of hydrocarbons at high shock strengths. It was clear that a long contact period was advantageous to Fischer-Tropsch synthesis.

Table 5.5.2.I shows details of the runs plotted in Figures 5.5.2.I - IV. There were large variations in the quantities of hydrocarbons initially present; this was found to have no influence (Chapter 5.5.3).

The F-test was applied to confirm that the means of the long contact runs, sets A below, and short contact runs, sets B, were significantly different at 1100 and 1250<sup>o</sup>K. Results for the four hydrocarbons appear below.

Temp. °K	Set A (Run Nos)	Set B (Run Nos)	Calculated F	F at 1% Level	F at 5% Level
1100	14, 15, 16, 17, 20	23, 25	CH <sub>4</sub> - F <sub>1,5</sub> = 54,0 C <sub>2</sub> H <sub>4</sub> - F <sub>1,5</sub> = 20,5 C <sub>2</sub> H <sub>6</sub> - F <sub>1,5</sub> = 75,2 C <sub>3</sub> H <sub>6</sub> - F <sub>1,5</sub> = 28,8	F <sub>1,5</sub> = 16,3	F <sub>1,5</sub> = 6,6
1250	34, 36, 37, 38, 39, 40, 55, 58	52, 56	CH <sub>4</sub> - F <sub>1,8</sub> = 46,9 C <sub>2</sub> H <sub>4</sub> - F <sub>1,8</sub> = 30,3 C <sub>2</sub> H <sub>6</sub> - F <sub>1,8</sub> = 13,9 C <sub>3</sub> H <sub>6</sub> - F <sub>1,8</sub> = 13,3	F <sub>1,8</sub> = 11,3	F <sub>1,8</sub> = 5,3

For all components the means are significantly different at the 1% level.

Subramanyam and Rao (1969) investigated the change in the composition of the adsorbed phase at various intervals of time employing two Fischer-Tropsch iron catalysts. They reported that at about 50<sup>o</sup>C, the CO/H<sub>2</sub> ratio in the adsorbed phase required about 2 - 3 hours to reach a maximum value. At the start of adsorption the composition of the adsorbed phase was practically equal to the composition of the gas phase employed,

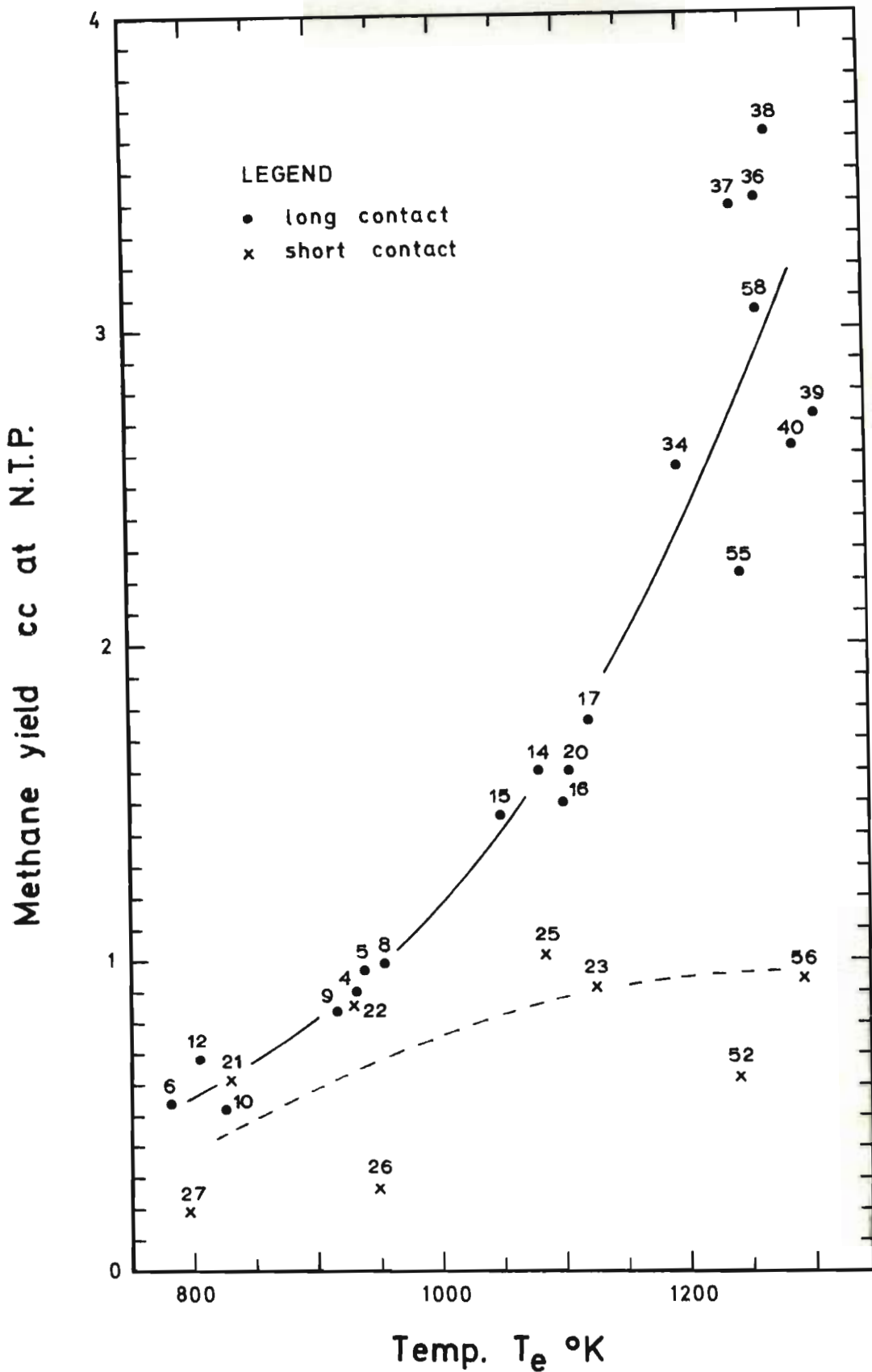


FIGURE 5.5.2.I Long and short contact runs ;  
Methane yield v. shock temp.

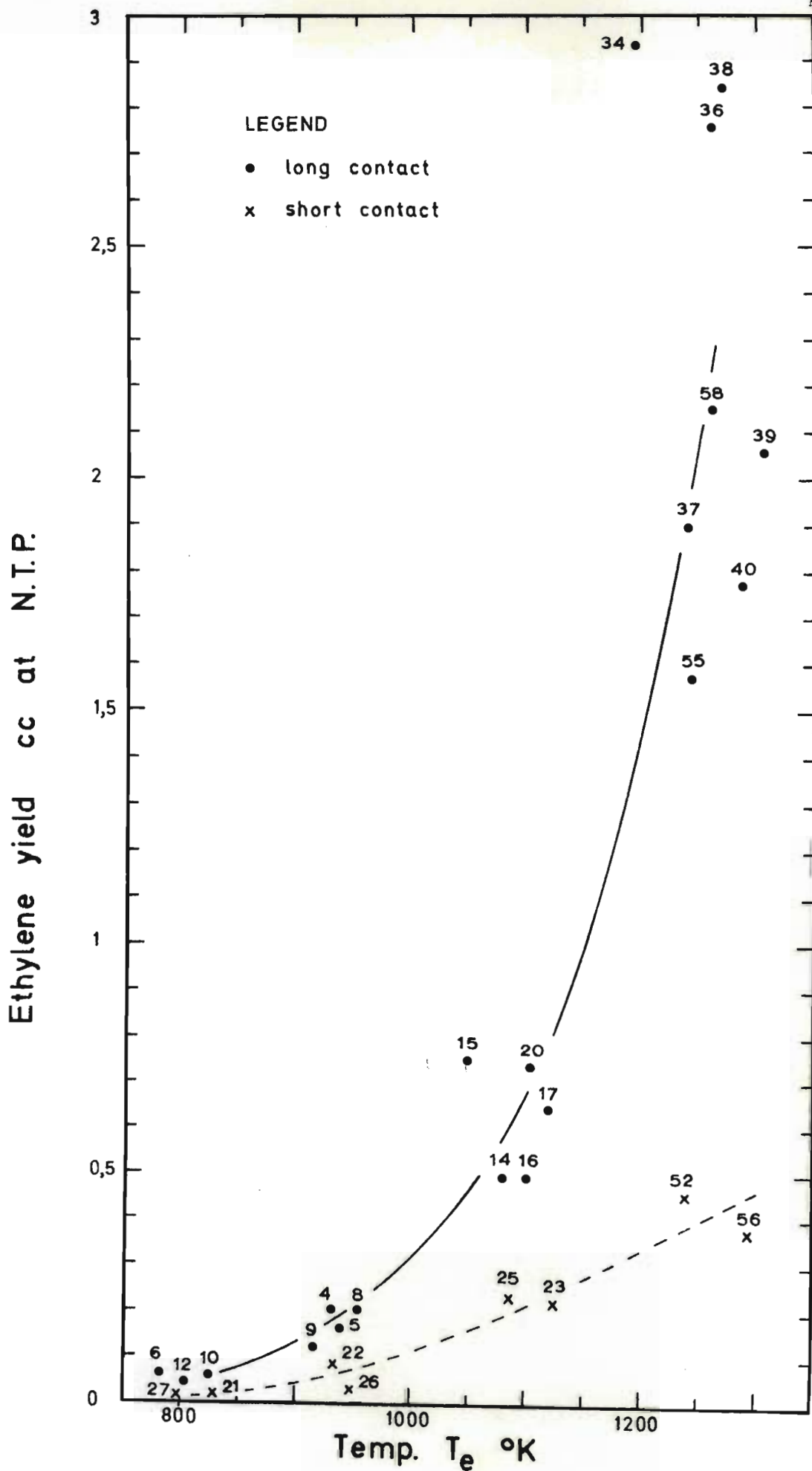


FIGURE 5.5.2.II Long and short contact runs ;

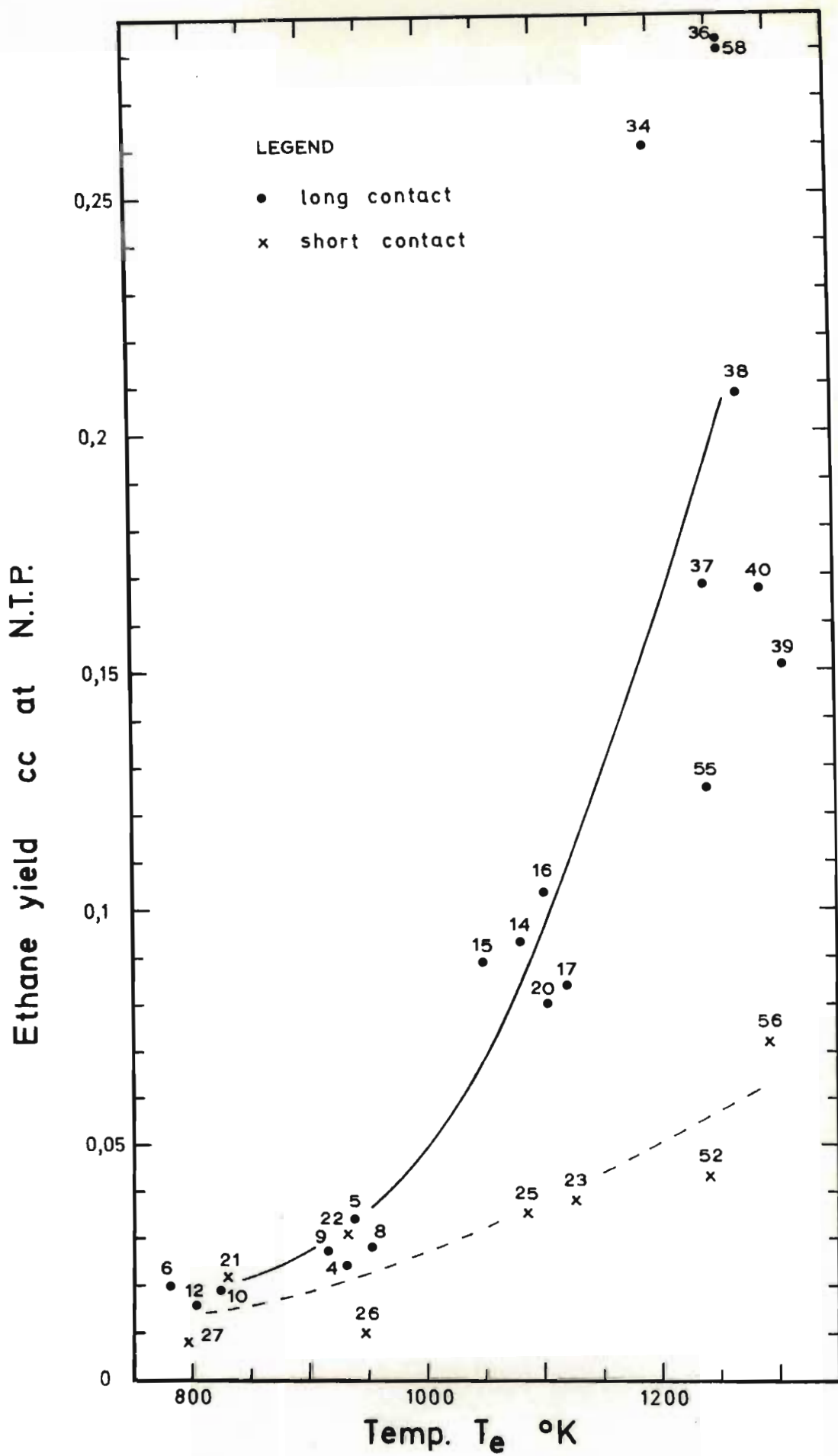


FIGURE 5.5.2.III Long and short contact runs ; Ethane yield  $\nu$  shock temp



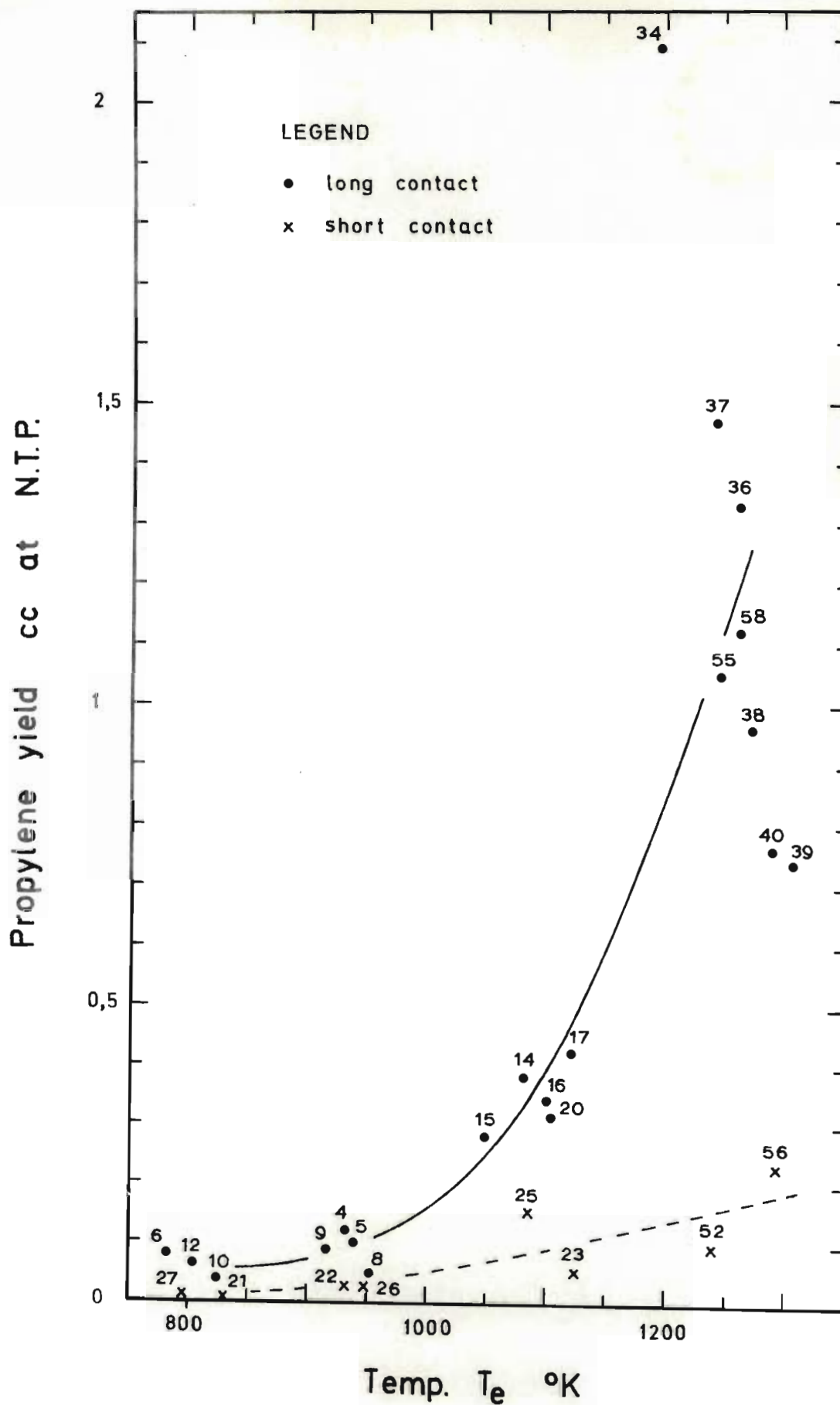


FIGURE 5.5.2.IV Long and short contact runs ; Propylene yield v. shock temp.

TABLE 5.5.2.I

Run No.	Measured Hydrocarbon Composition before Contact Period (estimated where stated)					Measured Hydrocarbon Composition after Contact Period (estimated where stated)					Hydrocarbon Yield due to Shock Wave cc at N.T.P.					Contact Period or Sample Time Min.	Catalyst Batch and Pre-Treatment	Shock Temp. T <sub>e</sub> °K
	CH <sub>4</sub>	C <sub>2</sub> H <sub>4</sub>	C <sub>2</sub> H <sub>6</sub>	C <sub>3</sub> H <sub>6</sub>	C <sub>3</sub> H <sub>8</sub>	CH <sub>4</sub>	C <sub>2</sub> H <sub>4</sub>	C <sub>2</sub> H <sub>6</sub>	C <sub>3</sub> H <sub>6</sub>	C <sub>3</sub> H <sub>8</sub>	CH <sub>4</sub>	C <sub>2</sub> H <sub>4</sub>	C <sub>2</sub> H <sub>6</sub>	C <sub>3</sub> H <sub>6</sub>	C <sub>3</sub> H <sub>8</sub>			
6	-	-	-	-	-	15,7	0,40	0,20	0,10	0,10	0,54	0,065	0,020	0,080	Nil	20	A 79%red.	782
						17,8	0,40	0,10	"	"						30		
10	9,0	0,04	0,04	<0,04	<0,04	18,3	0,10	0,10	<0,04	<0,04	0,52	0,055	0,019	0,038	0,013	A 80%red.	825	
	10,4	0,10	0,10	0,10	0,10	18,0	0,20	0,20	0,10	0,10								20
12	0,6	<0,04	<0,04	<0,04	<0,04	12,0	0,20	0,20	0,10	0,10	0,68	0,044	0,016	0,064	0,01	A 82%red.	804	
	1,9	"	0,04	"	"	20,8	0,30	"	"	"								20
21	2,39	0,06	0,06	"	"	-	-	-	-	-	0,61	0,019	0,022	0,007	0,005	B 86%red.	830	
	1,82	0,07	0,09	"	"	-	-	-	-	-								5
27	0,51	0,05	0,05	"	"	-	-	-	-	-	0,188	0,011	0,008	0,011	0,002	B,78%red.	797	
4	-	-	-	-	-	18,8	0,65	0,50	0,20	0,10	0,90	0,20	0,024	0,12	Nil	A 82%red.	932	
						15,3	0,60	0,40	0,20	"								25
5	-	-	-	-	-	20,8	0,30	0,30	0,10	0,15	0,97	0,165	0,034	0,10	Nil	A 80%red.	938	
						17,8	0,40	0,20	"	0,10								25
8	5,7	<0,04	<0,04	<0,04	<0,04	17,2	0,40	0,10	0,10	0,10	0,99	0,19	0,028	0,051	0,01	A 77%red.	953	
	12,8	0,10	"	"	"	17,2	0,30	0,20	"	"								25
9	21,4	0,04	0,04	"	"	21,3	0,20	"	"	"	0,84	0,12	0,027	0,089	0,016	A 82%red.	916	
	19,6	0,10	0,10	"	"	25,7	0,10	0,10	"	"								25
22	1,65	0,09	0,13	"	"	-	-	-	-	-	0,85	0,091	0,031	0,028	0,005	B 86%red.	932	
	1,48	0,11	0,07	"	"	-	-	-	-	-								5
26	0,27	0,11	0,13	"	"	-	-	-	-	-	0,266	0,033	0,01	0,028	0,006	B 82%red.	948	
	0,19	0,08	0,04	"	"	-	-	-	-	-								5

continued

TABLE 5.5.2.I Continued

Run No.	Measured Hydrocarbon Composition before Contact Period (estimated where stated) Vol. ppm					Measured Hydrocarbon Composition after Contact Period (estimated where stated) Vol. ppm					Hydrocarbon Yield due to Shock Wave cc at N.T.P.					Contact Period or Sample Time Min.	Catalyst Batch and Pre-Treatment	Shock Temp. T <sub>e</sub> °K
	CH <sub>4</sub>	C <sub>2</sub> H <sub>4</sub>	C <sub>2</sub> H <sub>6</sub>	C <sub>3</sub> H <sub>6</sub>	C <sub>3</sub> H <sub>8</sub>	CH <sub>4</sub>	C <sub>2</sub> H <sub>4</sub>	C <sub>2</sub> H <sub>6</sub>	C <sub>3</sub> H <sub>6</sub>	C <sub>3</sub> H <sub>8</sub>	CH <sub>4</sub>	C <sub>2</sub> H <sub>4</sub>	C <sub>2</sub> H <sub>6</sub>	C <sub>3</sub> H <sub>6</sub>	C <sub>3</sub> H <sub>8</sub>			
14	19,0*	<0,1*	<0,1*	<0,1*	<0,1*	26,13	0,61	0,66	0,22	0,32	1,60	0,49	0,093	0,38	0,044	50	A 82%red.	1079
						25,81	0,75	0,40	0,22	0,40						60		
15	"	"	"	"	"	23,15	0,69	0,47	0,34	0,27	1,46	0,75	0,089	0,28	0,029	50	A 80%red.	1048
						28,78	0,87	0,59	0,55	0,31						60		
16	2,50*	0,10*	0,50*	<0,04*	<0,04*	21,36	0,84	0,52	0,55	0,20	1,50	0,49	0,103	0,343	Nil	90	C,85%red.	1100
17	"	"	"	"	"	19,72	1,30	0,63	0,18	0,12	1,76	0,64	0,084	0,422	Nil	90	C,81%red.	1121
20	"	"	"	"	"	22,33	1,00	0,47	0,38	0,25	1,60	0,73	0,08	0,312	Nil	90	C,80%red.	1103
23	1,66	0,10	0,15	<0,04	<0,04	-	-	-	-	-	0,91	0,22	0,038	0,056	0,002	5	B 86%red.	1125
	2,04	0,09	0,10	"	"											10		
25	1,36	-	-	0,47	0,99	-	-	-	-	-	1,02	0,237	0,035	0,153	0,063	5	B 86%red.	1085
	-	0,07	0,12	<0,04	<0,04											10		
34	0,8*	<0,1*	<0,1*	<0,1*	<0,1*	18,67	0,50	<0,04	0,52	0,56	2,56	2,93	0,26	2,09	0,05	80	C 80%red.	1194
						21,59	0,55	"	0,21	0,17						90		
36	"	"	"	"	"	13,39	2,62	0,89	0,95	0,57	3,41	2,76	0,282	1,33	0,114	80	C 80%red.	1259
						19,64	2,35	0,87	1,63	1,57						90		
37	"	"	"	"	"	71,97	1,59	0,54	0,75	0,32	3,38	1,90	0,168	1,47	0,064	80	C 82%red.	1240
						18,21	2,70	0,73	1,29	0,29						90		
38	5,5*	1,0*	3,0*	0,4*	0,06*	11,05	2,22	1,31	0,17	<0,04	3,62	2,84	0,208	0,96	0,004	80	C 92%red.	1269
						14,68	2,80	2,29	0,56	0,20						90		
39	"	"	"	"	"	16,12	4,15	3,88	1,48	1,65	2,72	2,06	0,151	0,741	Nil	80	C 90%red.	1305
						14,99	2,71	2,06	0,41	<0,04						90		
40	"	"	"	"	"	13,05	2,42	0,99	0,64	0,20	2,62	1,77	0,167	0,762	0,035	80	C 92%red.	1287
						11,36	3,08	2,28	1,15	<0,04						90		
55	2,25	0,10	0,50	<0,04	<0,04	17,4*	3,40*	1,65*	0,85*	0,40*	2,22	1,57	0,125	1,05	Nil	95	C,86%red.	1243
58	-	-	-	-	-	56,4	5,32	3,64	1,05	0,18	3,05	2,15	0,28	1,12	0,005	90	C,82%red.	1260
52	3,80	0,30	0,57	<0,04	<0,04	-	-	-	-	-	0,62	0,45	0,043	0,095	Nil	15	C,80%red.	1239
56	61,5	5,82	3,43	0,95	"	-	-	-	-	-	0,93	0,375	0,072	0,23	Nil	15	C,80%red.	1292

Remarks: \* estimated via Simet setting

\* estimated from Figure 5.4.1.I

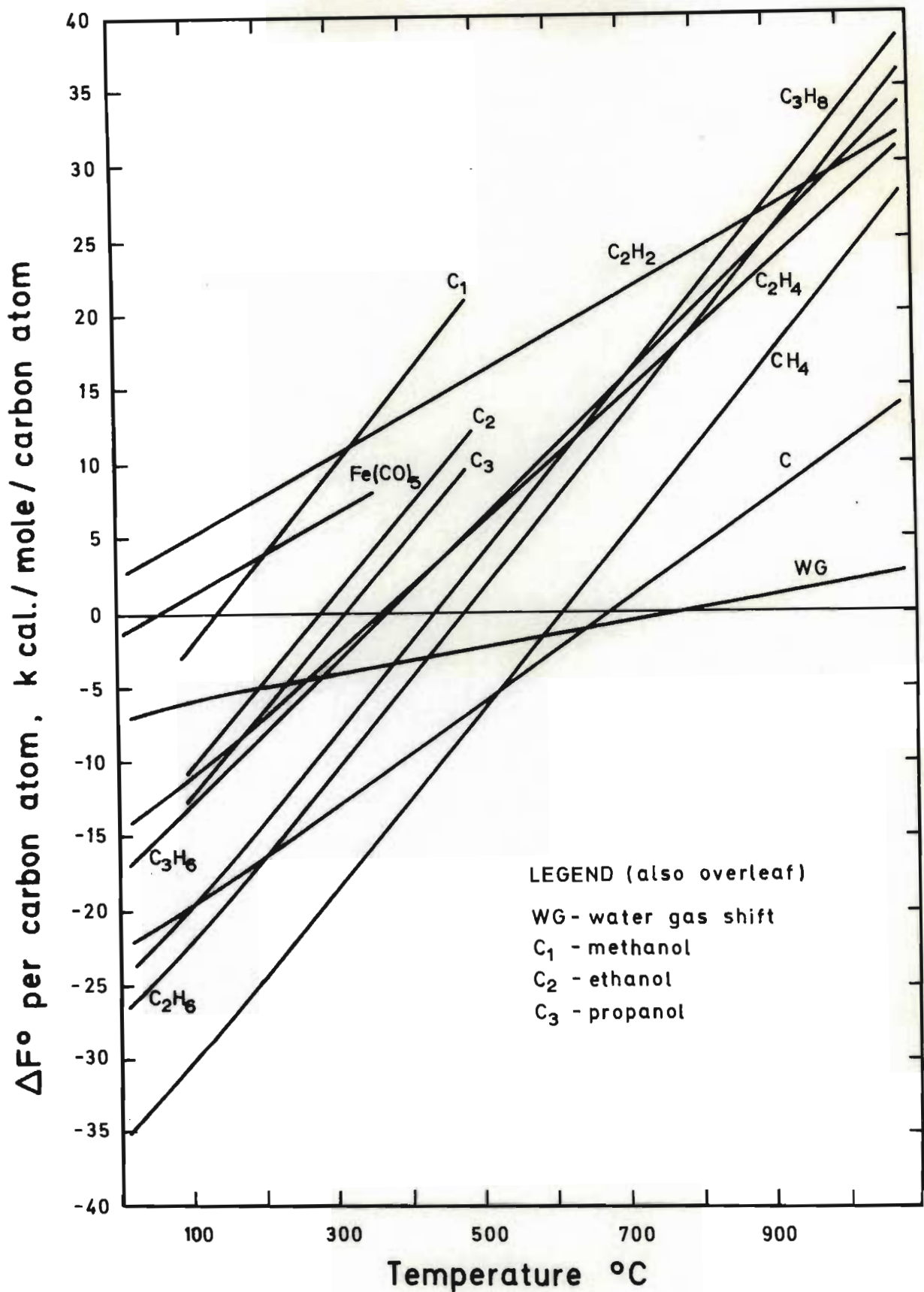
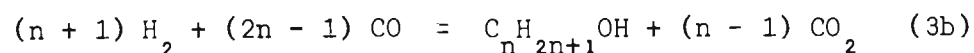
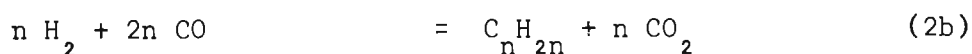
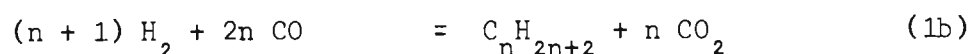
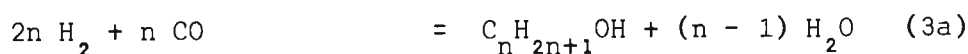
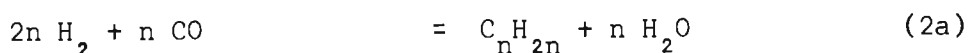
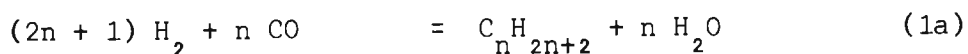


FIGURE 5.5.2.V Standard free energy changes versus temperature ; hydrocarbons, water gas and ironcarbonyl

Legend for FIGURE 5.5.2.V

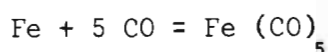
Reactions for the hydrogenation of carbon monoxide may be represented by equations 1 - 3 for the formation of paraffins, monoolefins and alcohols.



Equations marked (a) produce water and those marked (b) carbon dioxide.

Figure 5.5.2.V shows the standard state free energies of formation of hydrocarbons by reactions of type (a). Standard state free energies of reactions of type (b) may be obtained by adding the free energy of the water gas reaction (W.G.) to the free energies of reactions of type (a).

but with time the adsorbed phase became richer in carbon monoxide. This is thought to be one explanation of the beneficial effect of long contact periods especially since adsorbed molecules consisted entirely of hydrogen at the moment of catalyst introduction into the test gas. Another is the formation of iron pentacarbonyl in the catalyst lattice during the contact period. The standard free energy change,  $\Delta F^\circ$  for the reaction



was computed for the temperature range  $0^\circ\text{C} - 350^\circ\text{C}$ . This data was plotted in Figure 5.5.2.V so that comparison could be made with the thermochemical data of various hydrocarbons. Up to about  $60^\circ\text{C}$   $\Delta F^\circ$  was slightly negative indicating that the occurrence of this reaction was a possibility during the contact period. As already mentioned in Chapter 5.4.1, Probst et al (1952) observed the formation of iron pentacarbonyl at low temperatures,  $0 - 100^\circ\text{C}$ . The manner in which it might have acted as a catalyst or reaction promoting intermediate under shock conditions has not been investigated experimentally. Probst noticed a decrease in  $\text{Fe}(\text{CO})_5$  concentration with increasing temperature above  $65^\circ\text{C}$  - this could result in the liberation of CO with simultaneous active iron site production, both of which would tend to accelerate reaction under shock conditions (see Pichler's theory, chapter 1).

Using Subramanyam and Rao's findings it was estimated that the adsorbed phase after 90 minutes of circulation would contain  $\text{CO}/\text{H}_2 = 2,5$ . Synthesis requires on average a  $\text{CO}/\text{H}_2$  ratio of 0,5. Hence it was reasoned that the shock tube Fischer-Tropsch reaction was probably limited mainly by hydrogen availability at the sites of carbon monoxide chemisorption.

### 5.5.3 Effect of Gaseous Hydrocarbons Present before Shocking

Experimental results have been examined to ascertain whether hydrocarbons initially present had influenced the overall character of reaction.

TABLE 5.5.3.1.I

Run No.	Measured Hydrocarbon Composition before Contact Period (estimated where stated) Vol.ppm					Hydrocarbon Yield due to Shock Wave cc at N.T.P.					Contact Period or Sample Time Min.	Catalyst Batch and Pre-Treatment	Shock Temp. T <sub>e</sub> °K
	CH <sub>4</sub>	C <sub>2</sub> H <sub>4</sub>	C <sub>2</sub> H <sub>6</sub>	C <sub>3</sub> H <sub>6</sub>	C <sub>3</sub> H <sub>8</sub>	CH <sub>4</sub>	C <sub>2</sub> H <sub>4</sub>	C <sub>2</sub> H <sub>6</sub>	C <sub>3</sub> H <sub>6</sub>	C <sub>3</sub> H <sub>8</sub>			
41	0,70	<0,04	<0,04	<0,04	<0,04	1,13	0,31	0,025	0,053	Nil	60	None	1342
42	0,30	"	"	"	"	0,590	0,33	0,005	0,010	Nil	60	None	1392
45	17,5	0,17	0,07	0,85	"	0,44	0,134	0,012	0,005	Nil	15	None	1366
46	0,55	0,14	<0,04	<0,04	"	0,48	0,145	0,008	0,010	Nil	15	None	1423
48	69,7	64,0	"	"	"	0,994	0,312	0,067	0,013	Nil	15	None	1409
53	7,6	<0,04	0,55	0,15	"	0,861	0,614	0,044	0,050	Nil	15	None	1363
24	1,17	0,05	0,07	<0,04	<0,04	0,65	0,29	0,024	0,040	Nil	25	None	1216
	2,38	0,13	0,19	"	"						30		
28	1,23	<0,04	<0,04	"	"	0,87	0,23	0,036	0,08	0,003	25	None	1221
	0,19*	"	"	"	"						30		

Remarks: \* Analysis considered erroneous

### 5.5.3.1 Overall Homogeneous Reaction

Comparisons between runs 41, 42, 45, 46, 48 and 53 (Table 5.5.3.1.I) showed no significant dependence of reaction rate on varying amounts of hydrocarbons present before shocking; methane was added in the case of runs 45, 48 and 53 and ethylene in run 48. Runs 24 and 28 gave different hydrocarbon yields even though their pre-shock hydrocarbon concentrations were similar.

It was postulated therefore that the results showed no correlation between shock yields and quantities of hydrocarbons present initially. Naturally this holds only for the range of initial hydrocarbon concentrations investigated, i.e. 0,3 to 70 vol.ppm and for the reaction conditions used.

### 5.5.3.2 Overall Heterogeneous Reaction

Table 5.5.3.2.I contains a comparison between runs with similar catalyst activity and pre-shock contact time but with varying quantities of hydrocarbons present before shocking.

Two groups of runs were studied separately, namely short contact and long contact runs.

#### a) Short Contact Runs

Comparing runs 21 with 27; and 22 with 26 it was noticed that there was a slight variation in the yield of products especially methane. Runs 23 and 25 had approximately the same initial hydrocarbon content and yielded a similar product spectrum.

In run 56 methane and ethylene were injected into the gas before catalyst introduction. Yields were not significantly different from run 52 even though the concentrations of methane and ethylene were 15 fold and 20 fold higher respectively, see Table 5.5.3.2.I.

It should be noted that in the case of these runs there was no check on the extent of reaction which had taken place during the contact period. For this reason slight variations could be expected since the contact period reaction rate differed greatly from run to run; see Chapter 5.4.1.



TABLE 5.5.3.2.1

Run No.	Measured Hydrocarbon Composition before Contact Period (estimated where stated) Vol. ppm					Measured Hydrocarbon Composition after Contact Period (estimated where stated) Vol. ppm					Hydrocarbon Yield due to Shock Wave cc at N.T.P.					Contact Period or Sample Time Min.	Catalyst Batch and Pre-Treatment	Shock Temp. T <sub>e</sub> °K
	CH <sub>4</sub>	C <sub>2</sub> H <sub>4</sub>	C <sub>2</sub> H <sub>6</sub>	C <sub>3</sub> H <sub>6</sub>	C <sub>3</sub> H <sub>8</sub>	CH <sub>4</sub>	C <sub>2</sub> H <sub>4</sub>	C <sub>2</sub> H <sub>6</sub>	C <sub>3</sub> H <sub>6</sub>	C <sub>3</sub> H <sub>8</sub>	CH <sub>4</sub>	C <sub>2</sub> H <sub>4</sub>	C <sub>2</sub> H <sub>6</sub>	C <sub>3</sub> H <sub>6</sub>	C <sub>3</sub> H <sub>8</sub>			
	27	0,51	0,05	0,05	<0,04	<0,04	-	-	-	-	-	0,188	0,011	0,008	0,011			
21	2,39	0,06	0,06	"	"	-	-	-	-	-	0,61	0,019	0,022	0,007	0,005	5	B	830
	1,82	0,07	0,09	"	"											10	86% red.	
26	0,27	0,11	0,13	<0,04	<0,04	-	-	-	-	-	0,266	0,033	0,010	0,028	0,006	5	B	948
	0,19	0,08	0,04	"	"											10	82% red.	
22	1,65	0,09	0,13	"	"	-	-	-	-	-	0,85	0,091	0,031	0,028	0,005	5	B	932
	1,48	0,11	0,07	"	"											10	86% red.	
25	1,36	-	-	0,47	0,99	-	-	-	-	-	1,02	0,237	0,035	0,153	0,063	5	B	1085
	-	0,07	0,12	<0,04	<0,04											10	86% red.	
23	1,66	0,10	0,15	"	"	-	-	-	-	-	0,91	0,22	0,038	0,056	0,002	5	B	1125
	2,04	0,09	0,10	"	"											10	86% red.	
52	3,80	0,30	0,57	<0,04	<0,04	-	-	-	-	-	0,62	0,45	0,043	0,095	Nil	15	C,80%red.	1239
56	61,5	5,82	3,43	0,95	"	-	-	-	-	-	0,93	0,375	0,072	0,230	Nil	15	C,80%red.	1292
14	19,0*	<0,1*	<0,1*	<0,1*	<0,1*	26,13	0,61	0,66	0,22	0,32	1,60	0,49	0,093	0,380	0,044	50	A	1079
	"	"	"	"	"	25,81	0,75	0,40	0,22	0,40						60	82% red.	
15	"	"	"	"	"	23,15	0,69	0,47	0,34	0,27	1,46	0,75	0,089	0,280	0,029	50	A	1048
	"	"	"	"	"	28,78	0,87	0,59	0,55	0,31						60	80% red.	
17	2,50*	0,10*	0,50*	<0,04*	<0,04*	19,72	1,30	0,63	0,18	0,12	1,76	0,64	0,084	0,422	Nil	90	C,81%red.	1121
16	"	"	"	"	"	21,36	0,84	0,52	0,55	0,20	1,50	0,49	0,103	0,343	Nil	90	C,85%red.	1100

continued

TABLE 5.5.3.2.I Continued

Run No.	Measured Hydrocarbon Composition before Contact Period (estimated where stated) Vol. ppm					Measured Hydrocarbon Composition after Contact Period (estimated where stated) Vol. ppm					Hydrocarbon Yield due to Shock Wave cc at N.T.P.					Contact Period or Sample Time Min.	Catalyst Batch and Pre-Treatment	Shock Temp. T <sub>e</sub> °K
	CH <sub>4</sub>	C <sub>2</sub> H <sub>4</sub>	C <sub>2</sub> H <sub>6</sub>	C <sub>3</sub> H <sub>6</sub>	C <sub>3</sub> H <sub>8</sub>	CH <sub>4</sub>	C <sub>2</sub> H <sub>4</sub>	C <sub>2</sub> H <sub>6</sub>	C <sub>3</sub> H <sub>6</sub>	C <sub>3</sub> H <sub>8</sub>	CH <sub>4</sub>	C <sub>2</sub> H <sub>4</sub>	C <sub>2</sub> H <sub>6</sub>	C <sub>3</sub> H <sub>6</sub>	C <sub>3</sub> H <sub>8</sub>			
34	0,8*	<0,1*	<0,1*	<0,1*	<0,1*	18,67	0,50	<0,04	0,52	0,56	2,56	2,93	0,260	2,09	0,05	80	C 80% red.	1194
						21,59	0,55	"	0,21	0,17						90		
36	"	"	"	"	"	13,39	2,62	0,89	0,95	0,57	3,41	2,76	0,282	1,33	0,114	80	C 80% red.	1259
						19,64	2,35	0,87	1,63	1,57						90		
37	"	"	"	"	"	17,97	1,59	0,54	0,75	0,32	3,38	1,90	0,168	1,47	0,064	80	C 82% red.	1240
						18,21	2,70	0,73	1,29	0,29						90		
38	5,5*	1,0*	3,0*	0,4*	0,06*	11,05	2,22	1,31	0,17	<0,04	3,62	2,84	0,208	0,960	0,004	80	C 92% red.	1269
						14,68	2,80	2,29	0,56	0,20						90		
39	"	"	"	"	"	16,12	4,15	3,88	1,48	1,65	2,72	2,06	0,151	0,741	Nil	80	C 90% red.	1305
						14,99	2,71	2,06	0,41	<0,04						90		
40	"	"	"	"	"	13,05	2,42	0,99	0,64	0,20	2,62	1,77	0,167	0,762	0,035	80	C 92% red.	1287
						11,36	3,08	2,28	1,15	<0,04						90		
55	2,25	0,10	0,50	<0,04	<0,04	17,4*	3,40*	1,65*	0,85*	0,40*	2,22	1,57	0,125	1,05	Nil	95	C,86% red.	1243
58	-	-	-	-	-	56,4	5,32	3,64	1,05	0,18	3,05	2,15	0,280	1,12	0,005	90	C,82% red.	1260

Remarks: \* estimated via Simet setting

\* estimated from Figure 5.4.1.I

#### b) Long Contact Runs

Initial methane and ethylene concentrations varied from 12 to 56 ppmv and 0,2 to 5,3 ppmv respectively yet no significant influence on yields was apparent; see Table 5.5.3.2.I. Note that hydrocarbon yields were computed in these cases by subtracting the total quantity of hydrocarbons present in the system at the end of the contact period from the total quantity present after shocking.

#### 5.5.3.3 Summary of Chapter 5.5.3

The results and discussion have shown that hydrocarbons present in the gas before shocking, in the range of concentrations investigated, had no observable effect on reaction rate or product spectrum. Anderson et al (1964) found that methane acted as a diluent only and was not incorporated in reaction. Their experiments involved heavy doses of methane, of the order of percentages by volume, and were carried out under **normal processing conditions**.

Pichler (1970) however, through his tracer experiments showed that low molecular weight **olefins** took part **in** chain initiation; concentrations of olefins were much higher than those investigated here and normal synthesis conditions applied.

#### 5.5.4 Effect of Catalyst Activity

Pre-treatment of the catalyst was found to be important for paraffin yield but not critical in the case of olefins (true between 900 and 1150°K for olefins).

Comparison between reduced and, ~~unreduced and~~ re-oxidised catalysts has been made in Figures 5.5.4.I - IV. **It is** important to note that the runs depicted in these Figures have comparable contact periods, see Table 5.5.4.I.

Overleaf are results of the F-test applied to the data sets indicated.

Temp. °K	Set A Run Nos.	Set B Run Nos.	Calculated F	F at 1% Level	F at 5% Level
1000 to 1150	14, 15, 16, 17, 20	19, 29, 30, 43, 44	$\text{CH}_4 - F_{1,8} = 35,1$ $\text{C}_2\text{H}_4 - F_{1,8} = 0,82$ $\text{C}_2\text{H}_6 - F_{1,8} = 23,4$ $\text{C}_3\text{H}_6 - F_{1,8} = 1,59$	$F_{1,8} = 11,3$	$F_{1,8} = 5,3$

For methane and ethane the difference in yield was significant. It was inferred that hydrogen adsorption was more sensitive to catalyst activity than carbon monoxide adsorption.

In all cases it appeared that unreduced catalysts produced increasing amounts of products with increasing shock strength. This was attributed to two factors,

- a) these catalysts possessed some activity as mentioned in Chapter 5.4.3, and
- b) a gas bulk reaction did proceed in the absence of a catalyst, see Chapter 5.6.

There was no appreciable difference between unreduced and re-oxidised catalysts under shock conditions; see also Chapter 5.6.

In Table 5.5.4.I runs which used catalysts of slightly different degrees of reduction, namely 34, 36, 37 and 38, 39, 40, have been compared. The higher the degree of reduction the lower the yields of ethane and propylene; also true for runs 55 and 58 in respect of all products. It was impossible to comment on change in activity with degree of reduction from the narrow range of reduction extent studied in this work. According to Dorling et al (1958) no change in activity of an iron catalyst occurred once 50 per cent reduction had been reached. Apparently only a layer of limited depth of the catalyst makes an appreciable contribution to the catalyst activity which means that only the iron oxide in this outer layer must be reduced to give optimum activity. Under shock conditions this layer would be even shallower because of the heat sink effect of the catalyst particle.

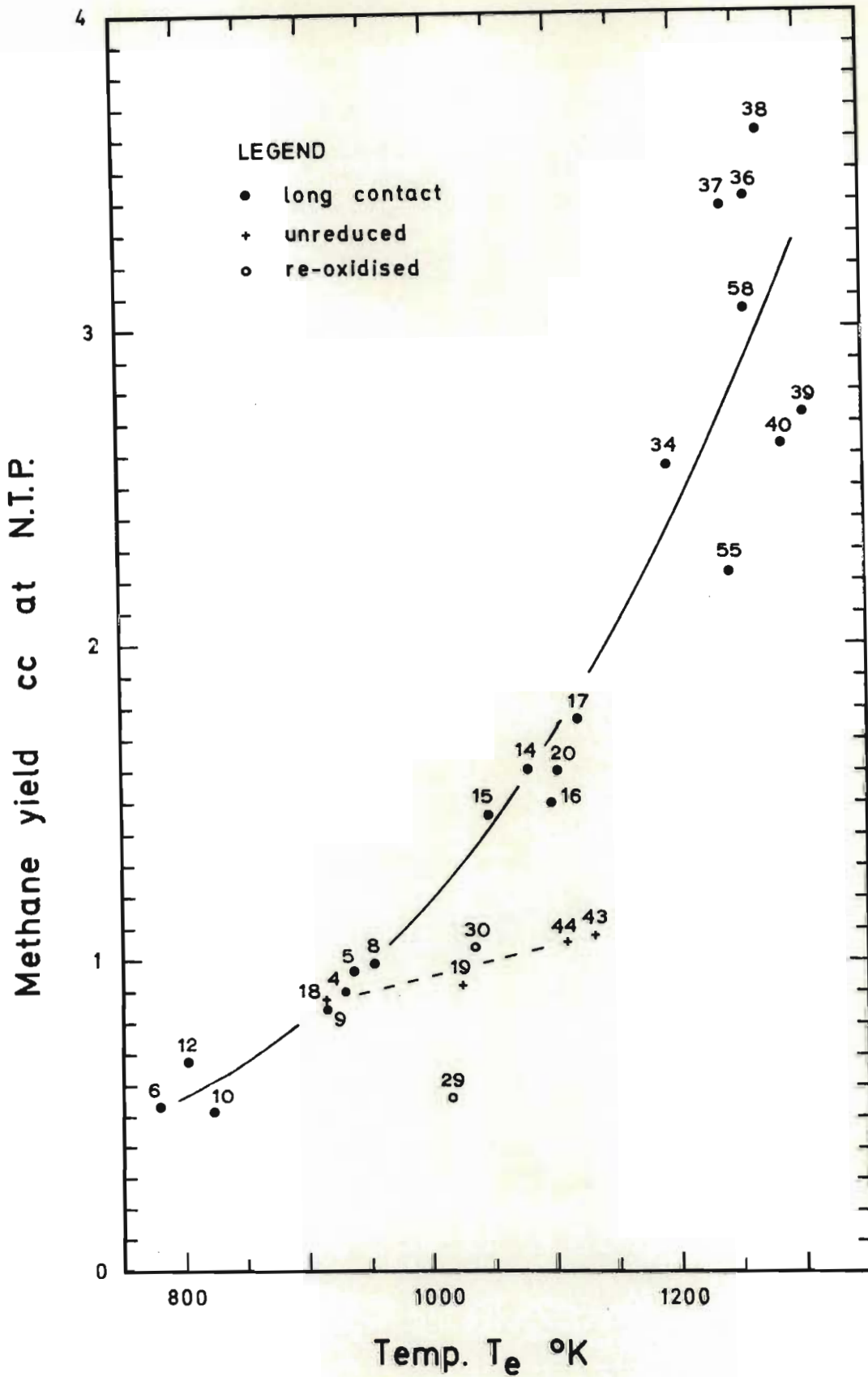


FIGURE 5.5.4.I Long contact, unreduced and re-oxidised runs ; methane yield v. shock temperature

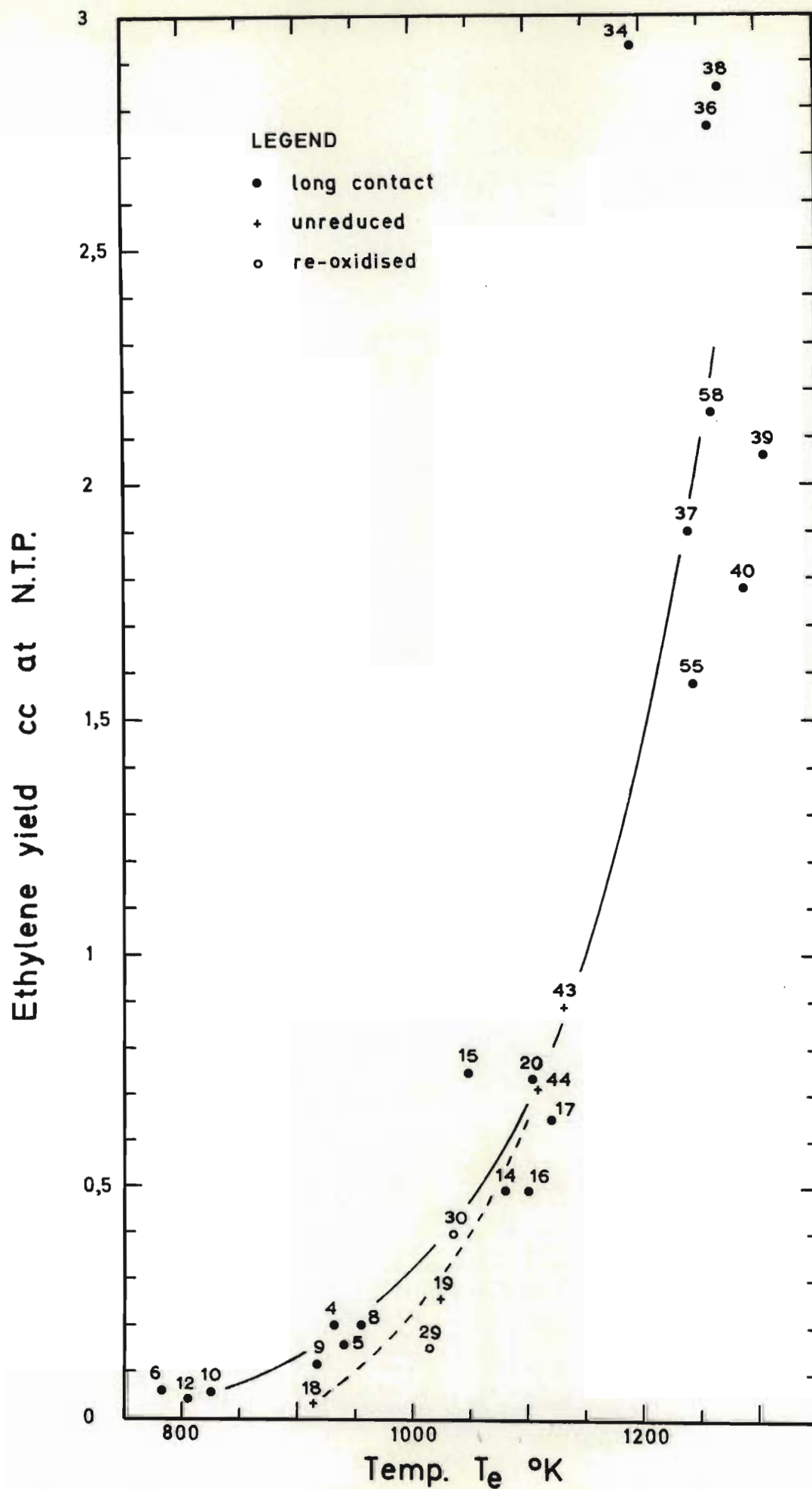


FIGURE 5.5.4.II Long contact, unreduced and re-oxidised runs; ethylene yield

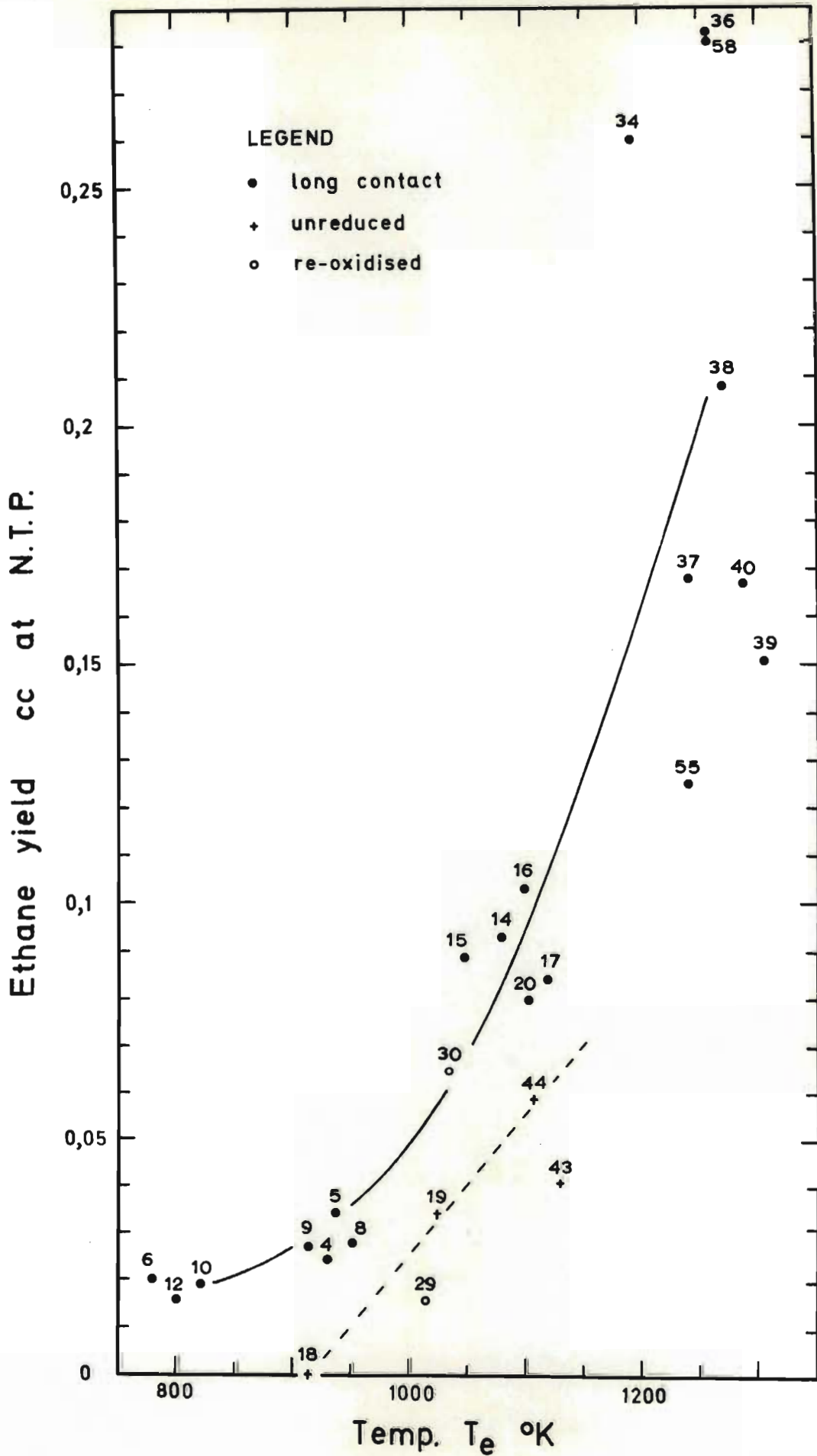


FIGURE 5.5.4.III Long contact, unreduced and re-oxidised runs ; ethane yield v. check temperature

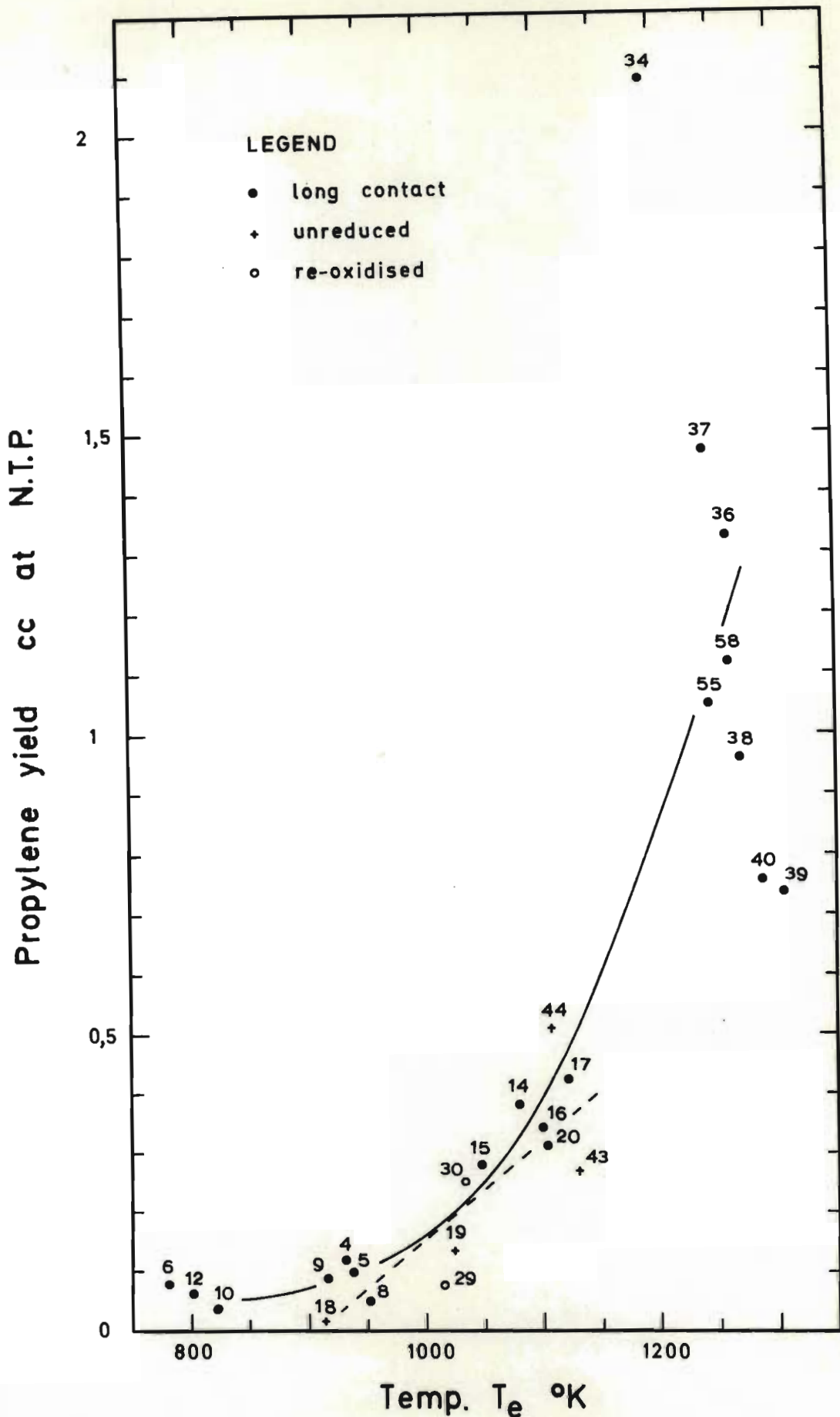


FIGURE 5.5.4.IV Long contact, unreduced and re-oxidised runs; propylene yield v. shock temperature



TABLE 5.5.4.I

Run No.	Measured Hydrocarbon Composition before Contact Period (estimated where stated) Vol.ppm					Measured Hydrocarbon Composition after Contact Period (estimated where stated) Vol.ppm					Hydrocarbon Yield due to Shock Wave cc at N.T.P.					Contact Period or Sample Time Min.	Catalyst Batch and Pre-Treatment	Shock Temp. T <sub>e</sub> °K
	CH <sub>4</sub>	C <sub>2</sub> H <sub>4</sub>	C <sub>2</sub> H <sub>6</sub>	C <sub>3</sub> H <sub>6</sub>	C <sub>3</sub> H <sub>8</sub>	CH <sub>4</sub>	C <sub>2</sub> H <sub>4</sub>	C <sub>2</sub> H <sub>6</sub>	C <sub>3</sub> H <sub>6</sub>	C <sub>3</sub> H <sub>8</sub>	CH <sub>4</sub>	C <sub>2</sub> H <sub>4</sub>	C <sub>2</sub> H <sub>6</sub>	C <sub>3</sub> H <sub>6</sub>	C <sub>3</sub> H <sub>8</sub>			
8	5,7	<0,04	<0,04	<0,04	<0,04	17,2	0,40	0,10	0,10	0,10	0,99	0,19	0,028	0,051	0,01	25	A 77% red.	953
	12,8	0,10	"	"	"	17,2	0,30	0,20	"	"						35		
9	21,4	0,04	0,04	"	"	21,3	0,20	"	"	"	0,84	0,12	0,027	0,089	0,016	25	A 82% red.	916
	19,6	0,10	0,10	"	"	25,7	0,10	0,10	"	"						35		
18	19,0*	<0,1*	<0,1*	<0,1*	<0,1*	71,0	3,63	7,74	2,11	3,18	0,88	0,03	Nil	0,018	Nil	50	B unreduced	914
						67,3	1,46	1,03	0,51	0,18						60		
14	19,0*	<0,1*	<0,1*	<0,1*	<0,1*	26,13	0,61	0,66	0,22	0,32	1,60	0,44	0,093	0,380	0,044	50	A 82% red.	1079
						25,81	0,75	0,40	0,22	0,40						60		
15	"	"	"	"	"	23,15	0,69	0,47	0,34	0,27	1,46	0,75	0,089	0,280	0,029	50	A 80% red.	1048
						28,78	0,87	0,59	0,55	0,31						60		
17	2,50*	0,10*	0,50*	<0,04*	<0,04*	19,72	1,30	0,63	0,18	0,12	1,76	0,64	0,084	0,422	Nil	90	C,81%red.	1121
16	"	"	"	"	"	21,36	0,84	0,52	0,55	0,20	1,50	0,49	0,103	0,343	Nil	90	C,85%red.	1100
19	19,0*	<0,1*	<0,1*	<0,1*	<0,1*	69,1	0,86	1,41	0,14	0,07	0,92	0,26	0,034	0,136	Nil	50	B unreduced	1024
						79,7	1,49	1,04	0,39	0,26						60		
29	0,38	<0,04	<0,04	<0,04	<0,04	12,35	0,14	0,23	<0,04	<0,04	0,56	0,153	0,016	0,074	0,004	80	B,89%red. re-oxid.	1015
	0,46	"	"	"	"	13,96	0,12	0,17	"	"						90		
30	2,76	"	"	"	"	20,41	0,13	0,08	0,04	"	1,04	0,404	0,065	0,250	0,004	80	B,100%red. re-oxid.	1034
	3,41	0,08	0,25	"	"	23,01	0,37	0,32	<0,04	"						90		

continued

TABLE 5.5.4.I Continued

Run No.	Measured Hydrocarbon Composition before Contact Period (estimated where stated)					Measured Hydrocarbon Composition after Contact Period (estimated where stated)					Hydrocarbon Yield due to Shock Wave					Contact Period or Sample Time Min.	Catalyst Batch and Pre-Treatment	Shock Temp. T <sub>e</sub> °K
	Vol.ppm					Vol.ppm					cc at N.T.P.							
	CH <sub>4</sub>	C <sub>2</sub> H <sub>4</sub>	C <sub>2</sub> H <sub>6</sub>	C <sub>3</sub> H <sub>6</sub>	C <sub>3</sub> H <sub>8</sub>	CH <sub>4</sub>	C <sub>2</sub> H <sub>4</sub>	C <sub>2</sub> H <sub>6</sub>	C <sub>3</sub> H <sub>6</sub>	C <sub>3</sub> H <sub>8</sub>	CH <sub>4</sub>	C <sub>2</sub> H <sub>4</sub>	C <sub>2</sub> H <sub>6</sub>	C <sub>3</sub> H <sub>6</sub>	C <sub>3</sub> H <sub>8</sub>			
34	0,8*	<0,1*	<0,1*	<0,1*	<0,1*	18,67	0,50	<0,04	0,52	0,56	2,56	2,93	0,260	2,09	0,05	80	C 80% red.	1194
					21,59	0,55	"	0,21	0,17	90								
36	"	"	"	"	"	13,39	2,62	0,89	0,95	0,57	3,41	2,76	0,282	1,33	0,114	80	C 80% red.	1259
						19,64	2,35	0,87	1,63	1,57						90		
37	"	"	"	"	"	17,97	1,59	0,54	0,75	0,32	3,38	1,90	0,168	1,47	0,064	80	C 82% red.	1240
						18,21	2,70	0,73	1,29	0,29						90		
38	5,5*	1,0*	3,0*	0,4*	0,06*	11,05	2,22	1,31	0,17	<0,04	3,62	2,84	0,208	0,960	0,004	80	C 92% red.	1269
						14,68	2,80	2,29	0,56	0,20						90		
39	"	"	"	"	"	16,12	4,15	3,88	1,48	1,65	2,72	2,06	0,151	0,741	Nil	80	C 90% red.	1305
						14,99	2,71	2,06	0,41	<0,04						90		
40	"	"	"	"	"	13,05	2,42	0,99	0,64	0,20	2,62	1,77	0,167	0,762	0,035	80	C 92% red.	1287
						11,36	3,08	2,28	1,15	<0,04						90		
55	2,25	0,10	0,50	<0,04	<0,04	17,4*	3,40*	1,65*	0,85*	0,40*	2,22	1,57	0,125	1,05	Nil	95	C, 86% red.	1243
58	-	-	-	-	-	56,4	5,32	3,64	1,05	0,18	3,05	2,15	0,280	1,12	0,005	90	C, 82% red.	1260
43	0,8*	<0,1*	<0,1*	<0,1*	<0,1*	11,07	2,93	0,50	<0,04	<0,04	1,08	0,89	0,041	0,27	Nil	90	C, unred.	1130
44	"	"	"	"	"	12,04	0,83	0,44	"	"	1,06	0,715	0,059	0,51	Nil	90	C, unred.	1107

Remarks: \* estimated via Simet setting

\* estimated from Figure 5.4.1.I

## 5.6 Homogeneous Reaction under Shock Conditions

Results have revealed the presence of a homogeneous (gas phase) reaction. Products were produced without the use of catalysts, in increasing amounts up to roughly 1100°K; above this temperature no further increase was apparent.

The F-test was applied to data sets in the temperature ranges 1000 to 1150°K and 1200 to 1430°K; see Table 5.6.I. It was clear that yields of hydrocarbons from runs with short contact time, unreduced catalyst and re-oxidised catalyst were indistinguishable in the range 1000 to 1150°K. Also in this range no-catalyst runs 60 & 61 gave significantly lower yields than runs with catalyst in the case of paraffins but not for olefins. It is interesting to note the similarity between this result and that of Chapter 5.5.4 where paraffins alone yielded a significant difference between long contact and, unreduced and re-oxidised catalyst runs.

In the higher temperature range only propylene gave rise to a significant difference between no-catalyst runs and short contact runs; the latter giving higher yields.

It appeared that reaction over the whole temperature span was mainly homogeneous in nature.

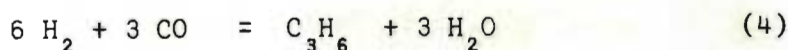
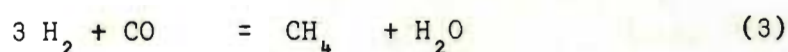
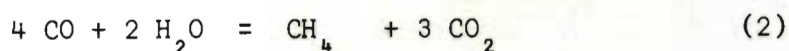
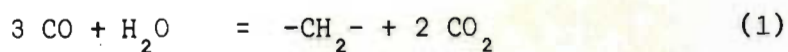
A parallel gas reaction has not been reported in the literature for Fischer-Tropsch synthesis under normal conditions. Speculation as to the full stoichiometry of the homogeneous reaction was not justified on account of insufficient measurements. However some possibilities have been considered below.

The considerations of Chapter 5.5.3.1 showed that the gas phase reaction could be regarded as independent of hydrocarbons initially present over the range of concentrations investigated, 0.3 to 75 volume ppm. Therefore initiation of the gas phase reaction by radicals such as  $\text{CH}_2$ ,  $\text{CH}_3$  etc., has been considered unlikely.

In Figure 5.6.I the change of free energy has been plotted against temperature for the following reactions:-

TABLE 5.6.I

Temp. °K	Set A Run Nos	Set B Run Nos	Set C Run Nos	Calculated F	F at 1% Level	F at 5% Level
1000 to 1150	23, 25	29, 30	19, 43 44	$CH_4 - F_{2,4} = 0,90$ $C_2H_4 - F_{2,4} = 1,79$ $C_2H_6 - F_{2,4} = 0,10$ $C_3H_6 - F_{2,4} = 1,10$	$F_{2,4} = 18,0$	$F_{2,4} = 6,94$
1000 to 1150	60, 61	23, 25, 29, 30, 19, 43, 44	-	$CH_4 - F_{1,7} = 13,05$ $C_2H_4 - F_{1,7} = 3,78$ $C_2H_6 - F_{1,7} = 7,71$ $C_3H_6 - F_{1,7} = 3,88$	$F_{1,7} = 12,25$	$F_{1,7} = 5,59$
1200 to 1430	52, 56	24, 28, 41, 42, 45, 46, 48, 53	-	$CH_4 - F_{1,8} = 0,02$ $C_2H_4 - F_{1,8} = 1,51$ $C_2H_6 - F_{1,8} = 4,48$ $C_3H_6 - F_{1,8} = 20,53$	$F_{1,8} = 11,26$	$F_{1,8} = 5,32$



Equations (1) and (2) have been observed by Kölbel and Hammer (1961) in a similar type of synthesis to Fischer-Tropsch called the Kölbel-Engelhardt synthesis. Equations (3) and (4) are the classical overall equations for the formation of methane and propylene respectively in the Fischer-Tropsch synthesis (Anderson (1956)).

Since hydrocarbons were produced by a homogeneous reaction at elevated temperatures then the most likely reactions (Figure 5.6.I) would have been (2) and (3). However (3) would have had preference over (2) as the initial concentration of  $\text{H}_2\text{O}$  was negligible compared to that of  $\text{CO}$ . The observation that the thermodynamic potential of reaction (1) was low demonstrated that the mechanism of the homogeneous reaction was probably not one involving polymerisation of  $\text{CH}_2$  free radicals.

---

## 5.7 Conclusion

The Fischer-Tropsch synthesis has been investigated under unique conditions in an attempt to reveal the character of its initial stages. Using the uniform reaction environment obtainable in a shock tube it has been shown that during the first millisecond of reaction the only products detected were, in order of descending magnitude, methane, ethylene, propylene and ethane. It was observed that these hydrocarbons were formed via two reaction routes namely, homogeneous and heterogeneous. Yield via the heterogeneous route as a function of temperature could be well described by an Arrhenius type relationship. From the form of the rate equation and a qualitative study of adsorption rates it was postulated that

the shock Fischer-Tropsch reaction was hydrogen adsorption controlled.

Although homogeneous reaction was detected nothing could be said about its nature or dependence of rate on temperature, with any certainty.

While it was shown that catalyst reduction was advantageous for obtaining higher reaction rates, no rate dependence on degree of reduction could be discerned for reduction variations between 77 and 92 per cent.

Fischer-Tropsch reaction was detected at very low temperatures ( $40^{\circ}\text{C}$ ) during the contact period between gas and catalyst.

As mentioned in Chapter 1 it was hoped that this work would result in constructive comment on the following aspects of the Fischer-Tropsch synthesis:-

- (i) The part played by oxygen compounds as intermediate products.
- (ii) The part played by heterogeneous hydrocarbon and oxygen-containing radicals at the start of chain formation and in the process of chain growth.
- (iii) Pichler's mechanism hypothesis versus that of Storch, Golumbic and Anderson.
- (iv) The part played by degradation processes in the formation of the final reaction products.

Naturally the observations made in the following paragraphs apply primarily to the Fischer-Tropsch reaction as carried out in the shock tube and may not reflect the situation in a particular commercial reactor.

Since oxygenated hydrocarbons were not detected in the product gas it was inferred that none were formed and that such compounds did not play an important role in synthesis up to  $\text{C}_3$ .

Heterogeneous hydrocarbon radicals formed by adsorption of hydrocarbon impurities appeared to have no influence on reaction rate (within the concentration range of impurities investigated).

Oxygenated hydrocarbon impurities were not studied in this work.

Owing to the absence of methanol as a product Pichler's hypothesis was favoured because it does not rely on methanol-type intermediates. Pichler's scheme would be expected to have a higher probability since it does not require two adjacent active sites for CO adsorption; the second site need only have sufficient energy to facilitate water removal.

In Table 5.7.I a comparison has been drawn up between SASOL's Kellogg process and Fischer-Tropsch synthesis carried out in the shock tube using similar catalyst, at three different temperature levels. The difference between commercial and shock tube reaction environment is clearly visible.

Table 5.7.III contains six product ratios computed from the surface reaction yields. Runs were grouped into three sets A, B and C as shown in Table 5.7.IV and the F-test applied to each ratio.

Choosing the 1 per cent level of significance the following was found to hold:-

Ratio 1 -  $\text{CH}_4/\text{C}_2\text{H}_4$  consistently decreased with temperature.

Ratio 5 -  $\text{C}_2\text{H}_4/\text{C}_2\text{H}_6$  increased at the high temperature end.

Ratio 6 -  $\text{C}_2\text{H}_6/\text{C}_3\text{H}_6$  decreased at the high temperature end.

Ratio 2 - $\text{CH}_4/\text{C}_2\text{H}_6$	] remained essentially constant throughout temperature range.
Ratio 3 - $\text{CH}_4/\text{C}_3\text{H}_6$	
Ratio 4 - $\text{C}_2\text{H}_4/\text{C}_3\text{H}_6$	

Similarly the F-test was applied to the selectivities of Table 5.7.II; the results appear in Table 5.7.IV. Observations here were:-

- (a) Methane selectivity decreased with increasing temperature.
- (b) Ethylene selectivity increased with increasing temperature at higher temperature levels.
- (c) Ethane selectivity was essentially independent of temperature.
- (d) Propylene selectivity increased with increasing temperature at lower temperature levels.

TABLE 5.7.I COMPARISON BETWEEN KELLOGG AND SHOCK TUBE REACTIONS

Reaction Conditions	SASOL KELLOGG Process	Shock Tube Experiments		
		Run 5	Run 16	Run 36
Temperature, °K	600	938	1100	1259
Total pressure, atm.	19	14,5	18,1	21,8
Partial pressure of reactants, atm.	11 in feed	2,18	2,71	3,90
H <sub>2</sub> /CO mole ratio in feed	5	1	1	1
Mean reaction time	20 sec.	0,655 m.sec.	0,680 m.sec.	0,713 m.sec.
Mass catalyst/mass gas	approx. 24	0,134	0,135	0,135
Pressure dependence of rate - total pressure	power 1		power 0	
- H <sub>2</sub> pp	power 0,60		-	
- CO pp	power 0,28		-	
- CO <sub>2</sub> pp	power 0,67		-	
Activation energy kcal/mole	5 - 10 based on H <sub>2</sub> O + CO <sub>2</sub> produced <sup>2</sup>		12 based on H <sub>2</sub> + CO consumed	



TABLE 5.7.II

Run No.	React. Temp. $T_e$ °C	Surface Reaction Yields cc at N.T.P.					Yield expressed as a percentage of Total Hydrocarbon Yield:Selectivity			
		CH <sub>4</sub>	C <sub>2</sub> H <sub>4</sub>	C <sub>2</sub> H <sub>6</sub>	C <sub>3</sub> H <sub>6</sub>	Total Hydrocarbon	CH <sub>4</sub>	C <sub>2</sub> H <sub>4</sub>	C <sub>2</sub> H <sub>6</sub>	C <sub>3</sub> H <sub>6</sub>
6	782	0,1511	0,05183	0,0200	0,0500	0,2729	55,37	18,99	7,329	18,32
10	825	0,1012	0,03592	0,01900	0,0080	0,1641	61,67	21,89	11,58	4,875
12	804	0,2757	0,02800	0,01600	0,0340	0,3537	77,95	7,916	4,524	9,613
4	932	0,4112	0,1582	0,02006	0,090	0,6799	60,48	23,33	2,950	13,24
5	938	0,4775	0,1220	0,03029	0,070	0,6998	68,23	17,43	4,328	10,00
8	953	0,4882	0,1428	0,01846	0,0210	0,6705	72,81	21,30	2,753	3,132
9	916	0,3613	0,08271	0,02421	0,0590	0,5272	68,53	15,69	4,592	11,19
14	1079	1,025	0,3966	0,0930	0,3500	1,8646	54,97	21,27	4,988	13,77
15	1048	0,9023	0,6699	0,08531	0,2500	1,9075	47,30	35,12	4,472	13,11
16	1100	0,9136	0,3870	0,09174	0,3130	1,7053	53,57	22,69	5,380	18,35
17	1121	1,162	0,5267	0,07221	0,3920	2,1529	53,97	24,46	3,354	18,21
20	1103	1,012	0,6256	0,07507	0,2820	1,9947	50,73	31,36	3,764	14,14
34	1194	1,925	2,777	0,2600	2,060	7,022	27,41	39,55	3,703	29,34
36	1259	2,744	2,565	0,2820	1,300	6,891	39,82	37,22	4,090	18,87
37	1240	2,723	1,718	0,1680	1,440	6,049	45,02	28,40	2,777	23,81
38	1269	2,949	2,638	0,1758	0,9300	6,693	44,06	39,41	2,627	13,90
39	1305	2,033	1,832	0,1175	0,7110	4,694	43,31	39,03	2,503	15,15
40	1287	1,941	1,555	0,1343	0,7320	4,362	44,50	35,65	3,079	16,78
55	1243	1,561	1,386	0,1025	1,020	4,070	38,35	34,05	2,518	25,06
58	1260	2,383	1,954	0,2572	1,090	5,684	41,92	34,38	4,525	19,18
600	SASOL KELLOGG Process Tail Gas - only Products CH <sub>4</sub> , C <sub>2</sub> H <sub>4</sub> , C <sub>2</sub> H <sub>6</sub> and C <sub>3</sub> H <sub>6</sub> considered						34,3	13,2	21,0	31,5

TABLE 5.7.III

Run No.	Product Ratios					
	1	2	3	4	5	6
	$\frac{CH_4}{C_2H_4}$	$\frac{CH_4}{C_2H_6}$	$\frac{CH_4}{C_3H_6}$	$\frac{C_2H_4}{C_3H_6}$	$\frac{C_2H_4}{C_2H_6}$	$\frac{C_2H_4}{C_3H_6}$
6	2,92	7,55	3,02	1,04	2,59	0,40
10	2,82	5,33	12,7	4,49	1,89	2,38
12	9,85	17,23	8,11	0,824	1,75	0,471
4	2,59	20,5	4,57	1,76	7,91	0,223
5	3,91	15,8	6,82	1,74	4,03	0,433
8	3,42	26,45	23,25	6,80	7,74	0,879
9	4,37	14,92	6,12	1,40	3,42	0,410
14	2,58	11,02	2,93	1,13	4,26	0,266
15	1,35	10,58	3,61	2,68	7,85	0,341
16	2,36	9,95	2,92	1,24	4,22	0,293
17	2,21	16,09	2,96	1,34	7,29	0,184
20	1,62	13,48	3,59	2,22	8,33	0,266
34	0,693	7,40	0,934	1,35	10,68	0,126
36	1,07	9,73	2,11	1,97	9,10	0,217
37	1,58	16,21	1,89	1,19	10,23	0,117
38	1,12	16,77	3,17	2,84	15,01	0,189
39	1,11	17,30	2,86	2,58	15,59	0,165
40	1,25	14,45	2,65	2,12	11,58	0,183
55	1,13	15,23	1,53	1,36	13,52	0,100
58	1,22	9,27	2,19	1,79	7,60	0,236
SASOL KELLOGG Process	2,6	1,6	1,1	0,42	0,63	0,67

TABLE 5.7.IV

Temp. Range °K	Set	Run Nos. Sets A and B	Run Nos. Sets B and C	
910 - 960	A	4, 5, 8, 9		
1040 - 1120	B	14,15,16,17,20	14,15,16,17,20	
1190 - 1310	C	-	34,36,37,38,39,40,55,58	
		Calculated F	Calculated F	Tabulated F
Product Ratios	1 CH <sub>4</sub> /C <sub>2</sub> H <sub>4</sub>	F <sub>1,7</sub> = 13,43	F <sub>1,11</sub> = 18,39	At 1% level
	2 CH <sub>4</sub> /C <sub>2</sub> H <sub>6</sub>	F <sub>1,7</sub> = 7,42	F <sub>1,11</sub> = 0,312	F <sub>1,7</sub> = 12,25
	3 CH <sub>4</sub> /C <sub>3</sub> H <sub>6</sub>	F <sub>1,7</sub> = 3,34	F <sub>1,11</sub> = 8,98	F <sub>1,11</sub> = 9,65
	4 C <sub>2</sub> H <sub>4</sub> /C <sub>3</sub> H <sub>6</sub>	F <sub>1,7</sub> = 1,04	F <sub>1,11</sub> = 0,256	At 5% level
	5 C <sub>2</sub> H <sub>4</sub> /C <sub>2</sub> H <sub>6</sub>	F <sub>1,7</sub> = 0,181	F <sub>1,11</sub> = 13,75	F <sub>1,7</sub> = 5,59
	6 C <sub>2</sub> H <sub>6</sub> /C <sub>3</sub> H <sub>6</sub>	F <sub>1,7</sub> = 3,00	F <sub>1,11</sub> = 12,84	F <sub>1,11</sub> = 4,84
Selectivities expressed as yield % of total hydrocarbon products	CH <sub>4</sub>	F <sub>1,7</sub> = 31,7	F <sub>1,11</sub> = 17,37	
	C <sub>2</sub> H <sub>4</sub>	F <sub>1,7</sub> = 4,99	F <sub>1,11</sub> = 11,88	
	C <sub>2</sub> H <sub>6</sub>	F <sub>1,7</sub> = 1,56	F <sub>1,11</sub> = 6,82	
	C <sub>3</sub> H <sub>6</sub>	F <sub>1,7</sub> = 9,28	F <sub>1,11</sub> = 2,19	

These observations are clearly visible in Figure 5.7.I where mean selectivities from Table 5.7.II have been plotted against hydrocarbon molecular types. Observation (b) corresponds to published trends in the commercial process but observation (a) does not. This was taken as further evidence of the reaction being limited by hydrogen availability. If the product spectrum of the commercial process was restricted to the four products of the shock tube reaction then the selectivities of ethane and propylene could be expected to decrease with increase in temperature. Observations (c) and (d) therefore may also be indicative of hydrogen starvation.

The above are important results; they indicate that methane production was independent of pyrolysis of higher molecular weight hydrocarbons even at such high temperatures. Hence, for the commercial process it was *inferred* that degradation processes involving  $C_2$  and  $C_3$  hydrocarbons would be negligible when the  $H_2/CO$  ratio was equal to 1.

Compared with the Kellogg process the shock tube synthesis tended to yield higher proportions of the two lighter compounds and lower amounts of the heavier products; as indicated by selectivities 2 to 6 in Table 5.7.III and percentage yields in Table 5.7.II. This trend was in keeping with published work on the effect of temperature under commercial conditions.

To summarise, there was evidence that the initial stages of the Fischer-Tropsch reaction using  $H_2/CO = 1$  yielded significant quantities of methane and that the reaction rate was limited by hydrogen adsorption. By studying various  $H_2/CO$  ratios strong rate dependence on hydrogen partial pressure has been observed at low conversions by Anderson (1956), Storch et al (1951), Dry et al (1972), and at high conversion by Roberts (1970) (see Table 5.7.I). Naturally under shock tube conditions the Fischer-Tropsch reaction rate was not influenced by the water gas shift reaction, effect of large quantities of adsorbed products or the extent of conversion of  $H_2 + CO$ .

In terms of the second objective of this work, techniques have been developed to define the reaction environment behind an inci-

dent shock front used as a heating medium in the study of heterogeneous catalysis. In particular unique theory has been developed for handling conditions of varying temperature and pressure. However the accuracies of these techniques have not been determined.

It is clear that initial rate studies are potentially a source of useful rate data for highly complex systems. The heterogeneous shock tube offers a possible means of obtaining such data, but that associated with its use are considerable problems involving mainly sampling and analytical procedures on which further refinements are clearly necessary before the technique as a whole can be said to be completely satisfactory.

---

## 5.8 Recommendations for Future Work

The results led to pointers for decreased methane selectivity in the commercial Kellogg process; (i) the  $H_2/CO$  ratio should be minimised throughout the reaction zone, and (ii) higher temperatures should be employed in the initial stages of reaction, subject to the Boudouard reaction  $2 CO \rightarrow CO_2 + C$  (Dry et al (1970)).

Anderson et al (1964) found that at low conversions methane yield was drastically reduced by water vapour but was increased by increasing  $H_2/CO$  ratio. Unfortunately the  $H_2/CO$  ratio of the gas increases rapidly with increasing conversion and the concentration of water either remains constant or decreases. The inhibiting effect of water vapour would soon be outweighed by the increasing  $H_2/CO$  ratio and methane yield would increase with increasing conversion.

In order to achieve conditions (i) and (ii) proposed above, it could be worth investigating the effect of superheated steam injection at the start of reaction and cold carbon dioxide injection at a later stage; see Figure 5.8.I. Carbon dioxide would have

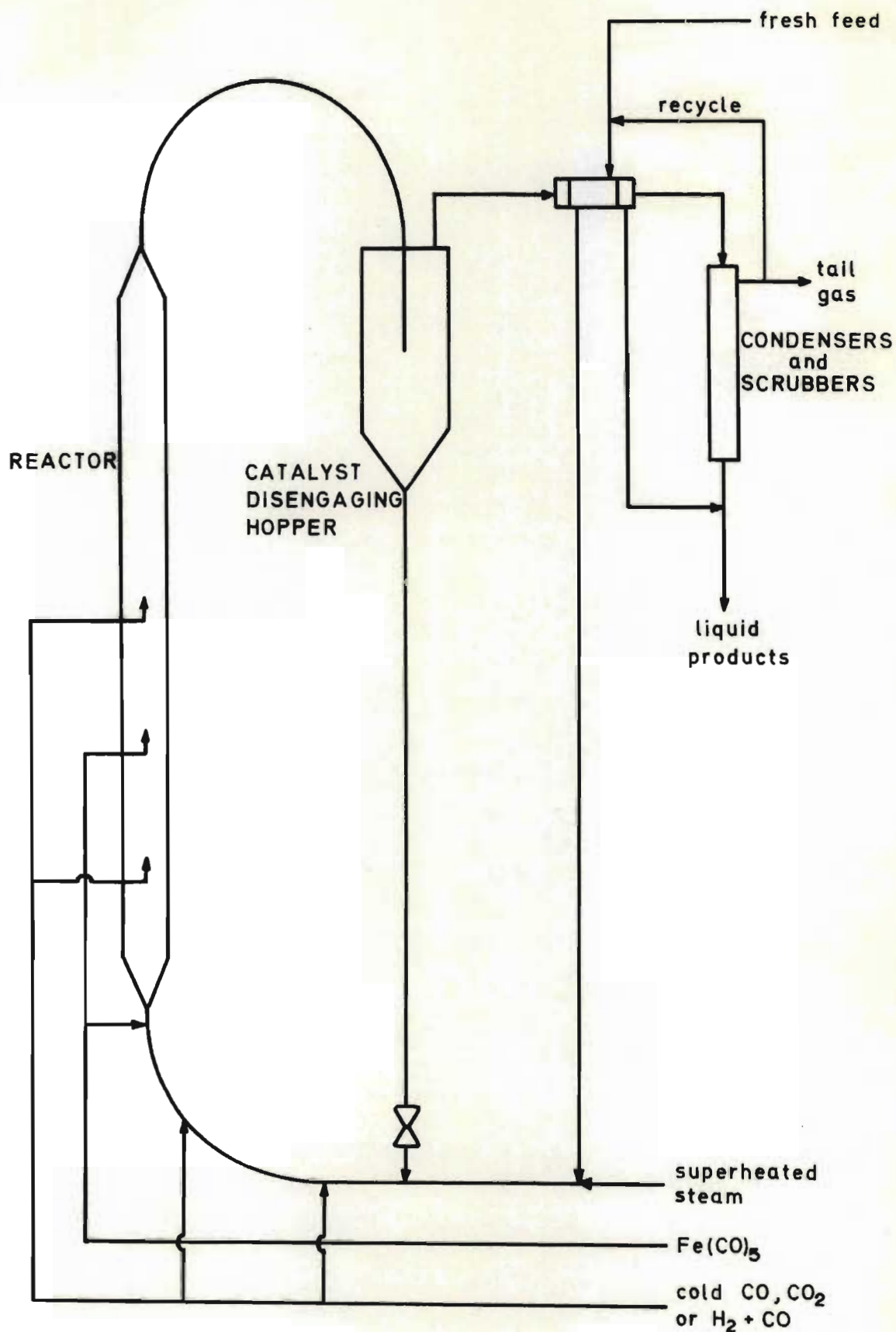


FIGURE 5.8.I Recommendations for future work on Kellogg synthesis

two functions namely to check the production of hydrogen via the water gas shift reaction and to cool the reacting mixture to a desired temperature after a certain time in order to obtain required macromolecular products. In this way it may be possible to utilise a higher overall reaction temperature yet benefit from lower methane and heavy product selectivities. Naturally the economic advantage gained must be weighed against possible loss in catalyst activity due to prolonged exposure to higher concentrations of water vapour and carbon dioxide (Anderson et al (1964)). Tramm (1959) found that water vapour considerably reduced the rate of synthesis while the effect of carbon dioxide was slight. This might be offset by utilising higher reaction temperatures with lower recycle ratios thus increasing production per unit time. Contrary to Tramm's findings Roberts (1970) stated that reaction rate was enhanced by carbon dioxide in the Kellogg process at SASOL; see Table 5.7.I. A possible explanation for Roberts' findings may be that with increasing conversion, rate control of synthesis might change from hydrogen adsorption to carbon monoxide adsorption; thus  $\text{CO}_2$  partial pressure would be important to check the consumption of CO via the water gas shift reaction.

A more practical method of decreasing reaction temperature at prescribed times might be the introduction of cold CO (or low  $\text{H}_2/\text{CO}$  ratio gas) as this would also counteract any tendency for the system to become CO adsorption controlled.

Another aspect which might be worth investigating is the effectiveness of iron pentacarbonyl gas as a homogeneous catalyst, which could lead to a reduction in macro-sized solid iron catalyst loadings and hence energy savings.

---

NOMENCLATURE

a	sound speed	$\text{cm}\cdot\text{sec}^{-1}$
$a_e$	sound speed in relaxed state 2 for gas alone	$\text{cm}\cdot\text{sec}^{-1}$
$a_{1,2,3\dots}$	sound speed in state 1,2,3 ...	$\text{cm}\cdot\text{sec}^{-1}$
A	frequency factor	
A	$= 16(\mu P/\rho a)_g \beta^2$	$\text{in}\cdot\text{mm Hg}$
ARZ	average sound speed in relaxation zone, gas alone	$\text{cm}\cdot\text{sec}^{-1}$
c	specific heat of catalyst particles	$\text{cal}\cdot\text{g}^{-1}\cdot\text{C}^{-1}$
$C_D$	particle drag coefficient	
$C_p$	specific heat of gas at constant pressure	$\text{cal}\cdot\text{g}^{-1}\cdot\text{C}^{-1}$
$C_v$	specific heat of gas at constant volume	$\text{cal}\cdot\text{g}^{-1}\cdot\text{C}^{-1}$
d	catalyst particle effective density	$\text{g}\cdot\text{cm}^3$
$d_{ST}$	shock tube internal diameter	cm
D	catalyst particle diameter	cm
$D_p$	catalyst particle mean diameter for a wide size distribution	cm
E	activation energy for reaction	$\text{kcal}\cdot\text{mole}^{-1}$
$E_a$	activation energy for adsorption	$\text{kcal}\cdot\text{mole}^{-1}$
FD	flow duration	m.sec.
$FD_i$	ideal flow duration	m.sec.
FDP	flow duration parameter	
g	gravitational acceleration	$\text{cm}\cdot\text{sec}^{-2}$
H	enthalpy of unit mass of gas	$\text{cal}\cdot\text{g}^{-1}$
$I_R$	relative intensity of turbulence	
k	Boltzmann's constant	
k	rate constant	
$k_t$	terminal rate constant	
$l_i$	length of cylinder of shocked gas contained between shock front and ideal contact surface	cm
m	mass flow rate of gas per unit area of shock front	$\text{g}\cdot\text{sec}^{-1}$
M	gas molecular weight	
$M_s$	$= u_1/\alpha_1$ Mach No. of shock front relative to gas/solid mixture in state 1	



$M_1$	$= u_1/a_1$ Mach No. of shock front relative to channel gas in state 1
$M_3$	$= u_3/a_1$ Mach No. of gas in state 3 relative to channel gas in state 1
$M'_3$	$= u''_3/a_1$ Mach No. $M_3$ corrected for boundary layer formation
$n$	mass flow rate of particles per unit area of shock front $g \cdot sec^{-1}$
$N$	mole fraction of component
$Nu$	Nusselt number
$N.T.P.$	normal temperature and pressure $25^\circ C$ and 755 mm Hg
$p$	partial pressure atm.abs.
$P$	total pressure atm.abs.
$P_c$	constant pressure in region between two incident rarefaction fans in the chamber gas atm.abs.
$P_e$	pressure in relaxed state 2 atm.abs.
$P_i$	varying pressure in region of compression wave coalescence to form a shock front
$P_I$	$= P_2$ but represents isentropically compressed channel gas atm.abs.
$Pr$	Prandtl number
$P_{1,2,3 \dots}$	pressure in state 1,2,3 ... atm.abs.
$P_{34}$	$= P_3/P_4$
$q$	consumption of $H_2 + CO$ during quench g moles
$Q$	hydrocarbon yield $cm^3$ at N.T.P.
$Q$	consumption of $H_2 + CO$ during reaction period (including or excluding quench) g moles
$r$	reaction rate
$R$	gas constant
$R_D$	extent of catalyst reduction; mass per cent of oxygen removed
$Re$	particle Reynolds number
$S$	surface area of catalyst after complete reduction $m^2 \cdot g^{-1}$
$S.T.P.$	standard temperature and pressure $0^\circ C$ and 1 atm.abs.
$t$	time m.sec.
$t$	statistical t-test
$t'$	time relative to centred reflected rarefaction fan in chamber gas m.sec.

$t''$	time relative to centred reflected rarefaction fan in channel gas m.sec.
$t_c$	time after diaphragm rupture when the head of the reflected rarefaction fan intersects the contact surface m.sec.
$t_E$	time after diaphragm rupture when the head of the reflected rarefaction fan intersects the tail of the relaxation zone m.sec.
$t_{FD}$	flow duration or mean flow duration m.sec.
$t_q$	quench period duration m.sec.
$t_s$	time after diaphragm rupture when the head of the reflected rarefaction fan intersects the shock front m.sec.
$t_Z$	total reaction period m.sec.
$t_3$	time after diaphragm rupture when the head of the reflected rarefaction fan intersects the tail of the incident rarefaction fan m.sec.
$t_4$	time after diaphragm rupture when the head of the incident rarefaction fan rebounds off the end of the chamber m.sec.
$t_6$	time after diaphragm rupture when state 6 is first formed m.sec.
$t_7$	time after diaphragm rupture when state 7 is first formed m.sec.
$T$	gas temperature $^{\circ}K$
$T_e$	gas temperature in relaxed state 2 $^{\circ}K$
$T_Z$	gas temperature below which reaction rate is negligible $^{\circ}K$
$T_{1,2,3,\dots}$	gas temperature in state 1, 2, 3 ... $^{\circ}K$
$u$	gas velocity relative to shock front $cm \cdot sec^{-1}$
$u'$	gas velocity relative to shock tube $cm \cdot sec^{-1}$
$u'_c$	gas velocity in region between two incident rarefaction fans in the chamber gas relative to the shock tube $cm \cdot sec^{-1}$
$u_e$	gas velocity in relaxed state 2 relative to shock front $cm \cdot sec^{-1}$
$u'_e$	gas velocity in relaxed state 2 relative to shock tube $cm \cdot sec^{-1}$
$u''_e$	gas velocity in relaxed state 2 relative to shock tube corrected for boundary layer formation $cm \cdot sec^{-1}$
$u_S$	= VEL shock velocity $cm \cdot sec^{-1}$
$u^+$	fluctuating component of gas velocity relative to shock tube $cm \cdot sec^{-1}$
$u_1$	= $u_S$ = VEL shock velocity $cm \cdot sec^{-1}$
$u_{1,2,3,\dots}$	gas velocity in state 1, 2, 3 ... relative to shock front $cm \cdot sec^{-1}$
$U$	= $u/a_1$ dimensionless gas velocity
$U_e$	= $u_e/a_1$
$U_R$	relative velocity between gas and catalyst particle $cm \cdot sec^{-1}$

UE	contact surface velocity relative to shock tube	cm·sec. <sup>-1</sup>
UE <sub>i</sub>	ideal contact surface velocity relative to shock tube	cm·sec. <sup>-1</sup>
U <sub>1</sub>	= M <sub>1</sub>	
v	catalyst particle velocity relative to shock front	cm·sec. <sup>-1</sup>
v <sub>e</sub>	catalyst particle velocity in relaxed state 2 relative to shock front	cm·sec. <sup>-1</sup>
V	= v/a <sub>1</sub> dimensionless catalyst particle velocity relative to shock front	
V <sub>e</sub>	= v <sub>e</sub> /a <sub>1</sub>	
V <sub>f</sub>	= u <sub>1</sub> /a <sub>1</sub> = U <sub>1</sub> dimensionless catalyst particle velocity in frozen state 2 relative to shock front	
VEL	= u <sub>1</sub> shock front velocity	cm·sec. <sup>-1</sup>
VRZ	velocity of the head of the reflected rarefaction wave in the relaxation zone relative to shock tube	cm·sec. <sup>-1</sup>
x	fraction of H <sub>2</sub> + CO reacted	
x	distance along shock tube measured from the diaphragm station, negative for chamber	cm
x'	distance in coordinate system for centred reflected rarefaction fan in chamber gas	cm
x'	particular value of x	
x''	particular value of x	
x''	distance in coordinate system for centred reflected rarefaction fan in channel gas	cm
x'''	particular value of x	
x <sub>C</sub>	value of x where the head of the reflected rarefaction fan intersects the contact surface	cm
x <sub>E</sub>	value of x where the head of the reflected rarefaction fan intersects the tail of the relaxation zone	cm
x <sub>RZL</sub>	reaction zone length	cm
x <sub>S</sub>	value of x where the head of the reflected rarefaction fan intersects the shock front	cm
x <sub>x</sub>	particular value of x	
x <sub>4</sub>	length of chamber	
X	shock tube similarity length parameter	
XAXIS	length of relaxation zone	cm
Y	hydrocarbon product apparent yield	cm <sup>3</sup> at N.T.P.
Z <sub>2</sub>	gas compressibility factor	

$\alpha_1$	sound speed of gas/solid mixture in state 1	$\text{cm}\cdot\text{sec}^{-1}$
$\alpha_{0,1,2,3,\dots}$	coefficients in reaction rate modelling	
$\beta$	boundary layer parameter	
$\gamma$	gas specific heat ratio	$C_p/C_v$
$\gamma_1$	specific heat ratio of channel gas (constant)	
$\gamma_4$	specific heat ratio of chamber gas (constant)	
$\Gamma$	specific heat ratio of gas/solid mixture	
$\delta$	$= c/C_p$ specific heat ratio catalyst/gas	
$\eta$	$= n/m$ mass flow ratio catalyst/gas	
$\theta$	fraction of surface covered by adsorbed specie	
$\theta$	$= T/T_1$ dimensionless gas temperature	
$\theta_e$	$= T_e/T_1$	
$\mu$	micron ( $10^{-6}$ m)	
$\mu$	gas viscosity	$\text{g}\cdot\text{sec}^{-1}\cdot\text{cm}^{-1}$
$\rho$	gas density	$\text{g}\cdot\text{cm}^{-3}$
$\rho_e$	gas density in relaxed state 2	$\text{g}\cdot\text{cm}^{-3}$
$\rho_{1,2,3,\dots}$	gas density in state 1, 2, 3 ...	$\text{g}\cdot\text{cm}^{-3}$
$T$	catalyst particle bulk temperature	$^{\circ}\text{K}$
$T_e$	catalyst particle bulk temperature in relaxed state 2	$^{\circ}\text{K}$
$\phi$	$= T/T_1$ dimensionless catalyst bulk temperature	
$\phi_e$	$= T_e/T_1$	
$\phi_f$	$= 1$ catalyst bulk temperature in frozen state 2 / $T_1$ dimensionless	

BIBLIOGRAPHY

- ANDERSON, R.B. 'Catalysis' ed. by Emmett, P.H., Reinhold, New York, Vol. 4, Chap. 1, 1 - 19 (1956)
- ANDERSON, R.B. 'Catalysis' ed. by Emmett, P.H., Reinhold, New York, Vol. 4, Chap. 3, 257-371 (1956)
- ANDERSON, R.B.;  
KARN, F.S. &  
SHULTZ, J.F. U. S. Bureau of Mines Bulletin 614 (1964)
- BOKHOVEN, C.;  
VAN HEERDEN, C.;  
WESTRICK, R. &  
ZWIETERING, P. Ch. in Catalysis, ed. by Emmett, P.H., Reinhold, New York, 3, p 265 (1955)
- BOUDART, M. Amer. Inst. Chem. Eng., 2, 62 - 64 (1956)
- BRADLEY, J.N. 'Shock Waves in Chemistry and Physics' Wiley, New York (1962)
- BRUNAUER & EMMETT J. Amer. Chem. Soc. 62, 1732 (1940)
- CARRIER, G.F. J. Fluid Mech. 4, 376 (1958)
- CHAPPELL, G.A. &  
SHAW, H. J. Phys. Chem. 72 (13), 4672 - 5 (1968)
- CHORNET, E. &  
COUGHLIN, R.W. J. of Catalysis 27, 246 - 265 (1972)
- CLAMEN, A. &  
GAUVIN, W.H. A.I.Ch.E. J., 15, 2, 184 (1969)
- CRAXFORD, S.R. &  
RIDEAL, E.K. J. Chem. Soc., 1604 (1939)
- CRAXFORD, S.R. Trans. Faraday Soc., 42, 576 (1946)
- DORLING, T.A.;  
GALL, D. &  
HALL, C.C. J. Appl. Chem. Sept. 8, 533 - 49 (1958)
- DRY, M.E.;  
SHINGLES, T.;  
BOSHOF, L.J. &  
OOSTHUIZEN, G.J. J. Catalysis 15, 190 - 199 (1969)
- DRY, M.E.;  
SHINGLES, T.;  
BOSHOF, L.J. &  
BOTH, C.S. van H. J. of Catalysis 17, 347 - 354 (1970)

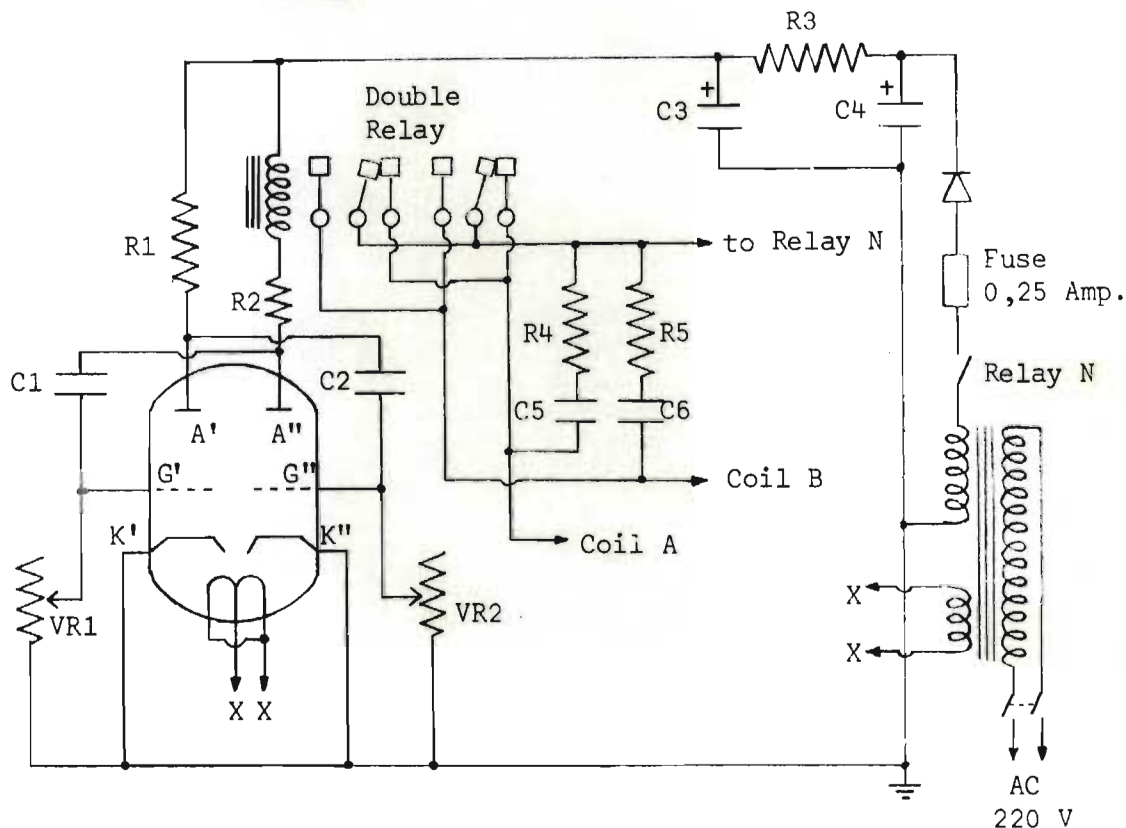
- DRY, M.E.;  
SHINGLES, T. &  
BOSHOFF, L.J. J. Catalysis 25, 99 - 104 (1972)
- DUFF, R.E. Phys. of Fluids, 2, 207 (1959)
- EIDUS, Ya. T. &  
ZELINSKI, N.D. Izv. Akad. Nauk SSSR, Otd. Khim. Nauk,  
190 (1942)
- EIDUS, Ya. T. Russian Chem. Reviews, 36(5), 338-351 (1967)
- ELVINS, O.C. &  
NASH, A.W. Nature, 118, 154 (1926)
- FISCHER, F. &  
TROPSCH, H. Brennstoff-Chem., 4, 276 (1923) &  
5, 201, 217 (1924)
- FISCHER, F. &  
TROPSCH, H. Brennstoff-Chem., 7, 97 (1926)
- FISCHER, F. Brennstoff-Chem., 24, 489 (1930)
- FISCHER, F. &  
PICHLER, H. German Patent Appl. St 56, 470, July 30, (1937)
- Fuel Research Board Report, Great Britain, D.S.I.R. London 62 pp (1953)
- Fuel Research Board Report, Great Britain, D.S.I.R. London 70 pp (1954)
- GALL, D.;  
GIBSON, E.J. &  
HALL, C.C. J. Appl. Chem., 2, 371 (1952)
- GAYDON, A.G. &  
HURLE, I.R. 'The Shock Tube in High-Temperature Chemical  
Physics' Chapman and Hall, London, p 113 (1963)
- GHOSH, SASTRI & KINI Ind. Eng. Chem. 44, 2463 (1952)
- GILBERT, M.;  
DAVIS, L. &  
ALTMAN, D. Jet Propulsion 25, 26 (1955)
- HARTUNIAN, R.A. Methods Exp. Phys., 7, Part B, 141 - 87 (1968)
- HOGLUND, R.F. A.R.S. J., 32, 662 (1962)
- HOOGENDOORN, J.C. &  
SALOMON, J.M. Brit. Chem. Eng. 308 - 312 (1957)  
and 368 - 373 (1957)
- HOOKE, W.J. Phys. of Fluids, 4, 12, 1451 (1961)
- HUGONIOT, H. J. Ec. Polyt., Paris, 57, 1 (1887)
- INGEBO, R.D. NACA TN 3762 (1956)

- KELLY, R.J. 'Design and Construction of a Simple Shock Tube'  
M. Sc. Thesis, University of Natal (1965)
- KNUDSEN, J.G. & 'Fluid Mechanics and Heat Transfer' McGraw-Hill,  
KATZ, D.L. N. Y., p 511 (1958)
- KÖLBEL, H. & Chem. & Process Engrg. 105 - 111 (1961)  
HAMMER, H.
- KÖLBEL, PATZSCHKE & Brennstoff-Chemie 47(1), 14 - 19 (1966)  
HAMMER
- KUMMER, J.T.; J. Amer. Chem. Soc., 70, 3632 (1948)  
DeWITT, T.W. &  
EMMETT, P.H.
- KUMMER, J.T.; J. Amer. Chem. Soc., 73, 564 (1951)  
PODGURSKI, H.H.;  
SPENCER, W.D. &  
EMMETT, P.H.
- KUMMER, J.T. & J. Amer. Chem. Soc., 75, 5177 (1953)  
EMMETT, P.H.
- KUNII, D. & Fluidization Engineering, John Wiley (1969)  
LEVENSPIEL, O.
- LESCHONSKI, K. 'A Course on Particle Technology' Nordwyk,  
Netherlands, p 11 (1970)
- MILLER, W. & J. Royal Tech. Coll., Glasgow, 3, Part 4,  
McINALLY, T.W. 682 (1936)
- MIRELS, H. Phys. of Fluids, 6, 9, 1201 (1963)
- NETTLETON, M.A. Amer. Inst. Aeronautics & Astronautics,  
4 (5) 939 (1966)
- PALMER, H.B. & J. Phys. Chem. 67, 709 - 711 (1963)  
HIRT, T.J.
- PERRY, J.H. Chemical Engineers' Handbook, 4th Edition,  
McGraw-Hill Book Company, 8 - 6
- PICHLER, H. 'Synthesis of Hydrocarbons from Carbon Monoxide  
and Hydrogen' U. S. Bureau of Mines Special  
Report, 158 pp (1947)
- PICHLER, H. 'Advances in Catalysis' ed. by Frankenburg, W.G.  
et al, Academic Press, New York, Vol. 4,  
271 - 341 (1952)
- PICHLER, H. Unpublished lecture to SASOL personnel (1970)

- PROBST, MEYERSON & SEELIG J. Amer. Chem. Soc. 74, 2115 (1952)
- RAAL, F.A. J. S.A.Chem. Inst. VIII(2) p 96 (1955)
- RANKINE, W.J.M. Phil. Trans. 160, 277 (1870)
- RESLER, E.L.; LIN, S.C. & KANTROWITZ, A. J. Appl. Phys. 23, 1390 (1952)
- RINK, J.P. J. Chem. Phys. 36, 1, 262 (1962)
- ROBERTS, H.L. S.A.Coal, Oil and Gas Corporation, unpublished data (1970)
- ROGINSKII, S.Z. Proc. 3rd International Congress on Catalysis, Amsterdam (1964)
- ROSHKO, A. Phys. of Fluids, 3, 6, 835 (1960)
- RUDINGER, G. Multiphase Symposium pub. by Amer. Soc. Mech. Engrs., New York, p 55 (1963)
- RUDINGER, G. Phys. of Fluids 7 (5), 658 - 63 (1964)
- RUDINGER, G. & CHANG, A. Phys. of Fluids 7, 11, 1747 (1964)
- RUMPF, H. Chemie-Ing.-Tech., 32, 129 (1960)
- SOO, S.L. J. Amer. Inst. Chem. Eng. 7, 384 (1961)
- SOO, S.L. I & EC Fundamentals, 3, 1, 75 - 80 (1964)
- STELLING, O. & KRUSTEUSTIERNA, O. Acta Chem. Scand., 12, 1095 - 1110 (1958)
- STERNBERG, H.W. & WENDER, I. Co-ordination Chem., 35 - 55 (1959)
- STORCH, H.H.; GOLUMBIC, N. & ANDERSON, R.B. 'The Fischer-Tropsch and Related Syntheses' Wiley, New York (1951)
- SUBRAMANYAM, K. & RAO, M.R.A. Current Sci. 38 (22), 539 - 41 (1969)
- THURSTON, E.G. J. Acous. Soc. Amer., 27, 735 (1955)
- TOENNIES, J.P. & GREENE, E.F. J. Chem. Phys., 26, 655 (1957)
- TOROBIN, L.B. & GAUVIN, W.H. Can. J. Chem. Engrg., 142 (1960)



- TOROBIN, L.B. & GAUVIN, W.H. A.I.Ch.E. J., 7, 4, 615 (1961)
- TRAMM, H. Erdoel u. Kohle, 12, 347 - 353 (1959)
- U.S. Bureau of Mines Bulletin 544, Bibliography of the Fischer-Tropsch and Related Processes, Part 1.
- VON KÁRMÁN, T. Engineering, 148, 210 - 213 (1939)
- VON KÁRMÁN, T. Trans. ASME, 61, 705 - 710 (1939)
- WEITKAMP, A.W.; SEELIG, H.S.; BOWMAN, N.J. & CADY, W.E. Ind. Eng. Chem., 45, 343 (1953)
- WELLER, S.; HOFER, L.J.E. & ANDERSON, R.B. J. Amer. Chem. Soc., 70, 799 (1948)
- WELLER, S. Amer. Inst. Chem. Eng., 2, 59 - 62 (1956)
- WHITE, D.R. J. Fluid Mech., 4, 585 (1958)
- ZOCCHI, F. J. Gas Chrom., 6, 100 (1968)

APPENDIX ACOIL TIMER CIRCUIT

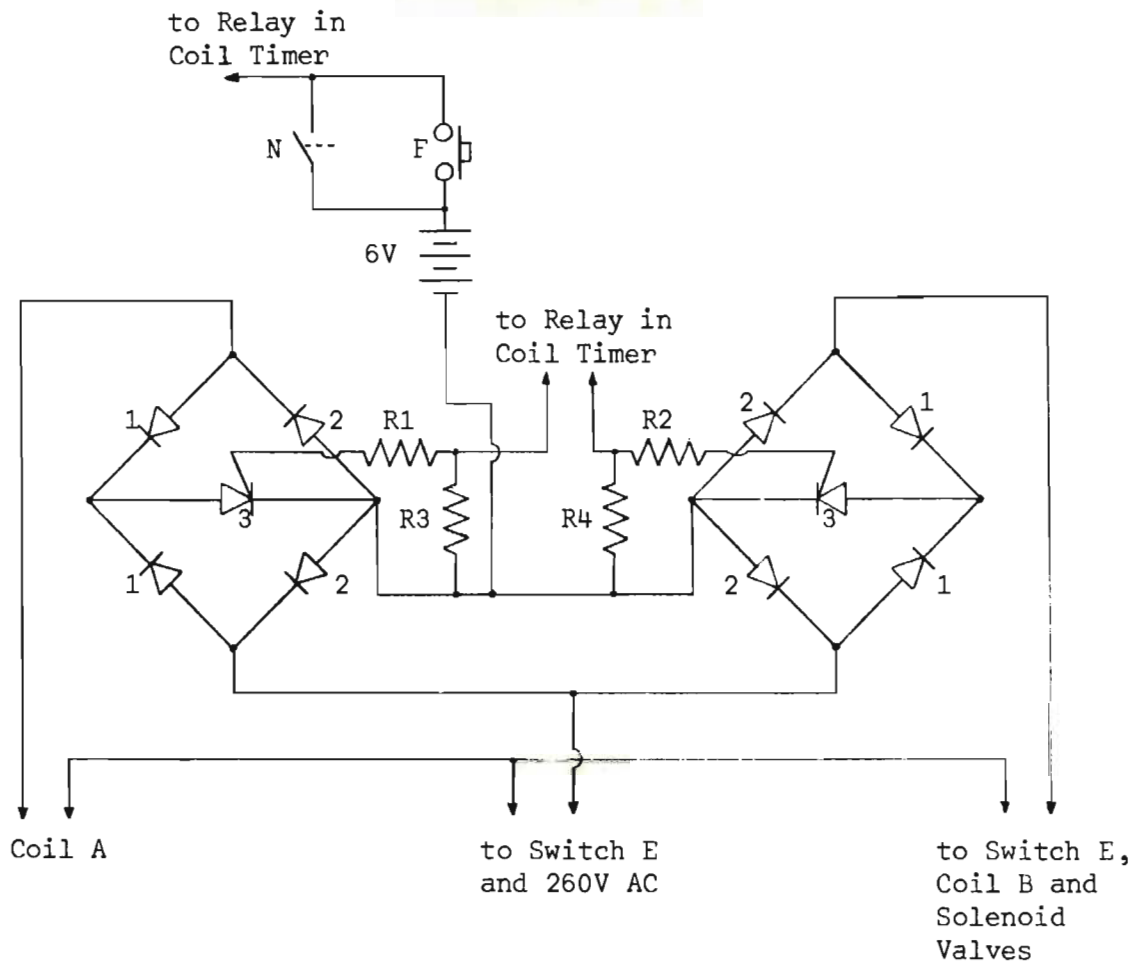
Coil A - Return

Coil B - Puncture

Component List

Valve	ECC81 with B9A base
Rectifier	20 mA, 220 V
Transformer	Douglas MT 22 CL Primary 210 - 220 V Secondary 230 - 6.3 V 2 amps
Relay	Schrack CAD11 D5 DPDT 24 VDC RN 210024 Coil resistance 500 $\Omega$ 200 V at 5 amps per contact
R1	10k, 1W
R2	9,5 k, 1 W for relay coil resistance of 500 $\Omega$
R3	2,2 k, 1 W
R4	56 k, 1 W
R5	56 k, 1 W
VR1	250 k lin. pot.
VR2	250 k lin. pot.
C1, C2	1 $\mu$ F, 600 VW paper
C3, C4	16 + 16 $\mu$ F, 600 VW electrolytic
C5, C6	1 $\mu$ F, 600 VW paper

CIRCUIT FOR THYRISTOR AC LOAD CONTROLLER



Component List

R1, R2	100 $\Omega$ 1 W
R3, R4	68 $\Omega$ 1 W
1	RCA 40212 R
2	RCA 40212
3	M MCR 2935 - 7

APPENDIX BSPECIMEN CALCULATION OF HYDROCARBON YIELDSPhysical Dimensions of Equipment

Bore of shock tube	5,3 cm
Length of chamber	60,6 cm
Volume of chamber	1,34 litre
Length of channel	498,0 cm
Volume of channel	11,25 litre
Volume of channel and circulation system (excl. chamber)	24,99 litre
(incl. chamber)	26,33 litre
Volume of gas mixing tank	36,92 litre

Sampling Data for Run 37

Pressure of first tank mixture	28,3 psig
Pressure of second tank mixture	9,5 psig
Pressure of third tank mixture	7,0 psig
Pressure of fourth tank mixture	6,7 psig

The pressures of the third and fourth tank mixtures were boosted with hydrogen having the following analysis

CH <sub>4</sub>	- 0,5 ppmv	C <sub>2</sub> H <sub>4</sub>	- 0,21 ppmv
C <sub>2</sub> H <sub>6</sub>	- 0,04 ppmv	C <sub>3</sub> H <sub>6</sub>	< 0,04 ppmv
C <sub>3</sub> H <sub>8</sub>	< 0,04 ppmv		

Pressure boosting was necessary so that two samples could be drawn from the tank each time.

The same hydrogen was used in the chamber.

Calculation of Methane Yield

$$\begin{aligned} \text{Volume of first tank mixture} &= 36,92 \cdot \frac{(28,3 + 14,6)}{14,6} \text{ litre} \\ &= 108500 \text{ cm}^3 \text{ at N.T.P.} \end{aligned}$$

where N.T.P. is defined here as 25°C and 755 mm Hg.

Similarly the volume of the 2nd tank mixture = 61000 cm<sup>3</sup> at N.T.P.  
 Volume of 3rd tank mixture = 54600 cm<sup>3</sup> at N.T.P.  
 Volume of 4th tank mixture = 54000 cm<sup>3</sup> at N.T.P.

The amount of methane present in each tank filling is

$$1\text{st tank} - 0,1085 \cdot 28,20 = 3,060 \text{ cm}^3 \text{ at N.T.P.}$$

$$2\text{nd tank} - 0,061 \cdot 22,64 = 1,382 \text{ cm}^3 \text{ at N.T.P.}$$

$$3\text{rd tank} - 0,0546 \cdot 17,17 = 0,937 \text{ cm}^3 \text{ at N.T.P.}$$

$$4\text{th tank} - 0,054 \cdot 11,74 = 0,635 \text{ cm}^3 \text{ at N.T.P.}$$

The arithmetic mean of the two sample analyses is used (see Table B.I). After the first and second tank fillings excess pressure was released so that conditions inside the tank before the second and third fillings were N.T.P. Hence methane present in the second tank filling due to residue gas from the first tank filling is:-

$$0,03692 \cdot 28,20 = 1,04 \text{ cm}^3$$

2nd tank residue:-

$$0,03692 \cdot 22,64 = 0,835 \text{ cm}^3$$

$$\text{Therefore 2nd tank contribution} = 1,382 - 1,04 = 0,342 \text{ cm}^3$$

$$3\text{rd tank contribution} = 0,937 - 0,835 = 0,102 \text{ cm}^3$$

Before the mixing tank was filled for the fourth time it was evacuated.

The quantity of methane remaining in the shock tube system after the fourth tank filling is calculated as follows

$$\frac{\text{volume of shock tube system}}{\text{volume of mixing tank}} \cdot \text{quantity of methane in 4th tank mixture}$$

Note that the conditions of temperature and pressure in the shock tube system and the mixing tank are identical at the time of filling of the tank. Hence this quantity is:-

$$\frac{26,33}{36,92} \cdot 0,635 = 0,453 \text{ cm}^3$$

The amounts by which the pressures of the third and fourth tank mixtures were boosted are 5,5 psi and 4,3 psi respectively. Hence the total hydrogen added for boosting purposes is 9,8 psi which equals

$$\frac{9,8}{14,6} \cdot 36,92 \text{ litre or } 24800 \text{ cm}^3 \text{ at N.T.P. Therefore methane added}$$

via this hydrogen is  $0,0248 \cdot 0,5 = 0,0124 \text{ cm}^3$ .

TABLE B.I GAS ANALYSES FOR RUN 37

Sample Description	Components													
	mol. %						ppmv							
	H <sub>2</sub>	Ar	CO	CO <sub>2</sub>	N <sub>2</sub>	O <sub>2</sub>	CH <sub>4</sub>	C <sub>2</sub> H <sub>2</sub>	C <sub>2</sub> H <sub>4</sub>	C <sub>2</sub> H <sub>6</sub>	C <sub>3</sub> H <sub>6</sub>	C <sub>3</sub> H <sub>8</sub>	CH <sub>3</sub> OH	C <sub>2</sub> H <sub>5</sub> OH
Pre-shock gas/catalyst mix after 80 min. of circulation	9,42	81,61	8,91	0,01	0,05	NDA*	17,97	NDA	1,59	0,54	0,75	0,32	NDA	NDA
Pre-shock gas/catalyst mix after 90 min. of circulation	9,47	81,44	8,97	0,01	0,11	NDA	18,21	NDA	2,70	0,73	1,29	0,29	NDA	NDA
First tank mix sample A	89,26	9,64	1,08	0,02	0,01	NDA	27,95	NDA	18,05	1,09	13,03	1,23	NDA	NDA
First tank mix sample B	88,97	9,79	1,14	0,02	0,08	NDA	28,42	NDA	16,73	1,05	10,51	0,04	NDA	NDA
Second tank mix sample A	92,47	6,80	0,71	0,02	0,01	NDA	21,16	NDA	12,18	1,44	7,71	0,04	NDA	NDA
Second tank mix sample B	92,40	6,84	0,74	0,02	0,01	NDA	24,12	NDA	13,45	1,70	7,36	0,04	NDA	NDA
Third tank mix sample A	80,65	17,38	1,92	0,01	0,04	NDA	18,45	NDA	7,02	0,55	4,06	0,04	NDA	NDA
Third tank mix sample B	80,36	17,59	1,93	0,02	0,10	NDA	15,89	NDA	7,54	1,74	8,30	0,04	NDA	NDA
Fourth tank mix sample A	62,14	33,75	3,75	0,01	0,35	NDA	12,30	NDA	1,36	0,21	1,08	0,04	NDA	NDA
Fourth tank mix sample B	62,36	33,90	3,40	0,01	0,33	NDA	11,18	NDA	1,30	0,48	1,18	0,12	NDA	NDA

\* NDA = non-determinable amount

The total quantity of methane present after shocking can now be computed:-

$$3,06 + 0,342 + 0,102 + 0,635 + 0,453 - 0,0124 = 4,58 \text{ cm}^3 \\ \text{at N.T.P.}$$

This quantity is not the yield of methane as methane was present initially in the channel gas mixture and also in the chamber hydrogen.

Methane present initially in the channel gas is

$$24,99 \cdot \frac{20}{14,6} \cdot 18,21 = 0,624 \text{ cm}^3 \text{ at N.T.P.}$$

(initially channel pressure is 20 psia)

Analysis used is that of the sample taken 90 minutes after start of circulation.

Methane added by chamber hydrogen is

$$1,34 \cdot \frac{1265}{14,6} \cdot 0,5 = 0,58 \text{ cm}^3 \text{ at N.T.P.}$$

(initial chamber pressure is 1265 psia)

Therefore the yield of methane due to the passage of the shock wave is

$$4,58 - 0,624 - 0,58 = 3,38 \text{ cm}^3 \text{ at N.T.P.}$$

#### Calculation of Ethylene, Ethane, Propylene and Propane Yields

The procedure is identical to that of methane. Propylene and propane content of the hydrogen was < 0,04 ppmv in both cases and this was treated as zero concentration.

Since the quantities of propane detected were very small this calculation was subject to large errors. For this reason propane was not considered as a product of synthesis.

---

APPENDIX CDATA PROCESSING FOR REACTION MODELC.1 Analytical Expressions for Homogeneous Yields

Analytical expressions for homogeneous yields were obtained by multilinear regression (\*\*\*) STEPWI).

Homogeneous run numbers were 24, 28, 31, 32, 41, 42, 45, 46, 48, 53, 60 and 61. Linear and exponential models were tested; for linear models the independent variables included were  $T_2$ ,  $P$ ,  $t_{FD}$ ,  $PT_2$ ,  $Pt_{FD}$  and  $Tt_{FD}$ ; for exponential models independent variables were  $-1/T_2$ ,  $P$  and  $t_{FD}$ . The dependent variable in each of the above cases was the corresponding hydrocarbon yield; see Table 5.5.1.I.

The best results obtained were as follows:-

$$Q_{CH_4} = 1,61 \cdot e^{\left(-\frac{1111}{T_2}\right)}$$

$$Q_{C_2H_4} = 16,22 \cdot e^{\left(-\frac{5564}{T_2}\right)}$$

$$Q_{C_2H_6} = -0,149 + 0,0002332 T_2 - 0,00003229 PT_2$$

$$Q_{C_3H_6} = 0,03 \text{ (by visual inspection)}$$

The expressions for  $Q_{CH_4}$  and  $Q_{C_2H_6}$  were bad fits; see details of regression results in Table C.1.I.

Since yields were low no distinction was made between homogeneous yield during flow duration (dwell time) and the quench period.

The homogeneous reaction yield of each heterogeneous run was estimated by inserting the appropriate independent variables into the above expressions. The yields due to heterogeneous reaction only were the differences between the observed yields and these estimated homogeneous yields.

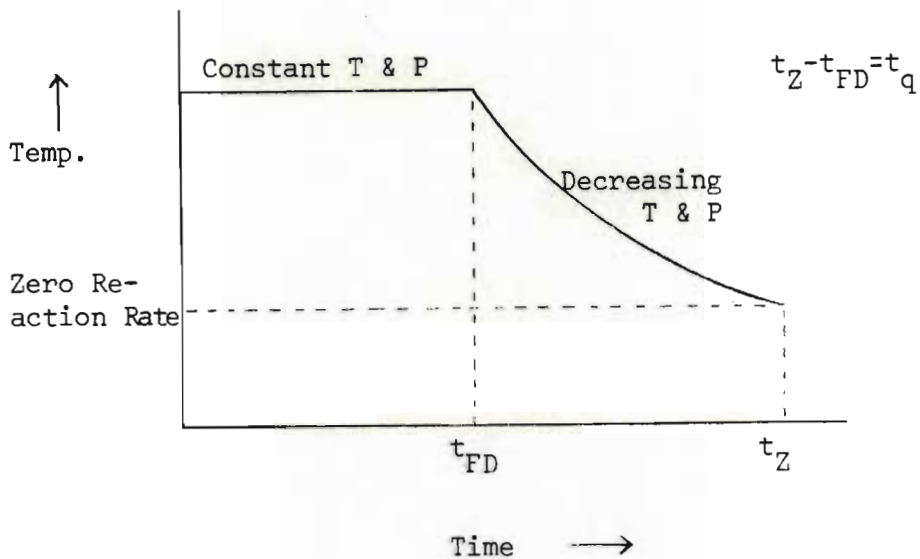


TABLE C.1.I     DETAILS OF REGRESSION ANALYSIS - HOMOGENEOUS YIELDS

	$Q_{CH_4}$	$Q_{C_2H_4}$	$Q_{C_2H_6}$
Sum of squares reduced	0,4205	10,55	0,001735
Proportion of variable of Q reduced	0,3037	0,7936	0,4525
Multiple correlation coefficient	0,551	0,891	0,673
F for analysis of variance	4,36 (D.F.=1-10)	38,45 (D.F.=1-10)	3,72 (D.F.=2-9)
Standard deviation of estimate	0,311	0,524	0,0153
Regression coefficient (a)	E/R = 1111	E/R = 5564	0,0002332
Standard deviation of regression coeff. (a)	532	897	0,0000931
Computed t - regression coefficient (a)	2,09	6,20	2,50
Regression coefficient (b)	-	-	-0,00003229
Standard deviation of regression coeff. (b)	-	-	0,0000147
Computed t - regression coefficient (b)	-	-	-2,19

### C.2 Allowance for Quench Period

Consider  $H_2 + CO$  consumption and assume temperature  $T$  and pressure  $P$  to be constant throughout the reaction period, i.e. assume the reaction period to be  $t_{FD}$  (mean flow duration, dwell time) and not  $t_Z$  the real period; see Figure C.2.I.



**FIGURE C.2.I TEMPERATURE-TIME DIAGRAM; REACTION ZONE**

Let  $Q$  represent  $H_2 + CO$  moles consumed. Using multilinear regression a yield expression such as

$$Q_{FI} = A_I e^{(-E_I/RT)}$$

was found to fit the data fairly well; see Table C.2.I, where  $Q_{FI} = Q_{FIT,initial} = H_2 + CO$  consumed according to the initial curve fit.

Corrections to  $Q$  for variation in mean reaction time  $t_{FD}$  and reaction length  $x_s$  were found to be negligible; see Table C.2.II. Therefore reaction rate could be expressed as  $Q/t_{FD}$ .

$Q_{FI}$  will yield higher values of  $Q$  than  $Q_{FA}$ , where  $Q_{FA} = Q_{FIT,actual} = H_2 + CO$  consumed according to the curve fit assuming instantaneous quenching; see Figure C.2.II.

TABLE C.2.I INITIAL CURVE FIT FOR CONSUMPTION OF H<sub>2</sub> + CO

Computer programme: *** STEPWI			
Relationship: $Q_{FI} = 3,8 \cdot 10^3 \cdot e^{\left(-\frac{7267}{T_e}\right)}$			
Note: $Q_{FI} = Q_{est.I} \cdot 10^4$			
Sum of squares reduced = 27,57			
Proportion of variable of Q reduced = 0,928			
Multiple correlation coefficient = 0,963			
F for analysis of variance (D.F. = 1 - 18) = 232			
Standard deviation of estimate = 0,345			
Variable	Regression coeff.	Standard deviation of regression coeff.	Computed t
$T_e$	E/R = 7267	478	15,2
Run No.	Temperature $T_e$ °K	Consumption of H <sub>2</sub> + CO observed ini- tially $Q_{obs.I} \cdot 10^4$	Estimated con- sumption of H <sub>2</sub> + CO from $Q_{FI}$ $Q_{est.I} \cdot 10^4$
6	782	0,612	0,3497
10	825	0,3356	0,5676
12	804	0,6865	0,4510
4	932	1,442	1,560
5	938	1,416	1,640
8	953	1,271	1,853
9	916	1,074	1,362
14	1079	4,179	4,515
15	1048	4,258	3,700
16	1100	3,836	5,134
17	1121	4,814	5,810
20	1103	4,417	5,228
34	1194	18,18	8,638
36	1259	16,28	11,826
37	1240	14,36	10,824
38	1269	15,13	12,377
39	1305	10,71	14,494
40	1287	10,01	13,408
55	1243	9,942	10,979
58	1260	13,36	11,880

TABLE C.2.II CORRECTIONS TO Q FOR VARIATIONS IN  $t_{FD}$  AND  $x_S$ 

With the following variables included in the regression the first variable selected was  $t_{FD}$ .

Variables:  $Q_{obs.I} \cdot 10^4$ ,  $P$ ,  $t_{FD}$ ,  $T_e$ ,  $R_D$ ,  $\eta$  and  $x_S$ .

Relationship:  $Q_{FI} = 1,63 \cdot 10^5 t_{FD}^{27,53}$  (a)

Without  $t_{FD}$ , the first variable selected was  $x_S$ .

Relationship:  $Q_{FI} = 1 \cdot 10^{26,74} \cdot x_S^{11,52}$  (b)

	(a)	(b)
Sum of squares reduced	28,94	28,46
Proportion of variable of Q reduced	0,974	0,957
Multiple correlation coefficient	0,987	0,979
F for analysis of variance	(D.F.=1-18) 672	(D.F.=1-18) 405
Standard deviation of estimate	0,207	0,265
Regression coefficient	27,53	11,52
Standard deviation of regression coeff.	1,06	0,572
Computed t	25,93	20,13

Continued overleaf

TABLE C.2.II Continued

Run No.	$t_{FD}$ m·sec.	$dt_{FD}$ $=t_{FD}-t_{FD}(\text{run 6})$ m·sec.	$\frac{dQ_{FI} \text{ due to } dt_{FD}}{Q_{FI}(\text{run 6})}$ from eqn. (a)	$x_S$ cm	$dx_S$ $= x_S - x_S(\text{run 6})$	$\frac{dQ_{FI} \text{ due to } dx_S}{Q_{FI}(\text{run 6})}$ from eqn. (b)
6	0,628	0	0	199	0	0
10	0,633	0,005	-	202	3	-
12	0,631	0,003	-	200	1	-
4	0,655	0,027	-	226	27	-
5	0,655	0,027	-	223	24	-
8	0,655	0,027	-	225	26	-
9	0,653	0,027	-	222	23	-
14	0,681	0,053	-	245	46	-
15	0,679	0,051	-	241	42	-
16	0,680	0,052	-	246	47	-
17	0,681	0,053	-	248	49	-
20	0,681	0,053	-	249	50	-
34	0,712	0,084	-	266	67	-
36	0,713	0,085	$1,18 \cdot 10^{-24}$	270	71	$7,08 \cdot 10^{-6}$
37	0,712	0,084	-	268	69	-
38	0,709	0,081	-	268	69	-
39	0,709	0,081	-	269	70	-
40	0,709	0,081	-	269	70	-
55	0,709	0,081	-	265	66	-
58	0,710	0,082	-	266	67	-

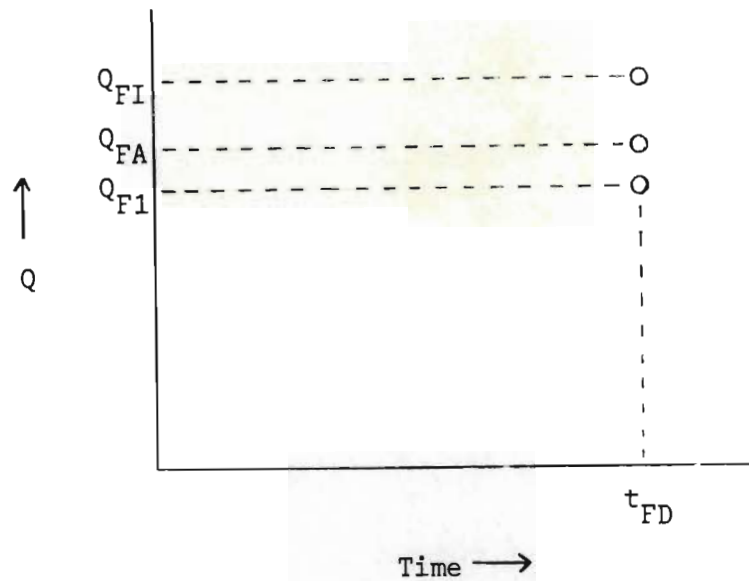


FIGURE C.2.II ITERATIVE APPROACH OF Q TO  $Q_{FA}$

By the following procedure it is possible to estimate the consumption of  $H_2 + CO$  ( $q$ ) during the quench period and hence obtain a better estimate of  $Q_{FA}$ , i.e.  $Q_{F1}$ .

In Figure C.2.III  $t_Z$  represents the instant when reaction rate becomes zero at the end of quench. The shaded area in Figure C.2.III b represents the quantity  $q$ .

$$\text{Now } q = \frac{A_I}{t_{FD}} \int_0^{t_q} e^{(-E_I/RT)} dt$$

It has been assumed here that the reaction rate expression developed for the range of  $t_{FD}$  investigated (0,628 to 0,713 m.sec.) can be extrapolated to the range  $0,713 < t < 2,40$  m.sec.; where 2,40 m.sec. is the total reaction period for category I in Figure C.2.IV. Category I is defined below.

Before the expression for  $q$  can be integrated  $T$  as a function of  $t$  must be determined.

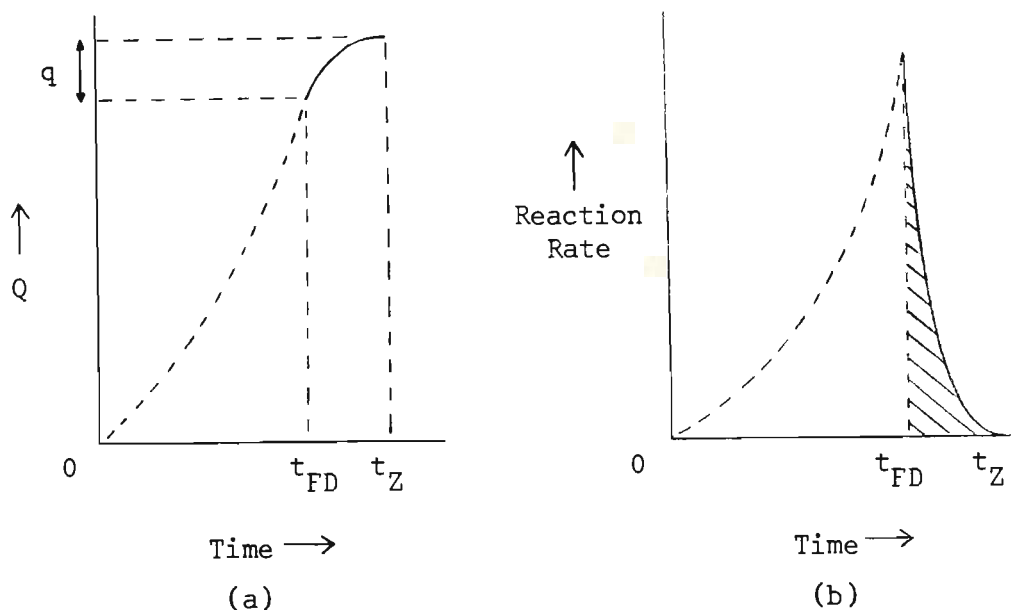


**FIGURE C.2.III YIELD AND RATE/TIME DIAGRAMS**

Experiments were grouped into four categories:-

- I High temperature, 1194 - 1305<sup>o</sup>K, runs 34, 36, 37, 38, 39, 40, 55 and 58.
- II Intermediate temperature, 1048 - 1121<sup>o</sup>K, runs 14, 15, 16, 17 and 20.
- III Low temperature, 916 - 953<sup>o</sup>K, runs 4, 5, 8 and 9.
- IV Extra low temperature, 782 - 825<sup>o</sup>K, runs 6, 10 and 12.

By means of the method described in Chapter 3.3.3 for the determination of quench rates, temperature-time curves for the quench periods were generated. Since there were very small differences between quench rates of individual runs within each of the above categories, a quench curve for one run was used to represent that category. The run chosen was that having a reaction temperature nearest the mean reaction temperature for that category:-

- Category I - run No. 36
- Category II - run No. 16
- Category III - run No. 5

H<sub>2</sub> + CO consumption figures for categories III and IV did not differ much (Table 5.5.1.1.I) and it was assumed therefore that

consumption of reactants during quench when temperature was below 800°K, was negligible.

Figure C.2.IV shows the curves obtained by the method of Chapter 3.3.3 and the curves fitted to these by multilinear regression. The quench periods of categories I and II were divided into two sections for better curve fitting. The quench curve for category III was well approximated by a single straight line. The beginning of quench in each case was considered to be zero time. Hence

$$q_{IIn} = \frac{A_n}{t_{FD}} \left( \int_0^{0,447} e^{-\left(\frac{E}{R}\right)_n \cdot \left(\frac{2,25+t}{2828}\right)} dt + \int_{0,447}^{1,737} e^{-\left(\frac{E}{R}\right)_n \cdot \left(\frac{t^{0,2049}}{897,2}\right)} dt \right)$$

$$q_{IIIn} = \frac{A_n}{t_{FD}} \left( \int_0^{0,23} e^{-\left(\frac{E}{R}\right)_n \cdot \left(\frac{2,16+t}{2372}\right)} dt + \int_{0,23}^{1,02} e^{-\left(\frac{E}{R}\right)_n \cdot \left(\frac{t^{0,1529}}{802,7}\right)} dt \right)$$

$$q_{IIIIn} = \frac{A_n}{t_{FD}} \left( \int_0^{0,38} e^{-\left(\frac{E}{R}\right)_n \cdot \left(\frac{2,20+t}{2068}\right)} dt \right)$$

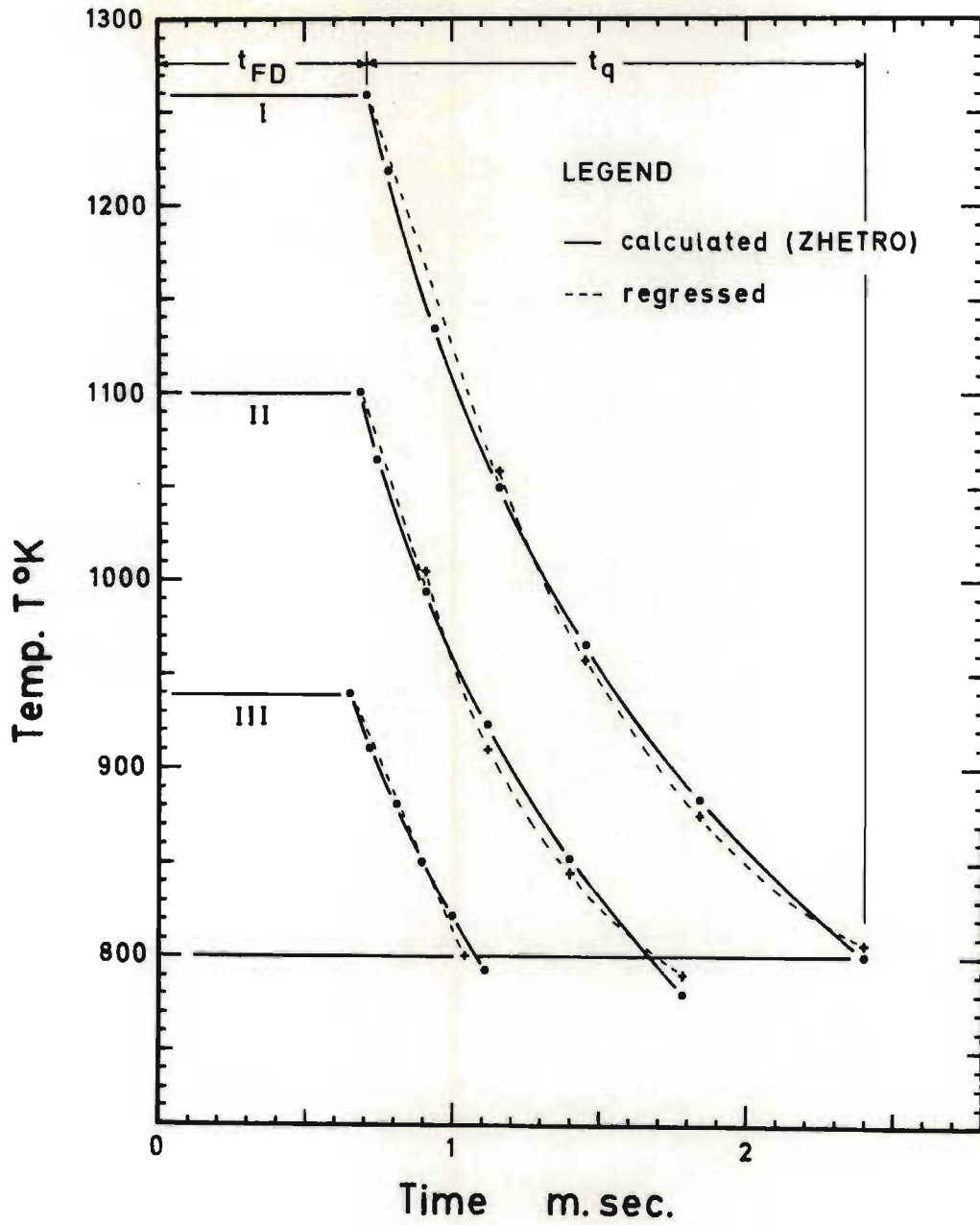
q values were calculated for each run, thus

$$\begin{aligned} q_{run,n} &= \left( \frac{Q_{observed}}{Q_{estimated}} \right)_n \cdot q_{category,n} \\ &= \left( \frac{Q_{observed}}{Q_{estimated}} \right)_n \cdot \frac{A_n}{t_{FD(run)}} \cdot (\text{Integral})_n \end{aligned}$$

where the form of the integral depends on the category to which the run belongs.  $Q_{estimated\ n}$  is the value of  $Q_{observed\ n}$  predicted by  $Q_{Fn}$ . The Rhombert integration technique was used to determine the values of the integrals.

$q_{run,1}$  values were subtracted from the initial  $Q_{obs.}$  values to yield a new set of consumption figures  $Q_{obs.1}$  which was in turn





CATEGORY	REGRESSED CURVES	TIME INTERVAL m. sec.
I	$T = 2828 / (2,25 + t_q)$	$t_q = 0 \text{ to } 0,447$
	$T = 8,972 \cdot 10^2 \cdot t_q^{-0,2049}$	$t_q = 0,447 \text{ to } 1,737$
II	$T = 2372 / (2,16 + t_q)$	$t_q = 0 \text{ to } 0,23$
	$T = 8,027 \cdot 10^2 \cdot t_q^{-0,1529}$	$t_q = 0,23 \text{ to } 1,02$
III	$T = 2068 / (2,20 + t_q)$	$t_q = 0 \text{ to } 0,38$

FIGURE C.2.IV Quench-temperature/time curves for categories I, II and III

regressed to give  $Q_{F1}$  a better estimate of  $Q_{FA}$ . From the  $Q_{F1}$  relationship another set of  $q$ 's ( $q_{run,2}$ ) was calculated followed again by subtraction from the initial  $Q_{obs.}$  values to yield  $Q_{obs.2}$ .  $Q_{obs.2}$  was then regressed to give  $Q_{F2}$  etc. The procedure was continued until variations in  $A$  and the exponent  $E/R$  were less than 5 per cent, i.e.

$$Q_{F(n-1)} = A_{n-1} e^{-\left(\frac{E}{R}\right)_{n-1}} \cdot \frac{1}{T}$$

$$\text{and } Q_{Fn} = A_n e^{-\left(\frac{E}{R}\right)_n} \cdot \frac{1}{T}$$

$$\text{constraints } 0,95 \left(\frac{E}{R}\right)_{n-1} \leq \left(\frac{E}{R}\right)_n \leq 1,05 \left(\frac{E}{R}\right)_{n-1}$$

$$0,95 A_{n-1} \leq A_n \leq 1,05 A_{n-1}$$

The final  $Q_{obs.n}$  values were then regarded as observed values had there been instantaneous quench, i.e.  $Q_{obs.A}$  ( $Q_{Fn} = Q_{FA}$ ). In this case  $Q_{Fg}$  satisfied the constraints; see Table C.2.III.

$Q_{obs.A}$  values were modelled using the expression:-

$$Q = A P^L \eta^M R_D^N e^{-E/RT}$$

In this way an activation energy for the Fischer-Tropsch reaction system studied here could be compared with published activation energies for normal systems. In addition the dependence of yield on the total pressure of the reactants, catalyst loading and reduction, could be observed; see Chapter 5.5.1.1.

TABLE C.2.III FINAL CURVE FIT,  $Q_{FA}$ 

$$Q_{FI} = 3,80 \cdot 10^3 \cdot e^{\left(\frac{-7267}{T}\right)}$$

$$Q_{F1} = 3,537 \cdot 10^2 \cdot e^{\left(\frac{-5433}{T}\right)}$$

$$Q_{F4} = 1,138 \cdot 10^3 \cdot e^{\left(\frac{-6366}{T}\right)}$$

$$Q_{F8} = 1,003 \cdot 10^3 \cdot e^{\left(\frac{-6260}{T}\right)}$$

$$Q_{F9} = 9,573 \cdot 10^2 \cdot e^{\left(\frac{-6221}{T}\right)} = Q_{FA}$$

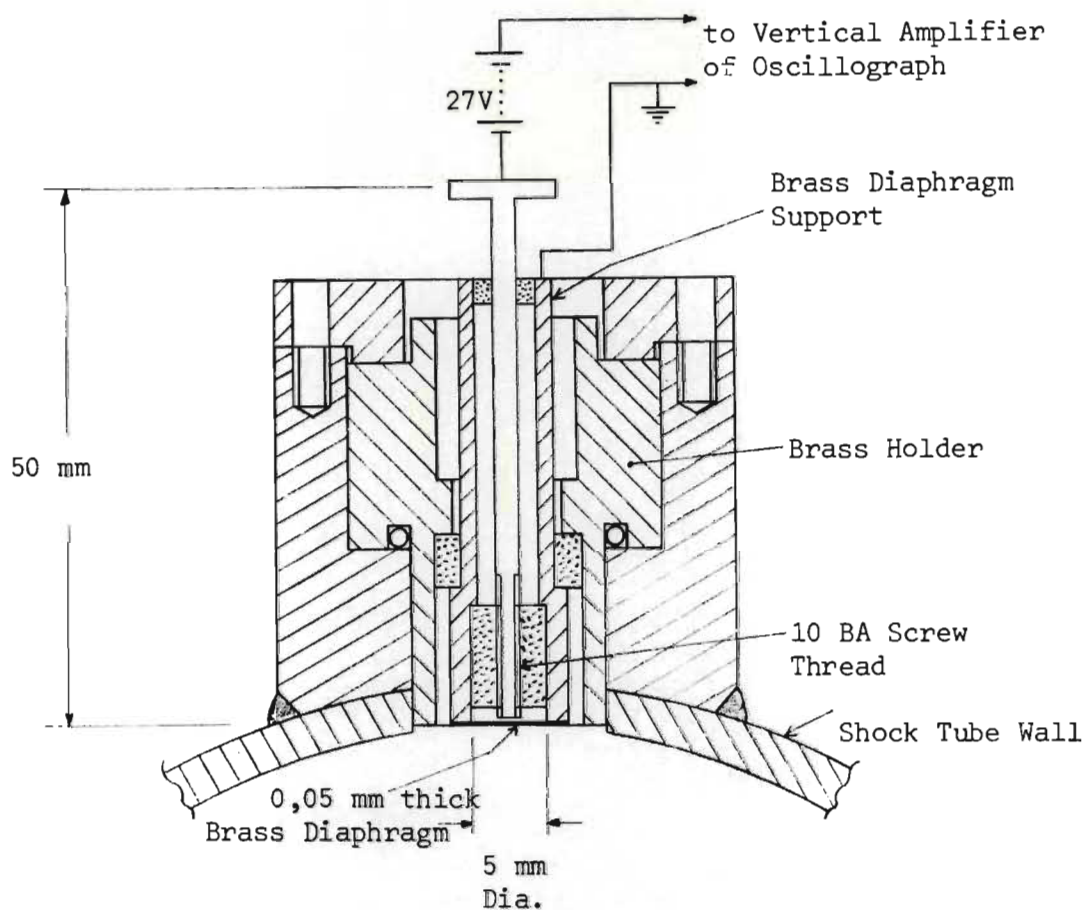
Analysis of  $Q_{F9}$

Sum of squares reduced	=	20,20
Proportion of variable of Q reduced	=	0,917
Multiple correlation coefficient	=	0,958
F for analysis of variance (D.F.=1-18)	=	198
Standard deviation of estimate	=	0,319
Regression coefficient	=	6221
Standard deviation of regression coeff.	=	442
Computed t	=	14,1

Run No.	$Q_{obs.9} \cdot 10^4 = Q_{obs.A} \cdot 10^4$	$Q_{est.9} \cdot 10^4$
6	0,612	0,336
10	0,3356	0,5081
12	0,6865	0,4173
4	1,059	1,208
5	1,051	1,260
8	0,968	1,399
9	0,762	1,075
14	2,627	2,999
15	2,468	2,528
16	2,510	3,347
17	3,264	3,722
20	2,831	3,399
34	8,44	5,225
36	9,90	6,838
37	8,10	6,340
38	9,33	7,110
39	6,94	8,140
40	6,34	7,614
55	5,85	6,417
58	8,13	6,865

APPENDIX D

PRESSURE SWITCH




 Fibre Insulation Glued in Position with 'Araldite' Resin

FIGURE D.I PRESSURE SWITCH

Note: The diaphragm was clamped to the support and lightly soldered around its outer circumference. This procedure avoided solder creep onto the free surface of the diaphragm thus ensuring uniformity of response between pressure switches.

Construction details of pressure switch used for shock speed measurement are given in Figure D.I.

APPENDIX E

DETAILS OF SOLENOID OPERATED EQUIPMENT

Figure E.I shows the bottom solenoid valve and electrical circuit for indicating when the valve is shut.

Figure E.II depicts the rupture pin and its solenoid drive; the diaphragm is shown in the flexed position.

---

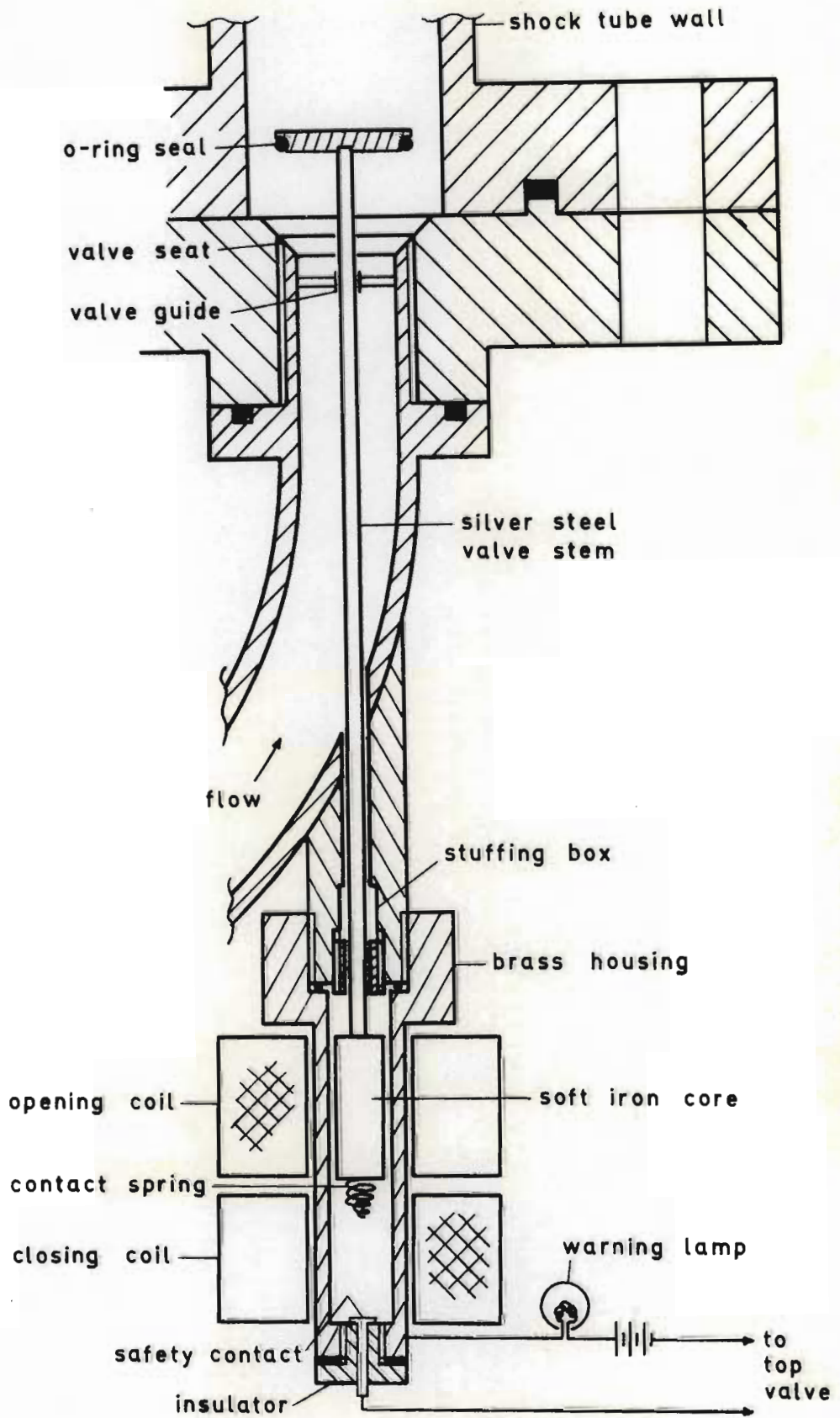


FIGURE E.1 Bottom solenoid valve

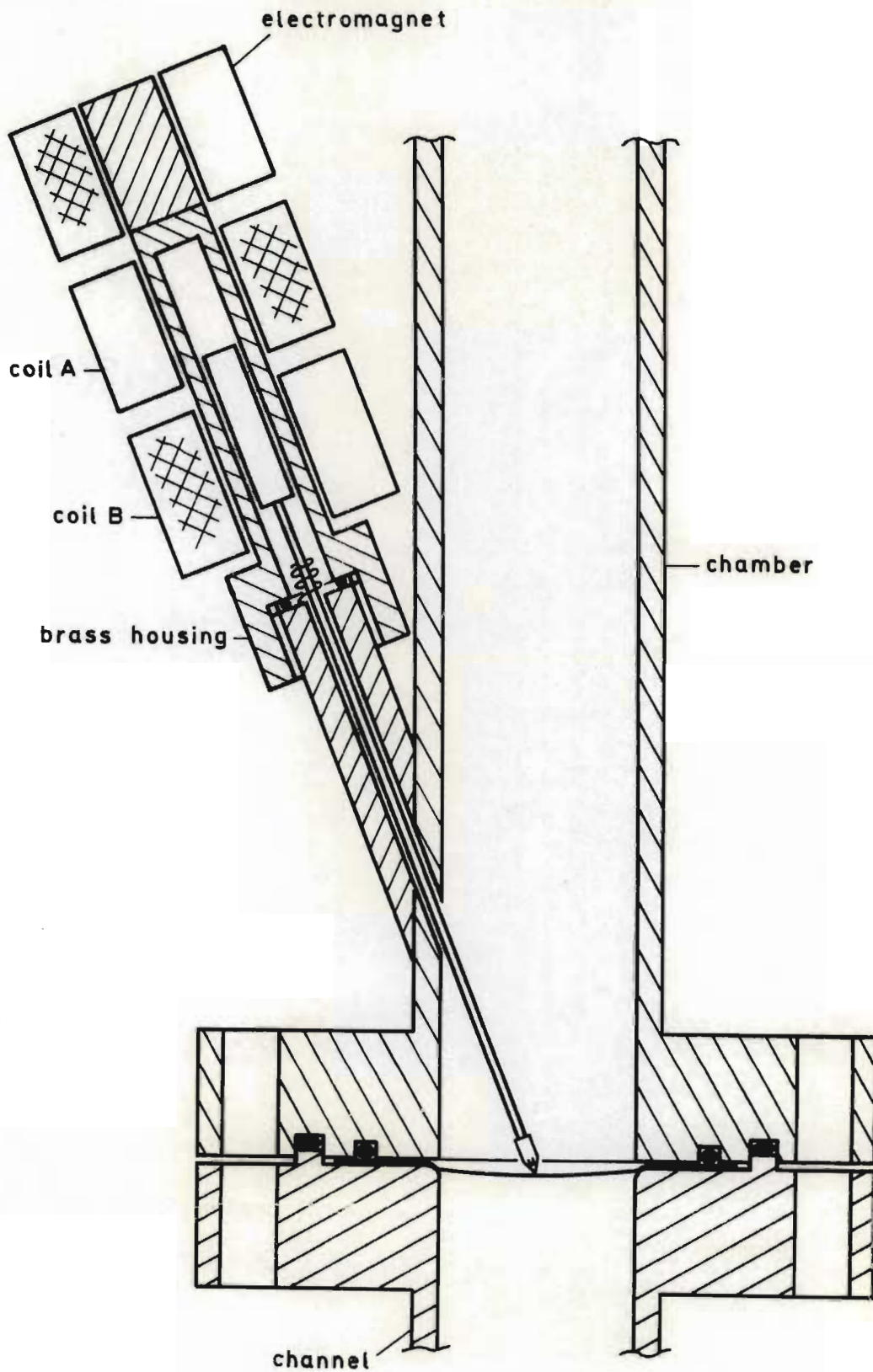
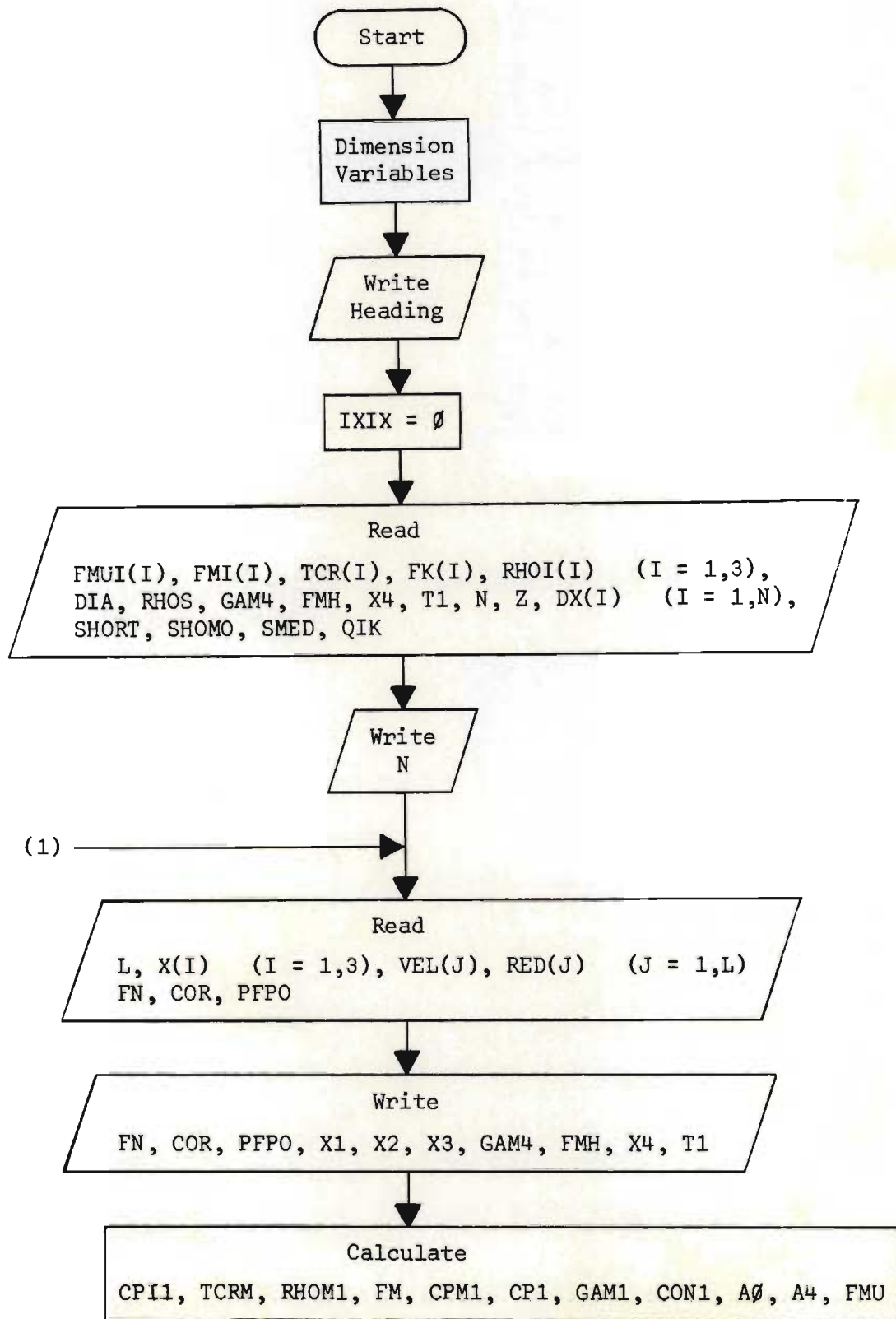
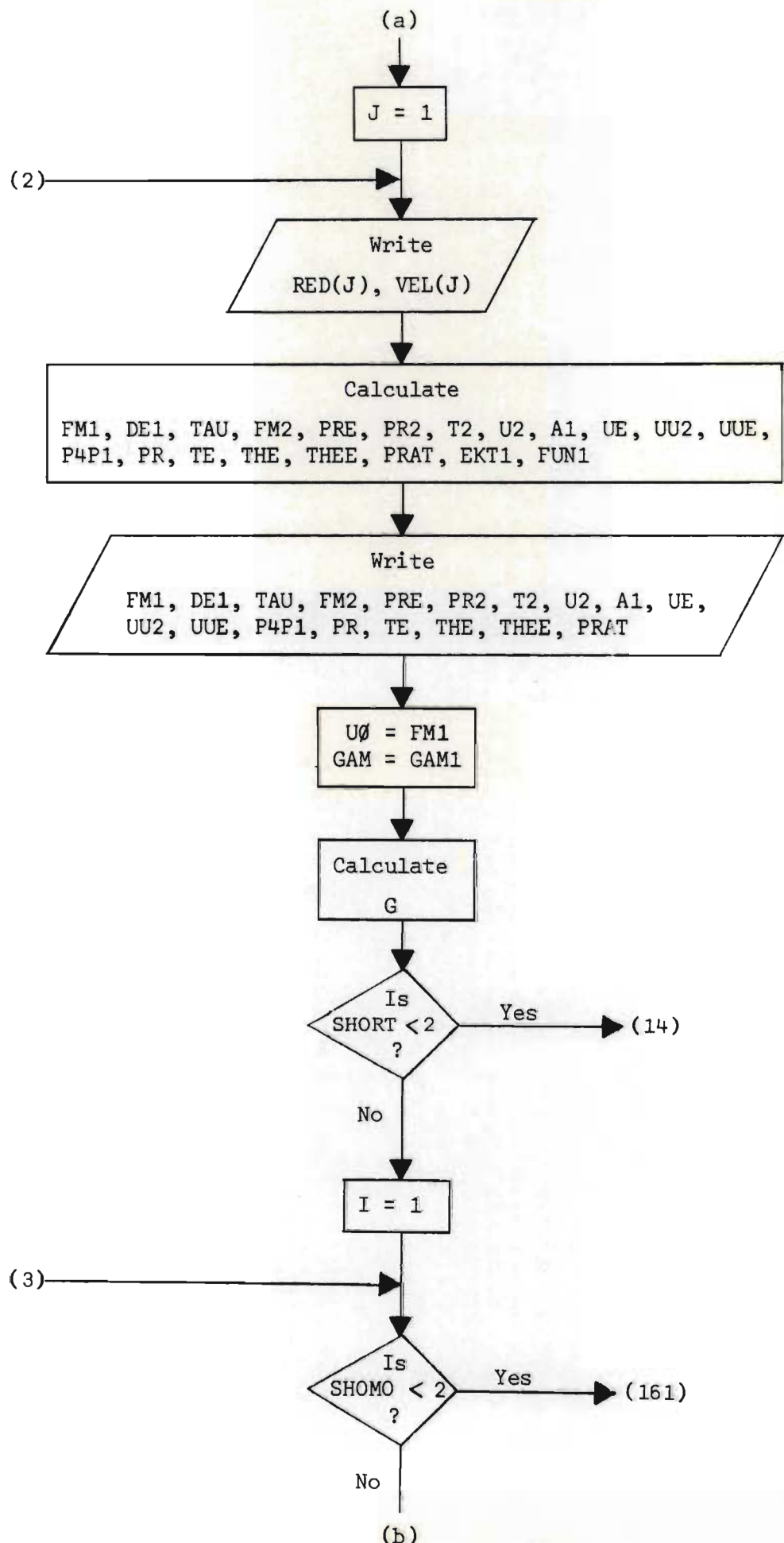
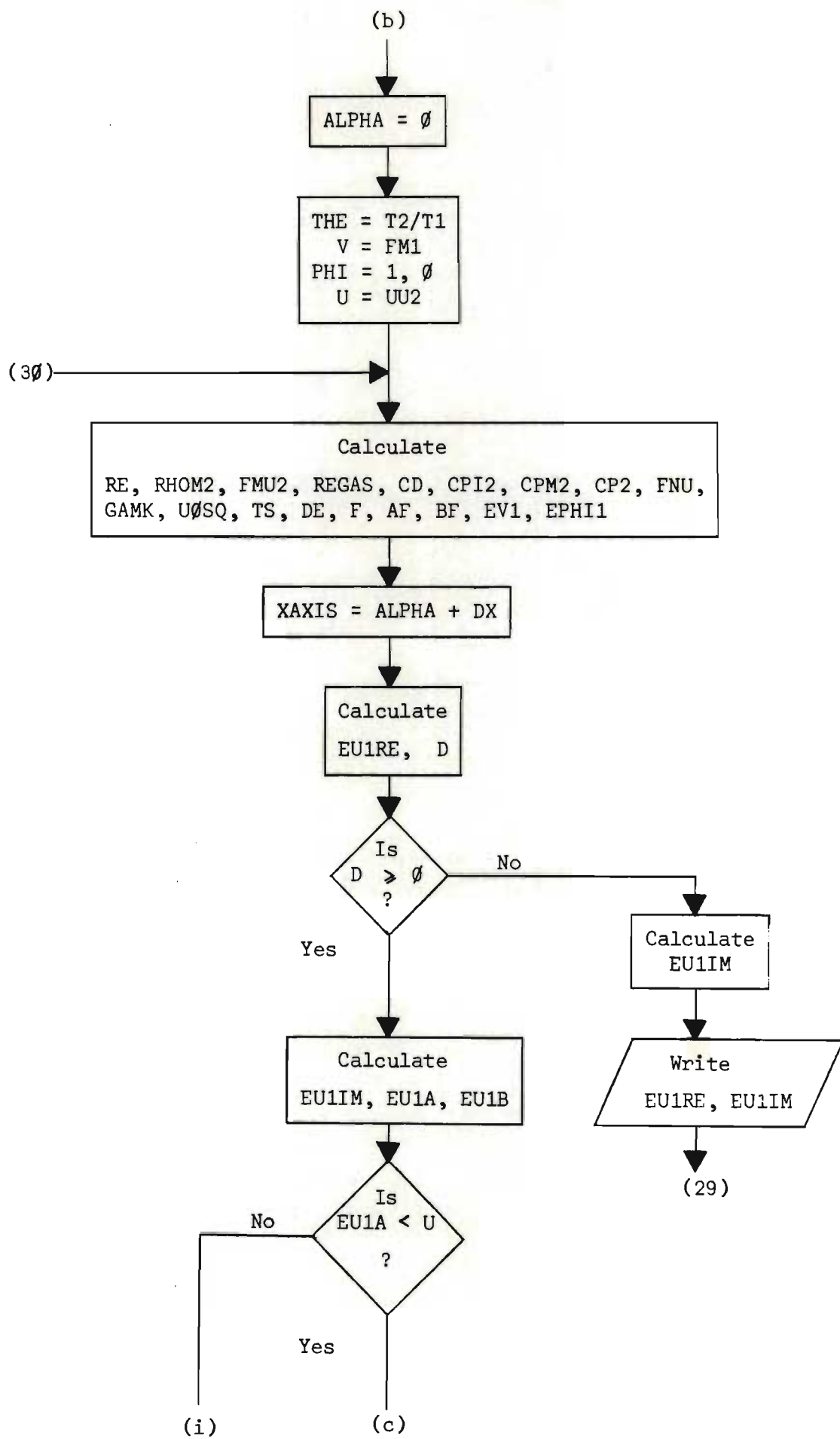


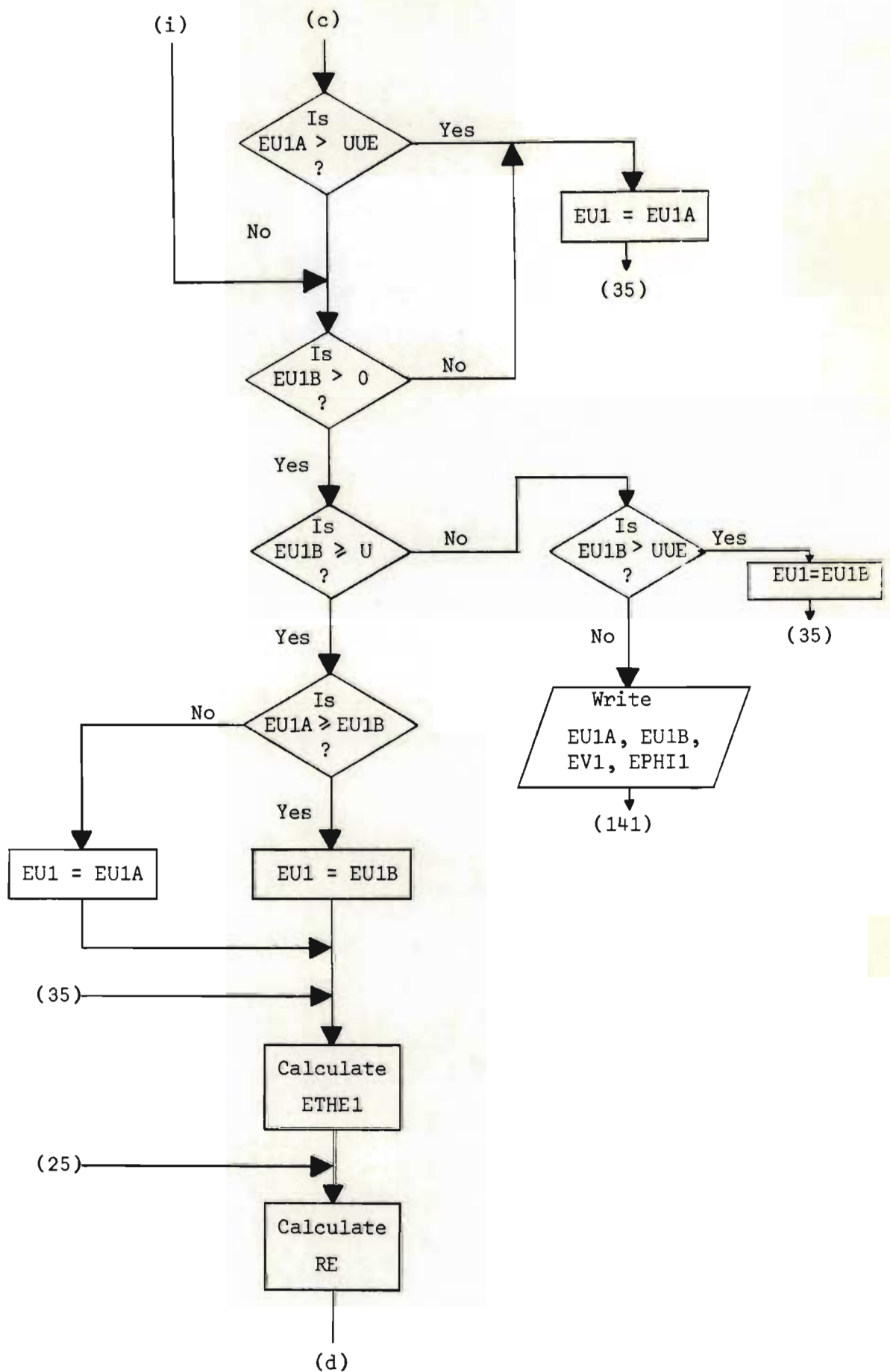
FIGURE E.II Rupture pin

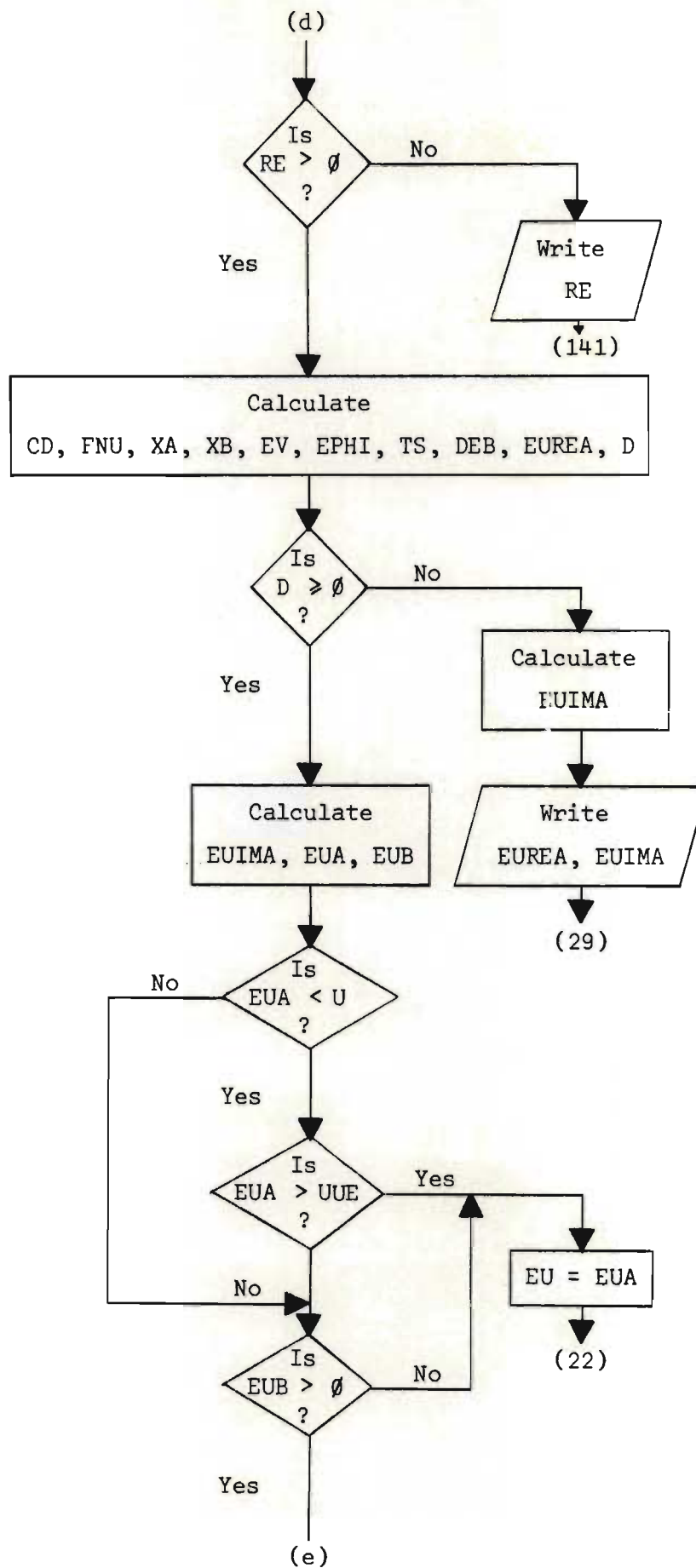
APPENDIX FPROGRAMME ZHETRO-HETEROGENEOUS STATE 2 (FORTRAN V)

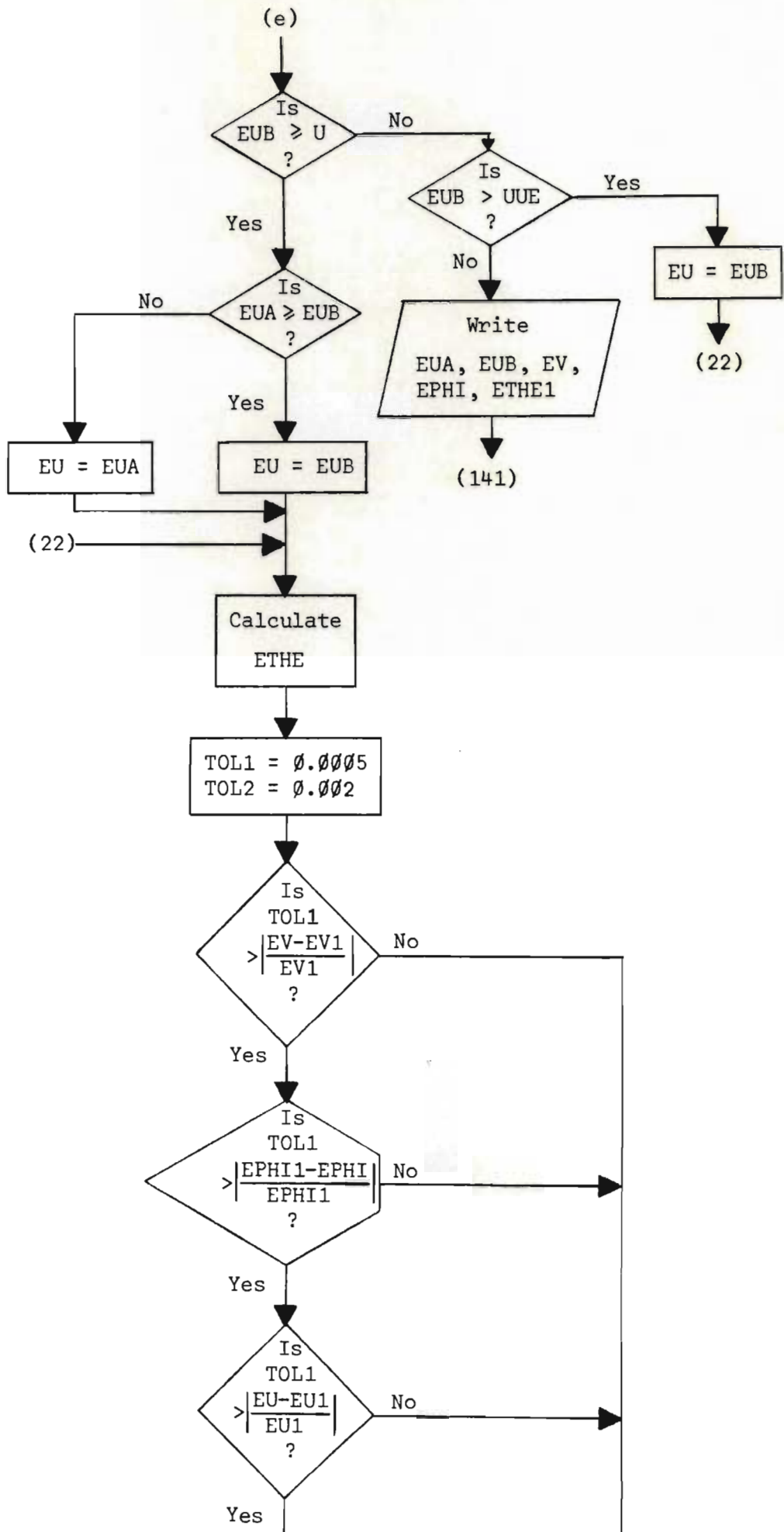


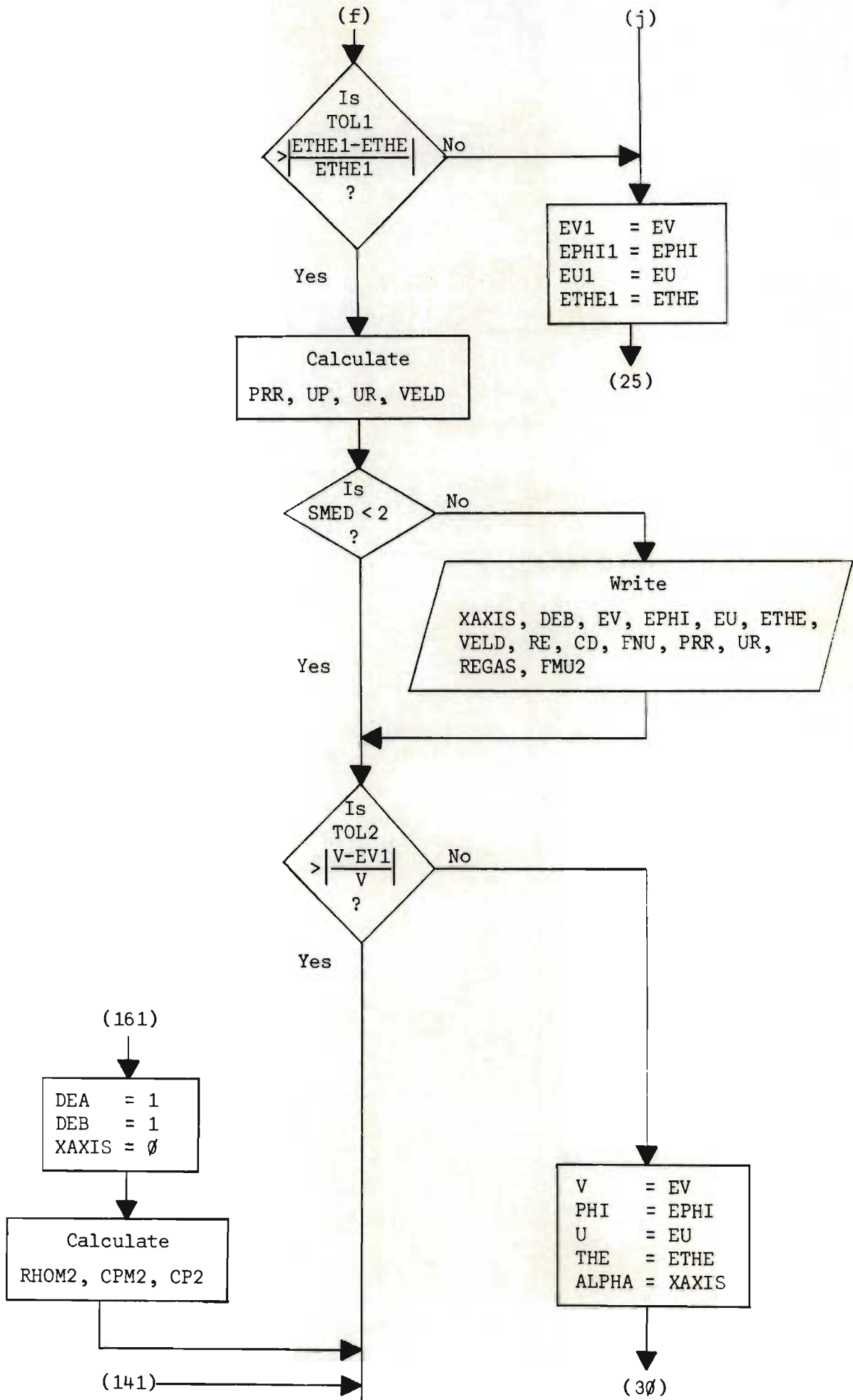


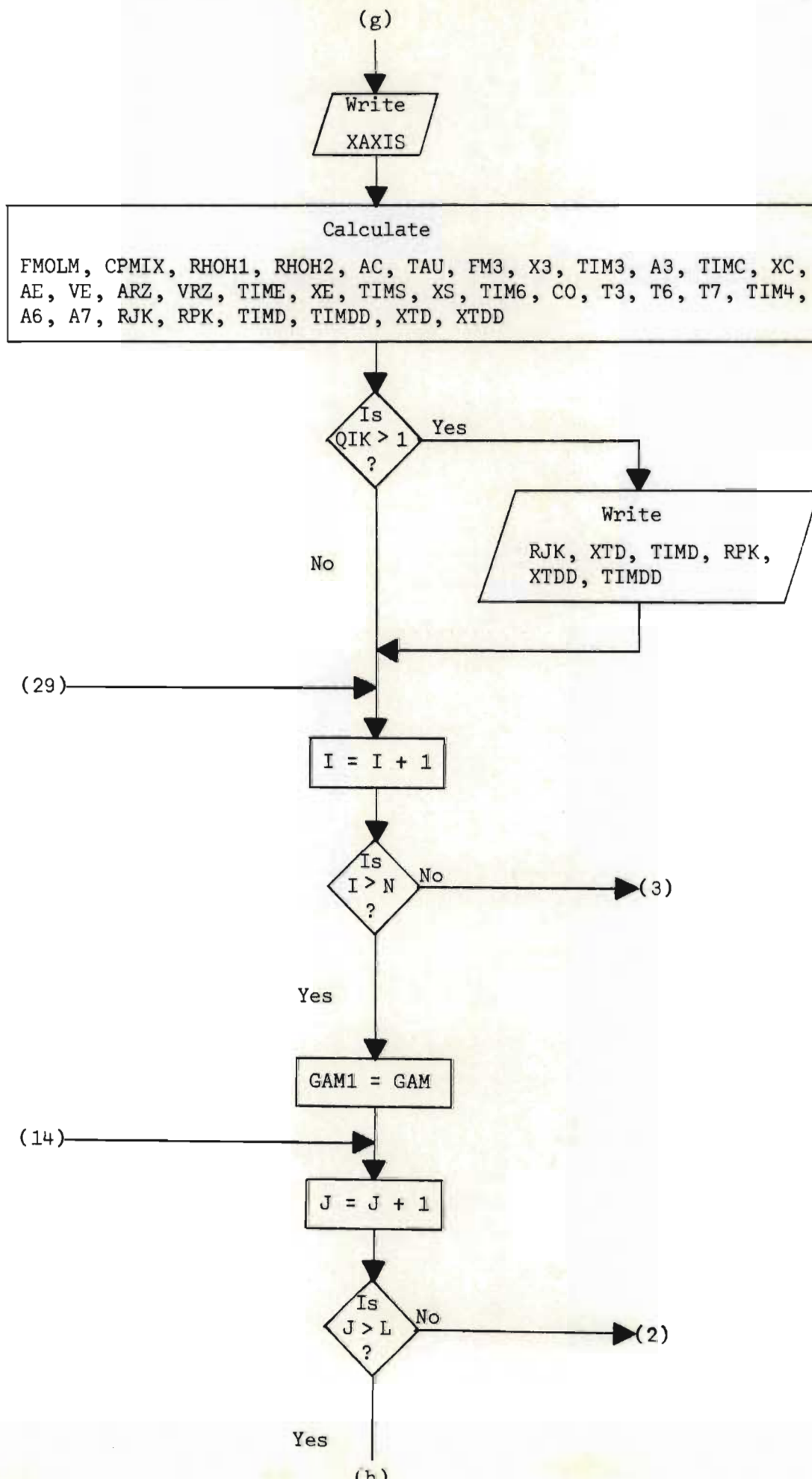


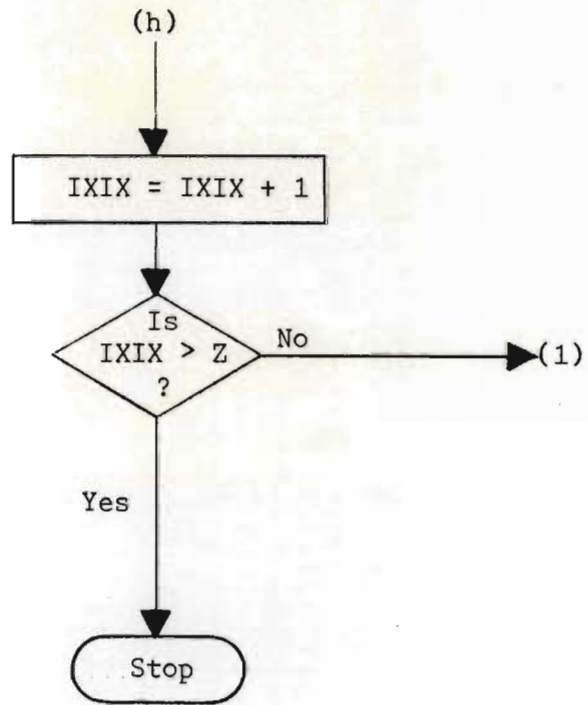














NOMENCLATURE FOR PROGRAMME P1

A $\emptyset$	gas mixture sound speed in state 1	cm·sec. <sup>-1</sup>	
A1	gas/solid mixture sound speed in state 1	cm·sec. <sup>-1</sup>	
A3	gas mixture sound speed in state 3	cm·sec. <sup>-1</sup>	
A4	chamber gas sound speed in state 4	cm·sec. <sup>-1</sup>	
A6	gas sound speed in state 6	cm·sec. <sup>-1</sup>	
A7	gas sound speed in state 7	cm·sec. <sup>-1</sup>	
AC	= $16(\mu p/\rho a)_s \beta^2$ , used in estimation of boundary layer drag (see Chapter 3.2.4)		
AE	gas sound speed in relaxed state 2	cm·sec. <sup>-1</sup>	
AF	dV/dx, for V see below and eqn. 3.2.2.VII		
ARZ	average gas sound speed in relaxation zone	cm·sec. <sup>-1</sup>	
BF	d(PHI)/dx, for PHI see below and equation 3.2.2.VIII		
CD	catalyst particle drag coefficient; equation 3.2.2.X		
CO	boundary layer correction factor for UE in chamber gas		
CON1	gas mixture thermal conductivity in state 1	cal·sec. <sup>-1</sup> ·cm <sup>-2</sup> ·°C <sup>-1</sup> ·cm	
COR	boundary layer correction factor for UE in channel gas		
CP1	gas mixture specific heat in state 1	cal·g <sup>-1</sup> ·°C <sup>-1</sup>	
CP2	gas mixture specific heat in state 2	cal·g <sup>-1</sup> ·°C <sup>-1</sup>	
CPI1	gas component specific heat in state 1	cal·g mole <sup>-1</sup> ·°C <sup>-1</sup>	
CPI2	gas component specific heat in state 2	cal·g mole <sup>-1</sup> ·°C <sup>-1</sup>	
CPM1	gas mixture specific heat in state 1	cal·g mole <sup>-1</sup> ·°C <sup>-1</sup>	
CPM2	gas mixture specific heat in state 2	cal·g mole <sup>-1</sup> ·°C <sup>-1</sup>	
CPMIX	specific heat of gas/solid mixture	cal·g <sup>-1</sup> ·°C <sup>-1</sup>	
D	= $B^2 - 4AC$ in solution of quadratic eqn. 3.2.2.XIII		
DE	specific heat of solid/specific heat of gas in frozen state 2		
DE1	specific heat of solid/specific heat of gas in state 1		
DEA	specific heat of solid/specific heat of gas in relaxation zone		
DEB	= (DE + DEA)/2, average for increment of relaxation zone		
DIA	catalyst particle mean diameter		cm (Appendix G)
DX	increment of distance behind shock front		cm
EKT1	= $1,33 \cdot T_r$ where $T_r$ is the reduced temperature of the gas in state 1		
EPHI	intermediate values of PHI at end of an increment DX		
EPHI1	final value of PHI at end of an increment DX		

ETHE	intermediate values of THE at end of increment
ETHE1	final value of THE at end of increment
EU	final value of U at end of increment
EU1	= EU, return designation in the iteration
EU1A	first solution for U from quadratic equation 3.2.2.XIII
EU1B	second solution for U from quadratic equation 3.2.2.XIII
EU1IM	first imaginary solution for U
EU1RE	first real solution for U
EUA	second and subsequent estimates of EU1A
EUB	second and subsequent estimates of EU1B
EU1MA	second and subsequent estimates of EU1IM
EUREA	second and subsequent estimates of EU1RE
EV	= V, return designation in the iteration
EV1	= EV, return designation in the iteration
F	variable for heat balance equation 3.2.2.VIII $= 6\mu/(D^2 \cdot d \cdot a_1 \cdot \delta \cdot Pr)$
FK	gas component thermal conductivity $\text{cal.} \cdot \text{sec.}^{-1} \cdot \text{cm}^{-2} \cdot \text{C}^{-1} \cdot \text{cm}$
FM	gas mixture molecular weight
FM1	Mach No. of shock wave w.r.t. gas only in state 1
FM2	Mach No. of shock wave w.r.t. gas/solid mixture in state 1
FM3	Mach No. of shock wave w.r.t. gas only in state 3
FMH	molecular weight of chamber gas g
FMI	gas component molecular weight g
FMOLM	molecular weight of gas/solid mixture g
FMU	gas mixture viscosity $g_{\text{mass}} \cdot \text{sec.}^{-1} \cdot \text{cm}^{-1}$
FMU2	gas mixture viscosity in state 2 $g \cdot \text{sec.}^{-1} \cdot \text{cm}^{-1}$
FMUI	gas component viscosity $g \cdot \text{sec.}^{-1} \cdot \text{cm}^{-1}$
FN	catalyst loading ratio, mass solid/mass gas
FNU	Nusselt No.; equation 3.2.2.XI
FUN1	viscosity temperature function based on the Lennard-Jones potential
G	variable for momentum balance equation 3.2.2.VII $= 3\rho_1 U_1 / 4Dd$
GAM	gas mixture specific heat ratio
GAM1	gas mixture specific heat ratio in state 1
GAM4	specific heat ratio of chamber gas
GAMK	= YK in equation 12 of Rudinger (1964) YK is the first criteria for negative sign of $(dU/dx)_{x=0}$

L	number of sets of RED and VEL to be calculated for particular X(I), FN, COR, PFPO
N	number of values for increment DX
P4P1	pressure ratio across the diaphragm for the homogeneous case
PFPO	experimental pressure ratio across the diaphragm
PHI	= $T/T_1$ (see Chapter 3.2.2)
PR	Prandtl number, equations 3.2.2.VIII and 3.2.2.XI
PR2	pressure of frozen state 2/pressure of state 1
PRAT	theoretical diaphragm pressure ratio for the heterogeneous case
PRE	pressure of relaxed state 2/pressure of state 1
PRR	pressure ratio at various points in the relaxation zone $P/P_1$
QIK	option to output quench rate results
RE	Reynolds No. for a particle; equation 3.2.2.IX
RED	reduction extent of catalyst; % $O_2$ removed
REGAS	gas Reynolds No. in relaxation zone, i.e. at velocity $(U_2+U_E)/2$ .
RHOH1	heterogeneous mixture density in state 1 $g \cdot cm^{-3}$
RHOH2	heterogeneous mixture density in relaxed state 2 $g \cdot cm^{-3}$
RHOI	gas component density at atmospheric pressure and temperature $T_1$ $g \cdot cm^{-3}$
RHOM1	gas mixture density in state 1 $g \cdot cm^{-3}$
RHOM2	gas mixture density at various points in the relaxation zone $g \cdot cm^{-3}$
RHOS	density of catalyst particle $g \cdot cm^{-3}$ (Appendix G)
RJK	various temperatures within the chamber gas expansion fan $^{\circ}K$
RPK	various temperatures within the channel gas expansion fan $^{\circ}K$
SHOMO	option to exclude relaxation zone calculations; for the homogeneous shock wave
SHORT	option to exclude all but frozen and relaxed state 2 calculations
SMED	option to output incremental calculation results within the relaxation zone
T1	temperature of state 1 = $T_1$ , $^{\circ}K$
T2	temperature of frozen state 2, $^{\circ}K$
T3	temperature of chamber gas in state 3, $^{\circ}K$
T4	temperature of chamber gas in state 4, $^{\circ}K$
T6	final temperature of expanded chamber gas, $^{\circ}K$
T7	final temperature of expanded channel gas, $^{\circ}K$

TAU	specific heat ratio for solid/gas mixture, equation 3.2.2.V
TCR	gas component critical temperature, $^{\circ}\text{K}$
TCRM	gas mixture critical temperature, $^{\circ}\text{K}$
TE	temperature of relaxed state 2, $^{\circ}\text{K}$
THE	temperature ratio $\theta$ , equation 3.2.2.II
THEE	$\theta_e$ , value in relaxed state 2
TIM3	$t_3$ , time after diaphragm rupture when the head of the reflected rarefaction wave intersects its incident tail - see Figure 3.3.2.I, m·sec.
TIM4	$t_3$ , see Figure 3.3.2.1, m·sec
TIM6	$t_6$ , see point B in Figure 3.3.3.I, m·sec.
TIMC	$t_c$ , see Figure 3.3.2.I, m·sec.
TIMD	$t'/t'_c$ for the values of RJK - see equation 3.3.3.IX
TIMDD	$t''/t''_c$ for the values of RPK - see equation 3.3.3.X
TIME	$t_E$ , see Figure 3.3.2.I, m·sec.
TIMS	$t_s$ , see Figure 3.3.2.I, m·sec.
TOL1	tolerance test for completion of iterative calculation over each DX
TOL2	tolerance test for attainment of relaxed state 2 conditions
TS	T, temperature of catalyst particle, $^{\circ}\text{K}$
U	$u/a_1$ , see Chapter 3.2.2
UØ	= FM1 = $U_1$ in Chapter 3.2.2
UØSQ	second criterion for negative sign of $(dU/dx)_{x=0}$ , equation 12 of Rudinger (1964)
U2	velocity of gas in frozen state 2 w.r.t. shock tube wall, $\text{cm}\cdot\text{sec}^{-1}$
UE	velocity of gas and solid in relaxed state 2 w.r.t. shock tube wall, $\text{cm}\cdot\text{sec}^{-1}$
UP	catalyst particle velocity relative to shock tube wall, $\text{cm}\cdot\text{sec}^{-1}$
UR	velocity of gas relative to catalyst particles in the relaxation zone, $\text{cm}\cdot\text{sec}^{-1}$
UU2	velocity of gas in frozen state 2 w.r.t. shock front, expressed as Mach No., $u_2/a_1$
UUE	velocity of gas in relaxed state 2 w.r.t. shock front, expressed as Mach No., $u_e/a_1$
V	$v/a_1$ , Mach No. of catalyst particle w.r.t. shock front
VE	$v_e/a_1$ , Mach No. of catalyst particle in relaxed state 2 w.r.t. shock front
VEL	velocity of shock wave w.r.t. shock tube wall, $\text{cm}\cdot\text{sec}^{-1}$
VELD	$(V-U)/(UØ-UU2)$

VRZ	arithmetic mean velocity of reflected rarefaction head within the relaxation zone w.r.t. shock tube wall, $\text{cm}\cdot\text{sec}^{-1}$
X1	mol. fraction of argon in channel gas
X2	mol. fraction of carbon monoxide in channel gas
X3	mol. fraction of hydrogen in channel gas <u>and</u> distance along shock tube where the head of the reflected rarefaction wave intersects its incident tail - see Figure 3.3.2.I, cm
X4	length of chamber, cm
XA	arithmetic mean of the values for AF calculated at the beginning & end of an increment DX
XAXIS	length of relaxation zone, cm
XB	arithmetic mean of the values for BF calculated at the beginning and end of an increment DX
XC	distance along shock tube where the head of the reflected rarefaction wave intersects the contact surface, cm
XE	distance along shock tube where the head of the reflected rarefaction wave intersects the tail of the relaxation zone, cm
XS	distance along shock tube where the head of the reflected rarefaction wave intersects the shock front, cm
XTD	$x'/t'$ , characteristic slope for values of RJK, calculated using equations 3.3.3.II and 3.3.3.III; see Figure 3.3.3.I
XTDD	$x''/t''$ , characteristic slope for values of RPK calculated using equations 3.3.3.II and 3.3.3.III with $\Gamma$ instead of $\gamma$ ; see Figure 3.3.3.I
Z	number of complete sets of data to be calculated

---

ZHETRO PRINT-OUT OF RESULTS - RUN 36

402 HETERO STATE 2 PROG ONE  
403 #  
404 #  
405 #  
406 #  
407 N= 1  
408 #  
409 #  
410 FN= .135 COR= 1.027 PFPO= 63.25  
411 X1= .8200 X2= .0900 X3= .0900  
412 GAM4= 1.407 FMH= 2.016 X4= 60.6 T1= 298.0  
413 CP1= .1492 GAM1= 1.603 RHOM1= .001451  
414 TCRM= 138.9 CON1= .6408-04  
415 FM= 35.428 A0= 33478.909 A4= 131500.020  
416 FMU= .2201-03  
417 #  
418 #  
419 #  
420 RED= .80  
421 #  
422 #  
423 VEL= 112100.0  
424 FM1= 3.348  
425 #  
426 DE1= .786  
427 PRE= 16.01 FM2= 3.669 PR2= 13.58  
428 T2= 1214.1 U2= 78459.335 UE= 82521.905 TAU= 1.515  
429 UU2= 1.004832 UUE= .883484 A1= 30553.638  
430 P4P1= 33.22 PR= .5122

431 THE2= 4.074 THEE= 4.225 TE= 1259.1  
432 G= .3301 PRAT= 41.18  
433 GAMK= .410 UOSQ= 9.449 RE= 1540.0 CD= .826093  
434 REGAS= .4931+02 FMU2= .5912-03 DE= .777  
435 #  
436 DISTANCE= 2.00  
437 DEB= .831  
438 V= 2.544 PHI= 1.387 U= .996937 4.228 .66  
439 RE= 1024.6 CD= 1.155 FNU= .17367+02 PRR= 14.20  
440 UR= 51782.139 REGAS= .4931+02 FMU2= .5912-03  
441 #  
442 DISTANCE= 4.00  
443 DEB= .927  
444 V= 1.906 PHI= 1.730 U= .976374 4.308 .40  
445 RE= 613.7 CD= 1.761 FNU= .13893+02 PRR= 14.77  
446 UR= 31126.533 REGAS= .4808+02 FMU2= .6063-03  
447 #  
448 DISTANCE= 6.00  
449 DEB= 1.004  
450 V= 1.458 PHI= 2.030 U= .953526 4.335 .22  
451 RE= 336.6 CD= 2.895 FNU= .10808+02 PRR= 15.22  
452 UR= 16890.812 REGAS= .4748+02 FMU2= .6139-03  
453 #  
454 DISTANCE= 8.00  
455 DEB= 1.066  
456 V= 1.186 PHI= 2.276 U= .934225 4.331 .11  
457 RE= 171.0 CD= 5.095 FNU= .82776+01 PRR= 15.52  
458 UR= 8427.301 REGAS= .4729+02 FMU2= .6165-03  
500 #  
501 DISTANCE= 10.00  
502 DEB= 1.115

503 V= 1.042 PHI= 2.467 U= .920021 4.314 .05  
504 RE= 83.8 CD= 9.360 FNU= .63951+01 PRR= 15.70  
505 UR= 4080.800 REGAS= .4731+02 FMU2= .6161-03  
506 #  
507 DISTANCE= 12.00  
508 DEB= 1.153  
509 V= .970 PHI= 2.611 U= .909943 4.296 .03  
510 RE= 42.4 CD= 17.188 FNU= .51270+01 PRR= 15.81  
511 UR= 2026.661 REGAS= .4743+02 FMU2= .6145-03  
512 #  
513 DISTANCE= 14.00  
514 DEB= 1.181  
515 V= .934 PHI= 2.722 U= .902590 4.279 .01  
516 RE= 22.3 CD= 32.014 FNU= .42670+01 PRR= 15.87  
517 UR= 1065.217 REGAS= .4757+02 FMU2= .6128-03  
518 #  
519 DISTANCE= 14.50  
520 DEB= 1.196  
521 V= .929 PHI= 2.746 U= .900516 4.273 .01  
522 RE= 19.5 CD= 36.785 FNU= .41197+01 PRR= 15.89  
523 UR= 937.720 REGAS= .4770+02 FMU2= .6111-03  
524 #  
525 DISTANCE= 15.00  
526 DEB= 1.201  
527 V= .923 PHI= 2.768 U= .899103 4.270 .01  
528 RE= 16.9 CD= 42.912 FNU= .39717+01 PRR= 15.90  
529 UR= 811.241 REGAS= .4774+02 FMU2= .6106-03  
530 #  
531 DISTANCE= 15.50  
532 DEB= 1.206  
533 V= .919 PHI= 2.789 U= .897768 4.266 .01



534 RE= 14.6 CD= 50.110 FNU= .38373+01 PRR= 15.91  
535 UR= 703.111 REGAS= .4777+02 FMU2= .6102-03  
536 #  
537 DISTANCE= 16.00  
538 DEB= 1.210  
539 V= .915 PHI= 2.809 U= .896502 4.263 .01  
540 RE= 12.7 CD= 58.736 FNU= .37132+01 PRR= 15.92  
541 UR= 610.287 REGAS= .4780+02 FMU2= .6099-03  
542 #  
543 DISTANCE= 16.50  
544 DEB= 1.215  
545 V= .911 PHI= 2.829 U= .895300 4.259 .01  
546 RE= 11.1 CD= 69.165 FNU= .35980+01 PRR= 15.93  
547 UR= 530.250 REGAS= .4782+02 FMU2= .6096-03  
548 #  
549 DISTANCE= 17.00  
550 DEB= 1.219  
551 V= .908 PHI= 2.847 U= .894155 4.256 .01  
552 RE= 9.6 CD= 81.898 FNU= .34908+01 PRR= 15.94  
553 UR= 460.922 REGAS= .4785+02 FMU2= .6093-03  
554 #  
555 DISTANCE= 17.50  
556 DEB= 1.223  
557 V= .905 PHI= 2.864 U= .893062 4.253 .01  
558 RE= 8.4 CD= 97.623 FNU= .33905+01 PRR= 15.95  
559 UR= 400.599 REGAS= .4787+02 FMU2= .6089-03  
600 #  
601 DISTANCE= 18.00  
602 DEB= 1.227  
603 V= .902 PHI= 2.881 U= .892017 4.250 .00  
604 RE= 7.3 CD= 117.302 FNU= .32962+01 PRR= 15.95  
605 UR= 347.856 REGAS= .4789+02 FMU2= .6086-03

606 #  
 607 DISTANCE= 18.50  
 608 DEB= 1.230  
 609 V= .900 PHI= 2.897 U= .891017 4.247 .00  
 610 RE= 6.3 CD= 142.308 FNU= .32070+01 PRR= 15.96  
 611 UR= 301.522 REGAS= .4792+02 FMU2= .6084-03  
 612 #  
 613 DISTANCE= 19.00  
 614 DEB= 1.234  
 615 V= .898 PHI= 2.913 U= .890058 4.244 .00  
 616 RE= 5.5 CD= 174.668 FNU= .31222+01 PRR= 15.97  
 617 UR= 260.613 REGAS= .4794+02 FMU2= .6081-03  
 618 #  
 619 DISTANCE= 19.50  
 620 DEB= 1.237  
 621 V= .896 PHI= 2.927 U= .889138 4.242 .00  
 622 RE= 4.7 CD= 217.460 FNU= .30409+01 PRR= 15.97  
 623 UR= 224.307 REGAS= .4796+02 FMU2= .6078-03  
 624 #  
 625 DISTANCE= 20.00  
 626 DEB= 1.240  
 627 V= .894 PHI= 2.942 U= .888253 4.239 .00  
 628 RE= 4.0 CD= 275.559 FNU= .29624+01 PRR= 15.98  
 629 UR= 191.913 REGAS= .4798+02 FMU2= .6076-03  
 630 #  
 631 DISTANCE= 20.50  
 632 DEB= 1.243  
 633 V= .892 PHI= 2.955 U= .887403 4.237 .00  
 634 RE= 3.4 CD= 357.052 FNU= .28858+01 PRR= 15.99  
 635 UR= 162.851 REGAS= .4800+02 FMU2= .6073-03  
 636 #  
 637 XAXIS= 20.50

638	CPMIX=	6.25	FMOLM=	40.2	RHOM2=	.005470			
639	RHOH1=	.001647	RHOH2=	.006208	AC=	.06281			
640	-46.46	.000556	120.74	.001425					
641	189.12	.001870	270.58	.002414					
642	.000690	.000461	142.0	630.4	90785.2	48691.9	200.3	107805.1	
643	142.0	.90785+05	2.7627	630.4	.47578+05	6.0662			
644	145.9	.98075+05	2.5509	672.3	.55879+05	5.1294			
645	149.8	.10527+06	2.3603	714.2	.63924+05	4.3815			
646	153.7	.11237+06	2.1882	756.1	.71737+05	3.7765			
647	157.6	.11938+06	2.0326	798.0	.79336+05	3.2812			
648	161.5	.12631+06	1.8914	839.9	.86738+05	2.8715			
649	165.3	.13315+06	1.7630	881.8	.93958+05	2.5293			
650	169.2	.13991+06	1.6461	923.8	.10101+06	2.2410			
651	173.1	.14660+06	1.5393	965.7	.10790+06	1.9963			
652	177.0	.15321+06	1.4415	1007.6	.11464+06	1.7871			
653	180.9	.15975+06	1.3519	1049.5	.12125+06	1.6070			
654	184.7	.16622+06	1.2696	1091.4	.12772+06	1.4511			
655	188.6	.17262+06	1.1939	1133.3	.13407+06	1.3154			
656	192.5	.17896+06	1.1241	1175.3	.14031+06	1.1967			
657	196.4	.18523+06	1.0596	1217.2	.14643+06	1.0922			

APPENDIX GAVERAGE PARTICLE DIAMETER, PARTICLE DENSITY AND SURFACE AREA

Roller analysis of unreduced catalyst:-

diameter $\mu$	mass fraction
0 - 8,8	0,06
8,8 - 12,6	0,17
12,6 - 25,2	0,30
25,2 - 34,0	0,145
34,0 - 46,0	0,21
46,0 - 50,0	0,115

According to Torobin and Gauvin (1960) there is much controversy over the method for evaluating the average particle diameter of a mixture of irregular particles having a wide size distribution.

From Perry (4th ed.),

$$\text{harmonic mean diameter } D_p = 1/\Sigma(\Delta W/D_m) \quad \text{G.I}$$

$$\text{weight average diameter } D_p = \Sigma(\Delta W \cdot D_m) \quad \text{G.II}$$

where  $\Delta W$  is the incremental mass fraction of particles and  $D_m$  is the arithmetic mean diameter of the increment.

For the above mixture equation G.I yields  $D_p = 17,3 \mu$  while G.II gives  $D_p = 26\mu$ .

Equation G.I yields  $D_p$  which is more compatible with the concept of hydraulic radius underlying the calculation of pressure drop across fluidised beds of particles. However, since this work is not concerned with fluidised beds of particles but rather transport in very dilute phase it was deemed more accurate to use equation G.II.

SASOL has observed that reduction of the catalyst at 400 - 450°C results in 18 per cent shrinkage in volume. Catalyst used in this work was reduced at 600°C but no particle size analysis was performed after reduction. Maximum possible shrinkage (for 100% reduction) is determined thus:

measured density of unreduced catalyst material  
 (by benzol immersion) =  $5,2 \text{ g} \cdot \text{cm}^{-3} = 0,1925 \text{ cm}^3 \cdot \text{g}^{-1}$   
 density of Fe =  $7,86 \text{ g} \cdot \text{cm}^{-3} = 0,1270 \text{ cm}^3 \cdot \text{g}^{-1}$   
 per cent shrinkage =  $\frac{0,1925 - 0,1270}{0,1925} \cdot 100 = 34$

Pore volume after reduction (100%) =  $0,1925 - 0,1270$   
 =  $0,0655 \text{ cm}^3 \cdot \text{g}^{-1}$   
 therefore effective particle density =  $1/(0,0655 + 0,1925)$   
 =  $3,88 \text{ g} \cdot \text{cm}^{-3}$

assuming no shrinkage.

The relationship between pore volume and extent of reduction; and reduction temperature and degree of shrinkage, being unknown, an approximate effective particle density of  $4,6 \text{ g} \cdot \text{cm}^{-3}$  for 85% reduced catalyst ( $600^\circ\text{C}$ ) was calculated assuming 18% shrinkage at  $600^\circ\text{C}$  and a pore volume of  $0,0655 \text{ cm}^3 \cdot \text{g}^{-1}$ .

On the basis of 18% shrinkage the average diameter of reduced catalyst particles was taken to be  $24 \mu$  compared to  $26 \mu$  for unreduced particles.

No satisfactory experimental measurements were obtained of reduced catalyst surface area so the value reported by Anderson et al (1964) for a similar catalyst was used for qualitative purposes in this work. Anderson et al measured the surface area of iron catalyst which had been completely reduced at  $600^\circ\text{C}$  and obtained a value of  $1,6 \text{ m}^2/\text{g}$ ; according to them lower extents of reduction would result in a surface area of  $S \cdot R_D$  where  $S$  is the surface area after complete reduction and  $R_D$  is the extent of reduction expressed as the fraction of total oxygen removed. Here, average  $R_D$  was 0,85, therefore surface area =  $1,4 \text{ m}^2/\text{g}$ .

Unreduced catalyst was found to have a surface area of approximately  $1 \text{ m}^2/\text{g}$ .